ADAPTIVE STRUCTURE DESIGN OF A SUPERSONIC MISSILE ACTUATION SYSTEM

Jeffrey Craig Moonsamy
0303522E

School of Mechanical, Industrial and Aeronautical

University of the Witwatersrand

Johannesburg, South Africa.

Supervisors:
Prof. C. Law and Prof. R. Reid

A research dissertation submitted to the Faculty of Engineering and the Built Environment, University of the Witwatersrand, in fulfilment of the requirements for the degree of Master of Science in Engineering.

November 2021

Declaration

I declare that this dissertation is my own unaided work. It is being submitted in fulfilment of the requirements for the degree of Master of Science to the University of the Witwatersrand, Johannesburg. It has not been submitted before for any degree or examination to any other University.

……………………………:……...……………..……………..

(Signature of Candidate)

………14th…….. day of………November…….. year……2021………..

Abstract

Smart Materials' ability to alter shape by applying an external impetus excitation has significant potential within the aerospace industry. The ability to operate as an actuator has been the focus of numerous published studies. Missile actuation systems have benefited from this technology where Adaptive Structures actuated missile control fins. This research aims to determine how an Adaptive Structure, using Smart Materials as the Force Generation Mechanism, can alter the flight path of a supersonic missile with performance comparable to the generic Force Generation Mechanism system. This study adapted the Systems Engineering approach from IEEE 1220 to develop a Force Generation Mechanism for a Beyond Visual Range (BVR) class of missile that operates in the supersonic regime. The Force Generation Mechanism is acknowledged in the literature to benefit the most from Smart Material technology. The requirements for the design were compiled based on a holistic view. The conceptual missile design and actuator system design were conducted to determine the inputs for the Force Generation Mechanism system design. Functional Architecture, Physical Architecture, and Force Generation Mechanism concepts were developed based on the requirement baseline. A design decision tool comprising two scoring stages was then constructed to assess the performance of the different force generation concepts that would incorporate Smart Material technology. A concept utilising piezoelectric linear actuators was found to meet the requirements defined in this study, indicating that existing Smart Material technology can satisfy the requirements of a generic Force Generation Mechanism for a supersonic missile system.

.

Acknowledgements

I would first like to thank my supervisors Prof. Craig Law and Prof. Robert Reid of the School of Mechanical, Industrial, and Aeronautical Engineering at the University of the Witwatersrand, Johannesburg. I am grateful for their assistance and invaluable insight throughout my research.

I would also like to thank the various experts I consulted for this research; this includes the guidance I received from mentors at Denel Dynamics and other industry experts. Without their passionate participation and input, this study could not have been successfully conducted.

I must express my very profound gratitude to my wife, Amarinthea, my daughters Saoirse and Caoimhe, my parents Kevin and Sharon, my brother Christopher and his fiancée Jasantha for providing me with unfailing support and continuous encouragement throughout my years of study and through the process of researching and writing this dissertation. This accomplishment would not have been possible without them. Thank you.

Finally, I would like to express my gratitude to God for the perseverance and strength that carried me through my studies and for the opportunity to develop myself further.

Author

Jeffrey Craig Moonsamy

Table of Contents

List of Figures

List of Tables

List of Acronyms and Symbols

Abbreviation/Acronyms	***Meaning***
AAM	Air to Air Missile
ABS	Acrylonitrile Butadiene Styrene
AMRAAM	Advanced Medium-Range Air-to-Air Missile
ARCH1	First architecture
ARCH2	Second architecture
AS	Adaptive Structure
ASYS	Actuator System
ASARCH	Actuator System Architecture
ASM	Air to Surface Missile
BLAM	Barrel-Launched Adaptive Munition
BVR	Beyond Visual Range
CC	circulation control
CONUSE	Concept of Use
DAP	Directionally Attached Piezoelectric
DARPA	Defence Advanced Research Projects Agency
DC	Direct Current
FAA	Federal Aviation Authority
FFBD	Functional Flow Block Diagram
FGM	Force Generation Mechanism
FR	Functional Requirements
H(s)	Feedback Function
IEEE	Institute of Electrical and Electronics Engineers
IMU	Inertial Measurement Unit
INCOSE	International Council on Systems Engineering
LOS	Line-of-Sight
LP	Life profile
MCP	Missile central processor
MFC	Macro Fibre Composite
MOE	Measures of Effectiveness
MOE	Measures of Effectiveness
MORPHLet	Morphing Winglet
MSMA	Magnetic Shape Memory Alloys
NASA	National Aeronautics and Space Administration
Ni-Ti	Nickel Titanium
OEM	Original Equipment Manufacturer
PBP	Post-Buckled Precompressed Structures
PI	Physik Instrumente
PZT	Lead Zirconate Titanate
REAM	Range-Extended Adaptive Munition
SAM	Surface to Air Missile
SCREAM	Shipborne Countermeasure Range-Extended Adaptive Munition
SE	Systems Engineering
SEP	System Engineering Process

SMA	Shape Memory Alloy
SOI	System of Interest
SSM	Surface to Surface Missile
TVC	Thrust Vector Control
UAV	Unmanned Aerial Vehicle

Symbols	**Meaning**
α	Angle of Attack
a	Major dimensions of an elliptical cross-section
b	Minor dimensions of an elliptical cross-section
b	Body
c	Chord
C_{di}	Coefficient of induced drag
C_L	Lift coefficient
C_{MAC}	Aerodynamic chord
C_N	Normal force coefficient
$\mathrm{C_{N\ Total}}$	Total Coefficient of Normal Force
D	Drag
D	Displacement of Wire Bundle
D_1	Displacement input signal
D_e	Difference between the displacement input signal and measured output
D_f,	Friction drag
D_p	Pressure drag
dS	Surface element
D_θ	Rotational displacement
E	Young's Modulus
ε	Strain (Subscript indicates principle axes)
Fa	Force required to move the structure and overcome external load
γ	Shear strain (Subscript indicates principle axes)
$G(s)$	Transfer function
g	Acceleration due to gravity
$H(s)$	feedback function
I	Moment of Inertia
K_p	Proportional Controller Constant
L	Lift
L	Length
M	Moment
M	Mach
N	Normal Force
n	g manoeuvre
n_T	target manoeuvrability
P	Applied load to the beam structure
p	Pressure
p_l	Lower pressure
p_u	Upper pressure

Q	Heat Energy
q	Dynamic pressure
R	Resultant force
r_c	Moment arm for MFC patch force
Re	Reynolds number
S_{Ref}	Missile reference area
s_u	Upper surface
S_W	Wing surface are
T	temperature
T_e	The temperature at the edge of the thermal boundary layer
T_i	Internal temperature
t_o	Time to go
T_w	The temperature at the surface
u_e	Boundary-layer edge velocity
v	Poisson's Ratio (Subscript indicates principle axes)
v	Velocity
V	Volume
V_∞	Freestream velocity
W	Mass of missile
W_a	Total work done by MFC actuator
W_b	Work required to move the structure
W_f	Aerodynamic Work on System
z	Displacement of structure using the actuator without an external load
za	Combined displacement due to aerodynamic loads and actuator moving the structure
zn	Displacement due to the normal force
δ	Fin Deflection angle
ρ	Density of air
τ	Missile time constant
τ	Shear stress
τ_u	Upper shear stress
τ_l	Lower sheer stress
φ	Rotation of the elliptical cross-section about its axis

1. Introduction

1.1 Background and Motivation

Adaptive Structures, using Smart Materials, can change their shape, and in some cases, their properties in response to external stimuli. This stimulus can be in the form of a temperature, pressure, magnetic field, or electrical current change [1]. The design and development of such structures require a multidisciplinary approach which includes the understanding of the structural properties of materials, dynamics, control, the environment, and the system requirements. This approach presents innovative ways to improve existing structures and mechanisms.

The design and development of Adaptive Structure (AS) technology is rapidly advancing despite the perceived reluctance to adopt the technology in the aeronautical industry. It is understandable why Civil Aviation Authorities, like the Federal Aviation Authority (FAA), do not recognise some of the Smart Materials used to create Adaptive Structures when it comes to reliability and safety [2]. Thus, various other studies have been undertaken where the evaluation of recognised materials was done to advance adaptive technology [2]. The various studies form part of the effort in identifying Smart Material technology that can be considered to be reliable and safe. Reliability and safety are significant factors that form part of the decision making across the aerospace industry.

Within the Unmanned Aerial Vehicle (UAV) and missile industry, there have already been projects corresponding to the use of Adaptive Structures to replace the mechanisms that actuate ailerons, elevators and control fins. Their effectiveness has been demonstrated in small/micro UAVs but is yet to become an alternative to the generic systems [3][4].

Considering that missile systems have space and mass constraints, as highlighted by Goldshine *et al*. [5], it can be argued that there is a benefit with regard to the use of actuator systems that can meet such requirements and still produce or aid in producing, the necessary forces to manoeuvre the missile during flight. Adaptive aerostructures are currently not established replacements for generic actuation systems on missiles. A knowledge gap is apparent in the area relating to the suitable application of Adaptive Structures and the method of use of such structures/systems for supersonic missile applications.

1.2 Problem Statement

As mentioned in Section 1.1, the use of Smart Materials/Adaptive Structure technology for aerospace applications should allow them to be used on missiles. These materials/structures would provide the means to alter the flight path of the weapon. However, these materials or structures are not acceptable alternatives for missile actuation systems.

This study assessed the viability of existing Smart Materials or Adaptive Structures as replacements for current missile actuation systems. Beyond Visual Range (BVR) missiles with tail-mounted actuation system control surfaces were selected as the focus for the evaluation. These missiles were determined to benefit from the expected lower mass and reduced space occupied by the Adaptive Structures, given the space limitations in the missile. The resultant increase in the space available would also allow the increase in the amount of propellant for improved range if required. There is a gap in knowledge concerning Adaptive Structures used as part of a BVR missile actuation system. As such, an assessment of relevant existing Smart Materials for use within the missile actuation system would aid the decision process for the use of this technology in BVR missiles.

1.3 Research Question

BVR missiles usually fly at a velocity faster than that of their intended target and must be able to cover the distance to the target relatively quickly. These targets tend to be supersonic fighter aircraft capable of speeds at Mach 1-4. The supersonic regime (Mach 1-4) was therefore selected as the velocity regime for this study.

The problem statement has led to the creation of a primary research question:

Can existing Smart Materials satisfy all the requirements of a Force Generation Mechanism (FGM) that alters the flight path of a BVR supersonic missile?

This would require the Smart Material/Adaptive Structure system to satisfy (or exceed) the performance requirements of the generic FGM system of a supersonic missile. The all-around effectiveness of the replacement would be evaluated in order to determine the feasibility of using the Adaptive Structure system.

1.4 Objectives

The objectives of this research will, therefore, be to:

1. Develop the requirements baseline for an FGM for a BVR supersonic missile control system.
2. Generate the Functional and Physical Architecture for the System of Interest.
3. Generate FGM concepts using Smart Materials.
4. Develop a design decision tool or framework to evaluate the concepts' performance.
5. Evaluate potential candidates using the tool or framework developed.

1.5 Roadmap

This dissertation is structured as follows:

- Chapter 1 includes the background and motivation for this study. The problem statement, research question, and objectives are defined in the subsequent sections of the chapter.

- Chapter 2 describes the literature review carried out for this study. Areas of interest related to the study include:

    - Systems Engineering
    - Adaptive Structures and Smart Materials
    - Missiles
    - BVR Missiles
    - Aerodynamic Loads
    - Missile Actuation Systems
    - Missile Flight Control
    - Actuator Control Methods
    - Flow Effector Methods

- Chapter 3 details the description of the method used to carry out this study. The chapter describes the process to elicit inputs for the FGM system design, and it describes the development of the evaluation tool or framework.

- Chapter 4 includes the selection of the System of Interest and the Enabling System Development.

- Chapter 5 defines the FGM Physical Architecture system design.
- Chapter 6 defines the concepts developed by employing Adaptive Structures. This study used currently available Smart Materials to generate the concepts for the FGM, and these were evaluated along with the defined generic FGM.
- Chapter 7 focuses on the development of the decision tool or framework to aid in the performance evaluation and selection of missile actuation concepts.
- Chapter 8 describes the application of the decision tool or framework and the results of the concept performance evaluation.
- Chapter 9 contains a detailed discussion of the study.
- Chapters 10 draws the conclusion of this study and outlines recommendations for future work in this field of study.

2. Literature Review

The literature review covers topics related to the approach to answer the research question and the aspects that required investigation to answer said question. These topics are:

- Systems Engineering
- Adaptive Structures and Smart Materials
- Missiles
- BVR Missiles
- Aerodynamic Loads
- Missile Actuation Systems
- Missile Flight Control
- Actuator Control Methods
- Flow Effector Methods

These topics were all key to understanding their respective contribution to the scope of this study.

2.1 Systems Engineering

Based on the multidisciplinary nature of aerospace systems, specifically missiles and missile subsystems, the design and development of such systems require a multidisciplinary approach. As described in NASA's Systems Engineering Handbook [6], Systems Engineering is a multidisciplinary approach and has been described by Ryschkewitsch *et al.* [7] as "a critical core competency for successful NASA missions". The Systems Engineering approach was thus investigated as an approach to use for this study.

Systems Engineering (SE) is described as a viewpoint, a method, and a discipline in the INCOSE Systems Engineering Handbook [8]. It is a multi-disciplinary approach to enable the conceptualisation of successful systems. The focus of SE is directed at defining the customers' desires for a system early in the development process, documenting the requirements, carrying out the design of the system, and validating the system thereafter, all while considering the problem in its entirety. SE often requires the integration of diverse disciplines and the interfacing of different stakeholders. SE as a method is a top-down and iterative approach, and as a discipline, it focuses on the problem as a whole [8].

The SE approach involves the application of Systems Thinking. Systems Thinking is a shift in perspective that allows one to focus on the whole and how its inner components interact with one another [8]. This approach has been successfully used in various areas of industry. The areas to which such an approach has been applied to include:

- Technology product development
- Information-rich systems
- Vehicle Platforms
- Organisational and enterprise systems for service delivery
- Infrastructure system development

In Technology Product development, the V-model (or Vee model) depicts a typical life cycle [8]. According to the INCOSE handbook [8], "The Vee model is used to visualize the System Engineering focus, particularly during the Concept and Development Stages. The Vee highlights the need to define verification plans during requirements development, the need for continuous validation with the stakeholders, and the importance of continuous risk and opportunity assessment". This model is illustrated in Figure 1.

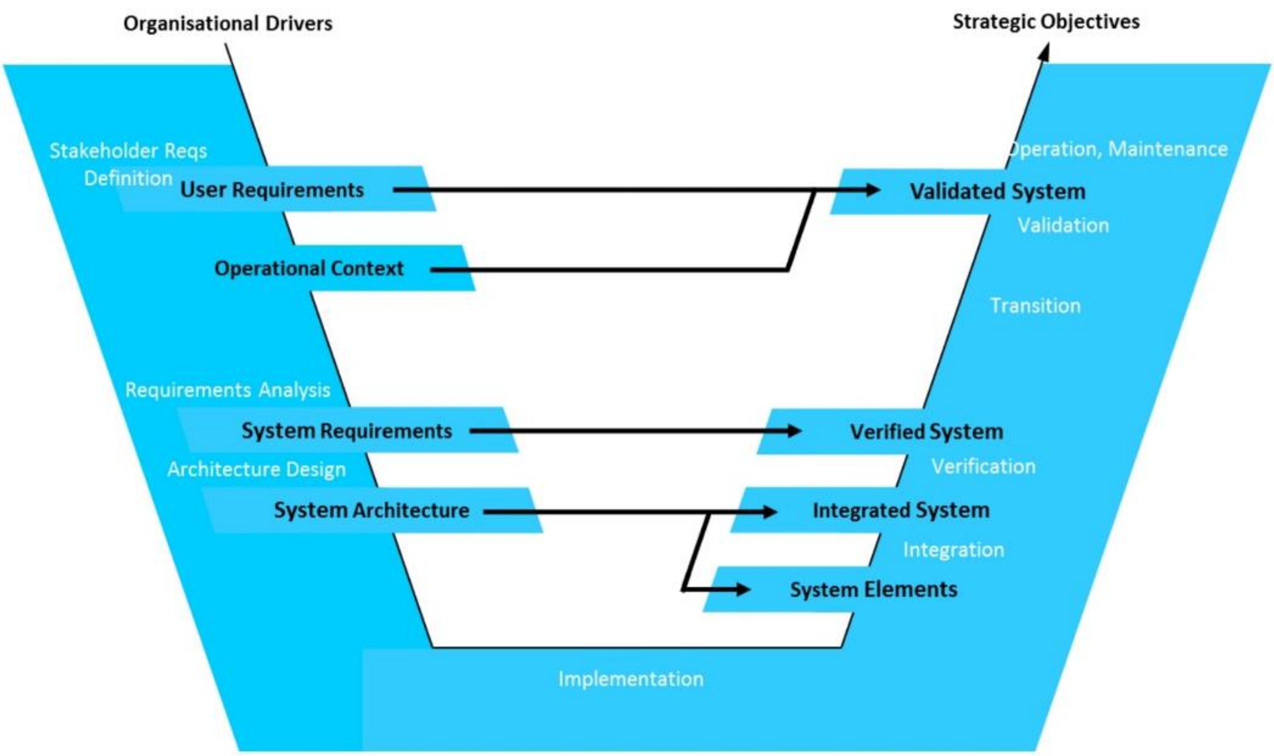

Figure 1: V-Model [9]

Figure 1 illustrates the major components of the SE approach. This includes the following [10]:

- Solicitation of user requirements
- The understanding of the operational context (required for the concept of use generation)
- The development of the system requirements during the Requirements Analysis (which includes a Function Analysis process)
- Architecture design where the system elements are conceptualised.
- System integration, and
- System verification and validation.

A SE approach emphasises the importance of the development of system requirements in the design of system products [8]. This approach was necessary due to the nature of this study and formed part of the methodology.

The requirements of the FGM needed to be determined to answer the research question. A SE approach gives a bird's eye view of the entire system's lifecycle. This ensures that the proper requirements and verifiable functions are elicited. The FGM is a subsystem within a missile's Actuation System (ASYS). The missile forms part of a larger weapon system which again sits within a larger system. There are relationships between these systems across various system boundaries. Applying the SE approach assisted in identifying the relationships that had an influence on the FGM. Hence this approach formed a central part of the method developed for this study.

For a structured approach, a suitable SE Process standard was investigated. The IEEE 1220- 2005 standard [11] describes a structured approach for product system development. It is known as the IEEE Standard for Application and Management of the Systems Engineering Process, and it describes the conversion of stakeholder needs, requirements, and system constraints through interdisciplinary processes over the system's life cycle in order to achieve the required solution [12]. It largely focuses on product-related systems such as aircraft and information systems. Figure 2 illustrates the IEEE 1220-2005 process.

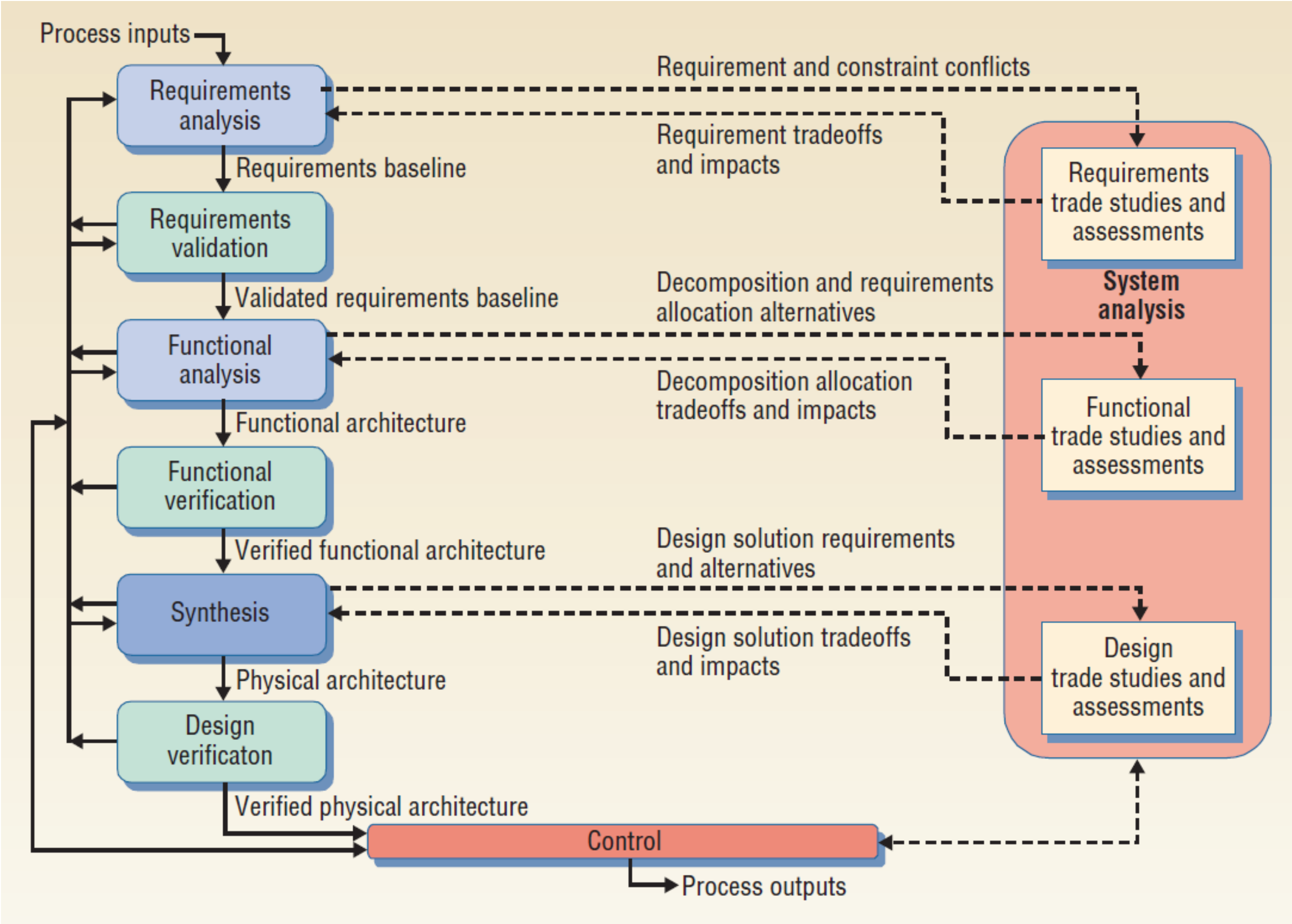

Figure 2: IEEE 1220-2005 System Engineering Processes [12]

The main stages of the IEEE 1220-2005 [11] [12] [13] process are:

1. Requirements Analysis
2. Requirements Validation
3. Functional Analysis
4. Functional Verification
5. Synthesis
6. Design Verification
7. System Analysis
8. Control

This process can be applied to the System of Interest (SOI), whether it be a single system consisting of basic system elements or a system of systems.

According to the INCOSE handbook [8], the SOI refers to the system whose lifecycle is being considered. The SOI interacts with enabling systems and various other systems within its operational context. This is illustrated in Figure 3.

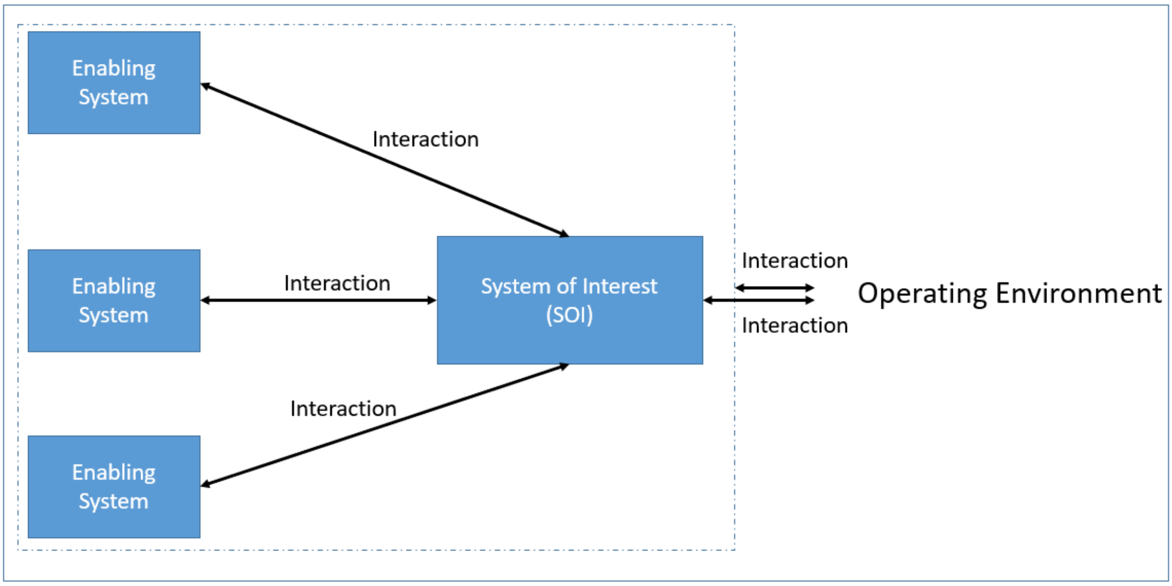

Figure 3: System of Interest within its operational context [8]

The SOI in this study was identified as the FGM based on the research question. As mentioned earlier in this chapter, the FGM is a subsystem within a missile's ASYS. According to the INCOSE handbook [8], it will interact with enabling systems such that both systems benefit from one another or receive inputs when required. Using the SE approach aided in understanding the relevant influences on the SOI and assisted in the Requirements Analysis.

As described by Doran [12], a Requirements Analysis defines the system's abilities and performance. The process outlines the operational context that includes the environment it will operate in, the interfaces involved (human and other system interfaces), the physical characteristics of the system, and other constraints that affect design solutions. The evaluation of stakeholder needs, requirements, and system constraints results in the identification of the requirements baseline for the system. The requirements should give a balanced view between the design, operation and function of the system. It was necessary to carry out a Requirements Analysis to gather the correct inputs and establish a more defined baseline of design inputs. During this process, the system requirements were specified as described in the IEEE 1220- 2005 [10]. The structure of this process is illustrated in Figure 4. To elicit a comprehensive list of requirements for the FGM, it was necessary to address all the aspects defined in the process in Figure 4. This assisted in understanding the interaction between the systems surrounding the FGM and its constraints. This process was helpful due to the complex nature of missile systems.

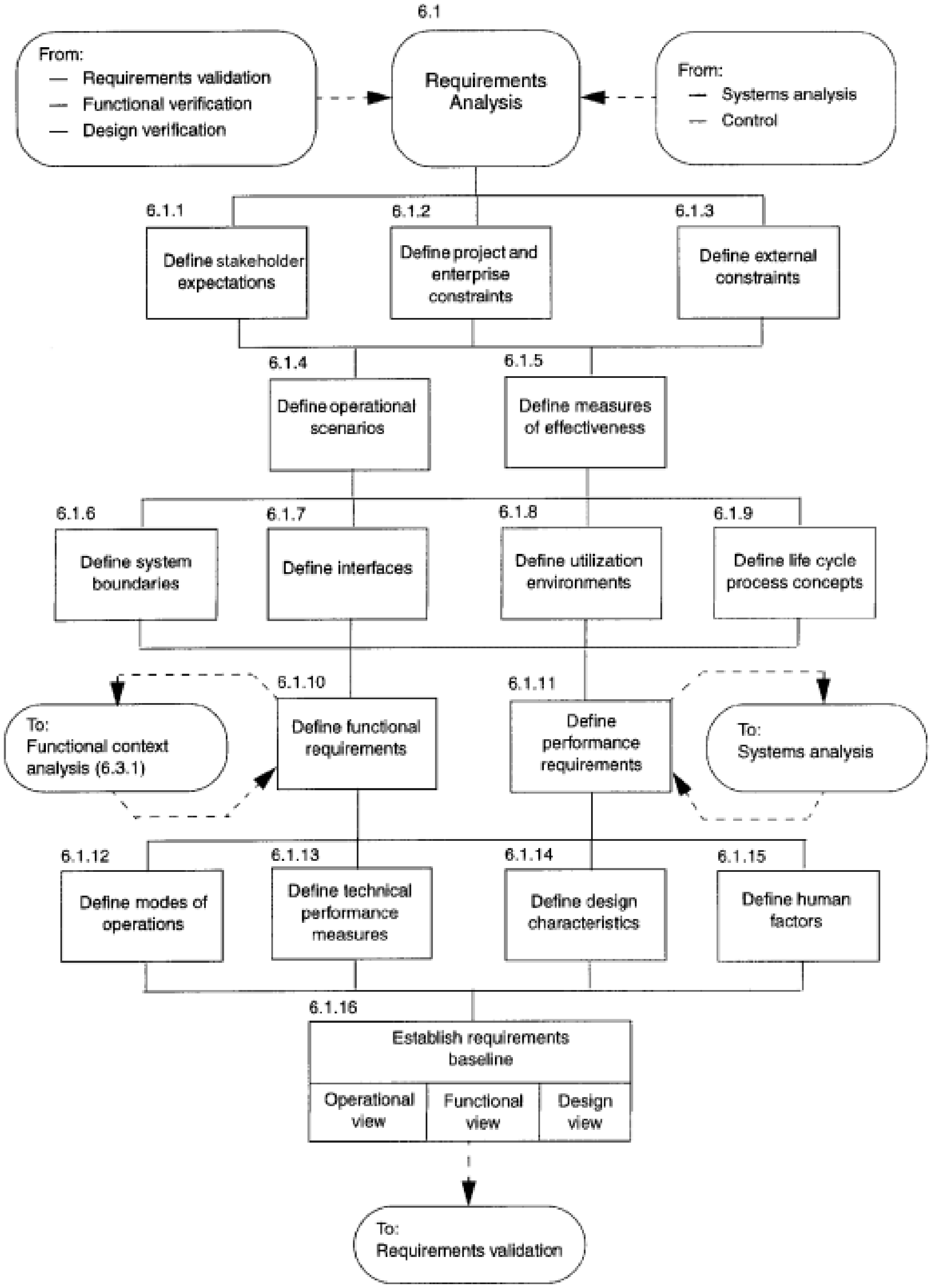

Figure 4: Requirements Analysis[11]

Following the establishment of the requirements baseline, they can be validated through the Requirements Validation stage. The Requirements Validation involves the requirements baseline being assessed to determine if the stakeholder needs, requirements, and system constraints have been accounted for. The Requirements Analysis stage is repeated if it is found that not all the needs have been satisfied. [12]. The validation process, according to Sparrius [13], involves:

- Examination of all requirements individually and as groups to see if they have been formulated correctly.
- Comparison with the stakeholder requirements and possibly reviewed by the stakeholders.
- Comparison with the constraints of the project
- Comparison with the external constraints, and
- Determining and fixing any requirement issues

This process was based on the Requirements Validation process illustrated in Figure 5. All the validation of requirements steps indicated in Figure 5 were relevant to this study as it is a check for the elicited requirements to ensure that the requirements addressed the needs of the FGM and to ensure robust requirements were used during the Functional Analysis phase.

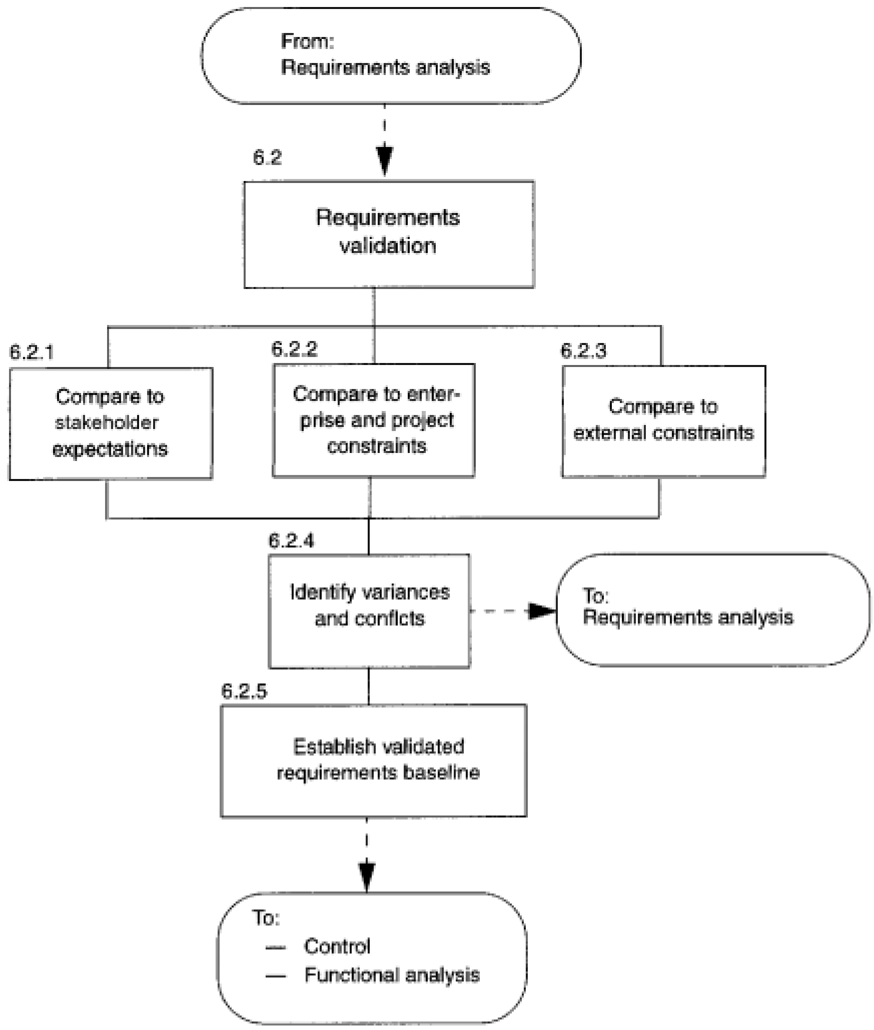

Figure 5: Requirements Validation [11]

As described in IEEE 1220- 2005 [11], during the Functional Analysis stage, the problem statement is moulded towards a system solution using the validated requirements baseline. The system functions are broken down into lower levels to fulfil system design components. The outcome of this stage is the system's Functional Architecture. The Functional Analysis process, from IEEE 1220- 2005 [11], is illustrated in Figure 6. This phase was needed in this study to assist in breaking down the functions for the FGM and to develop its Functional Architecture.

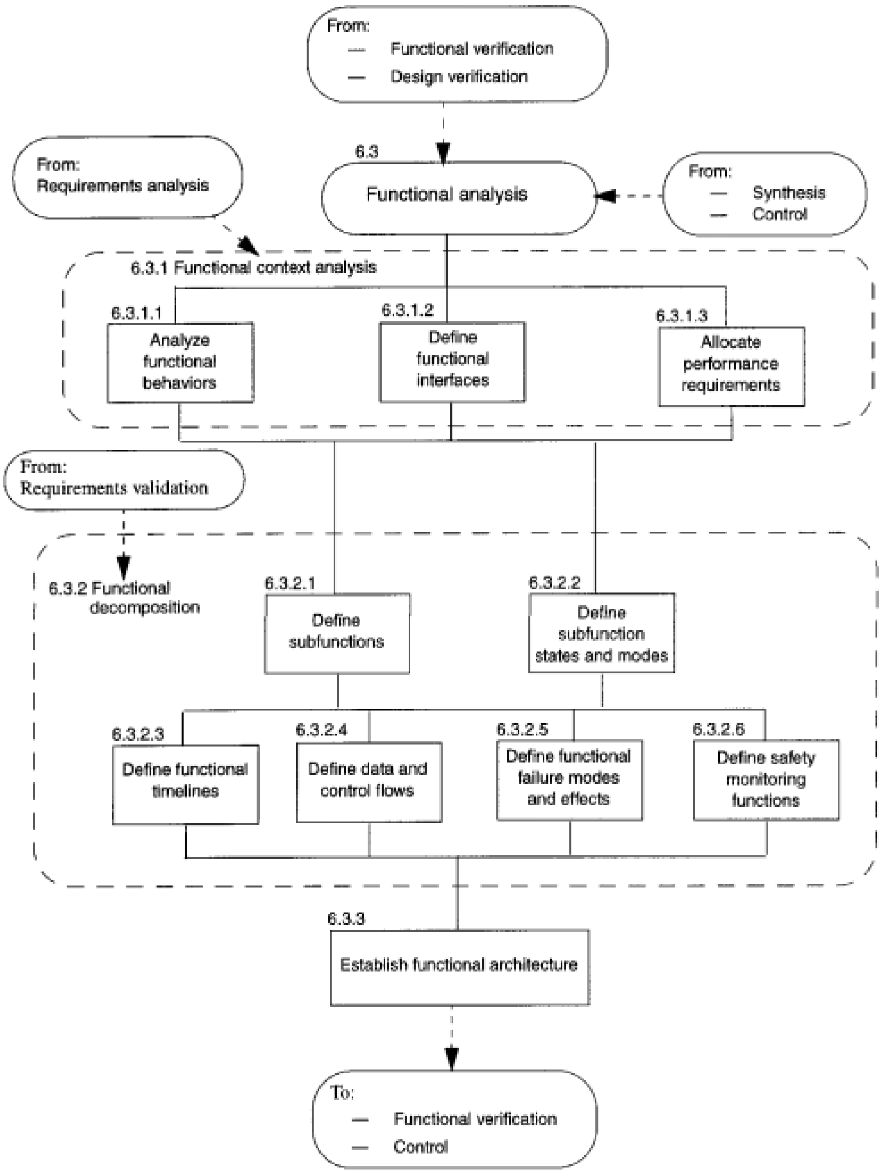

Figure 6: Functional Analysis [11]

According to IEEE 1220- 2005 [11], the Functional Architecture is evaluated, during the functional verification stage, for completeness by checking if it addresses the requirements defined. The functional verification process is highlighted in Figure 7. For a detailed functional verification, all the steps in the process should be followed. For this study, it was relevant to check the downwards and upwards traceability of the requirements and derived functions. This allowed for the establishment of a verified Functional Architecture that could be used during the Physical Architecture development.

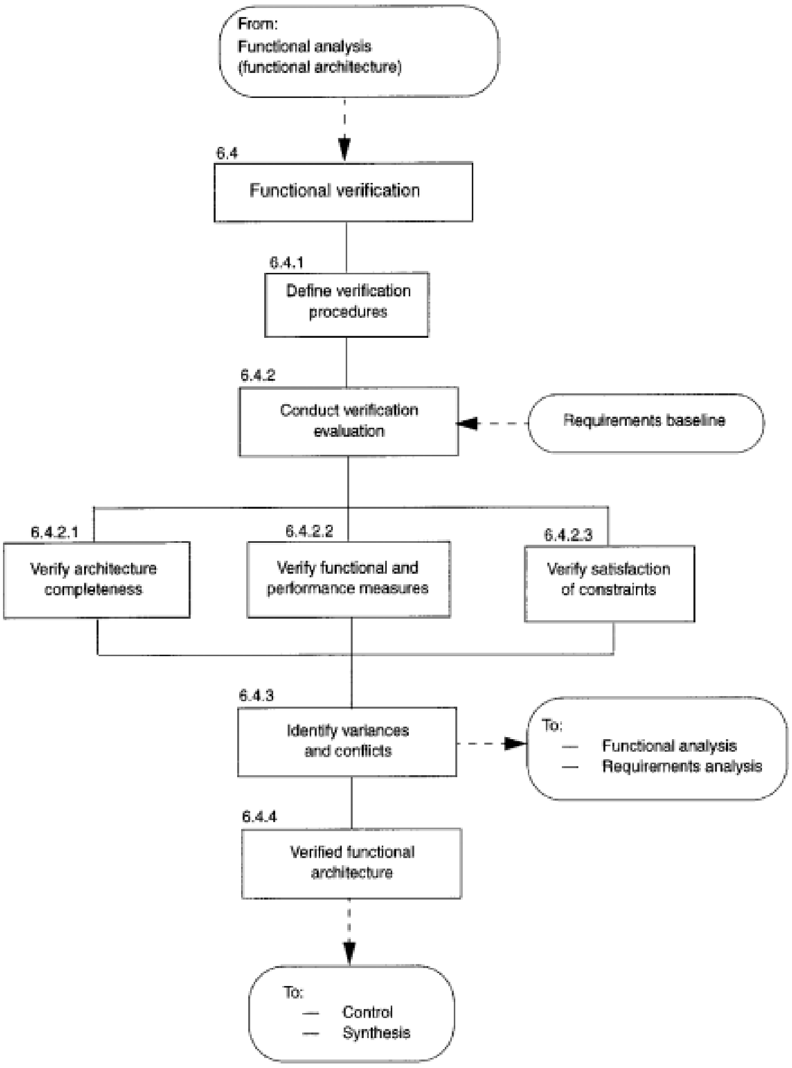

Figure 7: Functional Verification [11]

The design architecture is developed in the Synthesis stage according to IEEE 1220- 2005 [11]. As mentioned by Doran [12], the preferred solution is derived from a generated group of solutions, which are based on factors that include cost, project schedule, system performance, and other risks.

During the Physical Architecture design or the process of Synthesis, the Systems Engineering Body of Knowledge [10] mentions that the functional building blocks are transformed into physical blocks that details the organisation layout of crucial components, internal and external interfaces and relevant design constraints. A preferred solution is selected from a set of concepts.

The process is relevant to developing the Physical Architecture, which is the representation of the physical elements that make up the structure of the system. The physical elements are derived from the functions the systems are required to perform. Through this process, the components that could be replaced with Smart Materials can be identified. For this study, all the steps in the process were relevant to establish the concepts that would utilise Smart Material technology. This process is illustrated in Figure 8.

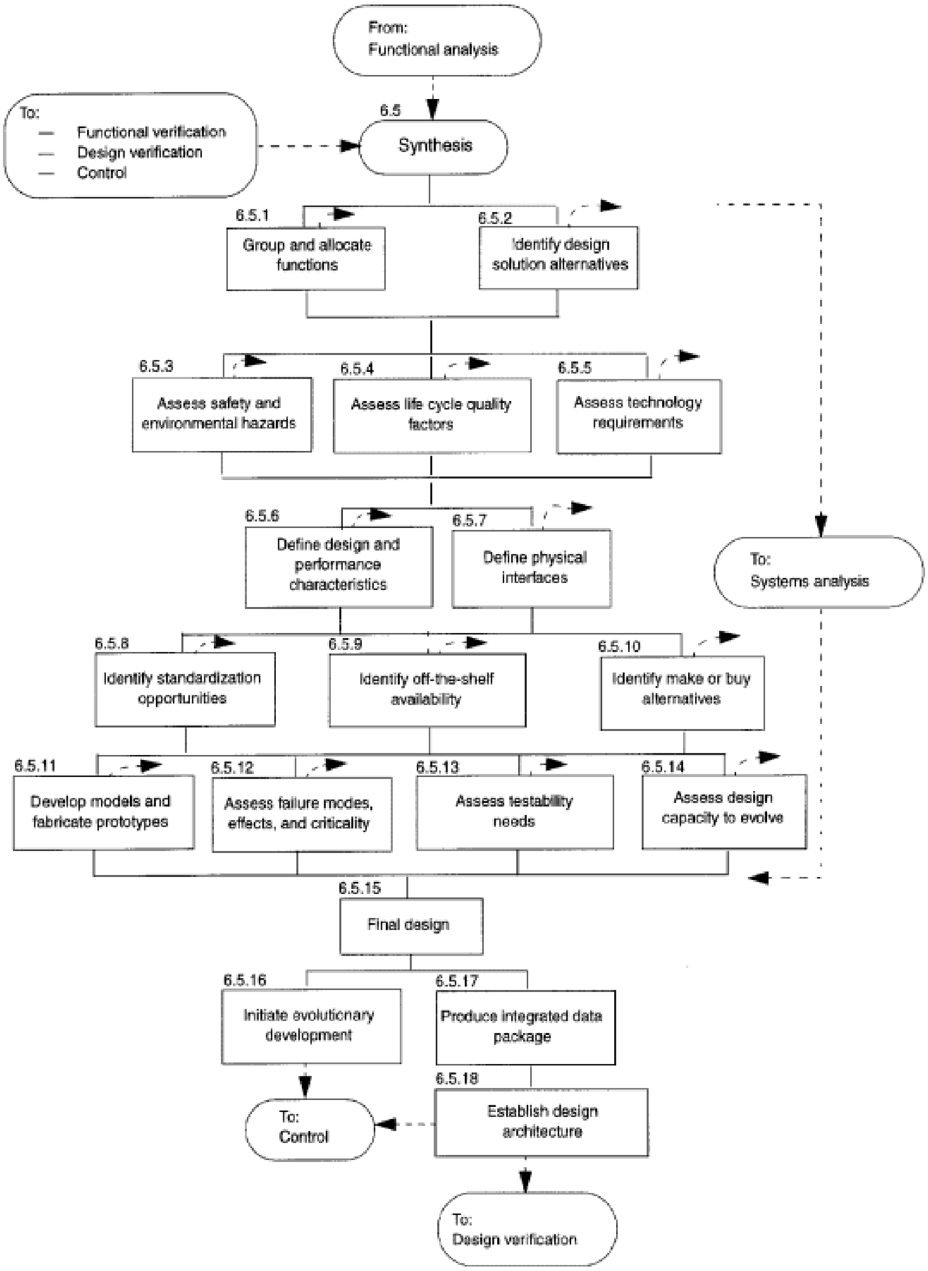

Figure 8: Synthesis Process [11]

Traceability between the lower-level components of the design and the Functional Architecture were confirmed through the Design Verification stage. This was applicable to this study so that the design architecture could be assessed to see if it meets the elicited requirements. The result was considered a verified physical system architecture as mentioned in IEEE 1220- 2005 [11]. The Design Verification process is depicted in Figure 9.

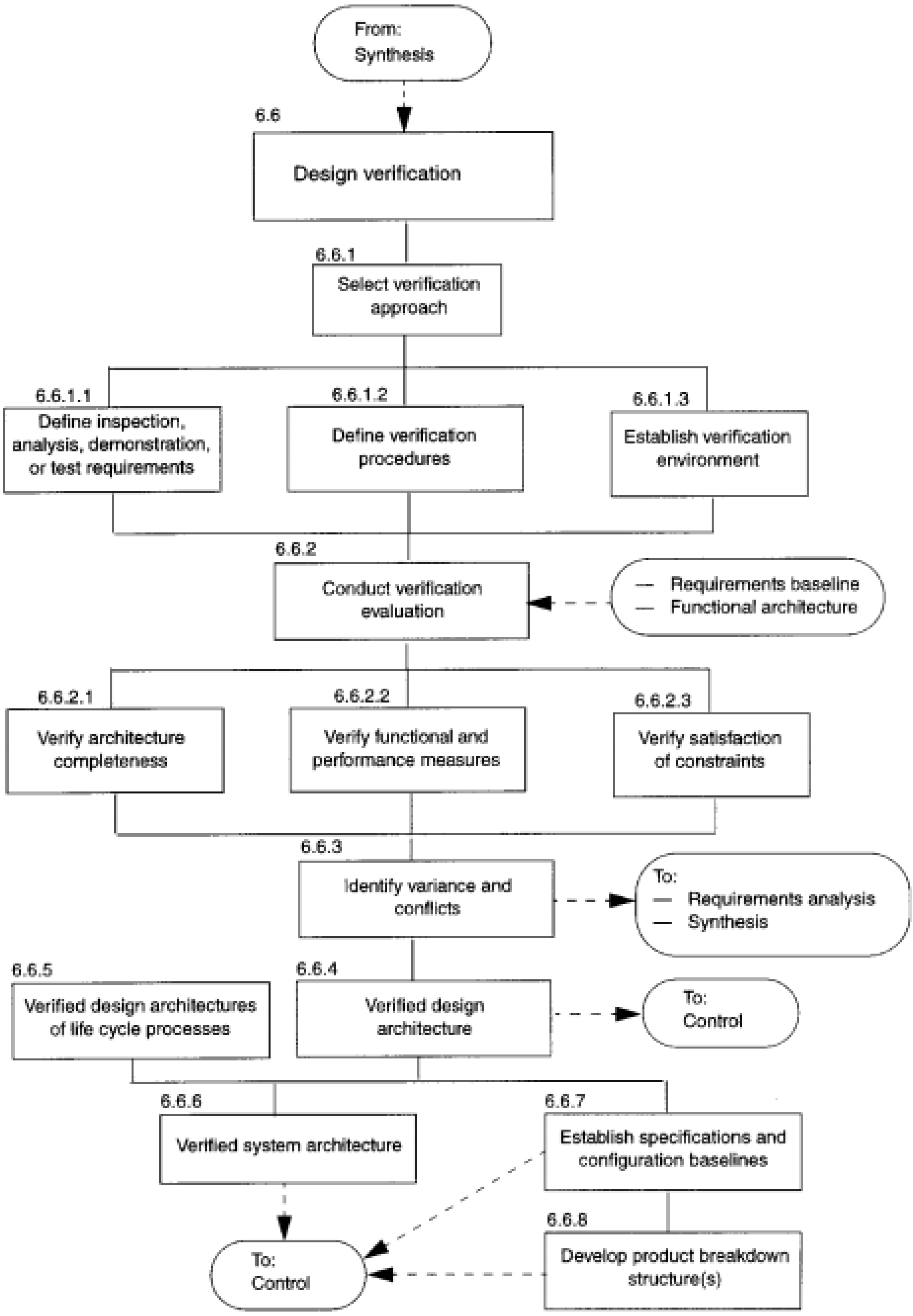

Figure 9: Design Verification [11]

During Systems analysis, Doran [12] mentions that the system is evaluated to determine and resolve requirement conflicts, establish the designed system effectiveness, manage risks related to the system, assist in the breakdown of functions, assess performance, and evaluate design alternatives. The process is shown in Figure 10. This process was relevant to this study as it aided in determining which concepts performed the best and where design could be improved.

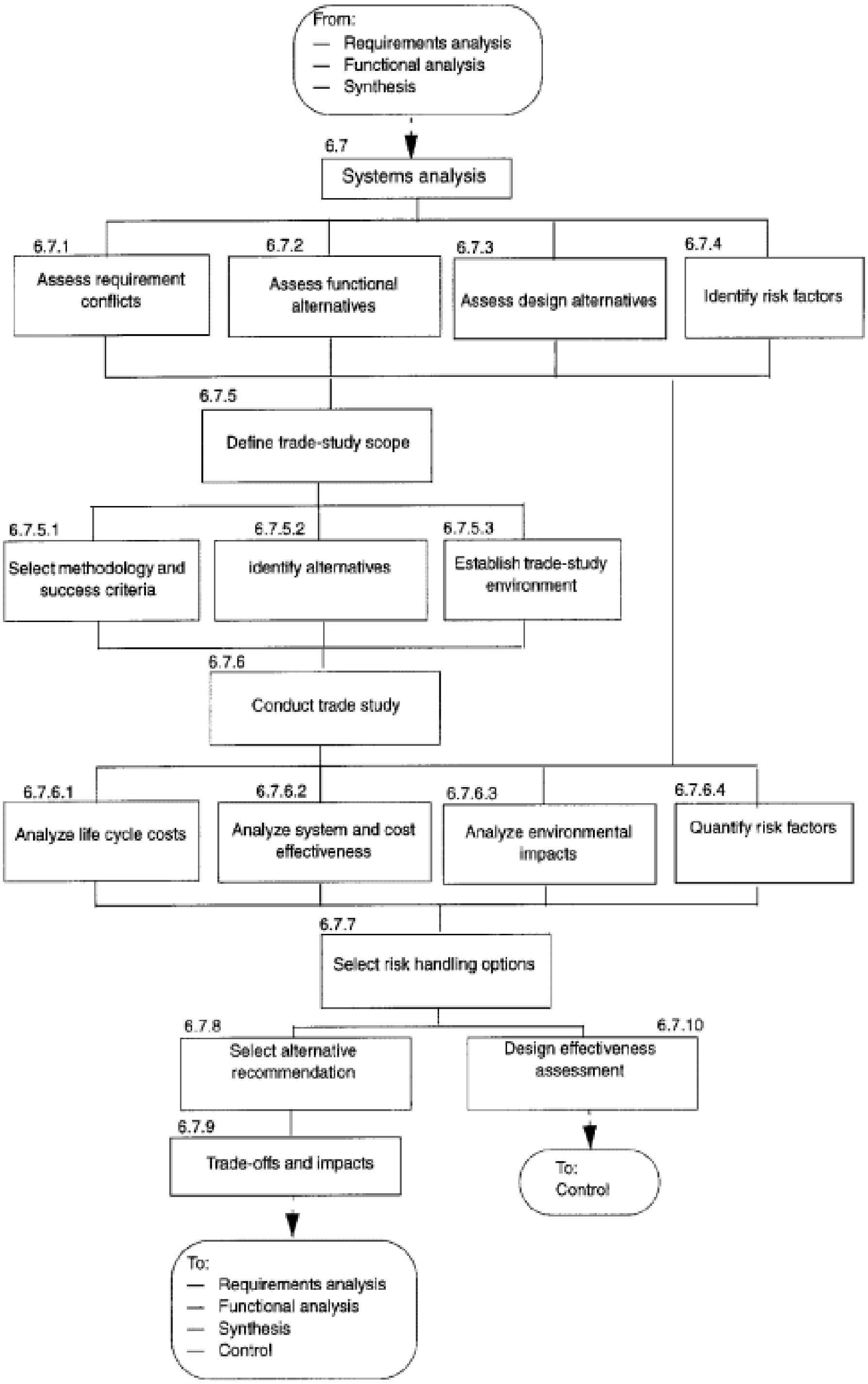

Figure 10: System Analysis [11]

Control tasks are performed to provide a framework for the documentation of the relevant activities in the SE plan and the related results [12]. The control process detail is depicted in Figure 11. This entire process was not included as part of this study. Only the outcome of the previous SE processes is documented in this paper.

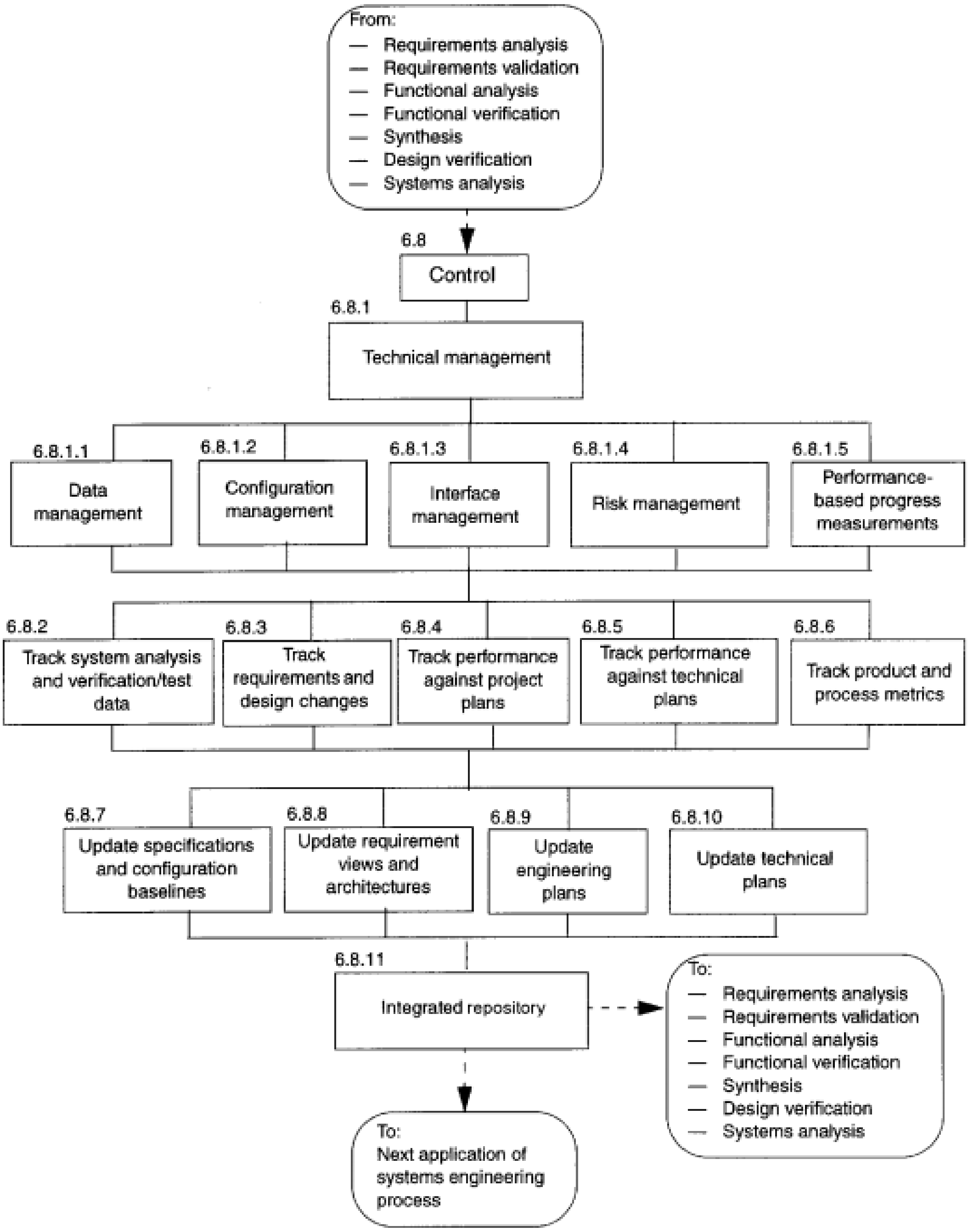

Figure 11: Control Process [11]

The adaptation of the IEEE 1220- 2005 by Sparrius [13] is utilised in this study's approach to SE. This is based on its use within the Aerospace and Defence industry. The multidisciplinary nature of the aerospace system in this study required the inherent multidisciplinary approach offered by SE to aid in the establishment of the requirement baseline through the Requirements Analysis and Validation processes. This baseline was used in the creation of the Functional Architecture through the Functional Analysis and Functional Verification processes. After this, the synthesis process allowed for the development of the Physical Architecture. The overview of the entire product lifecycle, using SE processes, allowed for a comprehensive list of requirements for the conceptual design of the FGM to be created.

With the SE process described, the topics required to answer the research question were addressed in the sections to follow.

2.2 Adaptive Structures and Smart Materials

An Adaptive Structure for an aircraft (or a missile) refers to a structure that can be morphed to influence the overall aerodynamic performance or characteristics. These elements include, but are not limited to, nose cone profile, the surface texture of fins, deflection of a fin or deflection of a wing. Adaptive Structures behave as a system, with the external stimuli (for example, electric current or forces) as the inputs and a change in structural geometry as the output. There are other types of Adaptive Structures, which change other structural characteristics. However, for this study, the focus is on structures that change in geometry. An Adaptive Structure can include specific materials, like Smart Materials that change their own structure or structures with built-in mechanisms that allow for the modification of the exterior structure's geometry.

This section is broken into two main subsections:

1. Adaptive Structure mechanisms used to morph Aircraft Structures, and
2. Smart Materials

In this study, various Adaptive Structures were reviewed to determine their usefulness for aerospace applications. The first subsection looks at the different ways Adaptive Structure mechanisms alter aircraft structures to affect the air flow over the aerodynamic surfaces. The methods to alter the aircraft structures focused on existing mechanisms and past studies to evaluate their feasibility for this study. The Smart Material subsection summarizes some of the Smart Materials used in the aerospace industry and again addresses the feasibility of such materials for use in this study's investigation.

2.2.1 Adaptive Structure mechanisms used to morph Aircraft Structures

Adaptive Structure technology has been extensively used in the aerospace industry. Wing Morphing has been used in Unmanned Aerial Vehicles (UAVs), created by companies like NextGen Aeronautics and Lockheed [4]. The NextGen Aeronautics UAV, the MFX-1, uses an adjusting internal scissor structure that aids in transforming the wing area by 40%, the sweep between 15°-35° and the span by 40% according to FlightGlobal [14]. This is a typical example of an Adaptive Structure. The MFX-1 can be seen in Figure 12.

Figure 12: NextGen MFX-1 (a) Extended Wings and (b) Swept Wings [14]

Changing the wings' shape had benefits for a different type of missions. Tests for this system were carried out at subsonic velocities [14].

An investigation into morphing winglets was carried out by Ursache *et al*. [15] to understand how they would improve a narrow body's flight performance. The morphing winglet or MORPHLet system was made up of four sections beginning at the outboard section of the wing. This can be seen in Figure 13. The structure was manipulated at each section to maximize the aircraft's performance during varying stages of the aircraft's mission profile through a multidisciplinary design optimisation study as described in Smith *et al*. [16]. A prototype of this winglet concept was created and tested for bending and torsion. The prototype can be seen in Figure 14. It was constructed using a corrugated skin to allow for the required deflections of the winglet.

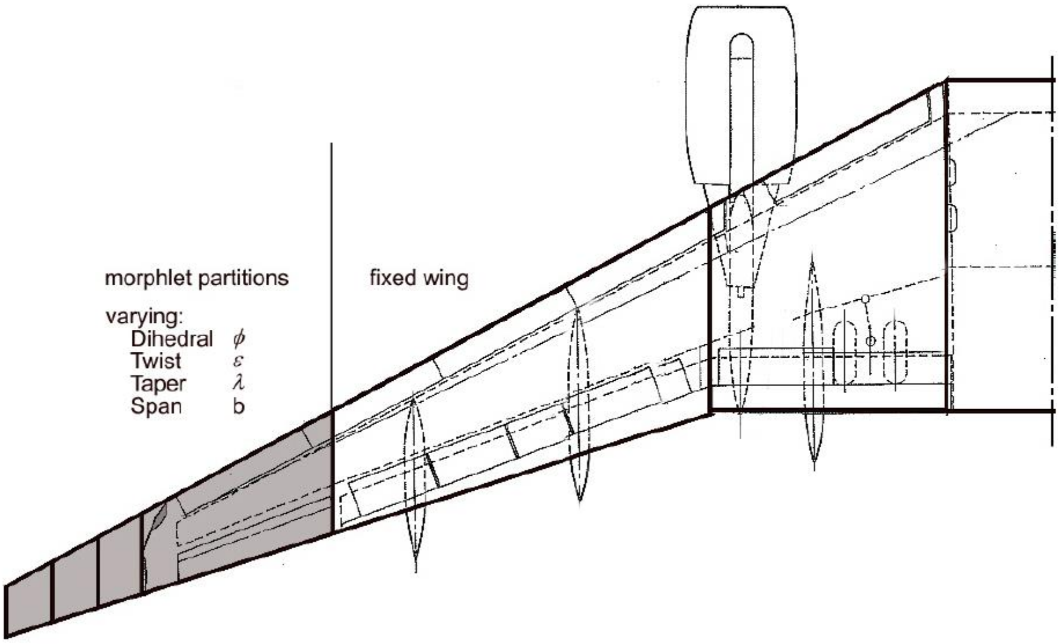

Figure 13: Baseline wing with MORPHLet Section [16]

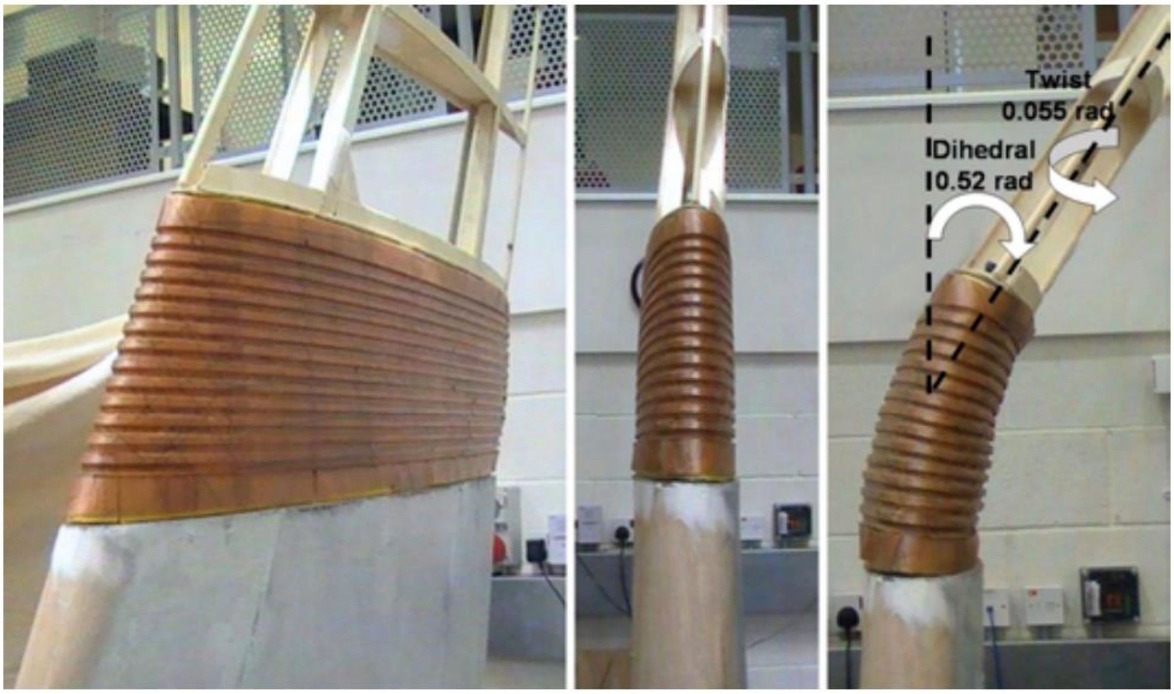

Figure 14: MORPHLet Demonstrator [17]

According to the optimization study by Smith [16], the morphing winglet showed improvement in the specific air range over the aircraft of 6%. The winglet was also able to sustain a specific air range improvement of 4.5% to 5.5% for the studies' defined flight stages. The generic winglet's specific air range was shown to drop to 3.5%. The results of the investigation indicated significant enhancements to:

- lift-to-drag ratios during the climb,
- take-off
- landing stages of the aircraft.

The previously mentioned mechanisms require a constant force to maintain the new morphed shape. This means an actuator would need to be constantly applying a load. With Bistable (or Multi-stable) structures, the structures are able to transition between two or more stable positions, as mentioned in Bilgen *et al*. [18] and Mattioni *et al*. [19].

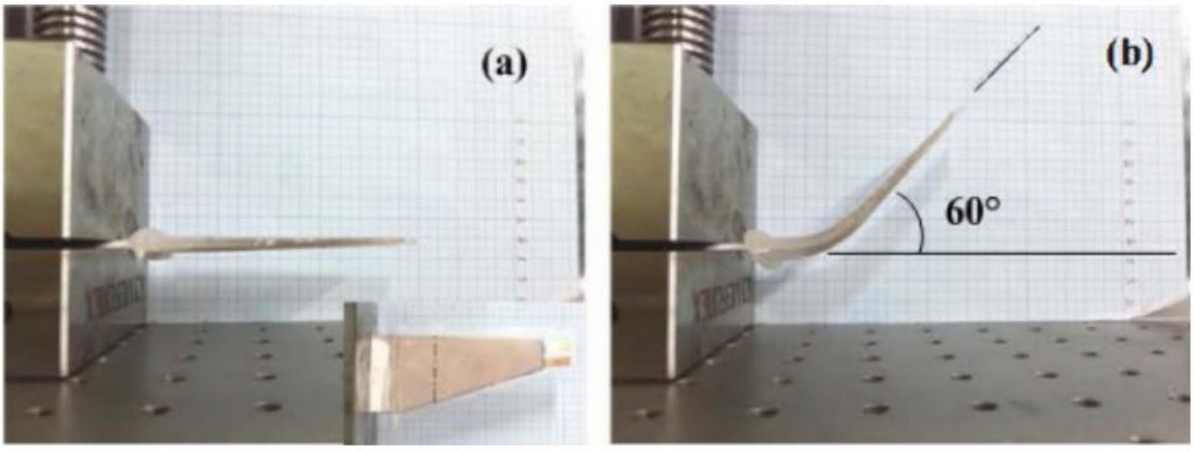

Figure 15: Bistable Winglet [20]

Bistable structure use in winglets (as seen in Figure 15 from a study by Kim *et al.* [20]) to alter the lift generation capabilities of a wing was investigated by Gatto *et al*. [21]. The bistable structure is made from an unsymmetric composite layup. It can shift to two static states depending on the load applied. For a range of subsonic flow speeds, the structure improved the lift characteristics of the wing. The study indicated some drawbacks related to the creation and transmission of dynamic loads. Therefore, the system would require a damper system to manage these loads.

These Adaptive Structure mechanisms showcased that their morphing ability improved the aerodynamics of the system. These mechanisms were only evaluated at subsonic speeds; therefore, for this study, their use in the supersonic regime may be limited. There were, however, lessons learned from these mechanisms, such as structural flexibility of some structures, support structures that can withstand the applied loads and actuators that can apply sufficient load to alter the structure and resistance to aerodynamic loads.

Table 1 and Figure 16 indicates some of the adaptive aerostructure developments between the late 1980s and the early 2000s. These include developments in Adaptive Structures for missile technology and where some were within the supersonic regime.

Table 1: Summary of Adaptive Structure Projects corresponding to Flightworthy UAVs [22]

Project *p=piezoelectric, s=shape memory alloy c=component testing only f=flight tested v = entire vehicle configuration tested with adaptive device*		**Modeling Techniques**		**Test Techniques**			**Agency/ Sponsor**
		closed	FEM	Bench	Stand/ Tunnel	Flight	
1 Bending-Twist Coupled Aeroelastic PZT Plate (1985-87)	*c,p*	•		•	•		*MIT*
2 Adaptive Flap (1987-89)	*c,p*	•		•	•		*MIT*
3 Twist-Active Subsonic DAP Missile Wing (1989-90)	*c,p*			•			*ARO*
4 Twist-Active DAP Rotor (1990-91)	*c,p*	•		•			*ARO*
5 Aeroservoelastic Twist-Active Wing (1990-92)	*c,p*	•					*Purdue*
6 Twist-Active Supersonic DAP Wing (1991-92)	*c,p*			•			*KU*
7 Constrained Spar Torque-Plate Missile Fin (1991-92)	*c,p*	•		•	•		*KU*
8 Free-Spar DAP Torque-Plate Fin (1992-93)	*c,p*	•		•			*KU*
9 Pitch-Active DAP Torque-Plate Rotor (1992-93)	*c,p*	•		•			*KU*
10 Subsonic Twist-Active DAP Wing (1993-94)	*c,p*		•	•			*WL/MNAV*
11 Subsonic Twist-Active SMA Wing (1993-94)	*c,s*		•				*WL/MNAV*
12 Subsonic Camber-Active DAP Wing (1993-94)	*c,p*		•				*WL/MNAV*
13 Subsonic Camber-Active SMA Wing (1993-94)	*c,s*		•				*WL/MNAV*
14 Supersonic Twist-Active DAP Wing (1993-94)	*c,p*		•	•			*WL/MNAV*
15 Supersonic Twist-Active SMA Wing (1993-94)	*c,s*		•				*WL/MNAV*
16 Supersonic Camber-Active DAP Wing (1993-94)	*c,p*		•				*WL/MNAV*
17 Supersonic Camber-Active SMA Wing (1993-94)	*c,s*		•				*WL/MNAV*
***18* UAV with Flexspar Stabilator (*Mothra* 1993-94)**	***v,f,p***	•		•	•	•	*AAL*
19 Flexspar TOW-2B Wing (1993-94)	*v,p*	•		•	•		*NSF*
20 Solid State Adaptive Rotor (SSAR) (1994-95)	*c,p*	•		•	•		*NSF*
21 Aeroservoelastic Flexspar Fin (1994-95)	*c,p*	•		•	•		*AAL*
***22* UAV with Solid State Adaptive Servopaddle Rotor (95-96)**	***v,f,p***	•		•	•	•	*NSF*
***23* MAV with Flexspar Stabilator (1994-97)**	***v,f,p***	•		•	•	•	*DoD CDTO*
24 Barrel-Launched Adaptive Munition (1995-97)	*v,p*	•		•	•		*AFOSR*
25 Smart Compressed Reversed Adaptive Munition (1995-97)	*v,p*	•		•	•		*WL/MNAV*
26 Monolithic Rotationally Active Linear Actuator (RALA1995-97)	*c,p*	•		•	•		*WL/MNAV/Boeing*
27 Pitch-Active Torque-Plate Wing (1997-98)	*c,p*	•		•	•		*AAL*
28 Range-Extended Adaptive Munition (1998-99)	*v,p*	•		•	•		*DARPA*
29 Hypersonic Interceptor Test Technology (1998-2000)	*v,p*	•		•	•		*SMDC/Schafer*
***30* Coleopter MAV with Flexspar Stabilators (1998-2001)**	***v,f,p***	•		•	•	•	*DARPA*
***31* UAVs with Pitch-Active SMA Wings (2000-01)**	***v,f,s***	•		•		•	*AAL*
32 Light Fighter Lethality MicroFlex Actuator (2000-01)	*v,p*	•		•	•		*TACOM/ARDEC*
33 Pitch-Active Curvilinear Fin Actuator (2001-02)	*c,s*	•		•	•		*AMCOM*
34 SC Range-Ex Adaptive Munition (SCREAM) (2000-03)	*v,p*	•		•	•		*TACOM ARDEC*
35 Thunder Multilaminate RALA Fin (2000-03)	*c,p*	•		•			*AFRL/MNAV*
36 Centerline Precompression RALA Fin (2000-03)	*c,p*	•		•			*AFRL/MNAV*
37 Center Pivot Flexspar Fin (2002-03)	*c,p*	•					*ARL*
***38* PBP StAB (2003-)**	***v,f,p***	•	•	•	•	•	*TU Delft/TNO*
***39* Convertible UAV with PBP Grid Fin (2003-)**	***v,f,p***	•	•	•	•	•	*TU Delft*
***40* Convertible UAV with PBP Turning Vane Flaps(2003-)**	***v,f,p***	•	•	•	•	•	*TU Delft*
***41* Extended-Range Gravity Weapons w/Active Wings (2003-)**	***v,f,p***	•	•	•	•	•	*AFRL/MN/Boeing*

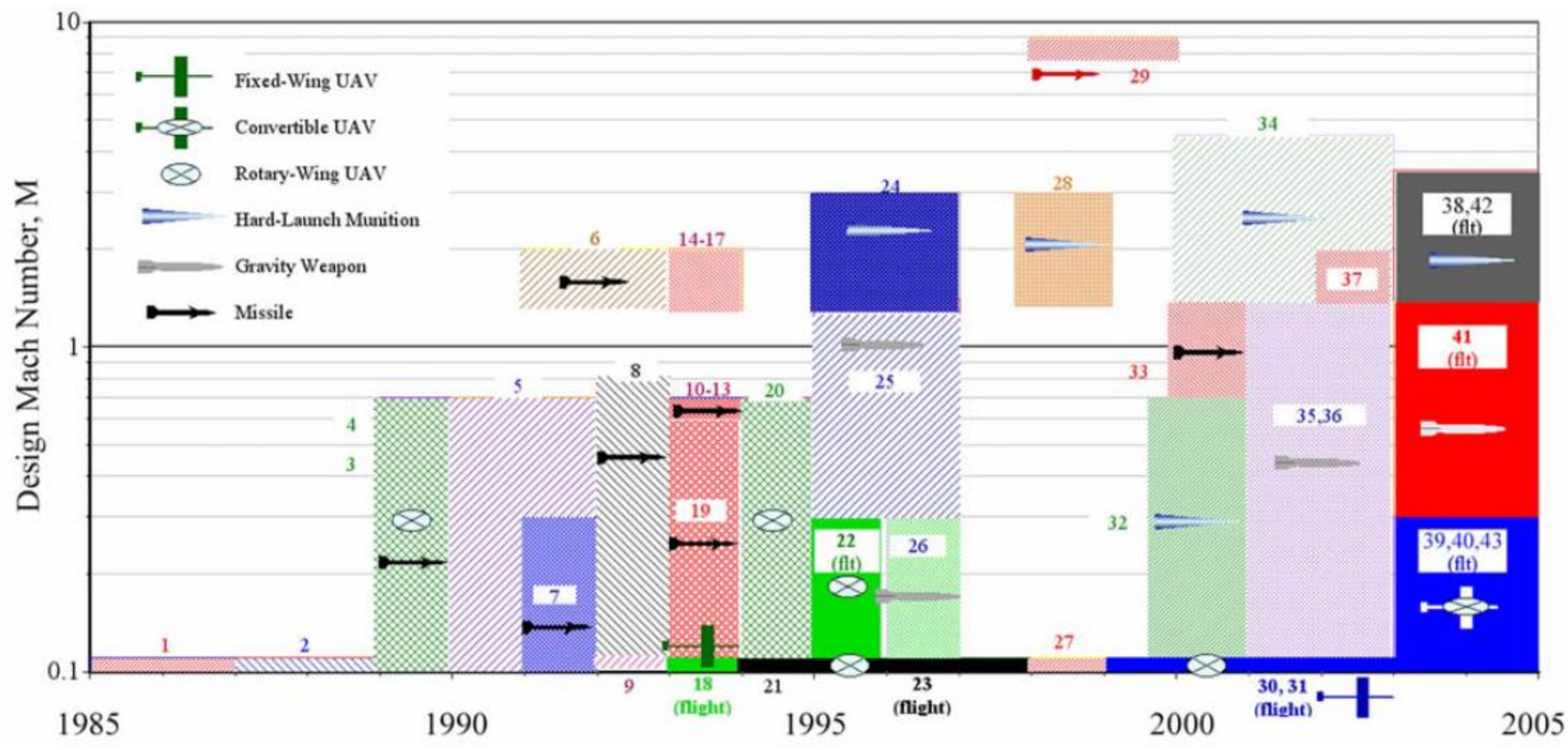

Figure 16: Overview of Adaptive Structure Projects corresponding to UAVs, Munitions, Gravity Weapons and Missiles [152]

The Adaptive Structures shown in Table 1 make use of Smart Materials to actuate the structures, which causes the change in geometry. For example, studies by Barrett [23] and Barrett [24] used Directionally Attached Piezoelectric (DAP) elements to twist an active structure for a subsonic and a supersonic missile fin.

As mentioned by Barret [23], a constrained Spar Torque-Plate Missile Fin was able to achieve ±4.5° static deflections. This was done without aeroelastic divergence issues and without the need for aeroelastic amplification. Figure 17 shows this fin during its operation. The fin performed well at low Mach numbers ($M < 1$), and as the Mach number increased, there was an improvement in the main spar's strength and torsional stiffness. There was a decrease in the deflection of the fin as the Mach number increased due to the mechanical joint between the plate and the spar. Decoupling the two resulted in higher static deflections in pitch of about 7 degrees at Mach 0.7, as mentioned in Barrett [25] originally from Barrett [26].

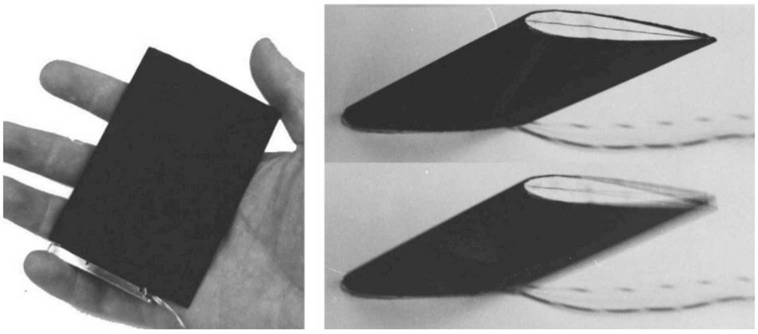

Figure 17: DAP fin

These studies indicated that suitable fin deflections for flight control could not be achieved. However, large rotational control surface deflections were shown to be necessary to generate the force and moments for subsonic and supersonic missiles. In Figure 18, the supersonic missile fin is experiencing deformation in its camber next to a subsonic missile fin being actively twisted.

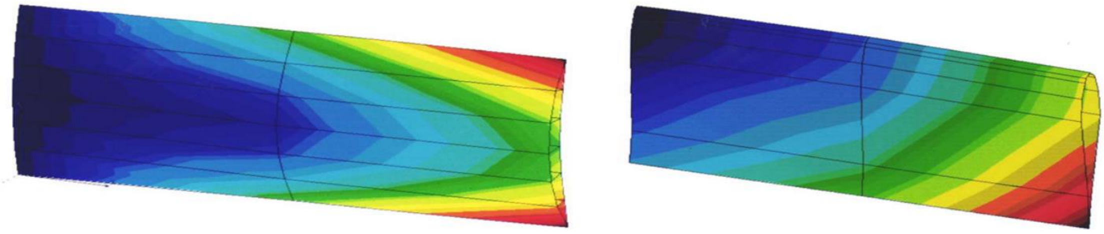

Figure 18: Finite Element models of the supersonic (left) and subsonic (right) fin

Flexspar technology, as mentioned by Barrett [22] (originally from Lee [27] and Lee [28]), was used for a Mach 3 projectile in 1998. Empirical studies such as bench tests and wind tunnel tests showed positive results for the mid-supersonic flow regime. Other investigative studies for BLAM and REAM programs described by Barrett [22] (originally from Lee [27] and Lee [28]) included flow speeds up to Mach 4.5. The Hypersonic Interceptor Technology Testbed program, described by Barrett [22] (originally from Lee [27] and Lee [28]), was designed for flight at Mach 8 and 9. In this program, carbon-carbon fins with piezoelectric devices were able to deflect in a Mach 9 flow within 4.5 ms. This meant that these actuators were able to overcome the high loads experienced at high Mach numbers and were able to perform comparably fast as an actuator for a missile fin. The hypersonic inceptor used for this test can be seen in Figure 19. This was taken from Barrett [22].

Figure 19: Hypersonic Interceptor [22]

The Flexspar actuators were later used in other projects, including the Light Fighter Lethality and Shipborne Countermeasure Range-Extended Adaptive Munition (SCREAM) projects as mentioned by Barrett [22] originally from Lee [29]. The Flexspar actuator was used in the construction of an aero elastically unbalanced fin configuration. This fin had a centreline spar pivot. Further details regarding the design and performance of the Adaptive Structures for the Flexspar design were not available as the source material is proprietary.

In a feasibility study carried out by Giurgiutiu and Pomirleanu [30], the objective was to see if Smart Materials could actuate a missile control surface from an energy or power requirement perspective. Smart Material actuators were used as part of the Adaptive Structure design. Two concepts were evaluated:

- A linear piezoelectric PZT actuator
- Smart Material motor.

The study highlighted the displacement limitation and introduced the Displacement Amplification mechanism. In the study, the parameters of such a device were developed. The outcome of the study indicated that the use of Smart Materials could be possible if an optimal design is achieved that allows a system, including the Displacement Amplification mechanism, to have a low gain and a high energy transfer.

Shape Memory Alloys have also been incorporated in a variety of systems to create Adaptive Structures, for example, air intake control (SAMPSON smart inlet), noise suppression, and flutter suppression [31]. These materials were used as actuator replacements in the aerospace application and thus advances the argument for the application of Smart Materials or, Adaptive Structures using Smart Materials to produce similar outcomes for a missile control system.

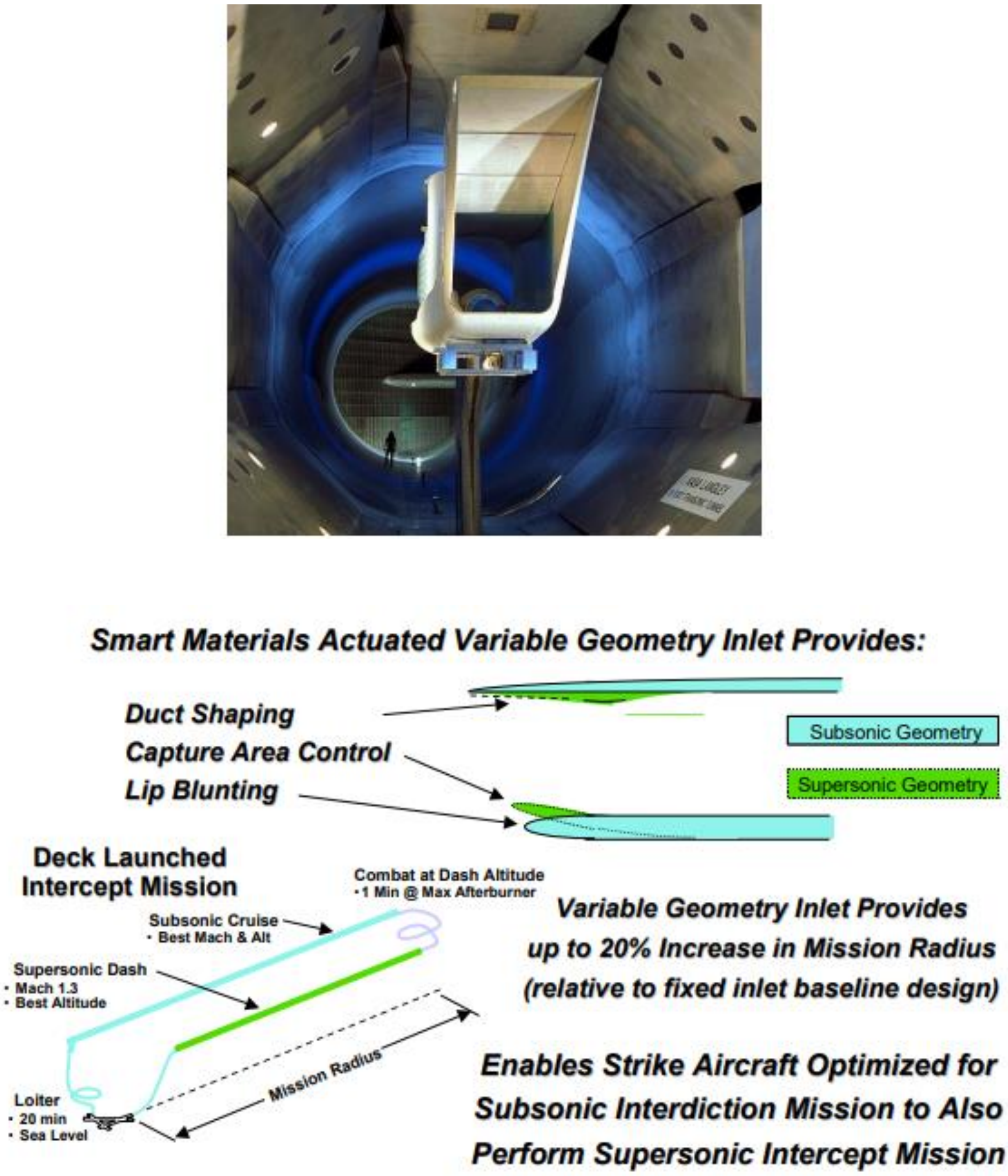

Figure 20: SAMPSON Smart inlet [32]

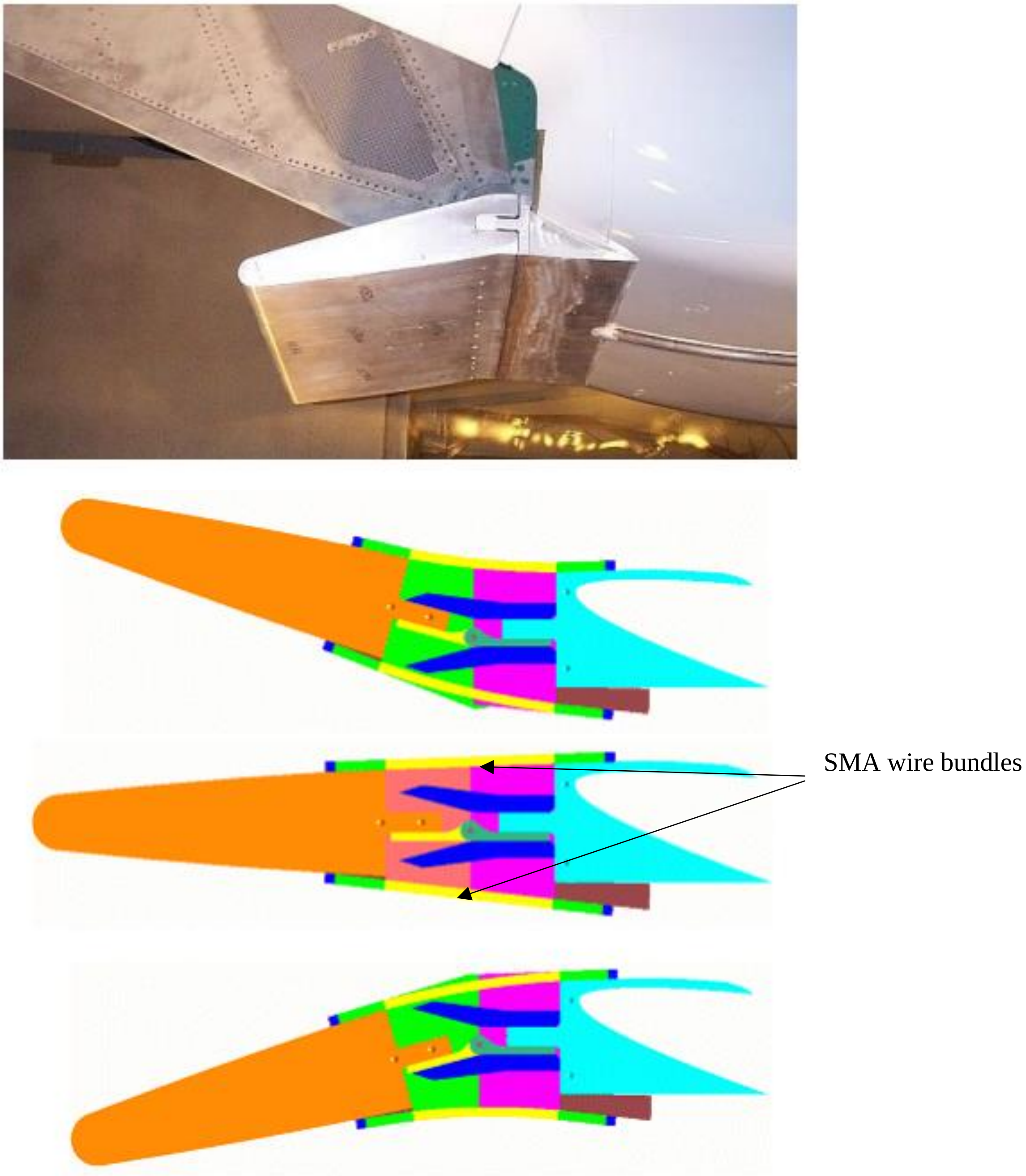

Figure 21: Rigid Lip Extension on the SAMPSON Smart Inlet [32]

For the SAMPSON inlet design, as seen in Figure 20 and Figure 21, a cable made from SMA wires carried out the cowl rotation as described by Pitt *et al*. [32]. The shaping of the duct provided an increase in the mission radius [32].

Many of the Adaptive Structures, as seen in this subsection, make use of Smart Materials to meet multidisciplinary Performance Requirements. In the aerospace industry, piezoelectric materials and Shape Memory Alloys have been firm favourites in past studies and applications.

2.2.2 Smart Materials

In this subsection, the Smart Materials, piezoelectric materials and Shape Memory Alloys (SMAs) used as actuators for the Adaptive Structures mentioned in Section 2.2.1 are showcased.

According to PI Ceramic [33], piezoelectric material uses the piezoelectric effect to generate charge from applied pressure to the material's surface. This effect is used for charge generation and for sensors. Piezoelectric actuators make use of the inverse of this effect. When an electric voltage is applied to the material, it changes in length. Piezoelectric materials include monocrystalline materials and polycrystalline ferroelectric ceramics.

Piezoelectric materials have been used to create a variety of Adaptive Structures, which include, amongst others, low-net passive stiffness structures [2], Post-Buckled Precompressed structures seen in Figure 22 [3], and Directionally Attached Piezoelectric (DAP) actuation system in Figure 23 [2].

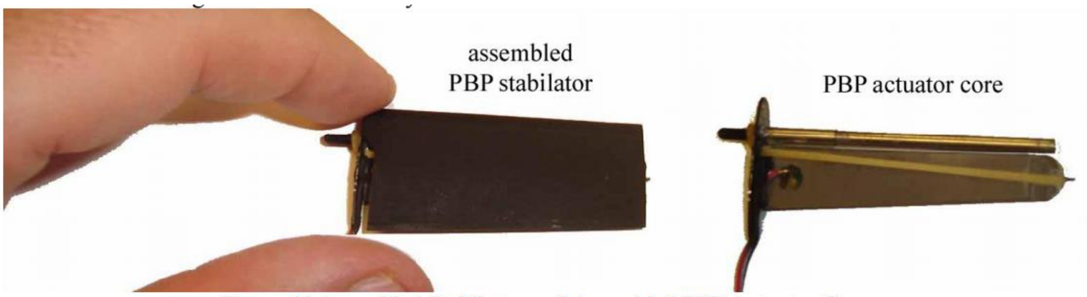

Figure 10 Assembled Stabilator and Assembled PBP Actuator Core

Figure 22: Post-Buckled Precompressed Structures [3]

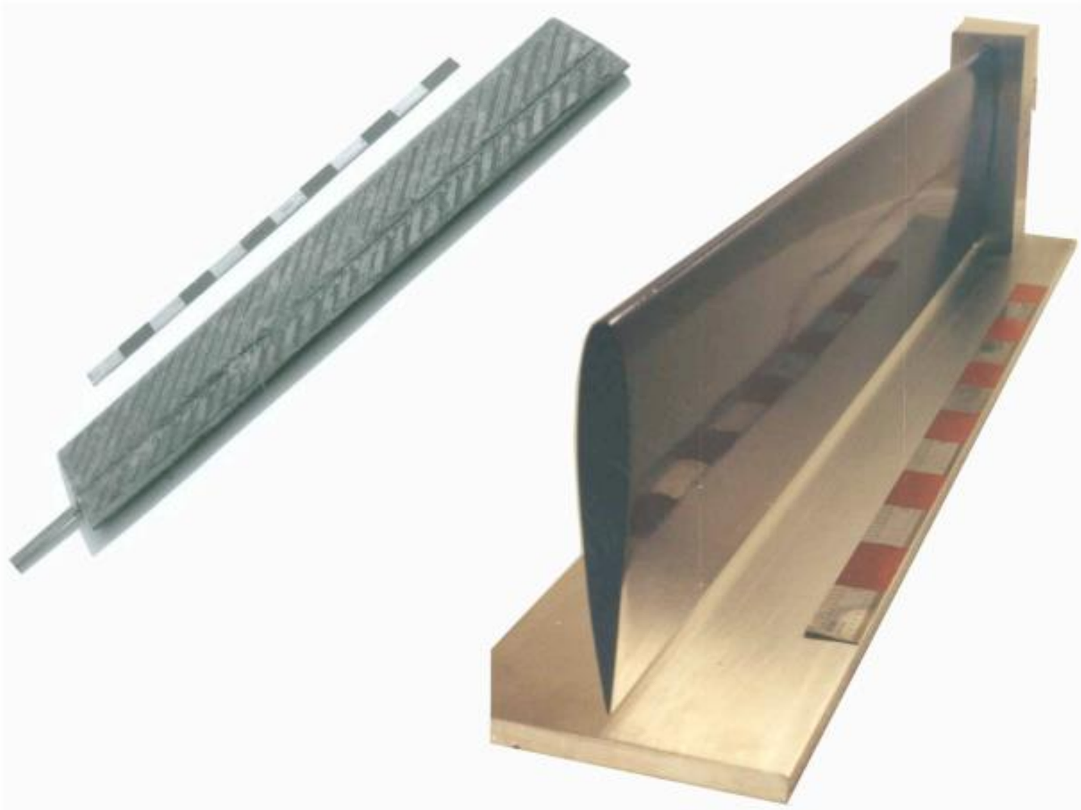

Figure 23: Directionally Attached Piezoelectric (DAP) [34]

Another piezoelectric actuator is the Macro Fibre Composite (MFC). According to Smart Material [35], it is a low-profile actuator and sensor invented by NASA in 1999. Smart Material began commercialising MFC in 2002. The MFC is constructed from rectangular piezo ceramic bars inserted between layers of adhesive, electrodes, and polyimide film and is sealed. The electrodes and the film are connected in an interlocked pattern that transfers the voltage to the piezo ceramics. The MFC construction allows for in-plane poling, actuation, and sensing. The piezoelectric device is usually bonded as a sheet to a structure or embedded within a composite. When a voltage is applied to the piezo structure, it will cause it to change shape or produce counter vibrations. The MFC can be used as a pressure sensor or as an energy harvester when a voltage is not applied. The actuator can be seen in Figure 24, and its properties can be seen in Table 2.

Figure 24: MFC Actuator [35]

Table 2: Overview of MFC properties [35]

Max. blocking force	28N to 1kN depending on width of MFC
Max. operating voltage	P1, S1, F1: -500V to +1500V P2, P3: -60V to 360V P2 Single Crystal: 0V to 500V
Max. operating frequency	Actuator: 10kHz Sensor, Harvester <1MHz
Typical lifetime	Actuator: 10E+9 cycles Sensor: 10E+11 cycles (< 400ppm) Harvester:10E+10 cycles (< 600ppm)
Typical thickness	300µm, 12mil
Typical capacitance	P1, S1, F1: 2nF to 12nF P2, P3: 25nF to 200nF

According to the MFC actuator datasheet [36], the MFC patches are environmentally sealed. The limits of the sealing were not found. The storage of the MFC actuator requirements dictates that the actuator must be stored within the temperature range of 10-60° C and less than 70% humidity. The actuator can be stored for 20 years (with maintenance at 6 to 7 years) according to the manufacturer Smart-Material [37]. In APPENDIX J, the email from Smart-Material affirming this statement can be seen.

The MFC was used as an actuator in the bistable winglets seen in Section 2.2.1. MFC patches can induce flexure in their supporting structures. This was shown in a study by Bowen *et al*. [38], where MFC actuators were used to deflect an aluminium plate. The experimental setup was as shown in Figure 25.

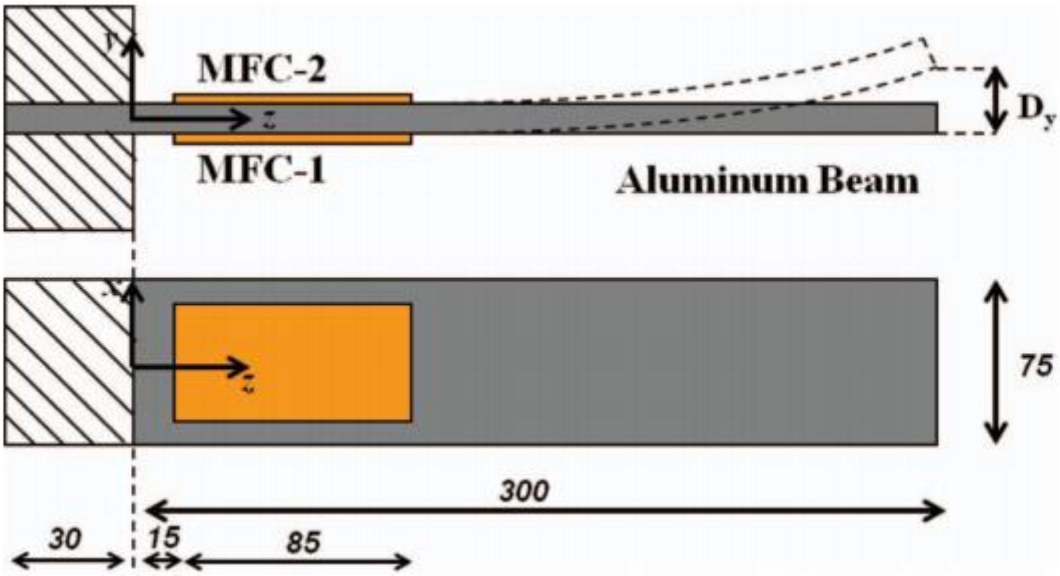

Figure 25: Experimental Setup of aluminium plate deflection using MFC actuators [38]

In a similar study by Zhang *et al*. [39], the results from the beam deflection are shown in Table 3. This was similar to the study in Bowen *et al*. [38].

Table 3: Validation Test results using MFC on an aluminium plate [39]

Θ^1 (mm)	Deflection (mm)
0	0
15	6.1445×10^{-4}
55	0.0372
100	0.1593
150	0.3453
200	0.5344
250	0.7242
300	0.9141

Based on the force from the extension of the MFC d33 P1 patches [36] and the placement of the actuator on the aluminium plate, a load would be induced on the plate, causing it to deflect. In the study by Zhang *et al*. [39], the MFC actuators were also used to deflect composite plates with various types of layer orientation.

Another type of piezoelectric actuator that could be utilised are Linear Actuators similar to the ones produced by PI [40]. These actuators use piezoelectric ceramic materials based on modified lead zirconate titanate (PZT) and barium titanate. The P-845.06 variant of this actuator (from PI) is able to push with a force of 3 kN and pull with a force of 700 N. The limitation of this actuator is the extremely small travel range of 90 µm. [41]

Shape Memory Alloys (SMAs), the other popular Smart Material, are described by Mohd Jani *et al.* [42] as metallic alloys that transform their shape due to a shift between the material's phases when subjected to temperature or magnetic field changes, called the Shape Memory Effect (SME). The material can be deformed by an applied force and through external heating or internal heating (like Joule heating) or subjected to a magnetic field (specific to MSMAs) [42].

Flexinol® wire is an SMA wire that is available in various diameters. The characteristics of the different diameters of the Flexinol® wire, including its pull force ability, can be seen in Table 4.

Table 4: Flexinol® Characteristics [43]

Diameter Size inches (mm)	Resistance ohms/inch (ohms/meter)	Pull Force* pounds (grams)	Cooling Deformation Force* pounds (grams)	Approximate** Current for 1 Second Contraction (mA)	Cooling Time 158°F, 70°C "LT" Wire *** (seconds)	Cooling Time 194°F, 90°C "HT" Wire *** (seconds)
0.001 (0.025)	36.2 (1425)	0.02 (8.9)	0.008 (3.6)	45	0.18	0.15
0.0015 (0.038)	22.6 (890)	0.04 (20)	0.016 (8)	55	0.24	0.20
0.002 (0.050)	12.7 (500)	0.08 (36)	0.032 (14)	85	0.4	0.3
0.003 (0.076)	5.9 (232)	0.18 (80)	0.07 (32)	150	0.8	0.7
0.004 (0.10)	3.2 (126)	0.31 (143)	0.12 (57)	200	1.1	0.9
0.005, (0.13)	1.9 (75)	0.49 (223)	0.20 (89)	320	1.6	1.4
0.006 (0.15)	1.4 (55)	0.71 (321)	0.28 (128)	410	2.0	1.7
0.008 (0.20)	0.74 (29)	1.26 (570)	0.50 (228)	660	3.2	2.7
0.010 (0.25)	0.47 (18.5)	1.96 (891)	0.78 (356)	1050	5.4	4.5
0.012 (0.31)	0.31 (12.2)	2.83 (1280)	1.13 (512)	1500	8.1	6.8
0.015 (0.38)	0.21 (8.3)	4.42 (2004)	1.77 (802)	2250	10.5	8.8
0.020 (0.51)	0.11 (4.3)	7.85 (3560)	3.14 (1424)	4000	16.8	14.0

Based on a discussion with Dynalloy (See APPENDIX H), the recommended work for the Flexinol® is 0.0981 Nm per strand of wire. The contraction distance of the wire is a percentage of the wire length according to Dynalloy [43], and as mentioned in APPENDIX H, one should consider the percentage of wire contraction to be approximately 4% of the original wire length. A contraction of 3.5 % of the wire length is considered to be more conservative. Table 4 highlights the current required for a 1-second contraction for the wire strands of various diameters.

According to Duerig [44], Ni-Ti alloys have been used as permanent Class III medical devices implanted inside a patient's vena cava as a filter to prevent possible embolisms. Therefore, it can be assumed that such material has a near-infinite shelf life. According to Dynalloy Inc. [43], Flexinol® wire is impacted by high stress and high temperatures, and it is possible for the wire to be permanently deformed when exposed to such conditions. The transformation temperatures for Flexinol® is between 60º and 110 ºC and for other Ni-Ti alloys can be adjusted from above 100 ºC to cryogenic values. [43]

The response rate of Flexinol® wires is determined by the heating of the wire, which is proportional to the rate and intensity of the current applied, as mentioned by Dynalloy [43]. The limiting factor on the rate of response of the wire is the inertia of the load the wire must pull, as damage in the wire can be introduced during rapid operation. For fast contractions, the inertia should be kept low, and the current should be applied in short high magnitude surges. Heating the wire using current, starting from room temperature, will cause the wire to reach 100 °C in 1 millisecond [43]. For the wire to return to its initial position, it is required to be cooled for relaxation to occur. These are some factors that limit the bandwidth of the actuator.

The bandwidth of a system, as described by Motion Control tips online [45], refers to the rate of the response to an input. The Smart Materials described previously perform the role of an actuator in the systems they are utilised in. The rate of response to a system input is an important attribute of an actuator as it links to its performance, with higher bandwidth being linked to better performance [45]. Within a system, the components connected to the actuator will tend to reduce the system's bandwidth [45].

The bandwidth for shape memory alloys from a survey of the literature, Lan and Fan [46], Grant [47], Moallem and Tabrizi [48], Moallem [49], Sunjai Nakshatharan *et al*. [50], Song *et al*.[51], Song *et al*. [52], Teh *et al*. [53] and Teh *et al*. [54], it was found to be between 0.3 to 3 Hz. With regard to Flexinol® wire, the literature also mentions that a significant contributing factor to the material's low bandwidth includes the cooling of the wire to return it to the initial set point and compensating for the hysteresis in operation [43].

In Fichera *et al*. [55], an MFC actuator was used for a camber morphing trailing edge. Through dynamic testing, as mentioned in Fichera *et al*. [55], the actuator was able to achieve a bandwidth of 25 Hz. The actuators consisted of an MFC patch sandwich (which comprises of two MFC patches with a 0.012 mm steel shim in between), 0.5 mm aluminium sheet metal, and fixed at the end with a non-deforming ABS plastic slider. The construction of the actuator plays a role in the bandwidth of the system, as mentioned in Wu *et al*. [56], where they argue the effect of the mechanical structure on the bandwidth and resonance and also indicates the influence of the electrical circuit. They affirm that PZT actuators have high-frequency bandwidths greater than 1 kHz. As seen in Table 5, the survey carried out indicated that the bandwidth for piezoelectric ceramics and single-crystal piezoelectric materials can be 5 kHz and 5.8 kHz, respectively.

SMAs, piezoceramics and other actuator performance are highlighted in Table 5 from Mohd Jani *et al*. [42].

Table 5: Actuator Comparison [42]

Actuator type	Stress (MPa)	Strain (%)	Efficiency (%)	Bandwidth (Hz)	Work per Volume (J/cm^3)	Power per Volume (W/cm^3)
NiTi SMA	200	10	3	3	10	30
Piezoceramic	35	0.2	50	5000	0.035	175
Single crystal piezoelectric	300	1.7	90	5800	2.55	15,000
Human Muscle	0.007–0.8	1–100	35	2–173	0.035	0.35
Hydraulic	20	50	80	4	5	20
Pneumatic	0.7	50	90	20	0.175	3.5

This study identified two dominant types of Smart Materials. These include shape memory alloys and piezoelectric ceramics. These were often the Smart Materials used in the creation of the Adaptive Structure systems. These can be seen in Table 6.

Table 6: Smart Material Actuator Comparison

Type of Smart Material	Force	Structural Load capacity	Bandwidth	Operating Cycles	Shelf Life	Density	Electronic Requirements
SMA – Flexinol®	3.5 – 68.5 N/mm (wire diameter)	70 MPa	0.3 to 3 Hz	10^7 cycles(under load L. Middleton [57])	Infinite (below annealing and aging temperature)	6450 kg/m^3	45 – 4000 mA
Piezoelectric MFC d33	28 – 1000 N (depending on width)	55.9 MPa (In fibre direction) 11.67 MPa (perpendicular to fibre direction) [58]	0-10 kHz (High Electric Field) 0-700 kHz (<33% of Electric Field)	107 cycles (at 2kVp-p)	20 years (with maintenance at 6 to 7 years) [114] [APPENDIX I]	5440 kg/m^3 [114]	1500 V
Piezoelectric PI P-845.06 (PZT)	3000 N [41]	30 MPa (due to an axial load)	Up to 5.5 kHz (No load) [41]	100^9 cycles [41]	Not specified	4836 kg/m^3 [41]	100 V [41]

Adaptive Structures have been evaluated for missile applications, as shown in Section 2.2.1. The use of adaptive aerostructures for missiles and other aerial vehicles were evaluated at different velocities. The Adaptive Structures used for the studies were used to create mechanisms that aided in the actuation of aerodynamics surfaces. The Smart Materials, seen in this section, would perform a more secondary function with regards to the control of the airflow over a control surface. The successes and shortcomings from the studies in this subsection and Section 2.2.1 are useful input to a conceptual design.

From the literature, the Smart Materials were found to have limitations with regard to stroke length (as was the case for the piezoelectric actuators) and low bandwidth (for the SMAs), amongst a few others mentioned in this section. Overall, the literature indicated that Smart Materials are able to produce high loads and have been evaluated in the supersonic regime.

Following the investigation into Adaptive Structures and Smart Materials, the system where these technologies would be applied was investigated, starting with missile systems.

2.3 Missiles

Missiles were examined to gain a greater understanding of how the Smart Materials or Adaptive Structures would be applied.

The Merriam-Webster Dictionary [59] refers to a missile as an object thrown or projected as a weapon, usually to strike something at a distance. The focus of this section will be on the guided, though not always self-propelled, flight vehicles used to carry warhead payloads to designated targets.

Missiles have sub-groups relating to their mission areas. These include the following:

- Air to Air Missile – AAM (e.g. AIM-120, Medium-Range) [60]
- Air to Surface Missile – ASM (e.g. AGM-65, Short-Range) [60]
- Surface to Surface Missile – SSM (e.g. BGM-109, Long-Range) [60]
- Surface to Air Missile – SAM (e.g. FIM-92, Short-Range) [60]

Further subcategories exist for each of the groups relating to, amongst others, the range, the type of targets the missiles intercept, and mission conditions. [60]

AAM and ASM are typically fired from an aircraft. Short-range AAM and ASM are usually used by an aircraft to defend itself and have a range less than 25 km (though it may be capable of achieving more). These missiles have control and seeker systems designed explicitly for short-range combat. These systems include Thrust Vector Control (TVC) which would allow for greater agility to engage targets behind the aircraft. Examples of AAMs include IRIS-T (manufactured by Diehl BGT Defence)[61], A-Darter (manufactured by Denel Dynamics) [62], and AIM 9X (manufactured by Raytheon) [63]. Examples of ASMs include AGM-114 Hellfire (manufactured by Lockheed Martin) [64] and Brimstone (manufactured by MBDA) [65].

Medium and long-range AAM and ASM missiles have ranges larger than 30 km. These are usually used in BVR scenarios. They tend to have radar seekers, larger warheads and larger rocket motors in comparison to the short-range missiles. Examples of AAMs include AIM-7 Sparrow (manufactured by General Dynamics and Raytheon) [66], AIM-120 AMRAAM (manufactured by Raytheon) [67], and Meteor (manufactured by MBDA) [68]. Examples of ASMs include AGM-65 Maverick [69] and AGM-88 AARGM [70] (both manufactured by Raytheon).

SSM and SAM are fired from the ground (ground-based launchers and ground vehicles) or the water (Ships). Examples include Javelin Weapon System missile (manufactured by Raytheon) [71] and the Tomahawk missile range (manufactured by Raytheon and General Dynamics) [72].

There are further subcategories to the missile groups relating to range and the type of targets the missiles intercept. The detail of these other sub-categories will be discussed in this study, where applicable.

Based on the research question, the missile investigation focused on the Beyond Visual Range (BVR) missile because of its operation in the supersonic regime. The application of Systems Thinking to design a BVR missile was the basis for the development of the requirements for an ASYS, which in turn were inputs to develop the requirements for the FGM. BVR missiles are a well-established class of missiles with adequate data for the AIM 120 (AMRAAM) missile and the Meteor missile to progress with this study.

2.4 Beyond Visual Range (BVR) Missiles

BVR missiles are a class of guided missiles that include the sub-categories of medium and long-range missiles.

BVR has been defined in various ways. According to Pierrot *et al*. [73], it is defined as 25 miles to 30 miles (which is about 40 km to 48 km) and beyond. Missiles that engage targets at this range tend to use radar seekers like the AIM 120 AMRAAM [74], though other seeker types have also been used.

The Meteor missile is also considered to be a BVR weapon. It has a radar guidance system, and it makes use of a ramjet for propulsion which enables the weapon to reach velocities above Mach 4 [68] and also achieve its 100 km range. The AIM 120 is also capable of reaching such velocities [75]. The high-velocity capability is a necessary trait for BVR missiles. It enables the missiles to engage high-velocity targets and have sufficient velocity to pursue them at long range and to allow for the interception of their high-velocity targets. It would also assist in reducing the time for a target to sense and avoid the incoming missile.

The AIM 120 was selected as the baseline for the conceptual missile design in this study. This BVR missile selection was based on the information available in the public domain. Its tail control actuator position was also the baseline used in this study. With a baseline selected, the next step was to understand how missiles and their control surfaces generate lift.

2.5 Aerodynamic Loads

Anderson [76] describes that the Lift (L) and Drag (D) for a constant angle of attack can be determined as follows in Equations (**1**) and (**2**):

$$L = \frac{1}{2}\rho_\infty V_\infty^2 S C_L \tag{1}$$

$$D = \frac{1}{2}\rho_\infty V_\infty^2 S C_D \tag{2}$$

Where ρ_∞ refers to the air density, V_∞ is the free stream velocity, S is the area of the wing area (or the missile's reference area), C_L is the coefficient of lift, and C_D is the coefficient of drag.

In most cases, aircraft make use of control surfaces such as ailerons, elevators and rudders to change their position about their roll, pitch and yaw axes. These surfaces affect the flow of air over the lift surfaces, which result in a change in the aircraft's motion [77]. Similarly, missiles make use of control surfaces to change their direction in flight.

BVR missiles, as mentioned in Section 2.4, operate in the supersonic regime. The aerodynamic loads experienced by a missile flying at supersonic velocities were considered relevant to this study. At these flow velocities, there are shock waves across which the properties of the flow change.

According to Chin [78], it is easier, in supersonic missile-design studies, to evaluate normal forces instead of lift forces when evaluating the aerodynamic loading on the missile. This is based on the generally symmetric nature of the missile's aerodynamic lifting surfaces. These are usually positioned symmetrically about the missile axis or chord of a control surface. The resultant pressure loads on these symmetrical bodies are therefore normal to the missile axis or chord of the control surface. This also is useful for wind tunnel studies as most wind-tunnel strain-gauge balance systems are configured to measure forces normal and parallel to the longitudinal axis of the model. Normal forces are also used in the stability analysis for the missile [78].

In Fleeman [78], the aerodynamic characteristics are determined for the different missile sections and summed together to obtain the overall aerodynamic characteristics of the missile. This is important as it has an impact on the control stability of the missile.

For the body normal force prediction, Fleeman [78] combines Slender Body Theory (based on a prediction method described by Pitts *et al*. [79]) and Body Cross Flow Theory (based on an analytical method described by Jorgensen [80]). Based on the combination of these prediction methods, the coefficient of normal force can be determined, as shown in Equation (**3**).

$$C_N = [(a/b)\cos\varphi + (b/a)\sin\varphi][\sin(2\alpha)\cos(\alpha/2) + 2(l/d)\sin^2\alpha] \quad (3)$$

Where a and b refer to the major and minor dimensions of an elliptical cross-section, φ is the rotation of the elliptical cross-section about its axis, α is the angle of attack of the missile body, and l/d is the length to diameter ratio of the body.

Both slender body theory and cross-flow theory are typically used for the analysis of "slender bodies" in a three-dimensional flow at any Mach number. The latter incorporates the effects of the vortices on the missile body. [81]

In Fleeman [78], the normal force coefficient, C_N, for a control surface or wing is a function of the freestream Mach number M, local angle of attack α', the wing surface planform area S_W and the missile reference area S_{Ref}.

$$For\ M^2 > 1 + \left(\frac{8}{\pi AR}\right)$$

$$C_N = \left[4\frac{\sin\alpha'\cos\alpha'}{\sqrt{M^2-1}} + 2\sin^2\alpha'\right]\frac{S_w}{S_{Ref}} \tag{4}$$

From Equation (**4**), as the supersonic Mach number increases, the normal force coefficient decreases. The inverse is true if the angle of attack or the wing surface area increases. The normal force coefficient is also proportional to the angle of attack and wing surface area. Equation (**4**) is based on a method determined in a study by Pitts *et al*. [79]. As mentioned in Fleeman [78], Linear Wing Theory and Newtonian Impact Theory are the basis for the evaluation of the normal force C_N at supersonic Mach numbers greater than 1.35.

The local control surface angle of attack α' in Equation (**4**) refers to the combination of the angle of attack α (the angle of the missile body relative to the freestream velocity V_∞) and the wing or control surface deflection δ (the angle the fin is deflected relative to the missile body axis). This is illustrated in Figure 26 from Fleeman [78] for a canard controlled and a tail control missile.

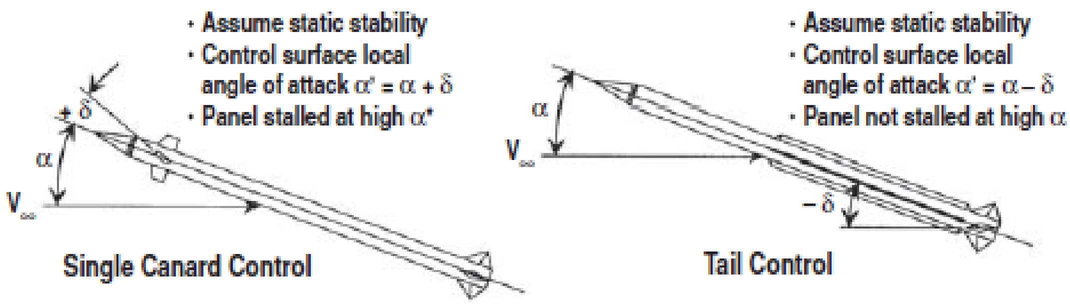

Figure 26: The definition of *α'* [78]

For a tail control missile, as the tail is deflected in the negative direction (as shown in Figure 26), the local angle of attack α' increases for a constant α.

The C_N can be used to determine the normal force in the same way that the coefficient of lift is used to determine the lift force. Using the lift equation from Equation (**1**) and replacing C_L with C_N and L with N, we get Equation (**5**):

$$N = \frac{1}{2}\rho_\infty V_\infty^2 S_{Ref} C_N \tag{5}$$

The flow over the body, in reality, has viscosity. According to Anderson [76], the viscous effects of fluid flow over a body have an impact due to the frictional forces generated. The flow over the surface of the body results in a boundary layer in a region near the surface of a body. Within this layer, the flow is stifled due to friction interaction with the body's surface. This layer has an impact on the friction drag, D_f, and the heat that the body will experience. Due to the viscous effects, the flow velocity at the surface of the body is zero. This is also known as the "no-slip" condition. The temperature of the fluid is the same as that of the surface, where the velocity is zero. The flow gradually increases in the *y*-direction, as illustrated in Figure 27, which depicts the viscous flow over a flat plate.

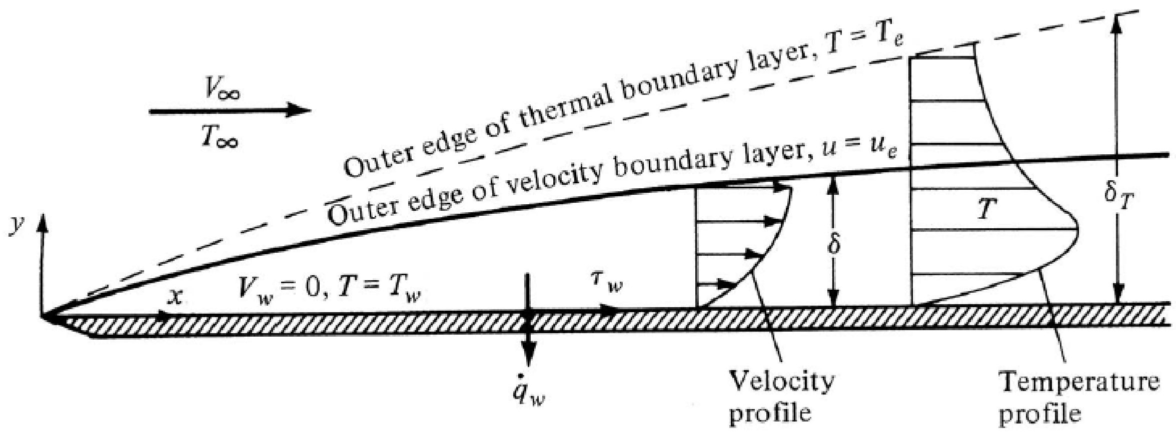

Figure 27: Boundary-Layer properties [76]

The velocity, *u*, increases until it is almost equal (0.99 times) to the freestream velocity, V_∞, which occurs at a height δ, the velocity boundary layer thickness, above the surface of the flat plate in Figure 27. The velocity at the edge of the boundary layer, u_e, is equal to V_∞. This velocity is determined by evaluating the inviscid flow at the effective body surface. The velocity profile is defined as $u = u(y)$. This is for *y* equal to zero until δ and varies for different *x* positions along the body. This is also true for the temperature variation on the outside surface of the body, which varies along the surface in the x-direction.

The temperature *T* changes from T_w at ($y = 0$) to *T* equal to $0.99T_e$ at *y* equal to δ_T. T_e refers to the temperature at the edge of the thermal boundary layer depicted in Figure 27.

The velocity gradient at the surface of the body (a result of the frictional effects of the fluid moving over the surface of the body) is the cause of the shear stress experienced by the body, and in a similar manner, the temperature gradient results in the heat transfer at the surface.

The friction forces on the fluid at the surface also reduce the velocity of the fluid as it moves in the x-direction. This eventually results in the separation of the flow from the surface. The separated flow influences the fluid by altering the body shape seen by the fluid downstream of the separation point. The separated flow results in a change in the pressure distribution on the surface of the body, which results in a drag force in the direction of the flow. This is known as Pressure Drag, D_p.

The type of flow, whether the flow is turbulent or laminar, also plays a role in the effects of the fluid on the surface. The shift from laminar to turbulent flow, usually occurring at the transition point, causes D_f to increase and D_p to decrease. Some factors which affect this transition include increased surface roughness, increased freestream turbulence, an adverse pressure gradient, heating of the fluid due to the surface, Mach number and Reynolds number (*Re*). As mentioned in Anderson [76], at high Mach numbers and low *Re*, the flow tends to be laminar in nature. An important flow attribute to consider when evaluating the transition from laminar to turbulent flow is *Re*. Turbulent flow tends to separate later than laminar flow due to its higher energy elements. Modifying the boundary layer usually involves delaying the flow separation. This can be done by causing a turbulent flow to remain attached to the surface at high angles of attack.

With the understanding of the boundary layer and the way the normal force is generated for a missile, it was important to investigate how these aerodynamic effects could be used to alter their trajectory in flight.

2.6 Missile Control Methods

Aircraft make use of control surfaces such as ailerons, elevators and rudders to change their trajectory in flight. These surfaces affect the flow of air over the lift surfaces, which result in a change in the aircraft's motion [77]. Similarly, missiles make use of control surfaces to change their direction in flight.

Rear-mounted servo-actuated fins (as seen in Figure 28) are traditionally used to manoeuvre the missile in flight. These fins are a subset of the actuator system. The fins at the centre of the missile, the wings in Figure 28, roles are to provide lift for the AIM 120 and are static compared to the tail fins.

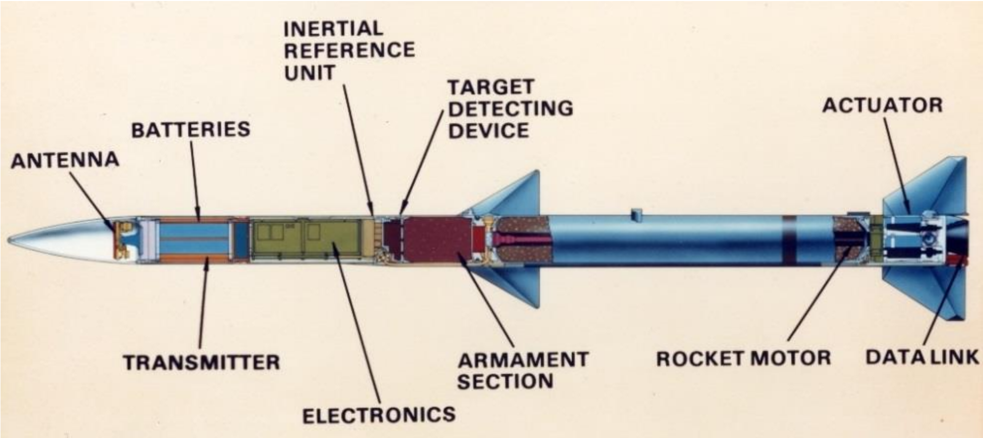

Figure 28: Major missile sections of the AIM 120 [82]

Typical types of control methods for missiles are shown in Figure 29.

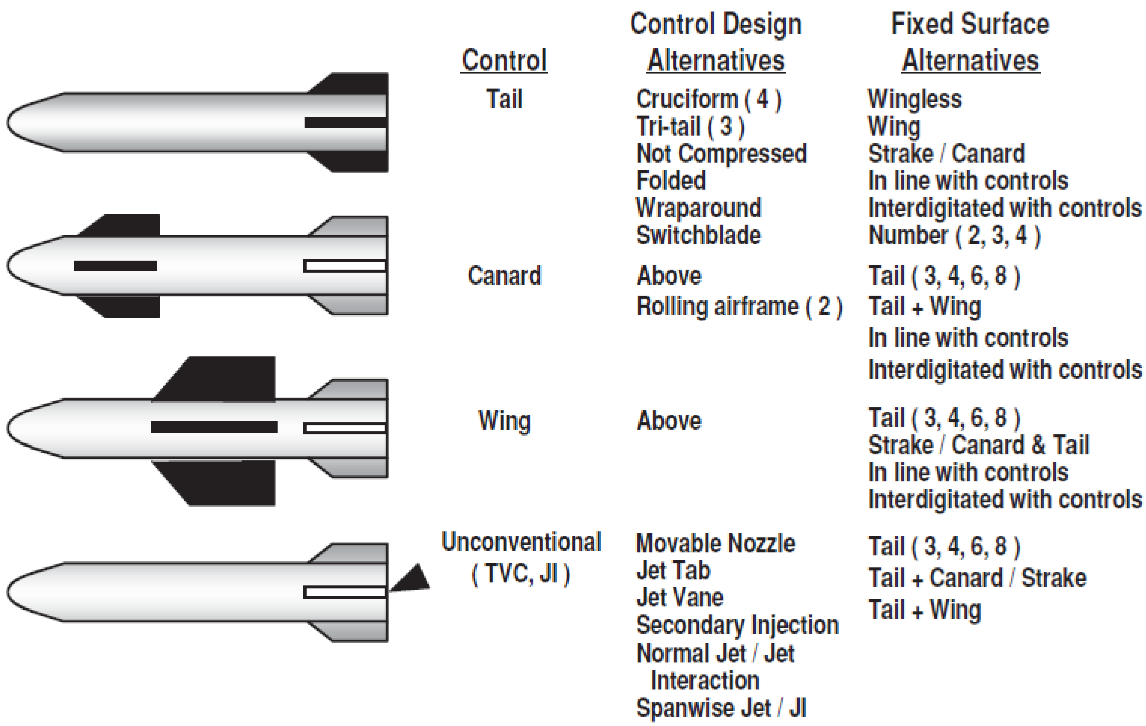

Figure 29: Missile Control Method Alternatives [60]

As seen in Figure 29 from Fleeman [60], the control alternatives involve tail, canard and wing control, Thrust Vector Control (TVC), and Jet Injection.

In changing a control surface (tail fins, canard fins, wings or a combination thereof) in-flight, results in changes in the lift vector of the missile. The altering of the surface position affects the magnitude and direction of the normal force produced. The control surfaces generate an unbalanced force, which will result in a change in the flight path of a missile. The unbalanced load will induce a moment about an axis or point inducing pitch, yaw, or roll, depending on the required vector change. Missiles generally employ this method for flight control by using either wings, canards, tail fins or a combination of the three, according to Fleeman [60].

In APPENDIX B, Figure 105 to Figure 107 highlight the effects of the different control surface positions as previously mentioned and give a visual representation of the advantages and disadvantages of the different placements of the control surfaces.

According to Fleeman [60], the advantages of Tail Control include:

- A compact packaging of the internal actuator components around a blast tube
- A small hinge moment
- A low actuator motor torque because of the small local angle of attack and the vortices shed by a tail deflection trail behind the missile result in a low induced rolling moment

Tail control surfaces also do not stall at higher angles of attack and perform better concerning the Pitching Moment and Lift Coefficients at these angles, as mentioned by Fleeman [60].

The disadvantages of tail control include:

- Reduced lift at small angles of attack [60]
- The reduced volume due to the rocket motor hardware (such as the blast tube) limits the selection of subsystems for the actuator system based on size. [60]

In APPENDIX B, Figure 105 (Fleeman [60]) highlights these advantages and disadvantages and the effect of tail deflections.

Fleeman [60] also describes that the advantage of Canard Control is that the canard placement provides additional space for internal systems as there is no blast tube from a rocket motor at those locations. The design for the actuator systems does not have to be as compact as the subsystems of a tail control actuator unless it is necessary to accommodate other systems. The deflection of a Canard Control surface generates an increase in normal force at low angles of attack. The disadvantages include stalling at high angles of attack and induced roll due to the interaction of vortices from the canard interacting with aft control surfaces of the missile.

Thrust vector control (TVC), as described by Fleeman [60], involves the manipulation of the thrust vector by altering the direction of the exhaust gas of the rocket motor. This is achieved by the injection of fluid into the exhaust, jet vanes, axial plates, jet tabs or movable nozzles.

The various methods and attributes of TVC systems can be seen in Figure 30.

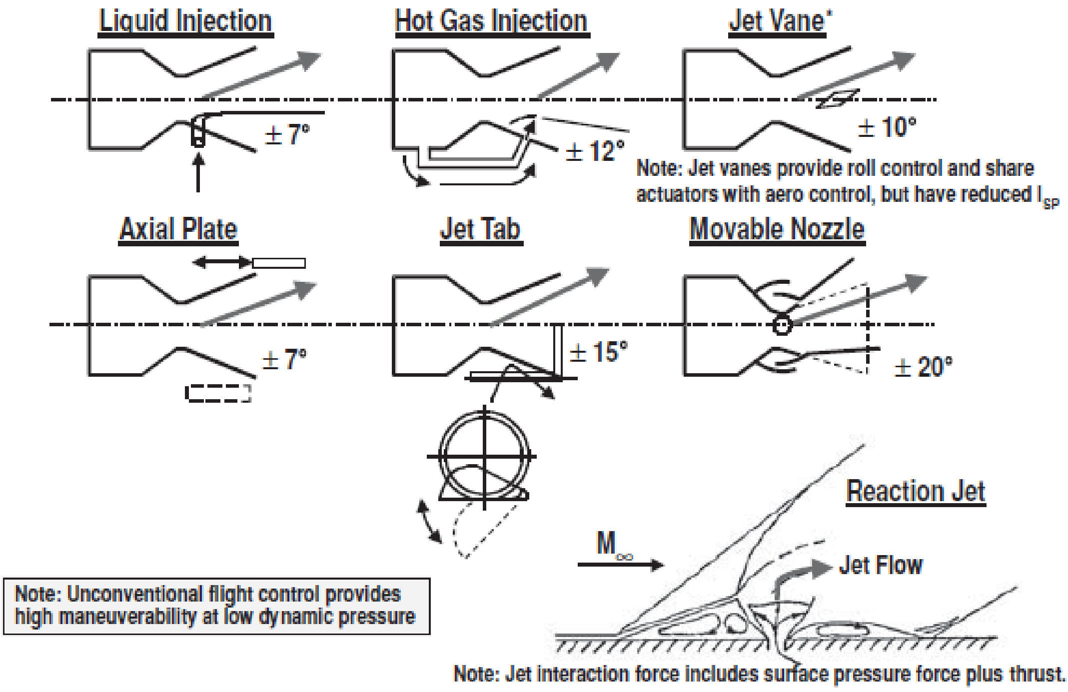

Figure 30: Thrust Vector Control Methods[60]

These attributes include:

- Deflection capabilities which range from 7 to 20 degrees
- Differential deflection for roll control (jet vanes)
- High manoeuvrability
- Fast response

The disadvantages mentioned in Fleeman [60] include:

- High operating temperature for TVC components
- High cost and short period of operation (due to the burn time of the rocket motor)

These viable control system methods were used to generate different concepts using Smart Materials/Adaptive Structures. The information was also helpful in eliciting requirements for the Actuator System design. For the actuator design, the detail of missile flight control systems was investigated. These inputs would later be used in the creation of the design decision tool as part of the verification of the concepts developed.

The control methods described in this section required additional systems to function as intended. The various missile flight control subsystems were therefore investigated to assist in the actuator system development and to identify possible enabling systems for the SOI, the Force Generation Mechanism.

2.7 Missile Flight Control System

While manoeuvring to a target, a sequence of events is triggered within the missile to adjust its flight path. Jackson [83] describes this sequence as the Homing Loop. This can be seen in Figure 31. In the Homing Loop, the missile motion (a function of the flight control) and the target motion are combined to create a relative geometry [83]. This is used by the Terminal Sensor to determine the Line-of-Sight (LOS) angle between the missile and the target. The State Estimator calculates the LOS angle rate, an input to the Guidance Law. The output from the Guidance Law is a control command, in the form of, amongst others, an acceleration which is the input into the Flight control system [83]. The missile systems involved in this loop include seekers, navigation and guidance systems, and flight control system components [83].

The system responsible for altering the missile's flight path is the missile Flight Control System. The flight control system is made up of the missile autopilot, actuator, airframe dynamics and the missile's Inertial Measurement Unit (IMU), as seen in Figure 32.

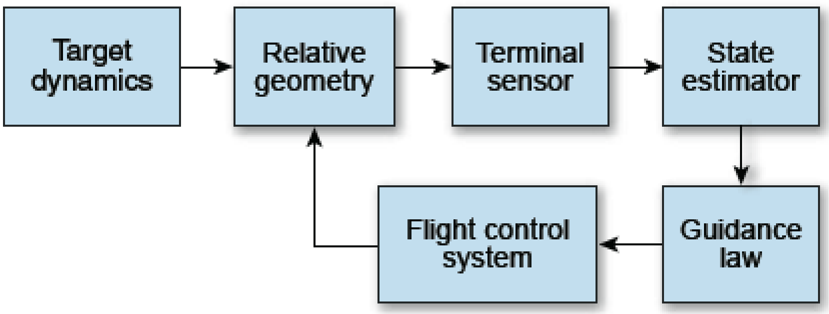

Figure 31: Missile Homing Loop [83]

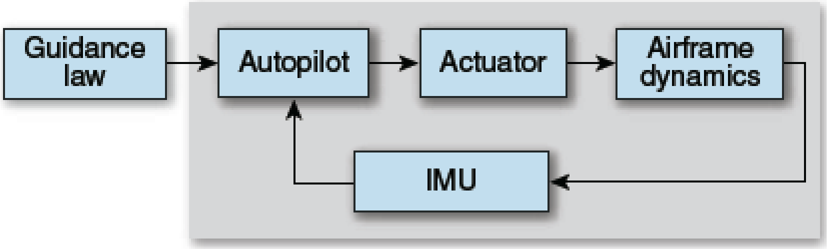

Figure 32: Missile Flight Control System [83]

While all these systems play their role in changing the missile's flight path, the Actuator is the system that provides the necessary physical input for the missile to manoeuvre. As mentioned by Jackson [83], the Actuator System translates the inputs from the autopilot system into the physical changes in the control surfaces or TVC systems that invoke changes in the airframe dynamics to follow the initial guidance input.

Missile actuator systems have historically used various mechanisms to achieve directional change. These include:

- Electrohydraulic Actuators
- Electro-pneumatic Actuators
- Electromechanical Actuators (like servo motors)
- Thrust vector control of the flow from nozzles of rocket motors.
- A combination of actuator types

Due to the space constraints within missile systems, the actuators are required to be compact to fit within the available space. This is illustrated in Figure 28. The increasing performance requirement for improved range, as well as lower mass requirements, has led to increased rocket motor volumes, further reducing the available space for actuator systems. The proximity to the rocket motor blast tube further reduces the available space for the Actuator System. Compact modular devices with reduced volume have become the industry norm for actuators in missile use, as discussed by Goldshine *et al*. [5]. This is significant as it indicates that there is a need to have a compact, low mass actuator system for tail control. The Smart Materials/Adaptive Structures identified in Section 2.1 can fulfil this need due to their low mass and can be deployed in various ways to optimally utilise the available space envelope within the system.

Due to the reduced size of the Missile Actuators, the force or torque output is lower than is often required. A Gearing System is deployed, using a system of gears [84], lead screws [85], or lever arms

[86], to deliver the necessary load. This is noteworthy in that, in conjunction with selected Smart Materials, a gearing system (or force-multiplying mechanism) must be considered when designing a missile actuator using Adaptive Structures, which would interface with the FGM.

In BVR missiles, electromechanical actuators in the form of brushless dc motors with a lead/ball screw arrangement are generally used, as seen in the AIM 120 AMRAAM mentioned by Global Security [87] online.

The abovementioned site [87] also indicates, in addition to the actuator devices, there are the power supply (in the form of lithium-aluminium batteries), control electronics, an encoder mounted to the output shaft to measure the fin position, and a load-bearing structure which is mounted to the rear of the missile's rocket motor.

The actuators discussed in this section make use of pressurised gas, hydraulic fluid, or electromagnetism to generate the force or torque necessary to move a control surface to affect the aerodynamic flow or exhaust flow from the rocket motor. These are considered to be the generic actuators mentioned in Section 1.3.

Understanding the components of the flight control system was necessary for the development and conceptual design of the FGM within the Actuator System.

2.8 Flow Effector Methods

Flow Effector Methods in this study refer to actuation methods that interfere with and alter the flow over lifting surfaces.

Fluidic Control or Boundary layer control involves the manipulation of the boundary layer on a lifting surface. This can be done using methods that involve Circulation Control (CC) [88][89][90] or the use of flow control actuator units [91] for active flow control.

During subsonic flight, CC uses the Coanda Effect [88] and allows the boundary layer over the lifting surface to remain attached for an extended period. This is done by blowing compressed air over the control surface to achieve an improvement in the lift. Figure 33 illustrates the effect on the flow over the lifting surface. Flapless aircraft such as the DEMON demonstrator [92] and the Magma aircraft [93], both UAVs, make use of this method, together with thrust vectoring, to manoeuvre in flight. The control mechanism for CC could make use of Smart Materials for control of flow openings. This method of actuation would, however, be best suited for subsonic cases and, therefore, would not be suitable for this study.

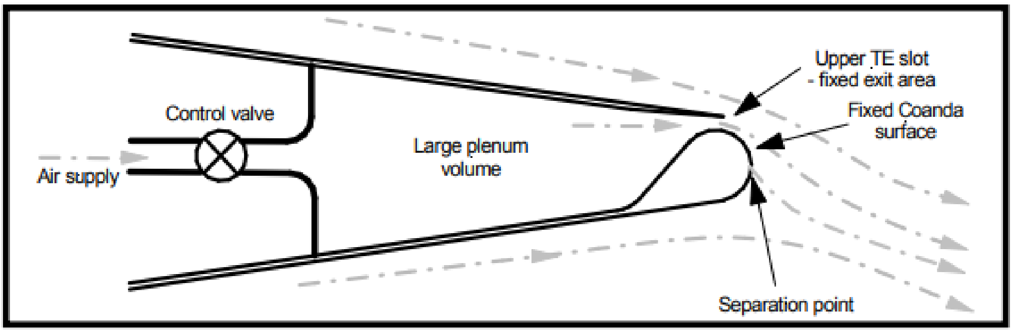

Figure 33: Circulation Control at wing Trailing-Edge [94]

Flow Control Actuator units similarly affect the airflow, except their placement is on top of the control surface instead of at the rear [91]. Examples of flow control actuators can be seen in Table 7.

Table 7: Flow control actuator examples [91]

Actuator Type	Actuator Transduction	Topology	Mechanism	Typical Application
(a) Air jet actuator [7] 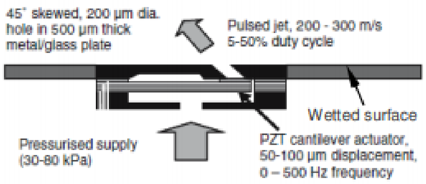	Fluidic	Hole	Injection of spatially periodic stream wise vortices	Boundary layer shape factor reduction → Separation control (High authority)
(b) Synthetic jet actuator [3] 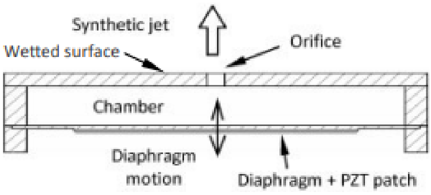	Electro-mechanical-fluidic (EMF)			
(c) Membrane actuator [8] 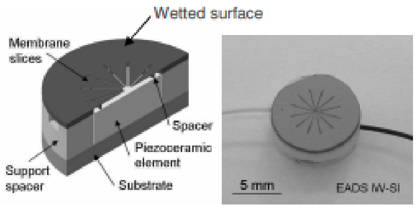		Surface (flow acceleration normal to surface)	Induction of wavelike disturbances	Attenuation of TS waves → Laminar-turbulent transition control (Low authority)
(d) Plasma actuator [9] 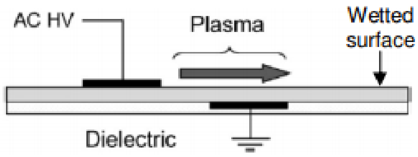	Electro-fluidic (EF)	Surface (flow acceleration tangential to surface)	Induction of span wise flow oscillations	Break up of turbulent streaks → Skin friction drag reduction (Low authority)

These methods are also known for their improvement of the lift properties of the lifting surface, which can be manipulated to manoeuvre the aircraft [91]. The method is, however, only viable at subsonic speeds due to the lack of circulation when the flow over the lifting surface is fully supersonic. This would not be effective if applied to a supersonic BVR missile due to the velocity requirement.

At the Center for Advanced Machine Mobility (CAMM) at Georgia Institute of Technology [95], another method of actuation using flow effectors was tested called a Bleed Port system. This system involves ports on the upper and lower surfaces of the wing, which can be opened to allow air to flow from the lower surface to the upper surface. As mentioned by Frink *et al*. [96], this reduces the lift (causes Lift dumping) on that surface, and this can be used to alter an aircraft’s flight path. In the study by Frink *et al*. [96], a concept called Passive Porosity Technology (PassPorT) was presented. The concept was originally envisioned for transonic aerodynamic surfaces but was also considered for supersonic delta-wing aircraft for the reduction of crossflow shock-induced separation. The envisioned use of the concept is illustrated in Figure 34.

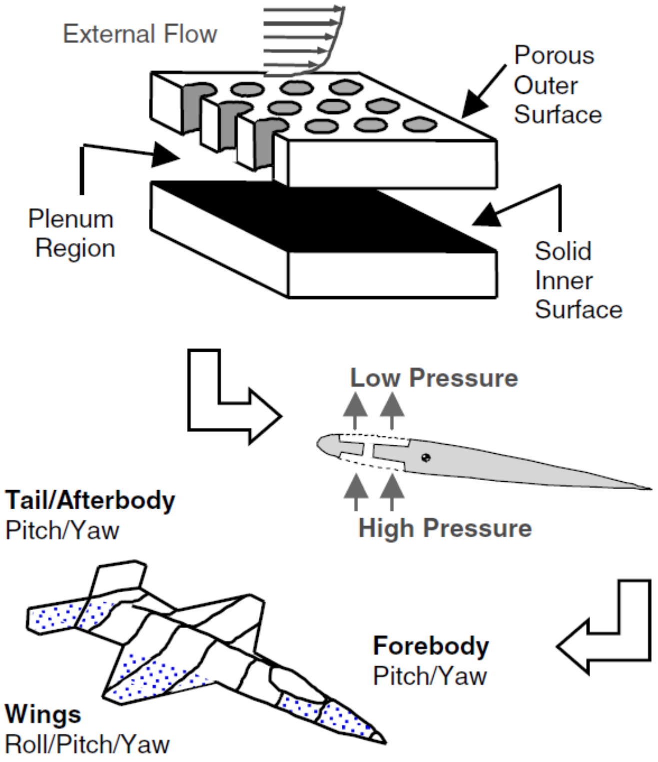

Figure 34: Vision for the use of the PassPorT concept on military aircraft

The study by Frink *et al.* [96] only evaluated the impact of this concept in subsonic conditions. In supersonic conditions, this concept would aid in reducing boundary layer separation and would act similar to the Flow Control Actuators in a subsonic flow mentioned in this section. As mentioned by Wallis & Stuart [97], discrete air jets were able to reduce the shock-induced separation of the boundary layer, which would result in the improvement of the performance of the aerodynamic surface.

A study by Bauer [98] found that the PassPorT, when applied to a supersonic delta wing, resulted in the "lift dumping". This provided roll and yaw control. This was achieved by linking the plenum region (shown in Figure 34) to the wing's high- and low-pressure region. This was mentioned by Frink *et al.* [96], but it was originally from the study by Bauer [98], which was carried out in the supersonic range. The connection of these high and low-pressure regions is associated with a decrease of the local normal force and translation of the centre of pressure, according to Hunter *et al*. [99]. One of the concluding remarks mentioned by Hunter *et al*. [99] was that for other flight regimes, this technology could work in a similar way.

Flow Effectors can also be in the form of protrusions that disrupt the flow over a lifting surface, such as those mentioned by Corriveau [100] and Wong *et al.* [101]. Figure 35 depicts the flow effectors on a missile used in the study by Corriveau [100]. These protrusions were tested at Mach 1.5 as the study investigated the feasibility of these protrusions to control a missile during supersonic flight. The tests were found to be successful as these protrusions were able to generate a significant force based on the study's requirements. The use of such a system was not considered because a tail control system was selected in this study, and further investigation would have to be carried out to determine the feasibility of this system at the tail location. This is due to the flow interactions that the tail control surfaces would experience due to the influence of the airflow from the forward lifting surfaces and the missile body.

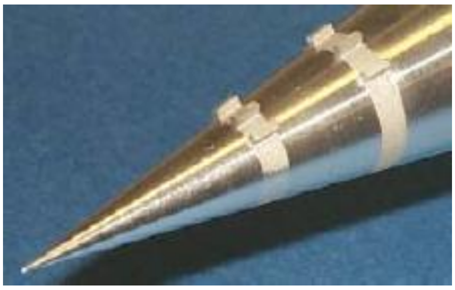

Figure 35: Micro-Actuated flow effectors [102]

Alternative methods for actuation were identified as potential applications for Adaptive Structures. The flow effector principal identified in this section was considered in this study as some applications already use Smart Materials/Adaptive Structures, and the others could benefit from the application of such materials/structures. Their possible use as part of a missile ASYS was considered during the concept development in this study.

3. Method

For this study, a quantitative and a combination of a deductive and inductive approach was adopted. Maree *et al.* [103] describes a range of research methods and based on this, a quantitative research approach is relevant for this study, as numerical data was collected during the literature review and used for comparison during the assessment of the concepts designed in this study.

An inductive approach was used to compile a set of observations relating to AS technology and methods of actuation of missiles (Goddard *et al.* [104] and Dudovskiy [105]). The concepts developed through this approach incorporated these observations. A deductive approach, as described by Dudovskiy [106], was then used to evaluate and determine relevant adaptive technologies to be considered based on methods of missile actuation.

This study used a systematic review, as described by Jesson & Lacey [107], to compile the required information from a review of the relevant published literature. The literature focused on answering the research question. The relevant studies were identified based on the requirements defined through the Systems Engineering approach at each level of the system design, down to the system of interest. The concepts were thereafter generated based on the relevant reviewed information and evaluated using an evaluation tool developed for this purpose.

A more detailed description of the methodology followed to meet the objectives of this study are included in the following subsections:

- Identification of the system of interest
- Defining the FGM requirements and developing concepts using Adaptive Structures with Smart Materials
- Developing the design decision tool for evaluation of the concepts
- Applying the design decision tool to the designed concepts

3.1 System of Interest identification

The FGM (FGM) was identified as the system of interest (SOI) based on the research question in Section 1.3. The research question referred to a system that would aid in altering the flight path of a missile. Hence the literature was also used to identify what systems play a role in altering the flight path of a missile. This was done to establish the system context for the FGM. From the literature presented in

Chapter 2, it became evident which system would benefit the most from the application of Smart Materials for Adaptive Structures.

Following the identification of the SOI, a conceptual missile design was initiated to identify the interaction between the enabling system, the missile, and the FGM. The mission requirements for a supersonic BVR missile were defined based on a potential competitor to the Meteor and AIM 120 AMRAAM BVR missiles mentioned in Section 2.4. The missile design was considered to develop inputs for the FGM system and to support the SOI selection.

Missiles are complex systems with a design process that requires multidisciplinary inputs. For this study, the missile design method described by Fleeman [60] was used to develop a generic missile to determine the necessary system inputs to the missile's ASYS design, another enabling system to the FGM. There are other methods to develop a missile system, for example, the method described by Viljoen [108]. However, the Fleeman [60] approach was selected as the method of choice due to its use in other missile studies such as Khalil [109] and Frits [110] due to the ease of use of this method.

The approach described by Fleeman [60] is illustrated in Figure 94.

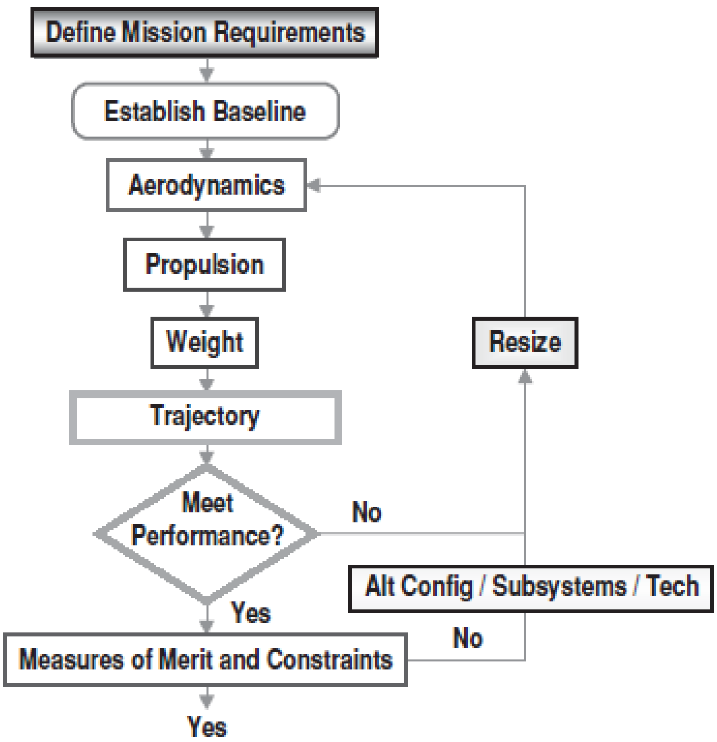

Figure 36: Fleeman's Missile Conceptual Design Approach [60]

With the mission requirements defined, a missile baseline from the BVR category of missiles, which comply with these requirements, was then selected. The aerodynamic characteristics of the missile were determined. This was followed by establishing the propulsion characteristics, the weight characteristics, and the missile's trajectory. The performance of the missile was evaluated along with the Measures of Merit. The process followed is illustrated in Figure 36.

The missile design process is usually iterative. For this study, the process was only carried out once to generate a conceptual missile, as this was not part of the scope of the study. As a result, no resizing was done. For an improved missile design, further investigation and iterations would be required. For the purpose of this study, the conceptual design provided sufficient information for the FGM Requirements Analysis.

Following the conceptual design of the BVR missile, the ASYS was designed. The Systems Engineering process described in Section 2.1 was followed to design the system. The outputs from this design and the conceptual missile design were then used as input for the FGM system design.

The design of the FGM also utilised the Systems Engineering process, as mentioned in Section 2.1. A description is presented in Section 3.2.

3.2 Force Generation Mechanism System Design

With the system of interest identified, the focus for the SE process was created. During the first stage of the process, the Requirements Analysis, the requirements baseline was defined.

During the Requirements Analysis the following aspects, based on the process described in Section 2.1, were defined:

1. Stakeholder needs, expectations and constraints.
2. Project constraints
3. End Date
4. Technology
5. Operational Context
6. Concept of Use envisioned for the Missile FGM
7. External Constraints
8. Scenarios or Mission Profiles
9. Measures of Effectiveness

10. Definition of system boundaries and external interfaces
11. Utilisation Environment
12. Life Profile
13. Functional Requirements
14. Performance Requirements
15. State and Mode Analysis
16. Technical Performance Measures
17. Physical characteristics
18. Human factors

As part of this stage, the literature was examined to determine the critical requirements of a supersonic missile actuator system's FGM. The missile system-level inputs identified through the conceptual missile design indicated that the actuator system design gave a more holistic approach to the Requirements Analysis phase. The Requirements Analysis aspects were then assessed and defined.

The Requirements Validation followed the Requirements Analysis. The requirements baseline was compared to the stakeholder needs and various system-related constraints. Requirement conflicts and shortcomings identified through this process would require another iteration of the initial stage. The validation followed the processes stated by Sparrius [13] described in Section 2.1. The outcome from this validation stage was a validated requirements baseline.

This validated baseline was then used to determine the functions of the system in the Functional Analysis stage. In this stage, the system functions were broken down into lower functions that are carried out by components of the system design. In order to define the actuator functions, a Functional Flow Block Diagram (FFBD) was generated.

According to the US Department of Defense Systems Management College [111], functional flow block diagrams are useful in functionally defining the system requirements. An FFBD is meant to define functions and not define solutions for the system to be designed. The process of defining lower-level functional decomposition was carried out to determine the FGM lower-level functions. This allows for the establishment of the Functional Architecture

This architecture was verified in the Functional Verification stage. The tabulation of the system requirements and their associated functions was chosen to check the traceability to the requirements baseline for the verification. The verified Functional Architecture was then used in the Synthesis stage, where the Physical Architecture was designed.

During this stage, the Physical Architecture was generated based on the Functional Architecture and the Physical Architecture from the actuator system architecture. Usually, alternatives would be created and assessed using trade studies to determine risks, risk-avoidance strategies and to determine their impact on performance, schedule, and cost. This would form part of the iterative approach, as seen throughout the Systems Engineering process, followed during this stage to mature the Physical Architecture solutions. In this study, alternate Physical Architectures were created and assessed for simplicity with regard to meeting the functions in the Functional Architecture. The aim was also to identify which Physical Architecture component could be replaced with a Smart Material or Adaptive Structure. The refinement of requirements was necessary to determine a better solution. This assessment is carried out in the System Analysis stage, which forms part of the iterative loop. In the end, the most suitable architecture was presented for Design Verification.

The verification requirements needed and the required environments were initially determined. These were then used to assess the architecture. For this study, it was decided to graphically verify the traceability between the lower-level components of the Physical Architecture and the Functional Architecture as an extensive verification process was considered to be outside the scope of this study.

The outcome of the Systems Engineering processes carried out in this study is captured in this document. This was considered part of the Control stage of the SEP followed.

By following the Systems Engineering process, the verified Physical Architecture can be traced back to the Functional Architecture, which was decomposed from the requirements elicited. This link, from the Physical Architecture to the system requirements, provided the basis for the evaluation of the concepts developed.

3.3 Concept Creation

The development of the concepts was based on the control methods and mechanisms indicated in Chapter 2 in conjunction with the Physical Architecture developed. The Smart Materials identified in Section 2.2 were utilised to produce the required mechanisms based on their abilities to function as actuators.

To aid in the development of the concepts, a Concept Combination Table approach, as described by Ulrich & Eppinger [112], was used to generate and select concept options.

Only concepts that m*et al*l the defined requirements were considered for evaluation with the design decision tool.

3.4 Developing the Design Decision Tool for Evaluation of Concepts

The vision of the Design Decision Tool was to evaluate the performance of the FGM concepts. It was also used to evaluate a generic FGM. This facilitated a comparison of the generic system with the solutions using Smart Materials/Adaptive Structures.

The FGM requirements baseline was used as the basis for the evaluation and for the creation of the tool. The requirements were used as decision criteria. These were weighted based on the Measures of Effectiveness and used to rank the concepts. This formed the first stage of the tool. The next stage was set up to evaluate how well the concepts meet the performance project-specific criteria.

The vision of the Design Decision Tool was to evaluate the performance of the FGM concepts. It was also used to evaluate a generic FGM. This facilitated a comparison of the generic system with the solutions using Smart Materials/Adaptive Structures. The weighting of requirements will highlight the level of importance to the system's performance, and the scoring assists in identifying how well a concept performs based on the requirements baseline.

3.5 Summary of the Method

The summary of the method followed is illustrated in Figure 37.

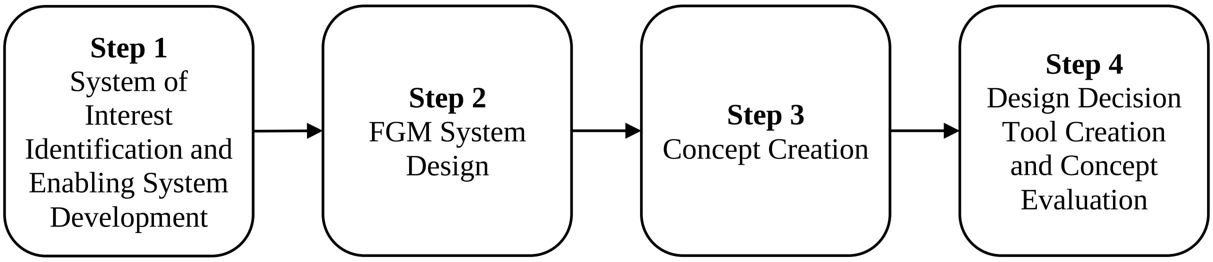

Figure 37: Summary of Method followed

Chapter 4 To Chapter 8 of this study fall within the steps highlighted in Figure 37.

The purpose of Step 1 was to define the SOI and develop the enabling system and operational context inputs for it. In Step 2, the requirements baseline and the functional building blocks of the FGM were developed and used to produce a Physical Architecture for the SOI. This formed the input to Step 3, where the concepts were generated. Step 4's purpose is to develop the method to rate and rank concepts to aid in a concept selection decision process.

4. System of Interest Identification and Enabling System Development

This chapter and its subsections fall within Step 1 of the method followed in this study. It is highlighted in Figure 38.

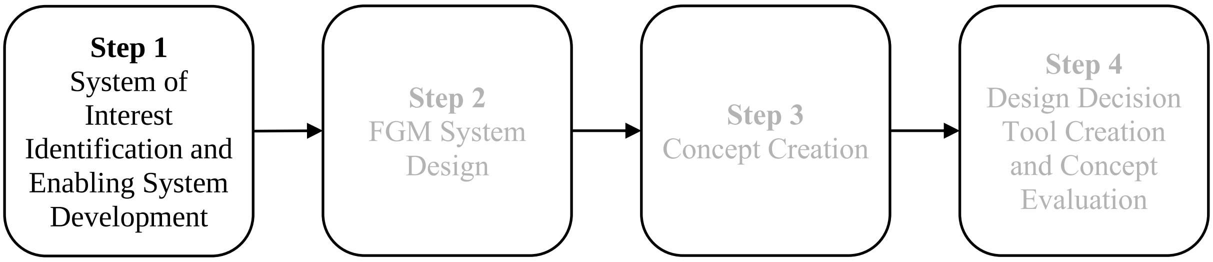

Figure 38: Step 1 of the Method

The purpose of this step is to identify the SOI, to develop its enabling systems and its operational context.

4.1 The System of Interest

As shown in Section 2.2, Smart Materials were used as actuators to influence aerodynamic structures that induce a change to the aerodynamic loading. Considering their application, they would be a system element of an actuator system.

Based on this, the Smart Materials and Adaptive Structures were considered for use within the Actuator System of a BVR missile. Therefore, the ASYS element, the FGM, was selected as the system of interest for this study. The SOI is depicted in Figure 39 in its system context.

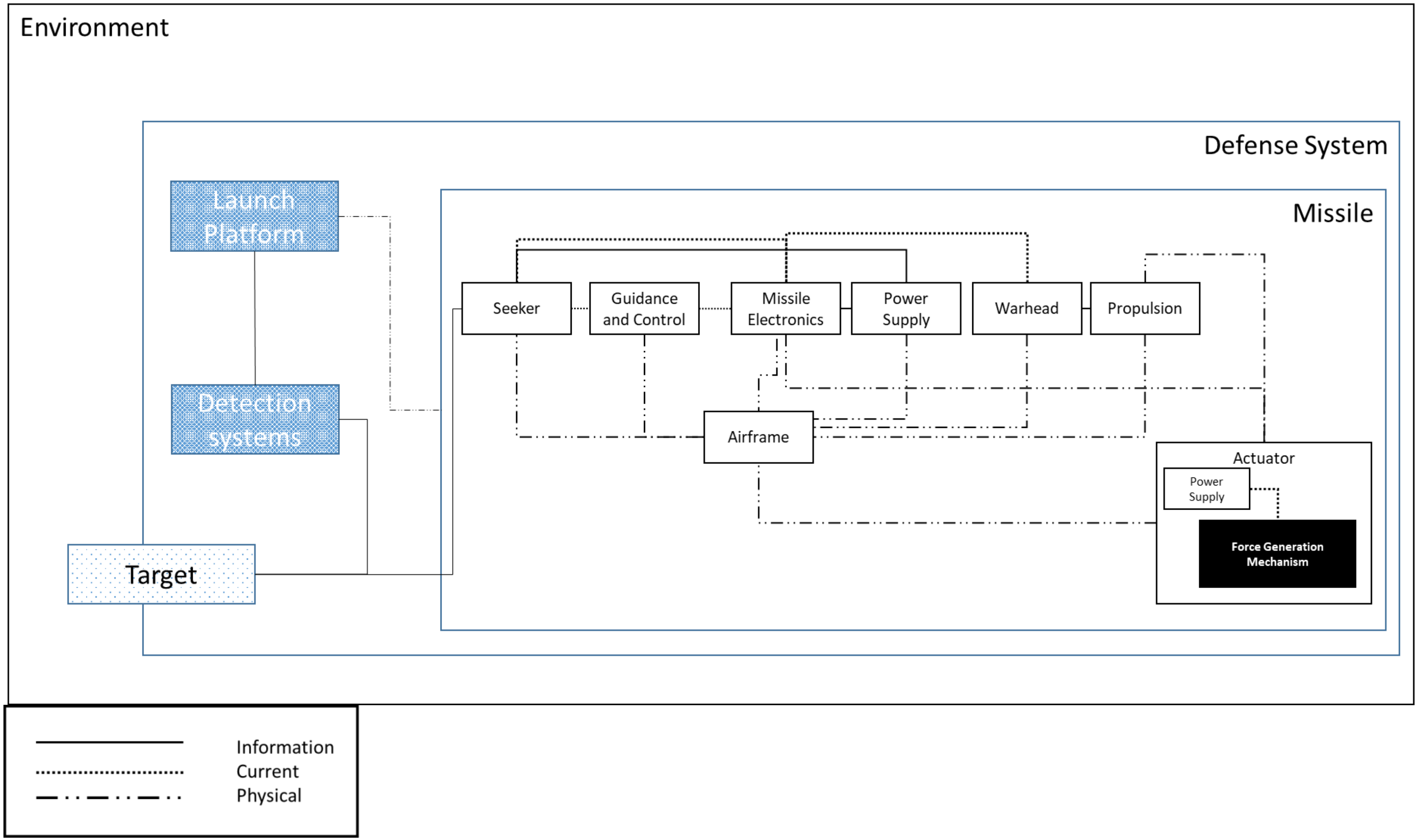

Figure 39: Force Generation Mechanism System Context

Following the identification of the system of interest, the missile design process, as described in Chapter 3.1, was initiated. The objectives of this process were to determine the interactions between the missile system and the FGM and to determine inputs for the ASYS.

4.2 Conceptual Missile Design

The requirements for the FGM are derived from the actuator system within a supersonic BVR missile system.

Based on the Systems Engineering approach to this design, the conceptual design of the missile system was necessary to develop the system requirements in which the ASYS would be used.

The iterative method described by Fleeman [60] was carried out. The outcomes from the design process that relate to the actuator system are described in this section.

The missile mission requirements are usually derived from the client, together with other stakeholders. The additional context for the design is extracted from the evaluation of the Concept of Use of the weapon. Once this is completed, a baseline can be selected. This assists the design process as the baseline provides a starting point for the design of the missile. As described in Section 2.3, Section 2.4, and Section 3.1, a BVR missile was selected.

The Concept of Use (CONUSE) describes how a product will be used in a variety of situations/scenarios [56]. To generate the required inputs to develop an ASYS, the higher-level system, the missile, needed a CONUSE to be defined.

The missile was envisioned to have the following post-integration life profile:

- Acceptance Testing (Using external power)
- Be transported.
- Be stored and remain in a dormant state.
- Enter Maintenance State (after extended storage periods of 5 years (assumed) after each flight cycle) (Using External Power)
- Be powered.
- Be tested (within missile system)
- Be powered down.
- Be repaired (if required)

- Carriage Flight
- Be utilised by the missile system (Free Flight)
- Decommission and dispose (if beyond proposed shelf life)

The CONUSE of the BVR missile to be designed is to engage an oncoming target at a range of 120 km at 30000 ft. The missile would be launched from an aerial launch platform (like a fighter aircraft such as a SAAB Gripen) with a velocity of Mach 0.9. As mentioned in Section 3.1, the missile mission requirements were based on creating a weapon as a potential competitor to the Meteor and AIM 120 AMRAAM missiles. Meteor is said to have a range of over 100 km, and it is utilised on the SAAB Gripen according to SAAB [113]. SAAB[114] also mentions that Meteor is launched at an altitude of 42650 ft.

The range for the conceptual missile was selected to be greater than that of Meteor so that it would have improved range performance. The operational altitude was selected to be lower than that of the Meteor missile as a conservative approach to the conceptual missile design. This is as the air density would be higher, which would increase the drag on the missile and therefore, the missile should have an improved range performance at higher altitudes. The launch velocity was based on the example used in Fleeman [60].

The CONUSE was introduced to assist in adapting and refining the missile Performance Requirements, as summarized in Table 8.

Table 8: Missile Performance Requirements

1	Range	120 km+
2	Launch Platform	Fighter Jet Aircraft
3	Launch Altitude	9144 m or 30000 ft.
4	Launch Platform Speed	Mach 0.9
5	Maximum Mass	160 kg
6	Maximum Carriage Volume	3.7m x 0.35 m x 0.35 m
7	Warhead Size	≥ 18kg Blast Fragmentation [115]
8	Engaging Platform Speed	M 0.9
9	Engaging Platform Altitude	30000ft
10	Engaging Platform Maximum Manoeuvre	9 g

Based on the missile's concept of use and its Performance Requirements, the AIM 120 AMRAAM was selected as the baseline for the conceptual design. The missile characteristics that have an impact on the FGM within the actuator system were determined, as seen in Table 9 through the Fleeman [60] process.

Table 9: Missile Characteristics

Characteristic	Value/Design Choice
Missile Diameter	0.178 m
Missile Body Geometry	Axisymmetric
Body Centre of Pressure	73% of the Nose Length (0.350 m)
Fin Design	Cropped Delta
Coefficient of Normal Force Prediction ($C_{N\ Total}$)	5.49
Normal Force Curve Slope	6.14/rad
Tail Centre of Pressure	3.39 m (0.081 m from Tail Leading Edge)
Flight Control	Tail Control
Missile Configuration	"+" configuration
Static Stability	Statically Stable (CG ahead of CP by 0.88 x Diameter value from Fleeman [60])
Missile Tail Sizing	0.233 m^2
Hinge Moment (total for two fins)	46.2 Nm
Fin Deflection (δ) (Trimmed Manoeuvre Condition)	-12.7 degrees (at 14.92 degrees Angle of Attack α)
Normal Force	1684.81 N (Minimum required for 30 g manoeuvre)
Velocity (not including Drag)	1312 m/s
Burn Time	7 s
Missile Mass	157 kg
Missile Length	3654 mm
Actuator Mass	14.4 kg
Actuator Length	410 mm
First Body Bending Frequency	48 Hz
Actuator Bandwidth	25 Hz
Maximum Missile Manoeuvre	30 g

The Actuator Length, seen in Table 9, together with the Missile Diameter, defines the volume of the Actuator. The components of the Actuator will be contained within this volume.

According to Fleeman [60], as a rule of thumb, the first body bending mode should be at least twice the flight control system's actuator bandwidth. This was used as the basis of the bandwidth requirement later in the study.

The missile's manoeuvrability was determined to be 30 g which is more than three times greater than the target's manoeuvrability, as per the rule of thumb stated in Fleeman [60].

The Measures of Merit for the missile that relate to the manoeuvring of the weapon were considered during the evaluation. Figure 40 highlights how the FGM can influence missile performance areas. This was based on the missile design detailed in APPENDIX A.

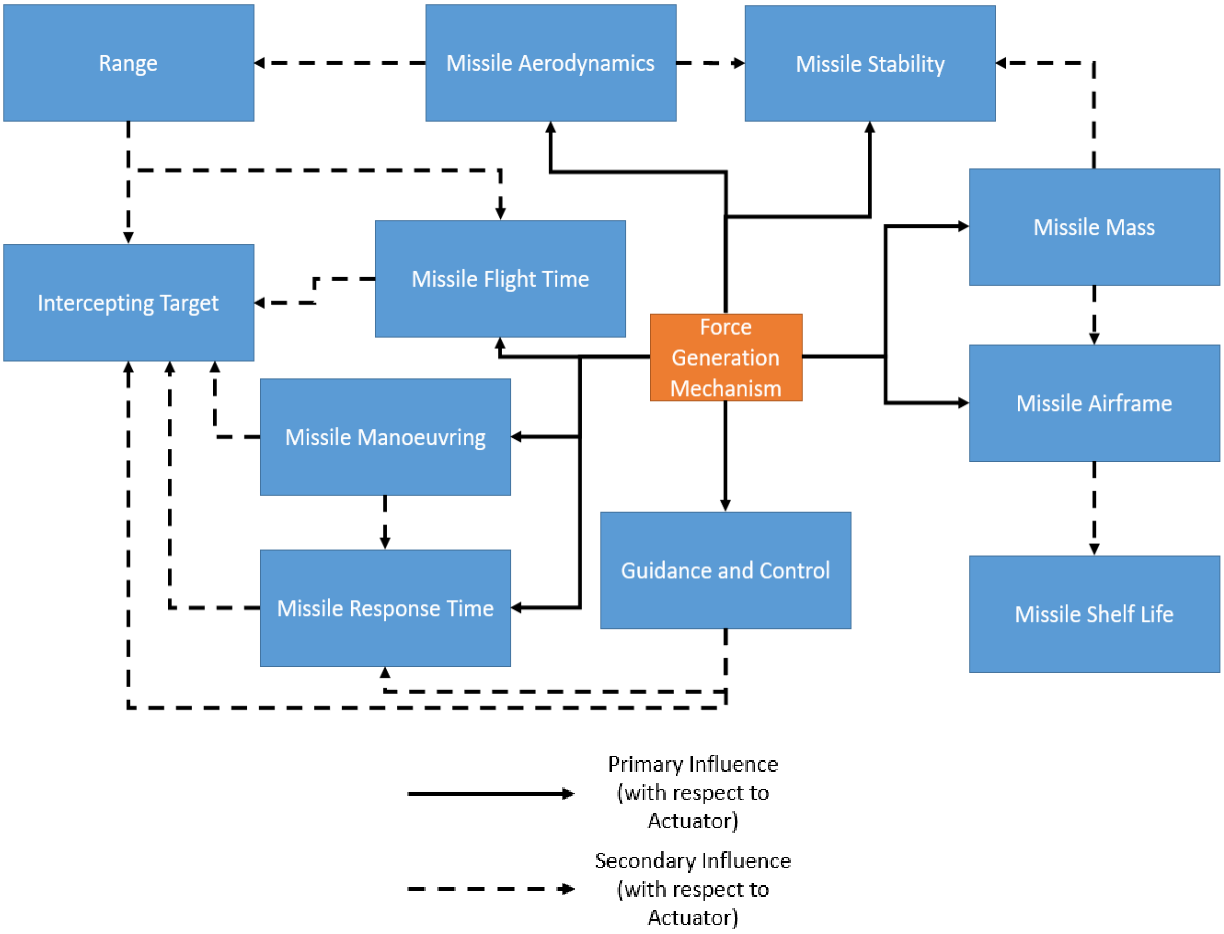

Figure 40: FGM influence on the Missile

In Figure 40, the primary influence of the FGM on different missile performance areas are depicted by the solid black arrows. The diagram also shows the secondary influences (dashed arrows) as a result of the FGM on other related missile performance areas when compared with the primary influences. The selection criteria will focus on performance areas that relate to the primary function of the actuator (i.e., to physically manoeuvre the missile to intercept the missile's target). The selection criteria were chosen to be as follows:

1. Missile Manoeuvring
    a) Response Time
    b) Missile Miss Distance
2. Missile Aerodynamics
    a) Contribution to Lift
    b) Impact on Drag.
3. Missile Guidance and Control
    a) Time Constant
4. Missile Airframe
    a) Effect of loading on Structure
    b) Influence due to Rocket motor.
5. Missile Mass
    a) Percentage contribution
6. Missile Stability
    a) Effect of force generation location
7. Missile Flight Time
    a) Operational Time

The performance areas are described as follows:

- Missile Manoeuvring (1) refers to the effect the FGM has on the change in the heading of the missile during flight. This affects the response time of the missile system and impacts the miss distance to the target.
- Missile Aerodynamics (2) refers to the FGM's contribution to lift and its influence on total missile drag.
- Missile Guidance and Control (3) refers to the influence the FGM has on the time constant used by the guidance and control system.
- The Missile Airframe (4) refers to the impact the FGM has on the interfaces to the missile airframe and the effect of the rocket motor (assuming a tail actuator) on the actuator.
- The Missile Mass (5) refers to the influence of the FGM's mass on the missile system's total mass. This has an impact on Missile Stability (6) and influences the actuation force generation location.
- Missile Flight Time (7) refers to the time the FGM will be operational after launch.

The influence of the FGM on the various missile performance areas described led to the development of the following requirements in Table 10:

Table 10: Missile Performance Requirements related to the FGM

	Performance Areas	**Approach**
1	Missile Manoeuvring	
1a	Response Time	A metric for missile response time is the angle of attack sensitivity to turn rate. [60]
1b	Missile Miss Distance	$\sigma_{MAN} = g n_T \tau^2 e^{-(t_O/\tau)[(tO/\tau)^2/2]}$ [60]
2	Missile Aerodynamics	
2a	Contribution to Normal Force	$C_N = C_{N\,Body} + C_{N\,Wing} + C_{N\,Tail}$ [60]
2b	Impact on Drag	Lift induced drag, drag due to the fin area exposed to the flow
3	Missile Guidance and Control	
3a	Time constant	$\tau_{Total} = \tau_{\delta} + \tau_{\dot{\delta}} + \tau_{Dome}$ [60]
4	Missile Airframe	
4a	Effect of loading on Structure	Evaluate the effect of load on the structure. In this study, it will be the same for all concepts except the C4
4b	Influence due to Rocket motor	Thermal impact on the actuator, space available
5	Missile Mass	
5a	Percentage contribution	Mass calculation, comparison
6	Missile Stability	
6a	Effect of force generation location	Comment on missile CP relative to missile CG

These requirements were determined based on a selected generic FGM.

A Generic FGM was selected to aid in the requirement elicitation. This would also be used as a baseline for comparison during the evaluation of the concepts. Based on the baseline missile's description online [87], the FGM was identified as brushless DC servo motors together with a ball screw arrangement. The details of the motors used on the baseline actuator were not available. Therefore, an existing servo motor was selected from a missile actuator servo motor supplier [116]. It was later determined that the supplier had discontinued the manufacture of the selected motor, but the motor data was still available to be used for the purpose of the analysis. The motor used for this analysis is the BLHP-20-04-8P; the datasheet can be seen in APPENDIX E.

The missile's manoeuvrability was assessed by evaluating the response time and the missile miss distance. The response time will be based on the angle of attack's (α) sensitivity to the missile's turn rate ($\dot{\gamma}$) as described in [60]. This will be assessed as seen in Equation (**6**):

$$Rate\ of\ Response = \frac{\alpha}{\dot{\gamma}} \tag{6}$$

The missile's response time is based on the sensitivity of the angle of attack to the missile's turn rate, which was measured based on the ratio $\alpha/\dot{\gamma}$. The FGM influence on the missile's response time is captured in the turn rate performance defined by $\dot{\gamma}$.

According to Fleeman [60], the turn rate performance is defined as seen in Equation (**7**):

$$\dot{\gamma} = gn/V = \left[qS_{Ref}C_{N\alpha}\alpha + qS_{Ref}C_{N\delta}\,\delta - W\cos\gamma \right]/[(W/g)V] \tag{7}$$

Where g is the acceleration due to gravity, n is the g manoeuvre, v is the velocity of the missile, q is the dynamic pressure, S_{Ref} is the reference area, $C_{N\alpha}$ is the normal force curve slope due to the angle of attack and the $C_{N\delta}$ is the normal force derivative due to pitch control deflection, W is the mass of the missile, α is the angle of attack, δ is the control surface deflection, and γ is the flight path angle (assumed to be zero for this study due to constant altitude used in this study).

Fleeman [60] indicates the actuator impacts the $C_{N\alpha}$, the $C_{N\delta}$, δ and W. $C_{N\alpha}$ is related to the ratio of the tail area (S_T) (which forms part of the actuator system in this study), and the missile S_{ref}. $C_{N\delta}$ would be related to the deflection of the tail control surface. δ would also be related to the tail's deflection. The mass of the actuator system would influence the missile's mass W. Based on the generic actuator for this study, the $C_{N\alpha}$ contribution from the tail was determined to be 1.03rad^{-1}. With the body's contribution of 2 rad^{-1} and the wing's contribution of 1.03 rad^{-1}, the $C_{N\alpha}$ for the missile would be 16.6 rad^{-1}(0.29 deg^{-1}) according to Equation (**8**).

$$C_{N\alpha} = C_{N\alpha\,Wing}\left(S_W/S_{Ref}\right) + C_{N\alpha\,Tail}\left(S_T/S_{Ref}\right) + C_{N\alpha\,Body} \tag{8}$$

This is based on an S_T/S_{ref} of 9.38 and an S_w/S_{ref} of 4.82.

The contribution and influence of the tail towards $C_{N\delta}$ are illustrated by the slope of the curve for $C_{N\ Tail}$ and $C_{N\ Total}$ in Figure 41. Based on a linear approximation, the slope of the $C_{N\ Tail}$ curve is 0.295 deg^{-1}.

As seen in Figure 41, the tail is the main contributor towards the $C_{N\delta}$ as the $C_{N\ Body}$, and $C_{N\ Wing}$ have no slope. Therefore, the total $C_{N\delta}$ would also be 0.295 deg^{-1}.

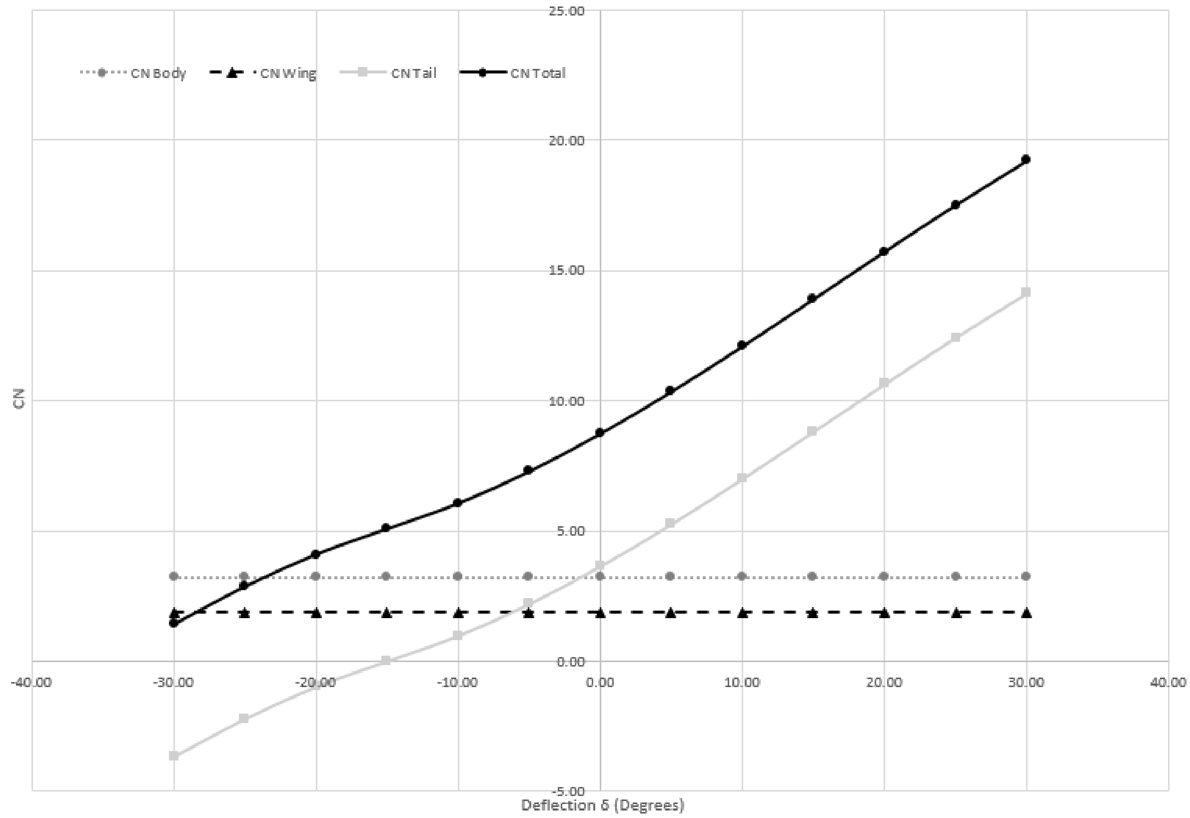

Figure 41: C_N vs δ for the missile body, wing, tail and for the entire missile

The relationship between the missile's C_N and C_M was established to evaluate trim condition, the tail fin deflection that would be required (δ_{Req}) to achieve C_{NReq} and a C_M of zero. Figure 42 depicts this relationship. APPENDIX C describes how the Normal Force coefficient and the Pitching Moment coefficient were calculated to create Figure 42.

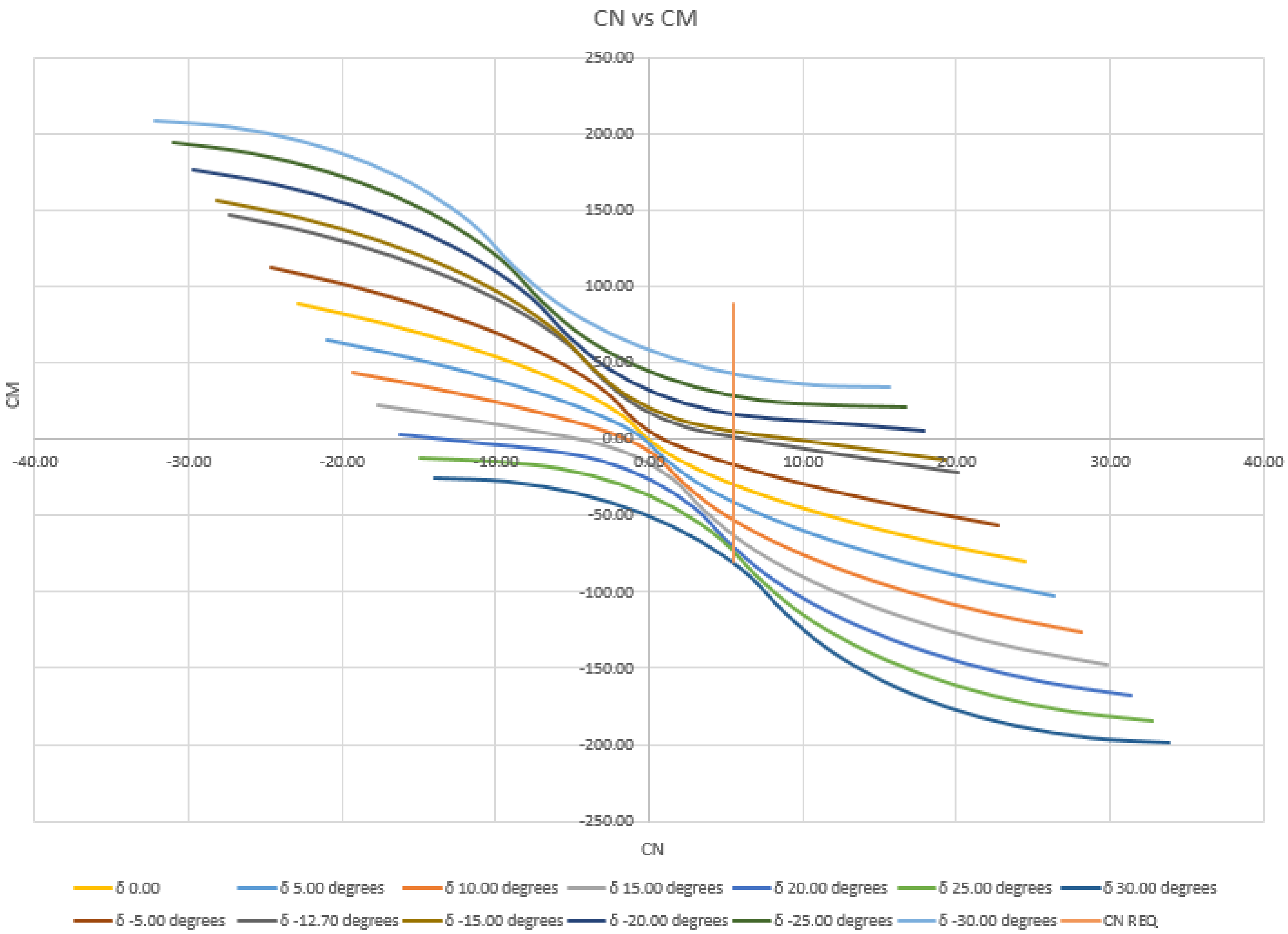

Figure 42: C_N vs C_M for the conceptual BVR missile

Based on Figure 42, the deflection that allows for the sustained g manoeuvre was determined to be -12.7°. This was based on the curve that passes through the x-axis at the required C_N value, which indicates the fin deflection that achieves the required Normal Force coefficient for a zero Moment coefficient. A negative fin deflection is defined as the "leading edge down - trailing edge up" deflection of the tail fin.

The conditions to produce the required C_N are highlighted in Table 11.

Table 11: Conditions for the Required C_N

Angle of Attack α (degrees)	Tail Deflection δ (degrees)
14.92	-12.7

Based on the calculations used to create Figure 42, it was determined that at an angle of attack of 14.92 degrees, the missile is trimmed with a tail deflection δ of -12.70 degrees (The first curve to cross the horizontal axis at the required C_N). This deflection would be required for a sustained 30 g manoeuvre at Mach 4. According to Fleeman [60], this gives control effectiveness, α/δ, of -1.18. This deflection was used as the maximum deflection for this study and was therefore used as δ for the evaluation of the turn rate performance.

The system of interest for the actuator system was the FGM, which is the servo motor for the generic ASYS. The selected motor for this study has a mass of 0.52 kg, as mentioned in the Montevideo Technology Inc. servo motor datasheet [116]. There would be four motors, one for each of the four tail control surfaces of the actuator system. This would mean the total mass of the servo motors combined would be 2.06 kg. Section 11.A.6, the mass summary of the conceptual missile used for this study, mentions that the actuator mass was 14.40 kg. This mass would include the structural components, power supply, motors and electronics. The servo motors selection, therefore, fits within the mass budget defined and would be a valid option, from a mass perspective, as the FGM for the generic actuator.

The mass of the missile, *W*, used for this evaluation included the actuator mass from the summary in APPENDIX A, as this forms part of the generic actuator used on the conceptual missile design. The missile mass is 157 kg. Assuming the missile reaches its maximum velocity of Mach 4 when all the propellant (52 kg) is spent and is then required to perform the 30 g manoeuvre, the mass of the missile would be reduced to 105 kg. This would be considered as *W* for the turn rate performance.

Therefore, based on Equation (**7**), the turn rate performance would be 20.95 °/s, which is greater than the intended target's turn rate performance of 16.64 °/s, which means that the missile is capable of intercepting the target.

The response time for 14.92 degrees angle of attack was determined to be 0.71 s.

The miss distance refers to the proximity of the missile to its manoeuvring target and is a measure of accuracy in intercepting the target. This is a function of the time to go (t_o), missile time constant (τ), target manoeuvrability (n_T) (which is the target acceleration in g's) and the acceleration due to gravity (g). An effective navigation ratio (N) of 3 is recommended by Fleeman [60]. The miss distance for an effective navigation ratio (N) of 3 is as described by Equation (**9**) according to Fleeman [60].

$$\sigma_{MAN} = g n_T \tau^2 e^{-(t_O/\tau)[(t_O/\tau)^2/2]} \quad (9)$$

For a target acceleration of 9 g, a time constant τ of 0.44 s, a time to go (t_O) of 0.41 s, and acceleration due to gravity of 9.81 m/s^2, the miss distance was calculated to be 11.48 m.

Assessment of the ASYS's influence on the missile's aerodynamics as a result of the use of a selected FGM was carried out by evaluating its impact on the contribution to the overall lift and drag of the missile.

For this study, the normal force was used as the measure for the force generated by the missile. The total normal force can be calculated as seen in Equation (**10**) from Fleeman [60]:

$$C_N = C_{N\,Body} + C_{N\,Wing} + C_{N\,Tail} \tag{10}$$

Based on the control surface position defined for this study, the C_{NTail} would be affected, which would impact the total normal force generated.

The contribution to the normal force of the missile is evaluated by assessing the actuator system's influence on the normal coefficient of the entire weapon as described previously. For the total C_N of 5.50, the tail contribution, C_{NTail}, is 0.4.

The C_{NTail} for the generic actuator system is a function of the tail fin area and the deflection of the fin. The servo motor for the generic actuator has a direct impact on the deflection.

Lift-induced drag was determined based on the coefficient of induced drag (C_{di}). This was determined as seen in Equation (**11**):

$$C_{di} = \frac{C_L^2}{\pi ARe} \tag{11}$$

Where *AR* is the aspect ratio of the control surface, and *e* is the efficiency factor for the control surface. Based on the relationship with regard to the coefficient of lift and the coefficient of normal force at high angles of attack, C_L can be approximated as seen in Equation (**12**):

$$C_L = C_N cos\alpha \tag{12}$$

Therefore Equation (**11**)becomes Equation (**13**):

$$C_{di} = \frac{(C_N cos\alpha)^2}{\pi ARe} \tag{13}$$

The coefficient of induced drag, together with the zero-lift drag coefficient (C_{do}), contributes towards the total drag coefficient (C_d) as seen in Equation (**14**):

$$C_d = C_{do} + C_{di} \tag{14}$$

The total drag was calculated as seen in Equation (**15**):

$$D = qS_{ref}C_d \tag{15}$$

The induced drag contribution due to the actuator system's control surface was determined to be 0.22 based on the induced drag calculation previously described. The C_{NTail} is the main influence from the actuator system.

With regard to the missile guidance and control, the time constant was determined, and the effect on the ASYS containing the FGM was evaluated. The time constant was calculated as recommended by Fleeman [60] as seen in Equation (**16**):

$$\tau_{Total} = \tau_\delta + \tau_{\dot{\delta}} + \tau_{Dome} \tag{16}$$

Where τ_δ is the time constant due to pitching moment control effectiveness, $\tau_{\dot{\delta}}$ is the time constant due to the deflection rate of the control surfaces, τ_{Dome} is the time constant due to the radome slope error, and τ_{Total} is the sum of the previously mentioned time constants, the total time constant for the missile. The time constants that contribute to the total time constant were determined as seen in Equations (**17**), (**18**) and (**19**):

$$\tau_\delta = \left[8I_y \frac{\frac{\alpha_{Max}}{\delta_{Max}}}{\rho V^2 S_{Ref} dC_{m\delta}}\right]^{\frac{1}{2}} \tag{17}$$

$$\tau_{\dot{\delta}} = 2\,\frac{\delta_{Max}}{\dot{\delta}_{Max}} \tag{18}$$

$$\tau_{Dome} = N\left(\frac{V_c}{V_M}\right)|R|\left(\frac{\alpha}{\dot{\gamma}}\right) \tag{19}$$

The variables and constants used in these calculations are defined in Table 12.

Table 12: Variables to determine the missile time constant

Variable/Constant	Definition	Units
α_{Max}	Maximum allowable angle of attack	Degrees
δ_{Max}	Maximum deflection angle of the control surface	Degrees
ρ	Air density	kg/m^3
v	Missile velocity	m/s
S_{Ref}	Reference Area	m^2
d	Missile Diameter	m
$C_{m\delta}$	Pitching Moment Coefficient	-
I_y	Pitch Moment of Inertia	m^4
$\dot{\delta}_{Max}$	Maximum wing control surface deflection rate	Degree/s
N	Navigation Ratio	-
v_c	Closing Velocity (related to the target and missile velocity)	m/s
v_M	Missile Velocity	m/s
R	Dome Slope Error	-
α/γ'	Angle of Attack sensitivity	s^{-1}

Based on the calculation previously described by Fleeman [60], the missile time constant τ is 0.44 s. The actuator system has a direct impact on the deflection δ, the pitching moment control effectiveness $C_{M\delta}$, the deflection (slew) rate $\dot{\delta}$, and the turn rate performance $\dot{\gamma}$. The FGM has an influence on all of these characteristics.

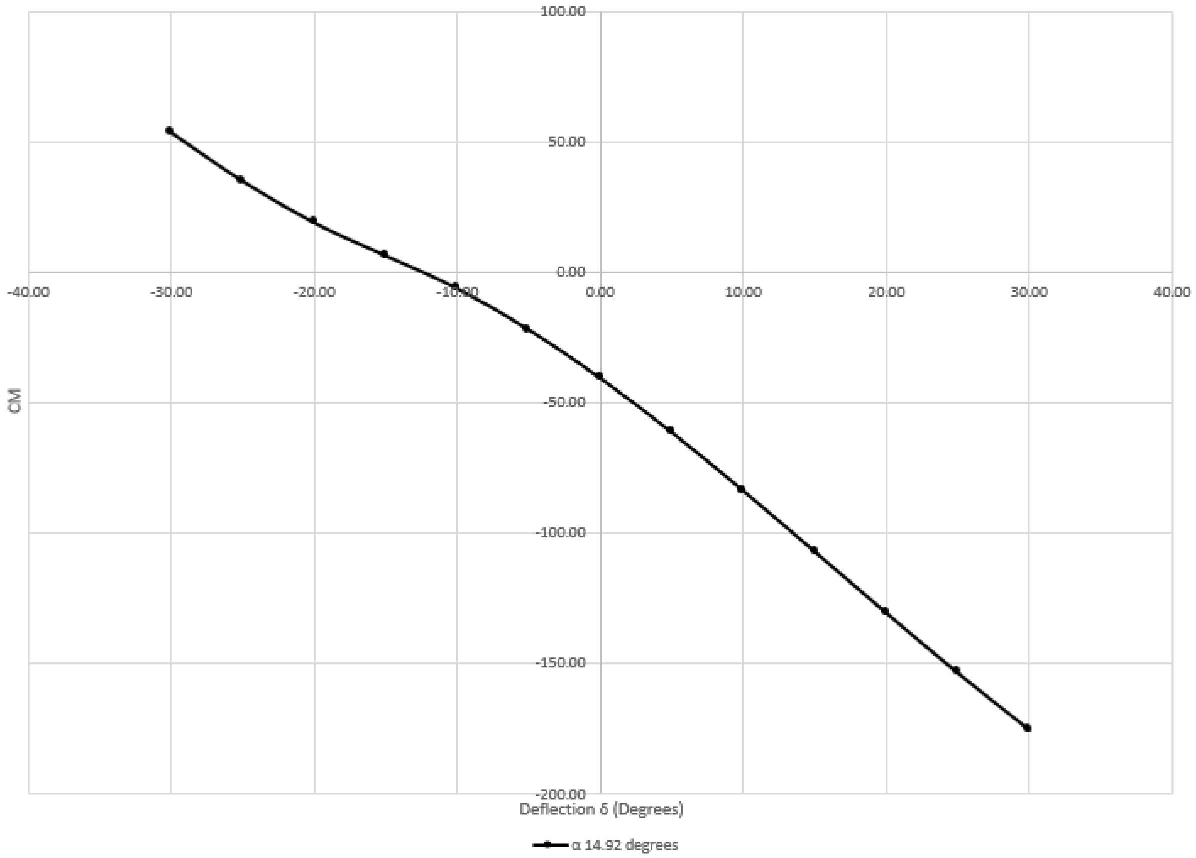

Figure 43: C_M vs δ at 14.95º angle of attack tail fin deflection for the conceptual missile

The slope of the curve in Figure 43 is -3.79. This slope is the pitching moment control effectiveness derivative $C_{M\delta}$.

The effect of loading on the missile airframe was evaluated based on the loads the missile structure would encounter in operation. The influence the ASYS has on this load was evaluated by its influence on the FGM.

The actuator system is subjected to aerodynamic loads, which is a function of altitude, geometry and velocity. The actuator system must be designed to withstand these loads and work against them in order to manoeuvre the missile. The loading around the actuator region would affect the interface to the missile airframe. For this evaluation, the focus was on the loading that would impact the FGM in a direct manner. This would be the normal force acting on the tail fin. The FGM would be expected to withstand and overcome this load to produce the necessary fin deflections. Hence the normal force is an important factor to consider. For the conceptual missile with a rotating fin, the hinge moment was determined to be 46.2 Nm based on the applied normal force.

To withstand this load and to operate when this load (assumed to be the maximum loading) is applied, a motor with a 20 % safety factor (20% more available torque) would be suitable for this study. This would mean that the servo motor should be able to hold the fin in its desired position regardless of the load applied, within the range the control fins would experience. These inputs were also needed to select the generic FGM to be used for comparison in this study.

Due to the selected placement of the actuator and the thermal influence of the rocket motor, the blast tube and the nozzle were evaluated. The thermal data for the rocket motor selected for the conceptual missile design was not available and thus could not be included in this study. In the absence thereof, the heat the actuator system would experience, i.e., the heat transfer from the rocket motor to the exterior surface of the rocket motor casing was estimated.

In G. P. Sutton *et al*. [117], which describes the transient heat transfer from the combustion chamber to the motor casing wall and through it, the temperature of the blast tube internal wall was determined based on Figure 44.

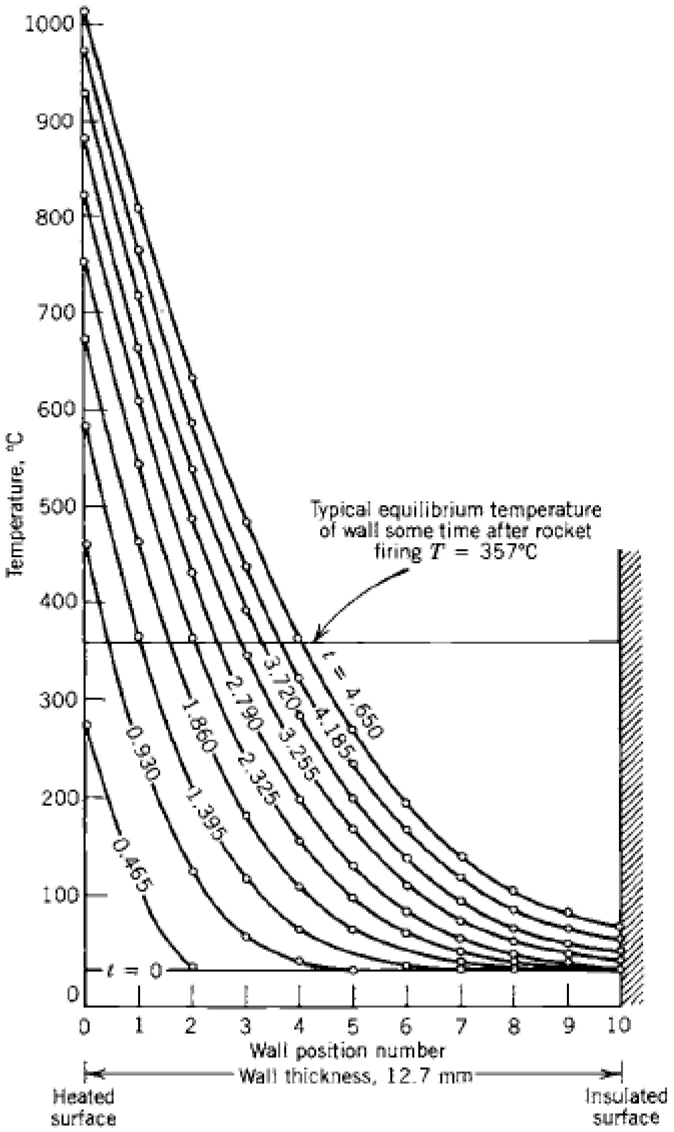

Figure 44: Typical temperature distributions through a motor casing thrust chamber wall as a function of heating time [117]

The internal temperature (T_i) was assumed to be the typical equilibrium temperature, namely 357°C, shown in Figure 44. Through conductive heat flow, the surface on the outside of the blast tube will eventually reach this temperature. The temperature inside the actuator system would start from an extremely low temperature (at the minimum operating temperature of the motor) and would start to increase as soon as the rocket motor is ignited and would continue to increase until all the propellant is burnt. According to Montevideo Technology Inc.[116], the maximum operating temperature of the selected servo motor is 220°C. As a similar type of motor is in use in the AIM-120, it is expected that the temperature does not reach a temperature higher than the maximum value operating temperature during the flight time.

The contribution to the overall missile mass was evaluated and compared to the conceptual missile's initial estimates. As previously described, the generic actuator system would contain four servo motors of 0.52 kg each, which make the total mass for the FGM 2.06 kg. This makes up 14.3 % of the 14.4 kg actuator, with the other components making up the remainder of the mass, as described in Section 11.A.6.

The stability of the missile was also evaluated based on the contribution of the actuator candidate mass and force generation location to the missile system. The positioning of the servo motor, the FGM within the actuator system, has an influence on the centre of gravity of the missile but has no direct effect on the centre of pressure of the weapon. This generic FGM placement would be similar to that of the AIM-120 baseline. The placement of the fins on the conceptual missile is also similar to the AIM 120. Therefore, the conceptual missile's stability is expected to at least be similar to that of the baseline selected.

The overall effect of the FGM on the operational time encompasses the time it is able to operate as well as the effects of its mass and influence on drag. The mass and the drag would tend to bleed energy from the system, reducing the missile range and ability to intercept the target.

As mentioned in Fleeman [60], a single degree of freedom approach was adopted to evaluate the operating time of the missile. For the evaluation, seen in APPENDIX A, the missile was assumed to fly at a zero angle of attack for the majority of its flight with only drag and thrust acting on it. Given that the rocket motor would burn for 7s, the motor produces 18 kN of thrust, the initial velocity is 1212 m/s, the reference area is 0.025 m2, the mass of the missile is 157 kg, and the coefficient of drag is 2, the missile would travel about 8.7 km. To achieve the range of 120 km and to ensure an intercept velocity of twice the target's velocity is achieved, the missile would have to travel for an additional 126 s. In the phase without the rocket motor, the missile is assumed to experience a constant drag that would reduce the missile's velocity from its maximum value to the desired intercept velocity. The flight time would therefore be about 133 s. This approach did not include the effects of manoeuvres, normal force or change in weight after burnout. The operational time was considered to be 180s to account for the influences of these effects on the missile as the system would be required for a longer period. This could be refined by carrying out a higher DOF investigation; however, this is beyond the scope of this study.

The additional inputs into the ASYS design are shown in Table 13. These inputs can be considered to be the minimum performance measures for a competitive generic FGM design.

Table 13: The Missile performance inputs related to the FGM

Selection Criteria		Generic	Units
Missile Manoeuvring	Response Time	0.71	s
	Missile Miss Distance	11.48	m
Missile Aerodynamics	Contribution to Normal force (C_N)	5.50	
	Impact on Drag (C_d)	0.22	
Missile Guidance and Control	Time constant	0.44	s
Missile Airframe	Effect of loading on Structure	23.15	Nm
	Influence due to Rocket motor	< 220	°C
Missile Mass	Percentage contribution	2.06	kg
Missile Stability	Effect of force generation location	Position Same as in Section 11.A.4	m (from Nose)
Missile Flight Time	Operational Time	180	s

Following the missile design, the stakeholders (this includes the Client, the end-user and the original equipment manufacturer (OEM)), as well as the operational context, were evaluated to elicit requirements for the ASYS, which includes the FGM.

4.3 Actuation System Design

The Systems Engineering approach was used for the design of the missile's Actuation System (ASYS). The purpose of the ASYS design, like the conceptual missile design, was to elicit requirements for the FGM. The details of the complete process and outcome are in APPENDIX D. This section contains a summary of the process and outcome.

The main stages of the process followed were also adapted from the IEEE 1220 standard (described in Section 2.1) and as described by Sparrius [13]

4.3.1 ASYS Requirements Analysis

The requirements for the actuator system are derived from the missile system. This is influenced by the stakeholders (this includes the Client, the end-user and the original equipment manufacturer (OEM) as well as the operational context. The process for the elicitation of requirements can be seen in Figure 4 in Section 2.1.

The functional and Performance Requirements for the actuator system were determined as summarized in Table 14. The detail of the ASYS Requirements Analysis can be seen in APPENDIX D.

Table 14: Functional and Performance Requirements for the Actuator System

	Functional Requirement	Performance Requirement	Value
1a	The Actuator Shall generate the required normal force	Generate a force to allow the missile to achieve a manoeuvre limit of 30 g (Minimum required for 30 g manoeuvre)	≥ 1685 N
1b		Ensure interfaces withstand generated forces.	Reserve Factor > 1
2a	Physical termination of missile flight (Once In-Flight termination mode)	Provide the means to terminate the flight	-
3a	Receive information from missile MCP	Information to be transferred at a rate of the system-level defined communication frame rate	Yes
4a	Send information to missile MCP	Information to be transferred at a rate of the system-level defined communication frame rate	Yes
5a	Assist in altering the missile flight path	Operate at a bandwidth	25 Hz
5b		Generate sufficient force to alter missile flight path as required	Based on 1a
5c		Maintain the required applied force for the required duration	180 s
6a	Maintain missile flight path	Operate at a bandwidth	25 Hz
6b		Generate sufficient force to alter missile flight path as required	Based on 1a
6c		Maintain the required applied force for the required duration	180 s
7a	Monitor Force generation	Measure force generated output	800 Hz ± 10 Hz
7b		Record force generated output	800 Hz ± 10 Hz
7c		Feedback measurements within the system to allow for system adjustment	800 Hz ± 10 Hz
8a	Run Pre-programmed flight paths	Operate at a bandwidth	25 Hz
8b		Generate sufficient force to alter missile flight path as required	Based on 1a
8c		Maintain the required applied force for the required duration	180 s
8d		Information to be transferred to and from MCP at a rate	800 Hz ± 10 Hz
9a	Run built-in maintenance tests	Operate at a bandwidth	25 Hz
9b		Generate sufficient force to alter missile flight path as required	Based on 1a
9c		Maintain the required applied force for the required duration	180 s
9d		Information to be transferred to and from MCP at a rate	800Hz ± 10 Hz
10a	Be transported	Endure all transportation within transportation packaging based on the Military Standard [66]	Yes
11a	Be stored	Have a Shelf life	Ten years
11b		Endure conditions within packaging based on the Military Standard [66]	Yes
12a	Be Programmed	Allow for multiple programming updates/modifications	Yes
13a	Be disposable at the end of its shelf life	Must adhere to environmental standards	Yes

The Measures of Effectiveness (MOE) refers to limits by which the system satisfies its mission when used by the end-user in the correct operational environment [10]. The MOE is meant to be defined in terms of anticipated outputs of the system but must be independent of any final design chosen. According to the INCOSE Systems Engineering Handbook [8], the defined MOE should be able to identify the overall performance of the final solution chosen.

The defined MOEs were used to check if the actuator system met or exceeded the requirements needed for the subsystem to be an effective solution for the intended missile system. The MOEs are as follows:

1. Bandwidth/Rate of Response
2. Energy Usage
3. Rate of change in Missile pitching moment.
4. Adherence to space requirements
5. Adherence to mass requirements

The ASYS boundaries were defined to assist in characterising other interacting systems which are out of the system designer’s control. The external interfaces were defined, and a greater understanding was achieved with regard to the input and output requirements of the system to be designed.

Figure 54 is an illustration of the ASYS and its related systems interaction. This illustration was created based on the inputs from the missile design (see Section 4.2) and other information related to the life cycle of the actuator system (derived from the missile system).

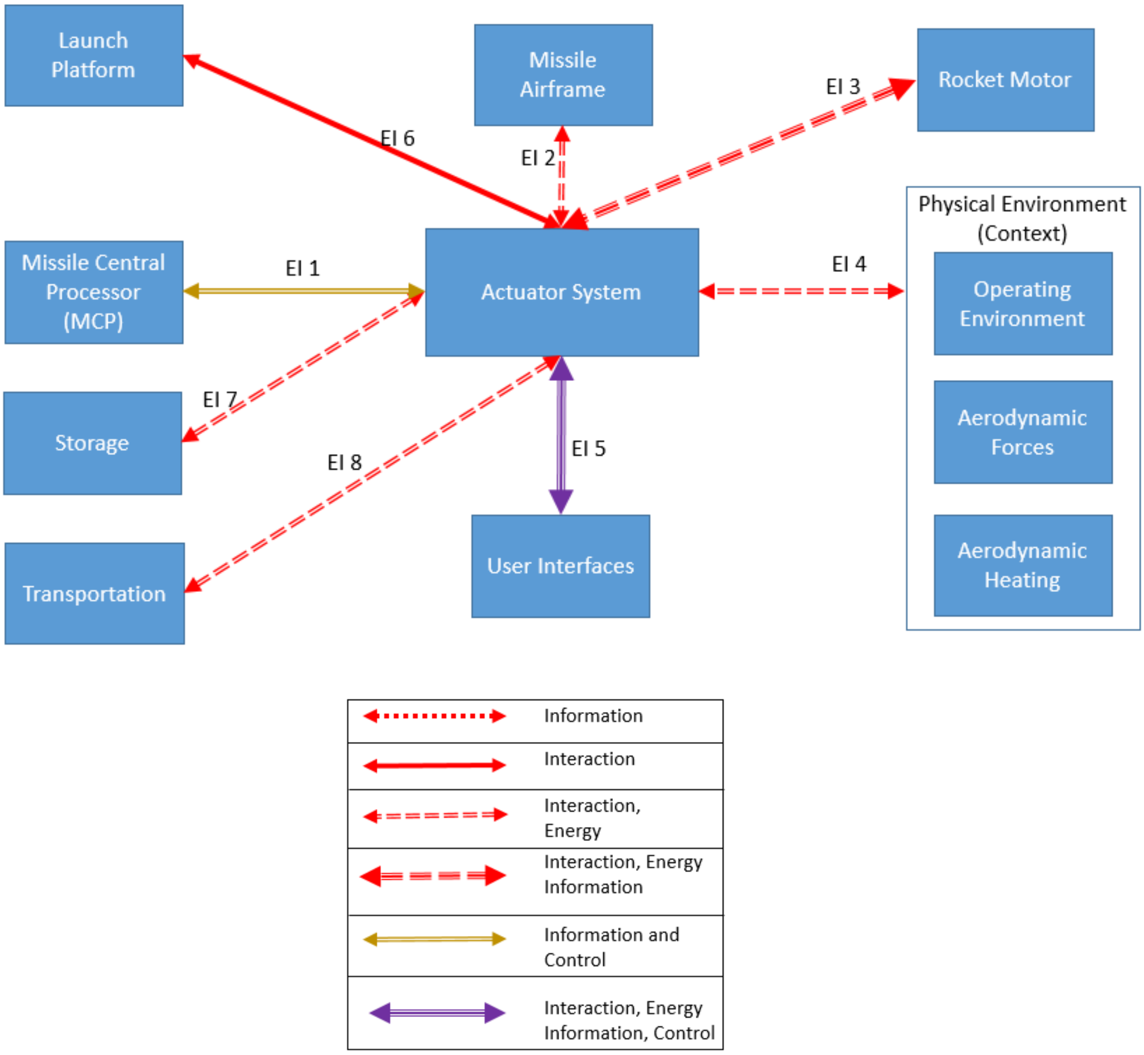

Figure 45: Context Diagram: Actuator System – External Interfaces

The details of these interfaces (the arrows labelled EI 1-8) are as follows:

1. The interface to the Missile Central Processor (MCP) is a communications link. The link is required for the MCP to send the actuator system information and to receive feedback from the actuator. (Information and Control)
2. The interface to the missile airframe refers to the physical connection the actuator will have with the rest of the missile system. (Interaction and Energy)
3. The rocket motor interface relates to the influence the rocket motor would have on the actuator. This was considered based on the general placement of a tail ASYS. The rocket motor affects the immediate environment of the actuator system due to the thermal impact. The rocket motor also constrains the volume the actuator can occupy. (Interaction, Energy and Information)

4. The physical environment is a significant influence on the actuator system. The physical environment refers to the operating environment and the aerodynamic loads that the actuator would have to overcome to function effectively. (Interaction, Energy)
5. The user interface refers to the interface the actuator would have before, during and after integration to the missile system. This would involve the consideration of human factors and other design criteria to ensure it can be integrated on the higher system level. (Interaction, Information, Control, Energy)
6. The launch platform has a direct influence on the volume the system can occupy. The interface is, therefore, a constraint to the actuator system. (Interaction)
7. The storage of the actuation system, before and after integration, is an interface that would have an influence on the volume. There may also be environmental effects that may affect the actuator system. (Vibration, temperature, humidity and other environmental factors) (Interaction, Energy)
8. The transportation of the actuator, like the storage interface, also has a similar influence on the actuator system. (Interaction, Energy)

In Figure 45, the different arrows used to depict the various flows between interfaces for the context diagram are defined. The flows such as information, control, energy and interaction were considered. Information flow refers to the flow of data feedback or measurements at the relative interfaces. Control flow refers to the control data sent at a specific interface that alters the function of the system. Energy flow refers to thermal energy and vibration. Interaction flow refers to the physical influence surrounding systems have on the actuator system. This relates to the space constraints the actuator would experience.

As seen in Figure 45, the actuator shall withstand the same environment as the next higher-level system, the BVR missile described in Section 4.2.

The Life Profile refers to a system's post-development life cycle, which includes where it will be used, how it will be integrated, how it will be accepted, user training, system support, and end of life processes (decommissioning and disposal). [10]

In order to define the life profile for the ASYS, the various processes post-integration of the system were envisioned, based on the Systems Engineering Body of Knowledge [10], and the following life profile was determined:

1. Acceptance Testing (Performance related testing pre-integration to the next higher-level system)
2. Physical integration to the missile system
3. Be transported.

4. Remain in a dormant state.
5. Enter Maintenance State
    a. Be powered.
    b. Be tested (within missile system)
    c. Be powered down.
    d. Be repaired (if required)
6. Be utilised by the missile system.
7. Decommission and dispose (if beyond proposed shelf life)

The remainder of the life profile was determined based on the life of the actuator incorporated into the missile system—the typical shelf life for a missile is 10 to 20 years, according to Howard *et al*. [118]. The shelf life of the missile system would give rise to a shelf-life constraint for the actuator and, therefore, for the FGM. The shelf life of weaponry is a concern, and an accurate performance specification could assist in developing products with better shelf life [118]. This points to the necessity of Systems Engineering as a basis for the design and to develop a maintenance plan.

It is important to note that during the process of deriving the Functional Requirements, the actuator was considered as a whole, and the Functional Requirements defined are that of the entire system. The functions relating to the defined requirements are described following the establishment of the requirements baseline. The links between the life profile of the actuator and the Functional Requirements defined can be seen in Table 15. The grey cells in the matrix depict the link between life profile and functional requirement.

Table 15: Actuator Life Profile and Actuator Functional Requirements

	FR1	FR2	FR3	FR4	FR5	FR6	FR7	FR8	FR9	FR10	FR11	FR12	FR13
LP1	■	■	■	■	■	■	■	■	■				
LP2	■	■	■	■				■	■	■			
LP3										■			
LP4											■		
LP5			■	■			■	■	■			■	
LP6	■	■	■	■	■	■	■	■	■				
LP7													■

The modes of the actuator were then determined. A mode is a label given to a set of user-based capabilities that can be used to command and control the system to achieve the required outcomes of the system. [119]

The modes for the actuator system were defined as follows:

- Power Off Mode refers to the mode when the system is not powered either from within the missile or an external source.
- Power-On Mode is when the actuator system is powered from within the missile.
- External Power Mode is when the actuator system is powered from outside the missile.
- Standby Mode is the mode the actuator enters where it awaits instruction.
- Operational Mode is when the actuator is able to execute the flight commands received from the MCP.
- Flight Termination mode is when the actuator performs a flight termination action.
- Test Mode is a mode used during the testing of the actuator. Within this mode, there are various built-in tests that assess the performance of the system.
- The failure mode is entered into once the actuator does not receive any feedback from the missile MCP. Upon entering this mode, the actuator then performs a series of system checks (built-in tests) to identify and resolve the problem.
- Repair mode allows the system to be adjusted to resolve issues affecting the functioning of the actuator.

Figure 46 highlights the modes for the ASYS. These modes are derived from the life profile of the actuator. Each blue block refers to a distinct mode, and the arrows indicate the conditions for each mode. The modes defined in Figure 46 are the internal modes of the actuator.

The FGM is impacted by all the modes identified. Table 16 illustrates the relationship between the defined modes and the previously defined Functional Requirements of the actuator system. The grey cells of the matrix depict the link between the functional requirement and the modes.

The complete correlation between the actuator modes and the missile system modes were not evaluated as it is beyond the scope of the study.

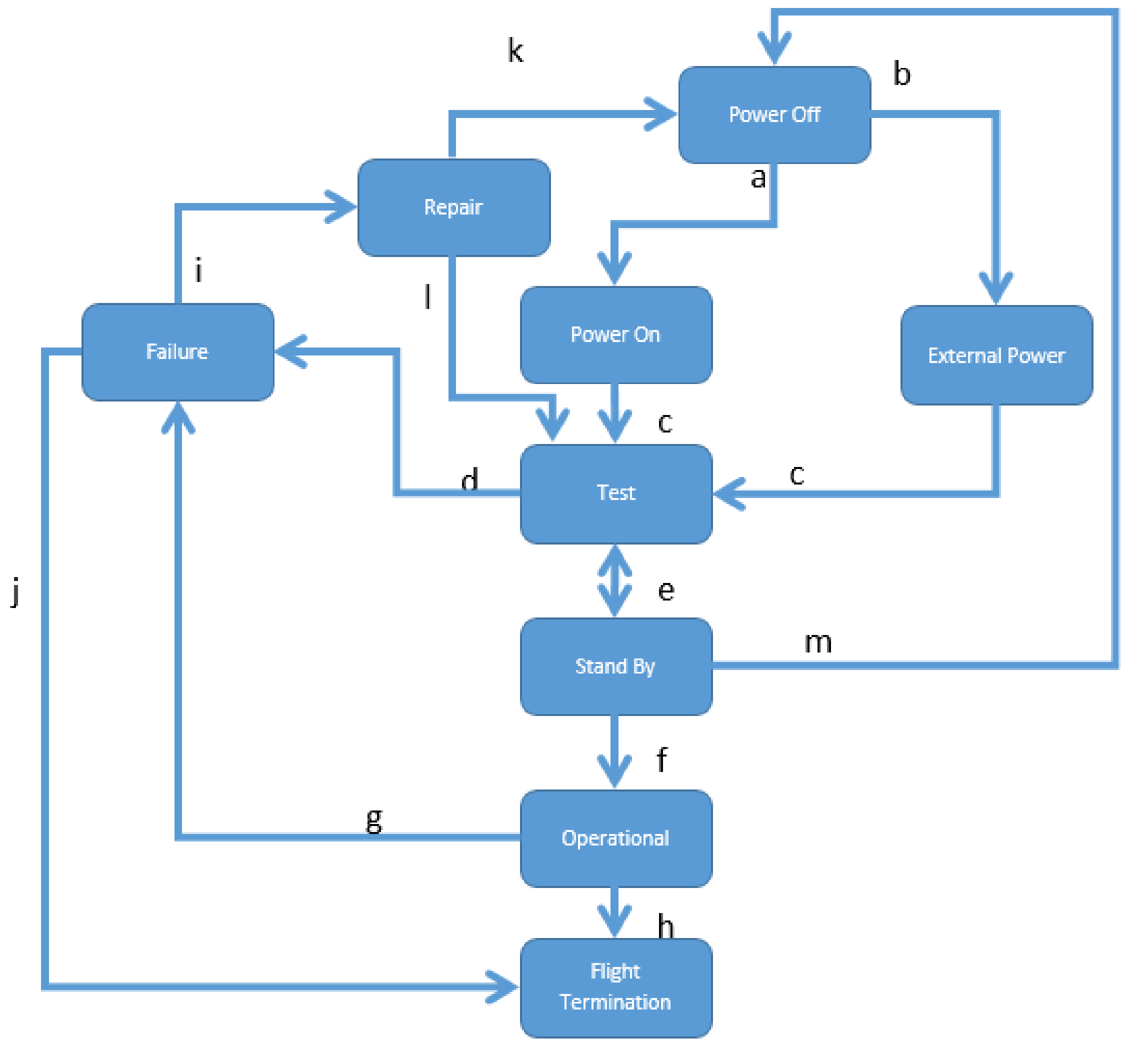

Figure 46: Actuator System - Modes of Operation flow diagram

The various conditions are defined as follows:

a) Refers to the fulfilment of the request from the Missile MCP to enter the Power On mode.
b) An external user initiates the External Power mode (for test purposes only).
c) After the power initiation has taken place (Power On/External Power modes) and the system is fully powered, the actuator system enters a test mode. Built-in tests are carried out to assess the integrity of the system.
d) If a failure occurs, the system enters a failure mode.
e) If the tests are successful, the system enters a standby mode. If required, the actuator system will be instructed to return to the test mode during system testing or maintenance.
f) When required by the missile system, the actuator is requested to enter the operational mode (by the MCP).

g) Should a failure occur with the actuator system, or if there is a communication failure between the MCP and actuator, the system enters a failure mode.

h) If a request is received from the MCP, the actuator enters flight termination mode.

i) If the failure can be resolved internally or by an external user (during maintenance or acceptance testing), the system will enter a repair mode.

j) If the failure cannot be resolved during free flight, the MCP will request the actuator to enter a flight termination mode.

k) During maintenance testing or acceptance testing, the system will reset itself if required by the solution to repair the failure and enter a Power Off mode.

l) If the solution to resolve the issue does not require a system reset, the system will enter the Test mode.

m) If required by the external user during acceptance testing/maintenance testing, the system can be manually switched to Power Off mode.

Table 16: Modes and associated Functional Requirements

	Power On	Standy By	Operational	Test	Maintenance	Failure	Flight Termination	Power Off	External Power
FR1			■	■					
FR2							■		
FR3	■	■	■	■	■	■	■		
FR4	■	■	■	■	■	■	■		
FR5			■	■			■		
FR6			■	■			■		
FR7	■	■	■	■	■	■	■		■
FR8				■					■
FR9					■				■
FR10								■	
FR11								■	

Assessing the Failure modes of a system is necessary in order to ensure a system continues to operate as intended. The conditions/events related to a failure occurring is referred to as Failure Modes in J. Moubray [120]. According to J. Moubray [120], it is crucial to define the functions and the Performance Requirements of the system to gain a better understanding of what the possible failure modes will be for the system.

Once failure occurs, the system enters a Failed State, also called a Functional Failure. It is named as such since the system is unable to function as intended [120]. The Failed State for the actuator is a sub-state of a Termination State. Within the failed state, there are two lower states, namely the internal power failure state or the External power failure state. The latter refers to a failed state experienced during testing and maintenance. During this period, the actuator can be repaired if required.

The former refers to when the missile is using the actuator in captive and free flight. During these periods, the actuator is not accessible for repair. It, therefore, results in the Flight Termination mode for the actuator, which in free flight would cause the missile to tumble from the sky, or in captive flight, it would send a signal to the missile that it is non-functional, which in turn would relay the message to the launch platform.

The effects of the failures are linked to the failure events, as detailed and discussed in Moubray [120]. The events and their descriptions are described further in APPENDIX D.

The actuator is a vital system with regard to flight path alteration of the missile system. The criticality of the failures was important to assess as they impact the surrounding systems and influence the missile's operation. For this study, the failures were assumed to have equal importance. The delay times in the failure mode analysis were assumed values as these values should be determined based on the needs of the system once components have been selected.

The actuator states were then determined. A system is in a state when the behaviour it showcases remains constant or steady for a meaningful period [121]. In a particular state, a variety of modes can occur as long as they align with the values of that state.

The states identified for the actuator are the Dormant State, the Operational State and the Termination State. These are indicated in Table 17 and are linked to the modes which align to the state values.

Table 17: States and associated Modes

Mode	State		
	Operational	Termination	Dormant
Power On	■		
Stand By	■		
Operational	■		
Test	■		
Maintenance	■		
Failure	■	■	
Flight Termination		■	
Power Off			■
External Power			■

The physical characteristics of the actuator (taken from the Missile Design in APPENDIX A) are shown in Table 18.

Table 18: Actuator Physical Characteristics

	Characteristic	Quantity
1	Shall fit within the missile diameter	178 mm
2	Shall fit within the defined actuator volume.	0. 0074 m^3

The human factors requirements were identified in Table 19.

Table 19: Actuator Human Factor Requirements

	Characteristics	Quantity
1	Shall have an external interface to a human user. The interface would allow for programming, maintenance and integration	Designated user interface

4.3.2 ASYS Requirements Validation

Validation of the outputs from the Requirements Analysis process is necessary to ensure the system will meet the required outcomes. The validation processes, as described in Section 2.1, were used. The requirements were evaluated and can be assumed to be validated as a detailed verification and validation of the actuator design is outside of the scope of this work.

4.3.3 ASYS Functional Analysis

In this study, functions are high-level operations performed by the system, and Functional Requirements are achieved through the system's functions. The Functional Requirements and other supporting detail developed previously were used to create a deeper understanding of the ASYS. This understanding provided the insights that aided in the definition of the system functions.

The functional flow diagram in Figure 47 illustrates the primary functions of the actuator. The format of the diagrams was based on the functional flow block diagrams from the Systems Management College [111].

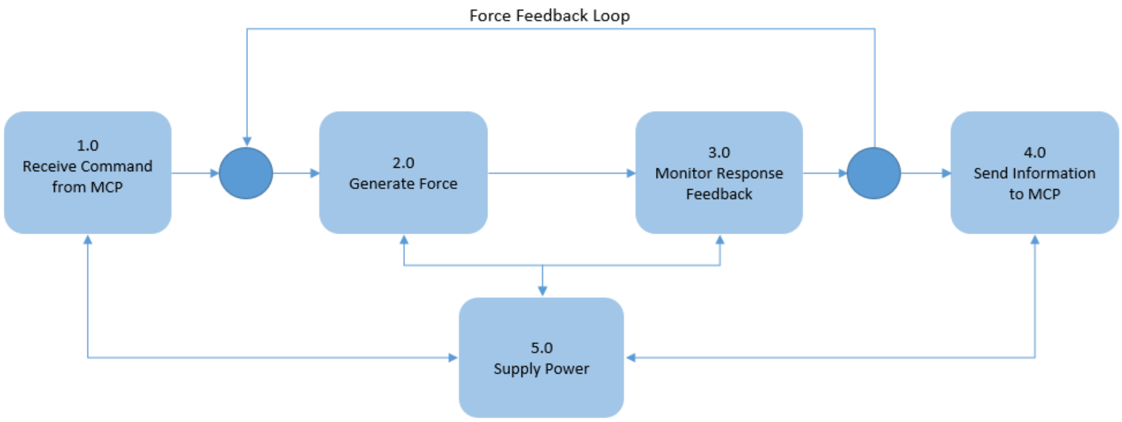

Figure 47: Actuator System-Level Functional Flow Block Diagram

The input from and the outputs to the missile system are not illustrated in Figure 47. It can be seen that the information enters the system at 1.0 Receive Command from the MCP function. It then enters the 2.0 Generate Force function, which then enters the 3.0 Monitor Response Feedback function. After this, the system then enters the 4.0 Send Information to MCP function.

An FFBD is meant to define functions and not define solutions for the system to be designed. The process of defining lower-level functional decomposition was carried out to determine the lower-level functions. This is required to develop the Functional Architecture required to carry out the design according to Systems Management College [111]. The lower-level functional decomposition for the ASYS can be seen in APPENDIX D.

The FGM, the system of interest, would be related to the "Generate Force" function. The sub-functions between the 2.0 Generate Force Function and the 3.0 Monitor the Response feedback for the actuator was broken down as seen in Figure 48 from the Functional Analysis for the actuator system from APPENDIX D.

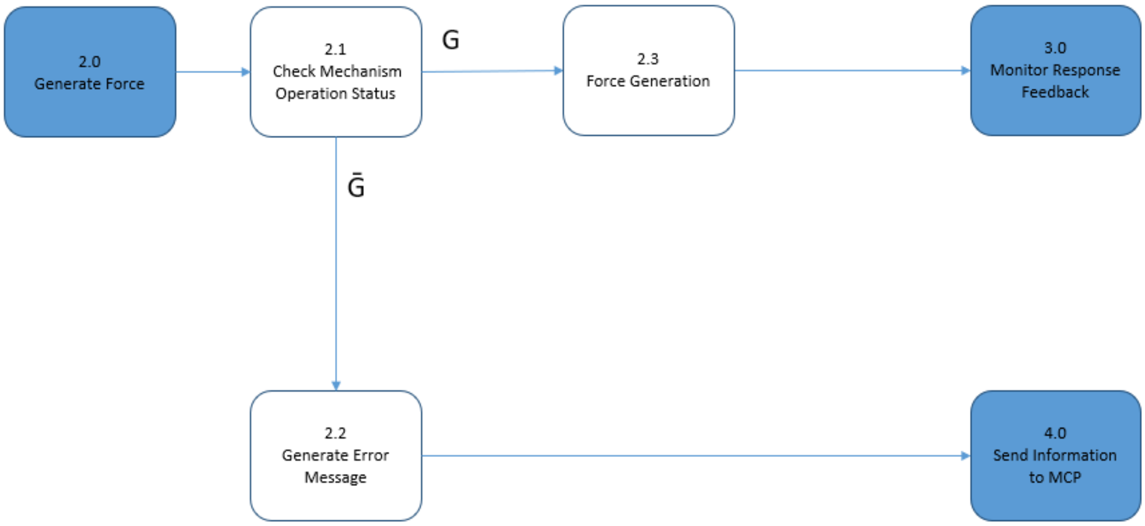

Figure 48: Functional Decomposition of the Generate Force Function

The lower-level functional decomposition of the "Generate Force" Function gave insight into the functions for the FGM.

4.3.4 ASYS Functional Verification

The purpose of functional verification is to verify the totality of the functional structure developed in the previous section. The verification involves evaluating the functions against the system requirements.

For this study, a tabulation of requirements and functions was employed. Table 20 highlights the relationship between the system requirements and the system functions.

Table 20: Downward and Upward traceability of Actuator System Requirements

Index	System Requirements and Constraints	Function	Functional Requirements	Performance Requirements
1.1.1	The Actuator must alter the missile flight path to intercept the intended target	1.0; 2.0; 3.0; 4.0; 5.0	1;2;5;6;7,9	1a;2a;2b;5a;6a;7a;7b;7c,9a
1.1.2	The Actuator must maintain the missile flight path	1.0; 2.0; 3.0; 4.0; 5.0	1;2;5;6;8;9	1a;2a;2b;5a;6a;8a;8b;8c;9a
1.1.3	The Actuator must not interfere with the launch platform	-	3	3a
1.1.4	Fit within the designated missile volume	-	3	3a
1.1.5	Operate within a required timeframe	1.0; 2.0; 3.0; 4.0; 5.0	7;8	7a;8a

The verified Functional Architecture was then used to develop the Physical Architecture in the Synthesis phase.

4.3.5 ASYS Architecture Definition

During the Physical Architecture design or the process of Synthesis [10], the functional building blocks are transformed into physical blocks that details the organisation layout of crucial components, internal and external interfaces, and relevant design constraints. A preferred Physical Architecture solution was selected from a set of concepts.

The functions and their related sub-functions were evaluated to develop suitable architecture as a first step. The top-level functions were separated into mechanical and electronic subsystems depending on the main focus of the function. In Figure 49, the demarcation of the subsystems, depending on the functions, are illustrated.

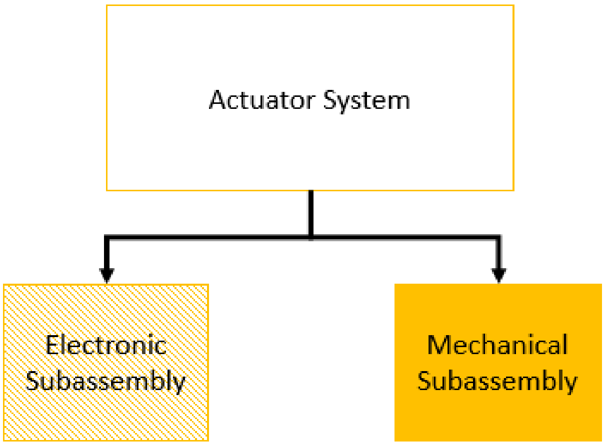

Figure 49: Initial Architecture Breakdown

The electronic architecture would manage the following functions:

- Receive Command from MCP
- Monitor response Feedback.
- Send Information to MCP
- Supply Power

The mechanical architecture would focus on the "Generate Force" function.

The hatched blocks will refer to electronic architecture, and the solid-coloured blocks will denote mechanical architecture.

During the next step, the functions were evaluated to determine the Physical Architecture. The diagram in Figure 50 illustrates the decomposition of the architecture.

The architecture decomposition of the actuator is only a single approach to the architecture that would be able to achieve functions defined for the actuator. An alternative architecture can be seen in Figure 51.

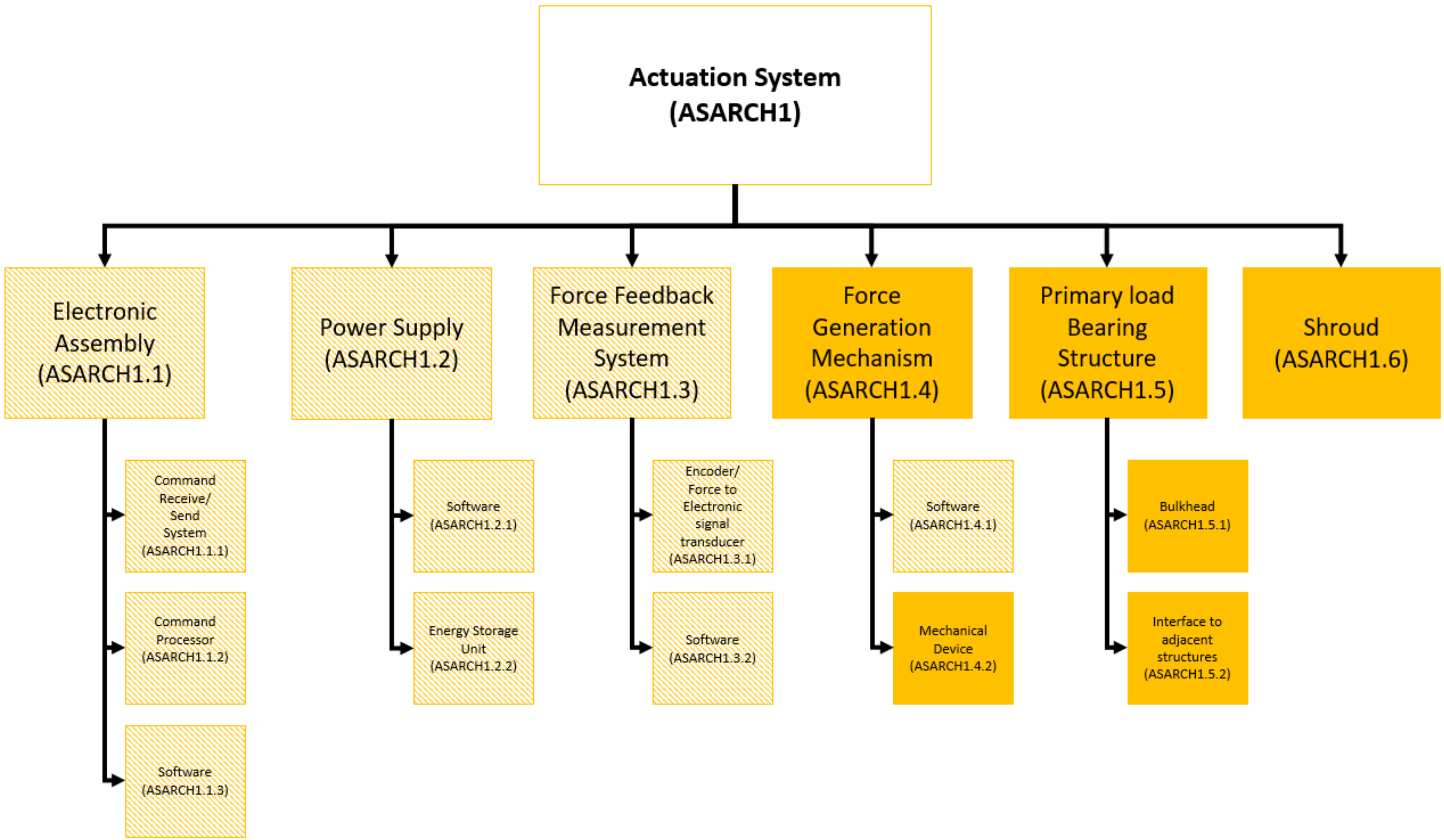

Figure 50: Actuator Physical Architecture based on Functions – Type A

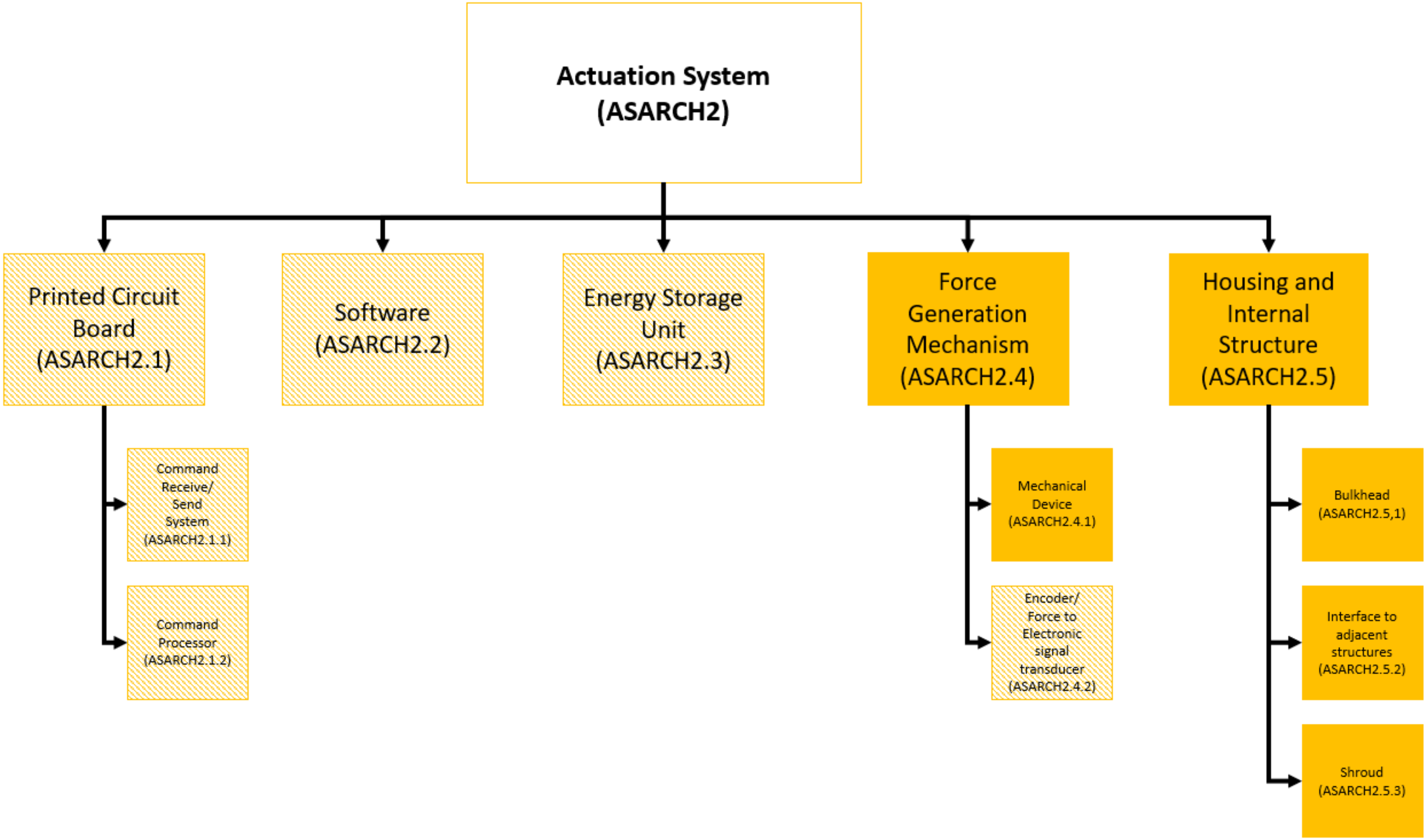

Figure 51: Physical Architecture based on Functions – ASACRCH2

Table 21 illustrates the relationship between the defined architecture and the main functions of the system. In places where the architecture is linked to more than one function, it refers to the architecture assisting in performing some of the functions.

Table 21: Relationship between the system architecture and the central system functions

		Functions				
		F1.0	F2.0	F3.0	F4.0	F5.0
		Receive Command from MCP	Generate Force	Monitor Response Feedback	Send Information to MCP	Power Supply
Architecture	ARCH1.1.1	■			■	
	ARCH1.1.2	■	■	■	■	
	ARCH1.1.3	■			■	
	ARCH1.2.1	■	■	■	■	■
	ARCH1.2.2					■
	ARCH1.3.1			■		
	ARCH1.3.2		■	■		
	ARCH1.4.1		■			
	ARCH1.4.2		■			
	ARCH1.5.1	■	■	■	■	■
	ARCH1.6	■	■	■	■	■
	ARCH2.1.1	■			■	
	ARCH2.1.2	■	■	■	■	■
	ARCH2.2	■	■	■	■	■
	ARCH2.3	■	■	■	■	■
	ARCH2.4.1		■			
	ARCH2.4.2			■		
	ARCH2.5.1	■	■	■	■	■
	ARCH2.5.2		■			
	ARCH2.5.3	■	■	■	■	■

The functional architecture was used to define two different physical architectures. The physical architecture is not limited to the structures created as other configurations may be possible. Its components, for each structure created, were able to be traced back to the defined functions, which were linked to the requirements baseline. This was mentioned in Section 4.3.4. Each of the structures created is, therefore, a viable option. The structure could be broken down further to better identify existing components and new design work. For the purpose of this study, however, the components were kept at the level defined to not limit the creativity when considering the use of Smart Material for the SOI. A selection process was necessary to determine which architecture is most suitable for this study. The Architecture Selection process is described in the following section.

4.3.6 ASYS Architecture Selection

The process of Architecture Selection is required to determine the most suitable system architecture to use for the concept generation. According to Cross [122], the practice relating to evaluating design alternatives is to evaluate them based on a set list of objectives. Through the Systems Engineering approach followed in the previous sections, a list of design objectives can be compiled. This will be based on user requirements, Functional Requirements, Performance Requirements, operational context requirements, and the defined functions of the system.

The method proposed by Cross [122] for evaluating alternatives, the Weighted Objective Method, was demonstrated through examples of concept evaluation. This method was employed for the architecture selection.

As seen in APPENDIX D, the second architecture (ARCH2) was found to be the preferred of the two architectures developed. Therefore, going forward, ARCH2 will be used as the ASYS Physical Architecture in this study.

With the conceptual missile designed and the ASYS architecture selected, some of the inputs for the FGM context were developed, which was used during the Requirements Analysis stage of the SOI design.

With the SOI identified, the missile-related inputs and the actuator system inputs determined, the Systems Engineering Process for the FGM was initiated. The Systems Engineering approach described in Chapter 3.2 was followed for the design of the missile's FGM, starting with its Requirements Analysis.

5. Force Generation Mechanism System Design

The system design for the Force Generation Mechanism (FGM) was carried out based on the method outlined in Section 3.2, which was derived from the system engineering approach defined in Section 2.1. This chapter is Step 2 of the method followed for this study, as seen in Figure 52.

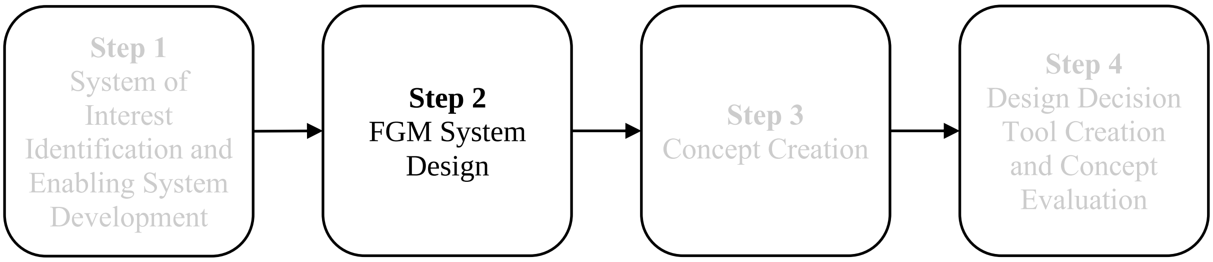

Figure 52: Step 2 of the Method

The purpose of this chapter was to develop the requirements baseline, the Functional Architecture and the Physical Architecture. The outcomes from the iterative approach are captured in this document.

5.1 FGM Requirements Analysis

The process followed for the FGM Requirements Analysis to gain additional inputs and to elicit better requirements, as mentioned in Section 3.2, can be illustrated as shown in Figure 53.

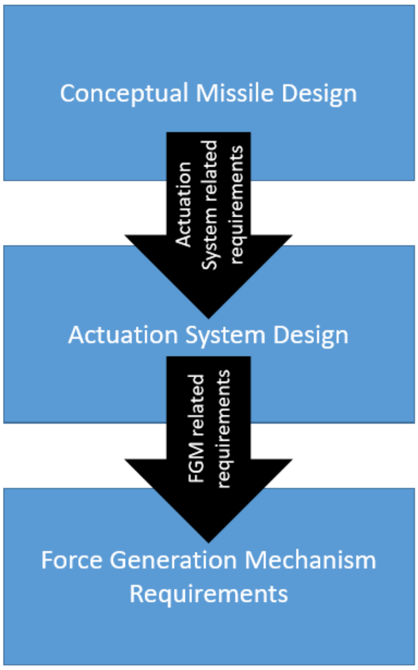

Figure 53: Illustration of the path followed for the FGM requirements

As shown in Figure 53 (from top to bottom), the conceptual missile design was carried out first, which was followed by the ASYS system design. The following sections will detail the FGM system design, the remaining step in the path illustrated in Figure 53.

5.1.1 FGM Stakeholder needs, expectations and constraints

Table 22 highlights the needs, expectations and constraints for all relevant stakeholders relating to the system of interest. For this study, only the stakeholder inputs seen in Table 22 were identified. These inputs will be used for the design going forward.

Table 22: Stakeholder Needs, Expectations and Constraints

Stakeholder	**S**	**Needs, expectations and constraints**
OEM of Missile	1.	The FGM shall provide a force that will be used to alter the missile flight path to intercept the intended target
	2.	The FGM shall aid in maintaining the missile flight path
	3.	The FGM shall fit within the designated missile volume
	4.	The FGM shall operate within a required timeframe
	5.	The FGM shall not interfere with the launch platform

5.1.2 FGM Project constraints

Project constraints are important inputs to consider, as they can have a significant impact on the design of a product. Examples of these constraints could include financial, end-user certificates, technology, suppliers and client constraints [123]. For this study, only the constraints highlighted in this chapter were identified to showcase the process followed.

5.1.2.1 FGM End Date

The conceptual design is to be completed in six months.

5.1.2.2 FGM Technology

Alternative technology and actuation methods should be investigated instead of generic missile actuation methods.

5.1.3 FGM Operational Context

The Operational Context refers to the environment in which the product to be designed would be required to function. It includes everything that has an influence on the operation of the product, whether it be constraints or system inputs.

5.1.4 FGM Concept of Use

The Concept of Use (CONUSE) describes how the product will be used in a variety of situations, and the CONUSE for the missile system was described in Section 4.2. The system of interest, the FGM, would have a CONUSE as follows:

"Assist the higher-level missile system to intercept a target at a range of 120 km by providing the required forces to keep the missile travelling along a required trajectory towards the target for as long as required by the missile system."

5.1.5 FGM External Constraints

External constraints refer to environmental and physical constraints that influence the system to be designed.

The FGM will form part of the actuator system within the missile system and will, therefore, be subjected to the same external environment. Based on the location of the actuator unit within the missile structure (refer to APPENDIX A), there would be an influence due to the interface to the missile system. The following external constraints were identified:

Table 23: FGM External Constraints

	Constraint	**Limits (Minimum and/or maximum)**
1.3.1	**Operating environment**	
1.3.1.1	Temperature	-40 to +85 Degrees Celsius
1.3.1.2	Aerodynamic Loads	1685 N
1.3.1.3	Aerodynamic Heating	334.76 K (for t = 90s) 891 K (Maximum temperature)
1.3.1.4	Vibration	Refer to MIL-STD-810G
1.3.1.5	G-Loading	30 g
1.3.2	**Missile Airframe**	
1.3.2.1	Space available	0.0074 m^3 (0.178 m Diameter)
1.3.3	**Rocket Motor**	
1.3.2.1	Thermal Loading	373- 473 K
1.3.2.2	Space constraint	0.08 m (Blast tube diameter)

The operating environment for the FGM would be the same environment the ASYS within the missile system would experience. The temperature that is expected to influence the FGM would be the environmental temperature range during the missile operation; this excludes the aerodynamic heating as the heat load path requires further analysis, which is beyond the scope of this study. The aerodynamic loads that have an impact on the FGM would be a result of its placement within the missile layout and the missile system aerodynamics.

The aerodynamic loads that impact the FGM have been estimated to be 1685 N based on the initial calculations in accordance with the conceptual missile design by Fleeman [60]. (Refer to Section 4.2)

Vibration refers to the vibration spectrum the missile will experience. This includes both carriage flight (experienced while still on the aircraft store) and free flight (in flight) vibration. Carriage flight vibration values are based on typical fighter aircraft flight vibration taken from MIL-STD-810G [124]. The free-flight vibration is based on military test specifications and established test data. Vibration test specifications should be evaluated based on the standard in MIL-STD-810G.

The g-loading was specified during the conceptual missile design. This is the expected worst case the missile is expected to see when engaging its specified target.

The Missile Airframe constraints refer to the limitations imposed onto the FGM based on its interface to the airframe. The space/volume allocated to the FGM is limited by the missile system. It is based on inputs from the conceptual missile design. Refer to APPENDIX A.

Due to the decision to have the actuator at the rear of the missile, the rocket motor would influence the FGM's operation. The thermal loading during and after the rocket motor is fired is a limiting factor. The rocket motor temperature values in Table 23 are based on rocket motor blast tube temperatures discussed in G. P. Sutton *et al*. [117]. The space available is influenced by the rocket motor blast tube. The blast tube diameter is based on the rocket motor's throat area, 0.003 m^2, which is a throat diameter of 0.061 m. According to Fleeman [60], the blast tube diameter is larger than the throat diameter, and therefore a diameter of 0.08 m was assumed.

5.1.6 FGM Mission Profiles

Defining scenarios or mission profiles allows one to outline how the system will operate or be operated by the end-user. The mission profile defined in this section is arranged in chronological order and highlights the various scenarios the FGM will face during its period of operation.

1. Once power is received from the launch platform, a system functional test is performed.
2. After the initial functional test, if the test was successful, then the FGM enters a standby mode. If not, it enters a failure mode, and a power reset from the launch platform is required.
3. Once the missile system is launched and is clear of the launch platform, the FGM will be fully functional.
4. The FGM will assist in maintaining the missile flight path towards the intended target by executing guidance and control commands.
5. The FGM will provide a force to alter the missile flight path to intercept the intended target by executing guidance and control commands.
6. If the missile does not intercept the target or is required to end its mission, the actuator shall enter a flight termination mode, and the FGM will assist the missile in tumbling towards the ground.

5.1.7 FGM Measures of Effectiveness

The Measures of Effectiveness (MOE) refers to limits by which the system satisfies its mission when used by the end-user in the correct operational environment [10]. The MOE is meant to be defined in terms of anticipated outputs of the system but must be independent of any final design chosen. According to the INCOSE Systems Engineering Handbook [8], the defined MOE should be able to identify the overall performance of the final solution chosen.

The defined MOEs will be used to check if the FGM meets or exceeds the requirements needed for the subsystem to be an effective solution for the intended actuator within the defined missile system.

1. Bandwidth/Rate of Response
2. Energy Usage
3. Rate of change in Missile pitching moment.
4. Adherence to space requirements
5. Adherence to mass requirements

5.1.8 FGM System boundaries and external interfaces

The definition of system boundaries assists in characterising other interacting systems which are out of the system designer’s control. The external interfaces can be defined, and a greater understanding can be obtained as to the input and output requirements of the system to be designed.

Figure 54 is an illustration of the FGM and its related systems interaction. This illustration was created based on the inputs from the missile design (see Section 4.2 and APPENDIX A) and other information related to the life cycle of the FGM.

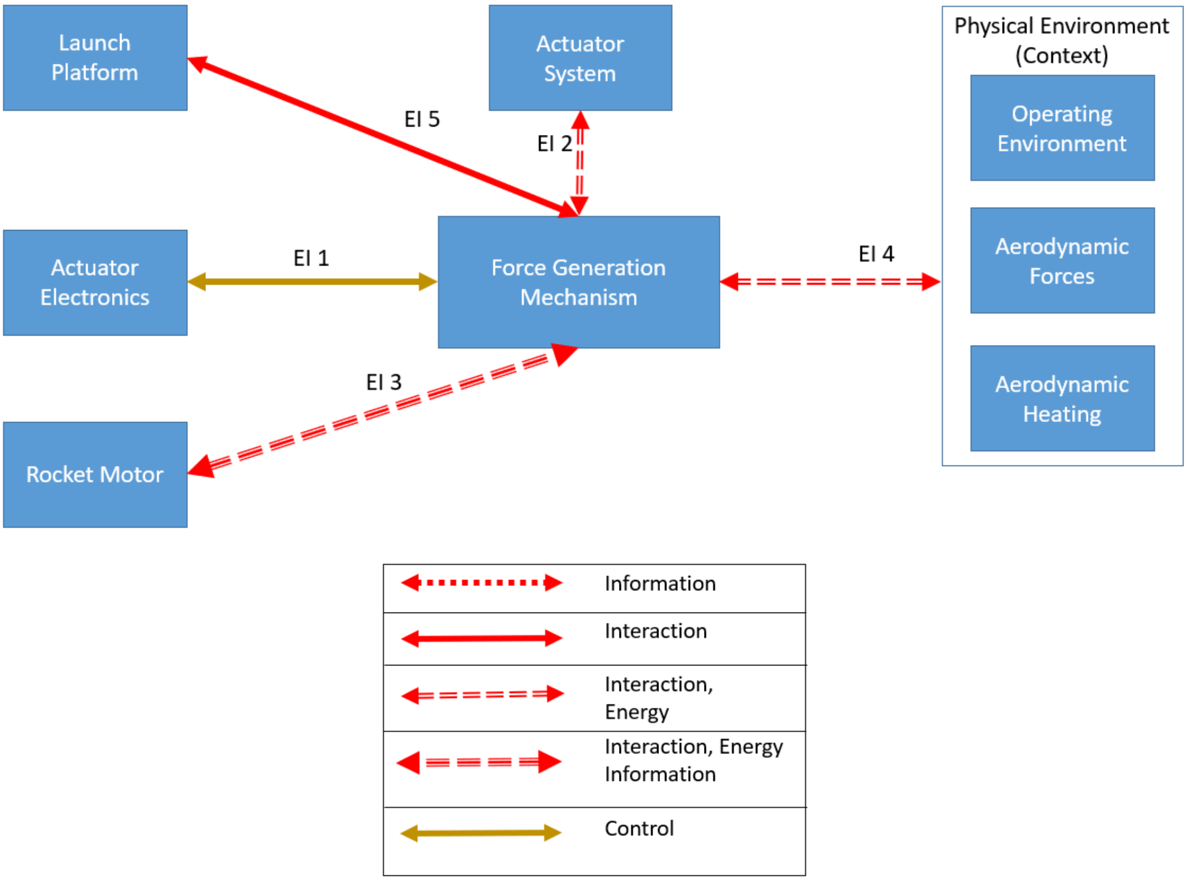

Figure 54: Context Diagram: FGM System - External Interfaces

Figure 54 depicts the external interfaces (the arrows labelled EI 1-8). The details of these interfaces are as follows:

1. This interface is the link is required for the Actuator Electronics to send the FGM inputs to operate. (Control)
2. The interface to the Actuator System refers to the physical connection the actuator will have with the FGM. (Interaction and Energy)
3. The rocket motor interface relates to the influence the rocket motor would have on the FGM. This was considered based on the general placement of a tail ASYS. (Interaction, Energy and Information)
4. The physical environment has an influence on the FGM. The physical environment refers to the operating environment and the aerodynamic loads that the FGM would have to overcome to function effectively. (Interaction, Energy)
5. The launch platform has a direct influence on the volume the system can occupy. The interface is, therefore, a constraint to the actuator system. (Interaction)

In Figure 54, the different arrows used to depict the various flows between interfaces for the context diagram are defined. The flows such as information, control, energy and interaction were considered.

Information flow refers to the flow of data feedback or measurements at the relative interfaces. Control flow refers to the control data sent at a specific interface that alters the function of the system. Energy flow refers to thermal energy and vibration. Interaction flow refers to the physical influence surrounding systems have on the actuator system. This relates to the space constraints the actuator would experience.

5.1.9 FGM Utilisation Environment

The FGM shall withstand the same environment as the next higher-level system, the actuator system for the BVR missile described in Section 4.2.

5.1.10 FGM Life Profile

The Life Profile refers to the item's post-development life cycle, which includes where it will be used, how it will be integrated, how it will be accepted, user training, system support, and end of life processes (decommissioning and disposal). [10]

In order to define the life profile, the various processes post-integration of the system were envisioned, based on the Systems Engineering Body of Knowledge [10], and the following life profile was determined:

1. Acceptance Testing (Performance related testing pre-integration to the next higher-level system)
2. Be transported.
3. Remain in a dormant state.
4. Enter Maintenance State
    a. Be powered.
    b. Be tested (within missile system)
    c. Be powered down.
    d. Be repaired (if required)
5. Be utilised by the actuator system.
6. Decommission and dispose (if beyond proposed shelf life)

Acceptance testing was considered as a part of the life profile as the ability to evaluate the actuation would be necessary if the system is to be tested for acceptance before the next level integration, and therefore the interface to allow for the acceptance testing would be a design consideration.

The remainder of the life profile was determined based on the life of the FGM incorporated into the actuator system—the typical shelf life for a missile is 10 to 20 years [118]. Therefore, the actuator system and its system elements, such as the FGM, would be subjected to this constraint. The shelf life of weaponry is a concern, and an accurate performance specification could assist in developing products with better shelf life [118]. This points to the necessity of Systems Engineering as a basis for the design and to develop a maintenance schedule.

5.1.11 FGM Functional Requirements

Deriving the Functional Requirements involves evaluating what the requirements of the system would have over its life profile [10].

The following list describes the functions identified (based on the life profile seen in Section 5.1.10) that the FGM is required to perform:

1. The FGM shall generate the required force when required.
2. The FGM shall perform during the entire operational period.
3. The FGM shall withstand the loads during transportation.
4. The FGM shall withstand the loads during operation.
5. The FGM shall be able to be functional after a set storage period.
6. The FGM shall be disposable at the end of its shelf life.
7. The FGM shall have sufficient no-load bandwidth.

It is important to note that during the process of deriving the Functional Requirements, the FGM was considered as a whole, and the Functional Requirements defined are that of the entire system.

The links between the life profile of the FGM and the Functional Requirements defined can be seen in Table 24. The grey cells in the matrix depict the link between life profile and functional requirement.

Table 24: FGM Life Profile and FGM Functional Requirements

	FR1	FR2	FR3	FR4	FR5	FR6	FR7
LP1	■	■		■	■		■
LP2		■	■				
LP3			■		■		
LP4	■	■			■		■
LP5	■	■	■	■	■		■
LP6						■	

5.1.12 FGM Performance Requirements

The Performance Requirements were based on the Functional Requirements developed in the previous Section (Section 5.1.11). The Performance Requirements are defined to characterise how well the function needs to be executed in order for the system to be valid based on the defined MOE [10].

The following is a summary of the previously defined functions and their related Performance Requirements:

1. The FGM shall generate the required force when required (to generate the required missile pitching, yaw or roll moment)
    a. Generate a maximum force to allow the missile to achieve a manoeuvre limit of 30 g (1685 N Minimum Required)
2. The FGM shall perform during the entire operational period.
    a. The FGM shall perform for > 180 s.
3. The FGM shall withstand the loads during transportation.
    a. Endure all transportation within transportation packaging based on the Military Standard [124]
4. The FGM shall withstand the loads during operation.
    a. Withstand the maximum force during the manoeuvre limit of 30 g (1685 N Maximum Applied Load)
5. The FGM shall be able to be functional after a set storage period.
    a. Shall have a Shelf life of 10 years
    b. Endure conditions within packaging based on the Military Standard [124]
6. The FGM shall be disposable at the end of its shelf life.
    a. Must adhere to environmental standards.
7. The FGM shall have sufficient no-load bandwidth.

a. The bandwidth should be greater than 25 Hz, with no load.

5.1.13 FGM State and Mode Analysis

5.1.13.1 Overview of System Modes

A mode is a label given to a set of user-based capabilities that can be used to command and control the system to achieve the required outcomes of the system. [119]

The modes are defined as follows:

a) Power Off Mode refers to the mode when the FGM is not powered either from within the missile or an external source.
b) Power-On Mode is when the FGM is powered from within the missile.
c) External Power Mode is when the FGM is powered from outside the missile.
d) Operational Mode is when the FGM is able to execute the flight commands received from the Actuator electronics.
e) Failure mode is entered into once the FGM does not receive any feedback from the missile MCP. Upon entering this mode, the actuator then performs a series of system checks (built-in tests) to identify and resolve the problem.

Figure 55 highlights the modes. These modes are derived from the life profile of the FGM. Each blue block refers to a distinct mode, and the arrows indicate the conditions for the transitions between the modes. The modes defined in Figure 55 are the internal modes of the FGM. A state mode analysis including was not carried as it is beyond the scope of this study.

Table 25 illustrates the relationship between the defined modes and the previously defined functional requirements of the FGM. The grey cells of the matrix depict the link between the functional requirement and the modes.

The complete correlation between the actuator modes and the missile system modes were not evaluated in this study.

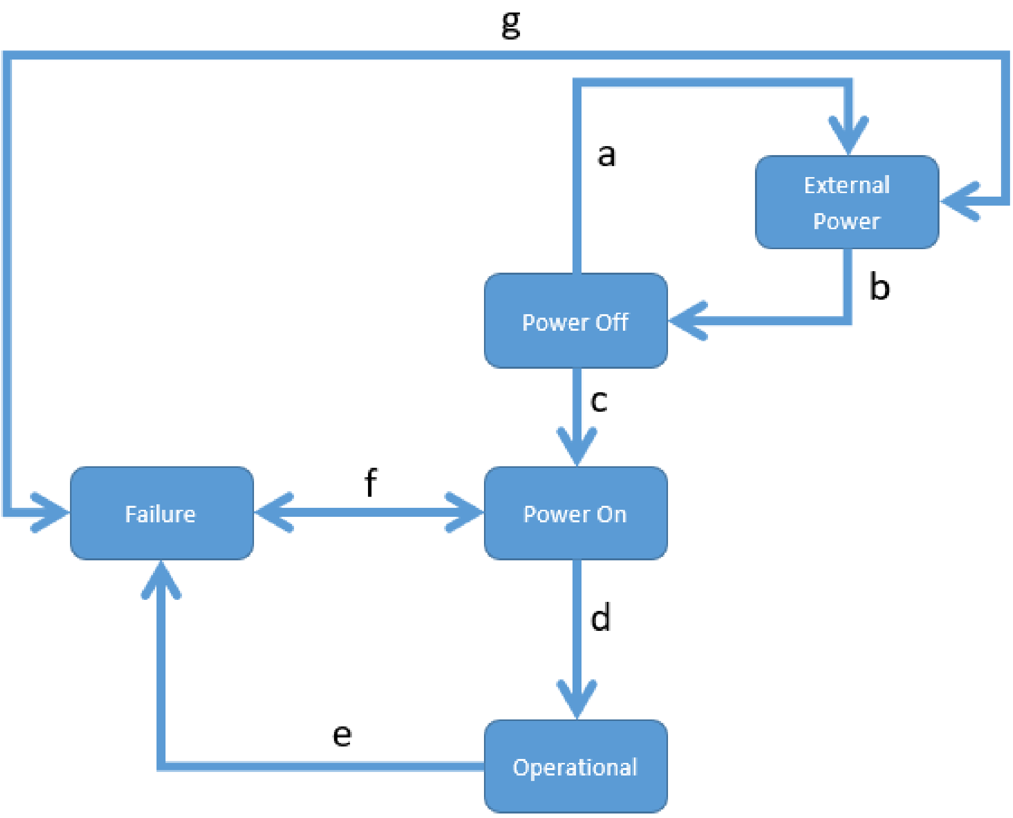

Figure 55: Modes of Operation of the FGM

The various conditions are defined as follows:

a) An external user initiates the External Power mode (for test purposes only).
b) The fulfilment of the request from the Actuator Electronics to enter the Power On mode.
c) After the power initiation has taken place (Power on Mode) and the system is fully powered, the actuator system enters a test sequence. Built-in tests are carried out to assess the integrity of the system.
d) If the tests are successful, the system enters Operational mode.
e) If a failure occurs, the system enters a failure mode.
f) Should a failure occur with FGM during the Power on Mode, the system enters a Failure mode.
g) Should a failure occur with FGM during the External Power Mode, the system enters a Failure mode.

Table 25: Modes and associated functions of the FGM

	Power On	Operational	Failure	Power Off	External Power
FR1		■			■
FR2	■	■	■		■
FR3				■	
FR4	■	■			■
FR5	■	■	■		■
FR6				■	
FR7	■	■			■

5.1.13.2 The Impact of Failure modes

Assessing the Failure modes of a system is necessary in order to ensure a system continues to operate as intended. The conditions/events related to a failure occurring is referred to as Failure Modes in J. Moubray [120]. As described in J. Moubray [120], it is crucial to define the functions and the Performance Requirements of the system to gain a better understanding of what the possible failure modes will be for the system.

For the FGM, these functional and Performance Requirements have been defined in Section 5.1.11 and 5.1.12.

Once failure occurs, the system enters a failed mode, also called a functional failure. It is named as such since the system is unable to function as intended [120].

The possible failure events or failure modes identified are as follows.

1. A reduced pitching rate of the missile due to a reduced force generation rate
2. A reduced roll rate of the missile due to a reduced force generation rate
3. A reduced yaw rate of the missile due to a reduced force generation rate
4. The FGM does not receive sufficient/any power for the system to operate.
5. FGM does not Power-On.
6. The FGM enters the Power on Mode but does not enter the Operation Mode.
7. The Force from the FGM cannot be utilised by the actuator system.

The effects of these failures are necessary to understand the impact on the surrounding systems. The effects of the failures are linked to the failure events, as detailed and discussed in J. Moubray [120]. A summary of these effects for the failure events are described as follows:

a. The missile does not head towards the target.
b. It is a threat to the performance of the missile.
c. There is an impact on the performance of the missile and could result in the missile missing its target.
d. The missile, due to the FGM not functioning correctly, could intercept something unintended.
e. If experienced in free flight, no repairs are possible. A system check and a system reset may be necessary.

The FGM is a necessary system with regard to flight path alteration of the missile system. Understanding the criticality of the failures was needed to assess their impact on the surrounding systems and their influence on the missile operation. For this study, the failures were assumed to have equal importance.

5.1.13.3 States

A system is in a state when its behaviour remains constant or steady for a meaningful period [121]. In a particular state, a variety of modes can occur as long as they align with the values of that state.

The states identified for the FGM are the Dormant State, the Operational State and the Failed State. These are indicated in Table 26 and are linked to the modes which align to the state values.

Table 26: States and associated Modes for the FGM

Mode	State		
	Operational	Failed	Dormant
Power On	■		
Operational	■		
Failure	■	■	
Power Off			■
External Power	■		■

5.1.14 FGM Technical Performance Measures

These are usually related to the measures of effectiveness. For this study, the Performance Requirements for the Functional Requirements will be used as the technical performance measures along with the measures of effectiveness stated in Section 5.1.7 of this chapter.

5.1.15 FGM Physical characteristics

The FGM must fit within the space allocated in the missile. The missile's diameter is 178 mm, and the FGM allocated length is 410 mm. These constraints are based on the conceptual missile design in Section 4.2 and are illustrated in Figure 56. The defined space is meant to house the FGM and other related actuator components.

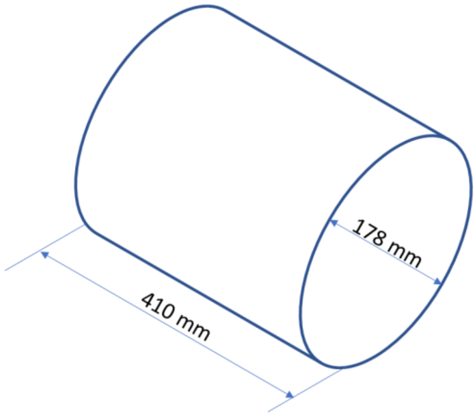

Figure 56: Illustration of actuator system dimensions

5.2 FGM Requirements Validation

The Requirements Analysis was repeated until the main requirements were elicited, as shown in Table 27.

Table 27: Summary of Requirements for the FGM

1	The FGM shall generate the required force when required	1685 N (Minimum)
2	The FGM shall perform during the entire operational period.	>180s
3	The FGM shall withstand the loads during transportation	See MIL-STD-810G
4	The FGM shall withstand the loads during operation	1735 N
5	The FGM shall be able to be functional after a set storage period	10 years (MIL-STD Conditions)
7	The FGM shall have a no load bandwidth greater than 25 Hz	> 25 Hz

The propagation of these requirements was validated, and the summary is in Table 28. The validation summary, based on the IEEE 1220-2005 [123] and as described in Section 2.1, focused on the assessment of the requirements baseline to check if the stakeholder needs, requirements, and system constraints have been accounted for during the Requirements Analysis phase.

Table 28: Summary of validation of requirements for the FGM

Index	System Requirements and Constraints	Functional Requirements	Performance Requirements
S1	The FGM shall provide a force that will be used to alter the missile flight path to intercept the intended target	FR1, FR2, FR3, FR4, FR5, FR7	FR1a, FR2a, FR3a, FR4a, FR5a, FR7a
S2	The FGM shall aid in maintaining the missile flight path	FR1, FR2, FR3, FR4, FR5, FR7	FR1a, FR2a, FR3a, FR4a, FR5a, FR7a
S3	Shall Fit within the designated missile volume	-	-
S4	Shall Operate within a required timeframe	FR2, FR4, FR7	FR2a, FR4a, FR7a
S5	Shall not interfere with the launch platform	-	-

The requirements have been evaluated and can be assumed to be validated for this study. This forms a portion of the expected outcomes from Step 2 seen in Figure 52. With the requirements validated, the system design entered the Functional Analysis stage of the process.

5.3 FGM Functional Analysis

Based on the Functional Requirements list in Section 5.1.11 of this chapter, the main Functional Requirements of the FGM were identified. This was done by evaluating the purpose of the system based on the higher-level system requirements.

The FGM was determined to be the system of interest in Section 4.1. Through the conceptual missile design and the actuator system design, the system of interest was also identified as the system that would provide the force needed to aid in the manoeuvring of the missile. This supports the initial decision to select the FGM as the system of interest. Therefore, the primary Functional Requirements of the actuator are to execute commands to alter and maintain the missile flight path.

According to Systems Engineering Fundamentals [111], Functional Flow Block Diagrams functionally define the system requirements. As described in Section 3.2, a Functional Flow Block Diagram (FFBD) was generated.

In this study, the functions are high-level operations performed by the system that achieve the Functional Requirements. The functional requirements developed in Section 5.1.11 were used to define the functions.

The FFBD in Figure 57 illustrates the primary function of the FGM. The format of the diagrams that follow was adapted from the functional flow block diagrams from the Systems Management College [111]:

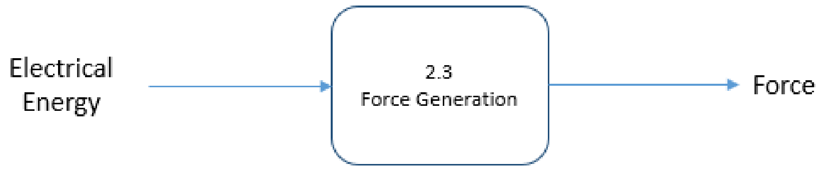

Figure 57: Actuator System-Level Functional Flow Block Diagram

Electrical energy is the input (indicated on the left of the function), and the output is the force utilised by the missile system.

The FFBD helped to develop the Functional Architecture required to carry out the design.

As described in APPENDIX D, once the command reaches the 2.0 Generate Force function (Function 2.0), the system must check the operational status of the FGM (Function 2.1, Check Mechanism Operational Status function). If the mechanism's status is acceptable, a "go" path is taken, denoted by the *G*. The system then enters the Force Generation function (Function 2.3), which would then ideally be able to increase, decrease or maintain the force required from the missile system. The Force Generation function was broken down into the sub-functions seen in Figure 58.

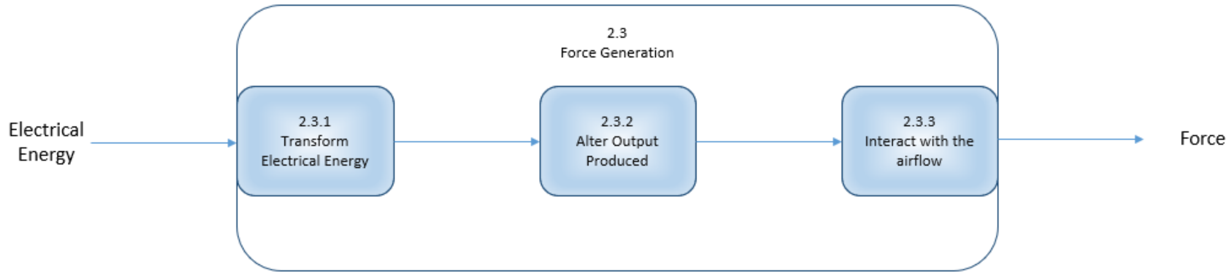

Figure 58: Functional Decomposition of the FGM Function

These sub-functions would include 2.3.1 Transform Electrical Energy, 2.3.2 Alter Output Produced, and 2.3.3 Interact with airflow. The FGM will experience the flow of functions mentioned to meet the force generation requirement. The electrical energy input will be transformed by the FGM into an output. This output may need to be altered to be usable by the system. Once that function is performed, it provides the input to interact with the airflow resulting in the force that will be utilised by the missile.

5.4 FGM Functional Verification

As mentioned in Section 2.1, the purpose of functional verification is to verify the totality of the functional structure developed in the previous section. The verification involves evaluating the functions against the system requirements.

The tabulation of the system requirements and the associated functions will highlight the downwards and upwards traceability of the requirements and derived functions. For this study, a tabulation of requirements and functions was employed.

Table 29 highlights the relationship between the system requirements and the system functions.

Table 29: Downward and Upward traceability of System Requirements

Index	System Requirements and Constraints	Functional Requirements	Performance Requirements	Function
S1	The FGM shall provide a force that will be used to alter the missile flight path to intercept the intended target	FR1, FR2, FR3, FR4, FR5, FR7	FR1a, FR2a, FR3a, FR4a, FR5a, FR7a	F2.3
S2	The FGM shall aid in maintaining the missile flight path	FR1, FR2, FR3, FR4, FR5, FR7	FR1a, FR2a, FR3a, FR4a, FR5a, FR7a	F2.3
S3	Shall Fit within the designated missile volume	-	-	F2.3
S4	Shall Operate within a required timeframe	FR2, FR4, FR7	FR2a, FR4a, FR7a	F2.3
S5	Shall not interfere with the launch platform	-	-	F2.3

The link between the FGM function and the system requirements have been established. Therefore, the Functional Architecture for the FGM can be considered to have been verified. This architecture will be used to define the Physical Architecture in the following chapter.

5.5 FGM Architecture Definition

As described in Section 2.1, during the Physical Architecture design or the process of Synthesis [10], the functional building blocks are transformed into physical blocks that details the organisation layout of crucial components, internal and external interfaces and relevant design constraints. A preferred solution is selected from a set of concepts.

The Physical Architecture is the representation of the physical elements that make up the internal structure of a system. The physical elements are derived from the functions the systems are required to perform.

The system's Functional Architecture, determined in Section 5.3, showcased a single top-level function for the FGM, Force Generation (Function 2.3 of the Actuator System).

This function and its related sub-functions were evaluated to develop suitable Physical Architecture as a first step. Using the Physical Architecture developed for the ASYS in Section 4.3.6, the FGM architecture was developed. The architecture labelled ASARCH 2.4.1 was used as the baseline architecture element for architectural development, as seen in Figure 59. In Figure 60, the demarcation of the subsystems depending on the functions are illustrated.

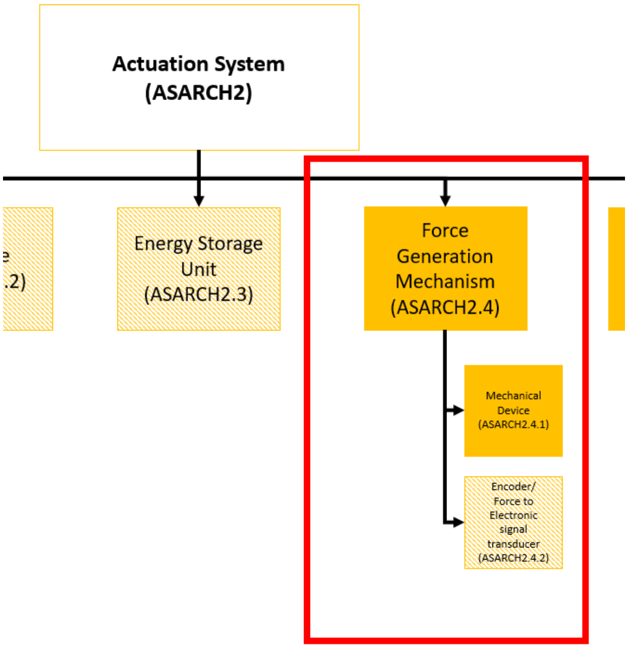

Figure 59: Selected ASYS Architecture

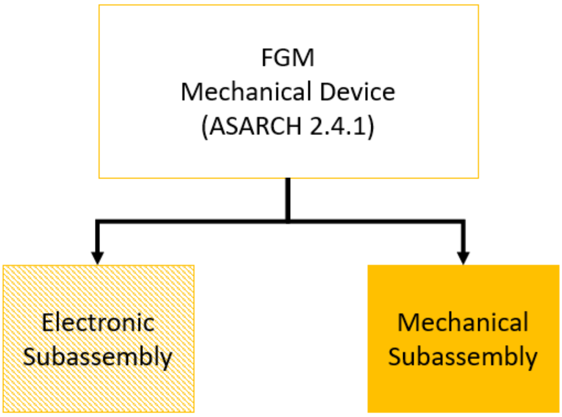

Figure 60: Initial Architecture Breakdown

The electronic architecture will handle Function 2.3.1, Transformation of the Electrical Energy. The mechanical architecture will also handle a portion of Function 2.3.1 as well as Function 2.3.2 Alter output produced and Function 2.3.3 Interact with the airflow.

The hatched blocks will refer to electronic architecture, and the solid colour blocks will denote mechanical architecture.

During the next step, the functions were evaluated to determine if there would be a possible Physical Architecture.

The Force Generation function requires different components to achieve the requirements. To identify the physical structure, the sub-functions were considered.

Focusing on the sub-function 2.3.1, the input electrical energy will be transformed by a device into useful work. This energy will be transferred through a train of components to give a final output force that the missile will during its manoeuvre process. These components will perform the sub-functions 2.3.2 and 2.3.3. This Physical Architecture for the FGM is illustrated in Figure 61.

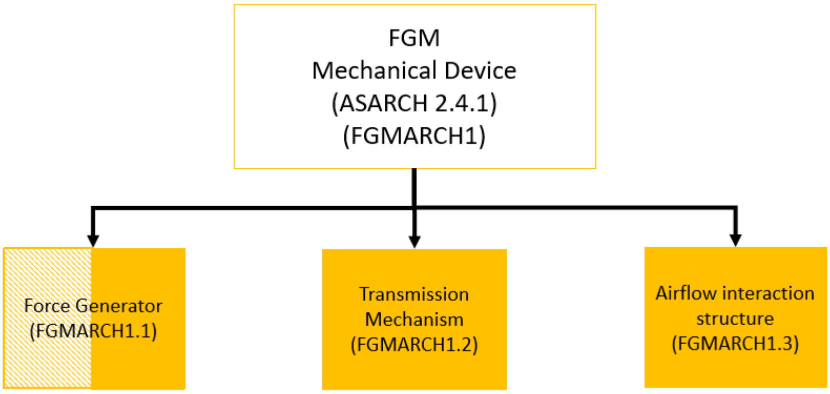

Figure 61: FGM Physical Architecture - ARCH 1

In Figure 61, the Force Generator (FGMARCH 1.1) transforms the electrical current into a force. The Transmission mechanism (FGMARCH 1.2) will alter the output produced by the force generator. The Airflow interaction structure (FGMARCH 1.3) will manipulate the airflow. Different components are capable of performing as these architecture elements; therefore, it was not broken down further to allow for freedom in the concept development.

For the generic FGM, the Physical Architecture would consist of a servo motor which would perform Function 2.3.1 by transforming the electrical energy into rotational motion, which would have an output torque. A lead screw and a nut would be coupled to the motor to change the rotational motion into linear motion, changing the motor torque into a linear force and amplifying the output load. This would fulfil Function 2.3.2. The fin would be the component that interacts with the airflow (Function 2.3.3), and the linear force from 2.3.2 would adjust how the fin interacts with airflow.

Table 30 illustrates the relationship between the defined architecture and the main functions of the system.

Table 30: Functional Allocation for the System Architecture

		Functions (FGM)		
		F2.3.1	F2.3.2	F2.3.3
		Transform Electrical Energy into a Force	Alter Output Produced	Interact with the airflow
Architecture (FGM)	ARCH1.1			
	ARCH1.2			
	ARCH1.3			

The outcomes of this chapter fulfil Step 2 defined in Section 3.5. During the Requirements Analysis, the inputs from the enabling systems, the missile and the actuator system, and the operational context aided in the elicitation of the FGM system requirements. This was considered to be validated as described in Section 5.2 and used as the basis of the Functional Architecture creation. This architecture was assumed verified through the traceability to the requirements baseline. The validation and verification mentioned here refer to the processes described in Section 2.1 based on IEEE 1220-2005 [123]. These functions, along with the Physical Architecture developed for the ASYS, were used as input for the FGM Physical Architecture generation. Through the SE processes mentioned in Section 2.1, the validated requirements baseline was developed, the Functional Architecture was generated, and the Physical Architecture was established. These inputs were used for the concept generation phase.

6. Concept Generation

The FGM system was developed using the Systems Engineering process mentioned in Section 3.2, where the requirements and functions were defined and from which a Physical Architecture was developed, as seen in Section 5.5. This architecture was used to develop the concepts described in this chapter.

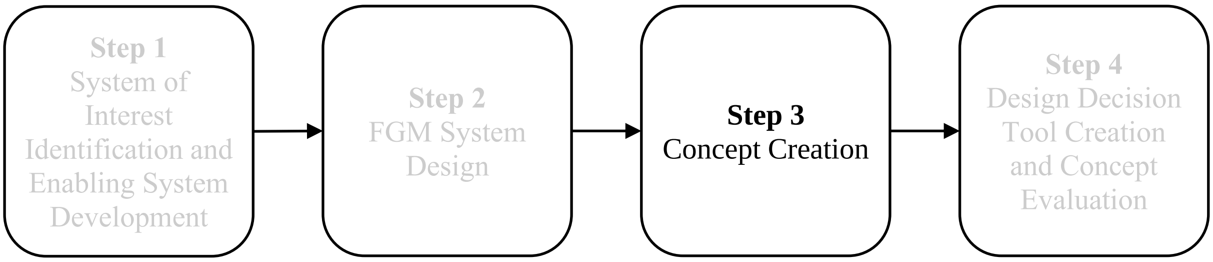

Figure 62: Step 3 of the Method

Based on the conceptual missile design carried out (described in Section 4.2), the actuator system was allocated space to the rear of the rocket motor for its placement. This decision was based on the placement of the actuator on the baseline missile (the AIM-120) used for the conceptual design and to reduce the scope of the study. The concepts were therefore developed with predefined placement in mind. Concepts that fall outside the prescribed placement were not considered for this study. Alternative ASYS placements outside the prescribed placement should be considered for future study.

As previously mentioned, these requirements were revised based on the system of interest, namely, the FGM. The design objective/requirement that refers to the primary function of the FGM is the generation of a force for the physical alteration of the missile's flight path (FR1). It was therefore considered during the evaluation of the requirements. The requirement value refers to the minimum force that is required to be produced by the actuator system for the system level to be utilised by the missile system for a 30 g manoeuvre. The force generation evaluation included analysing the defined FGM's ability to aid in meeting the force requirements. The concepts produce a force in different ways; therefore, the evaluation was adapted to accommodate the different ways between the concepts. The approaches are described in their respective sections. For the concepts that utilise the Smart Materials/Adaptive Structures to move a fin, the concepts were evaluated on their ability to deflect the fin. The geometry of the fin and the interactions between the body, wings and fins result in the aerodynamic force required to manoeuvre the missile. The evaluation, therefore, focused on the concept mechanism's force production to generate the required deflection, which required some gearing or mechanical advantage, to achieve the desired force. For this study, it was assumed that the Centre of Gravity (CG) position is not affected by the different concepts and that the moment arm measured from the CG to the point where the force generated acts was the same as the generic ASYS.

This force also needs to be generated within a specific time frame to be effective at the missile level. Therefore, the response of the system, the Bandwidth, was also important to consider. Therefore requirement/objective FR7 was also important. For the evaluation, a mathematical model for the different mechanism concepts was compiled in some cases based on an adaptation from literature. A transfer function was then determined, and MATLAB (a product from MathWorks used for computing and simulation) was employed to generate a Bode plot to determine the bandwidth. For some of the concepts, the bandwidth data obtained from the literature was referenced.

Evaluating interfaces and components requires some detailed design which is beyond the scope of this conceptual study. The verification of the structural integrity was therefore evaluated based on the Smart Material/Adaptive Structure's load-carrying ability as a standalone component.

The FGM also plays a role in maintaining the applied force for a required duration. This period is dependent on the type of manoeuvre the missile requires and the time and distance to the target. For this study, the analysis focused on the mission profile. The missile was thus expected to operate for a maximum period of 180 s ± 10 s and would engage a target at its maximum velocity (Mach 4).

In general, the actuator has low power requirements during most of the missile flight as the majority of the flight is spent making minor flight adjustments which does not require much energy to execute. At times the missile will be required to pull a high g-manoeuvre which requires high energy input. Therefore, the energy available for the FGM is a factor in maintaining the applied load, the other factor being the FGM's component fatigue life. For this study, it was assumed that the power supply is uncapped. However, limitations were described based on the power requirements of the generic actuator. The impact relating to available space was discussed. The fatigue life of the FGM was also described in terms of the operational time-related requirement.

As the FGM already forms part of an existing system that has its transportability governed by military standards like those mentioned in MIL-STD-810G [124]. The FGM should comply with these requirements as part of the ASYS. The influence (like damping effects) of other actuator system components not described in this study would play a role in the impact of the transportation of the FGM. Therefore, the transportability requirement was not assessed, and it was assumed that the system met the transportation requirements of the actuator system for this study.

The requirement for the disposability of the FGM was also not evaluated as it was considered to be beyond the scope of this study.

The storage requirement for the concepts was evaluated as it has a direct impact on the feasibly of the concepts.

Therefore, the requirements assessed during the concept development were as follows:

- Force Generation
- Structural Integrity
- Bandwidth
- Operation Time
- Storage

6.1 FGM Concepts

As mentioned in Section 2.6, a missile flight path can be physically varied by altering the position of a control surface. This change in position of the control surface influences the flow over its surface, modifying the lift generated as described in Section 2.5. As mentioned in Section 2.6, other methods that vary the missile's flight path include fluidic control or flow effectors and using thrust vectoring. The concept development was initiated with these various methods in mind. However, thrust vectoring was not considered for this study as the mechanism would only be useful while the rocket motor is in use.

A morphological box or concept combination table approach was used (as described in Section 3.3) to identify solutions that would correspond to the Physical Architecture developed in the previous chapter. The concept combination table can be seen in Table 31.

Table 31: FGM Concept Combination Table

Force Generator (FGMARCH1.1)	**Transmission Mechanism (FGMARCH1.2)**	**Airflow Interaction Structure (FGMARCH1.3)**
Servo Motor	Leadscrew, Nut and Lever Arm Assembly	Control Fin
Flexinol Wire	Lever Arm	Control Fin Exterior
Piezoelectric Linear Actuator	Support Rib and Spar	Fin Geometry
Piezoelectric MFC Actuator		

The first row indicates the headings for the columns, which correspond to the Physical Architecture elements developed in Section 5.5. Under each heading, various solutions were identified based on the Smart Materials identified in Section 2.2. The first row of solutions includes the generic force generation solution. This was included as a baseline for comparison. The evaluation of the generic FGM can be seen in APPENDIX F.

The concepts created were separated into concept categories. These can be seen in Figure 63.

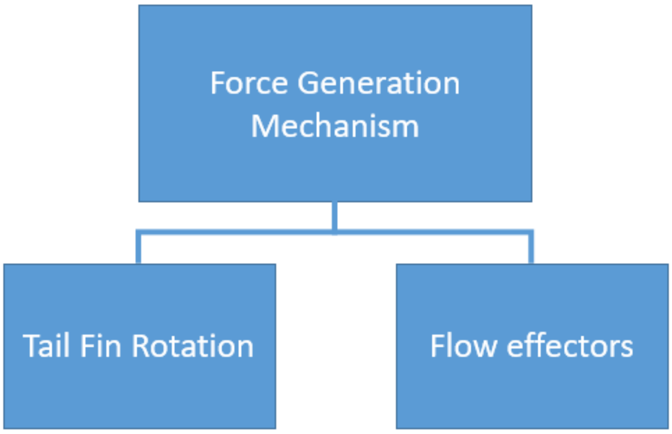

Figure 63: Concept Categories

Figure 63 presents an illustration of the understanding of the various types of force generation, as described in the Literature Review section, Chapter 2. Tail Fin Rotation was selected as a category based on the baseline missile from the conceptual missile design.

Tail Fin Rotation has two subcategories. These include Incidence and Morphing Control Surface Geometry. Incidence refers to the change to the incidence angle of the control surface with respect to the missile airframe, which also alters the control surface's angle of attack, as changing the angle of attack of the control surface changes the lift properties [81][125]. This is done by the rotation of a fin. The Morphing Control Surface Geometry is a broad category that refers to the changing of the control surface geometry. This can be done by altering the geometry's dimensions to change the structure's lift properties.

Flow effectors (see Section 2.8) refers to the category of FGMs, which make use of flow effectors to alter the flow around control surfaces to change the lift properties.

The concepts generated will be discussed under the sub-categories shown in Figure 63. It should be noted that the categories defined are not comprehensive, and other FGM categories may exist, but the focus of the study has been limited to the categories indicated in Figure 63. The concept creation was carried out as described in Section 3.3.

As mentioned in Section 2.5, the in-flight adjustment of the control surface position changes the pressure distribution on the surface, causing a variation to the normal force magnitude and direction. The concepts utilised the generic missile's fin geometry, as seen in Figure 64, to achieve the same normal force at the specified flight conditions.

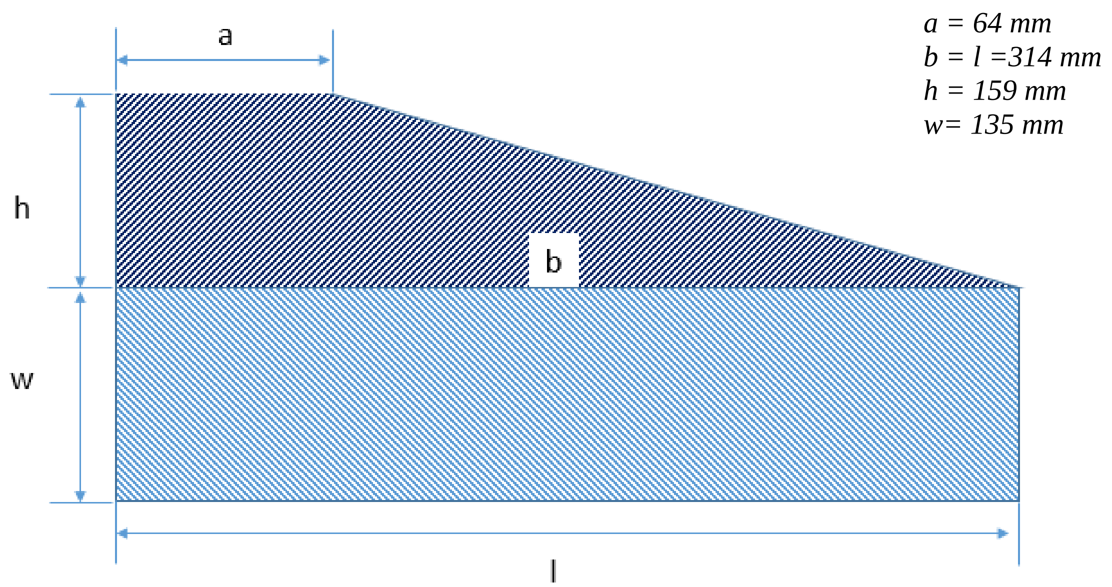

Figure 64: Control Fin planform used for the Generic Missile ASYS taken from the AIM 120 missile

Smart Materials or Adaptive Structures were employed to replicate a deflecting fin or simulate a servo motor mechanism.

6.1.1 Concept 1

As shown in Chapter 2.7, servo motors can be used as an actuating mechanism to rotate a fin. In this type of mechanism, the rotating motion of the motor shaft drives the rotation directly (see Figure 65), or the mechanism can translate the motion into linear motion to push or pull a lever to produce the required torque (see Figure 66).

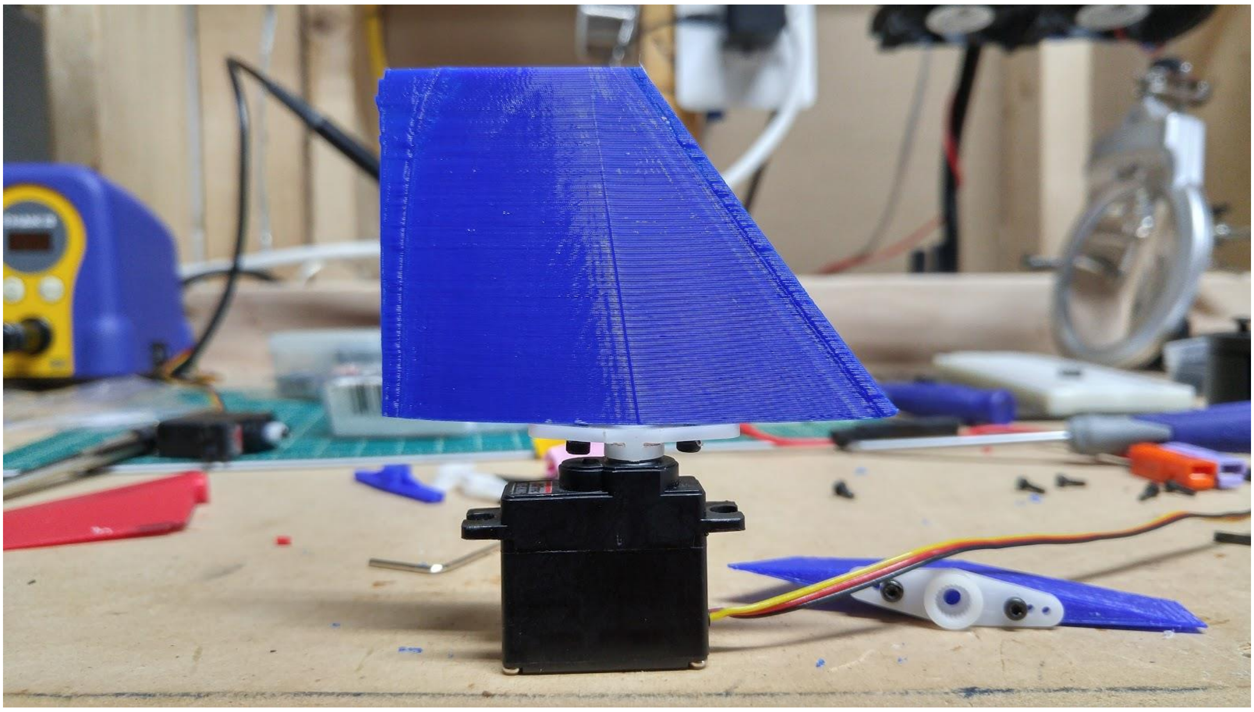

Figure 65: Missile Fin Coupled directly to a servo Motor for rotation [126]

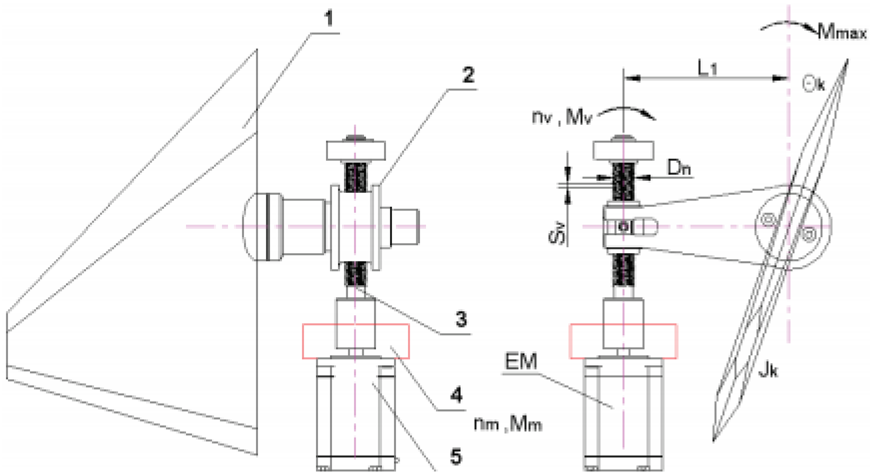

Figure 66: Servo Motor rotation translated into linear motion to rotate missile fin using a lever [127]

The concept is envisioned to replace the generic servo motor, as depicted in Figure 66. A Shape Memory Alloy (SMA) would provide the force to rotate the output shaft of the actuator, which would result in rotation of the fin, as seen in Figure 67 (a). The wire connected to the control unit would pull in the directions indicated to pull the wire wrapped around the spindle, which is connected to a leadscrew. As the lead screw rotates, the nut moves axially, rotating the missile fin in the directions indicated in Figure 67 (b) and (c). The SMAs would be controlled by the control unit indicated in Figure 67.

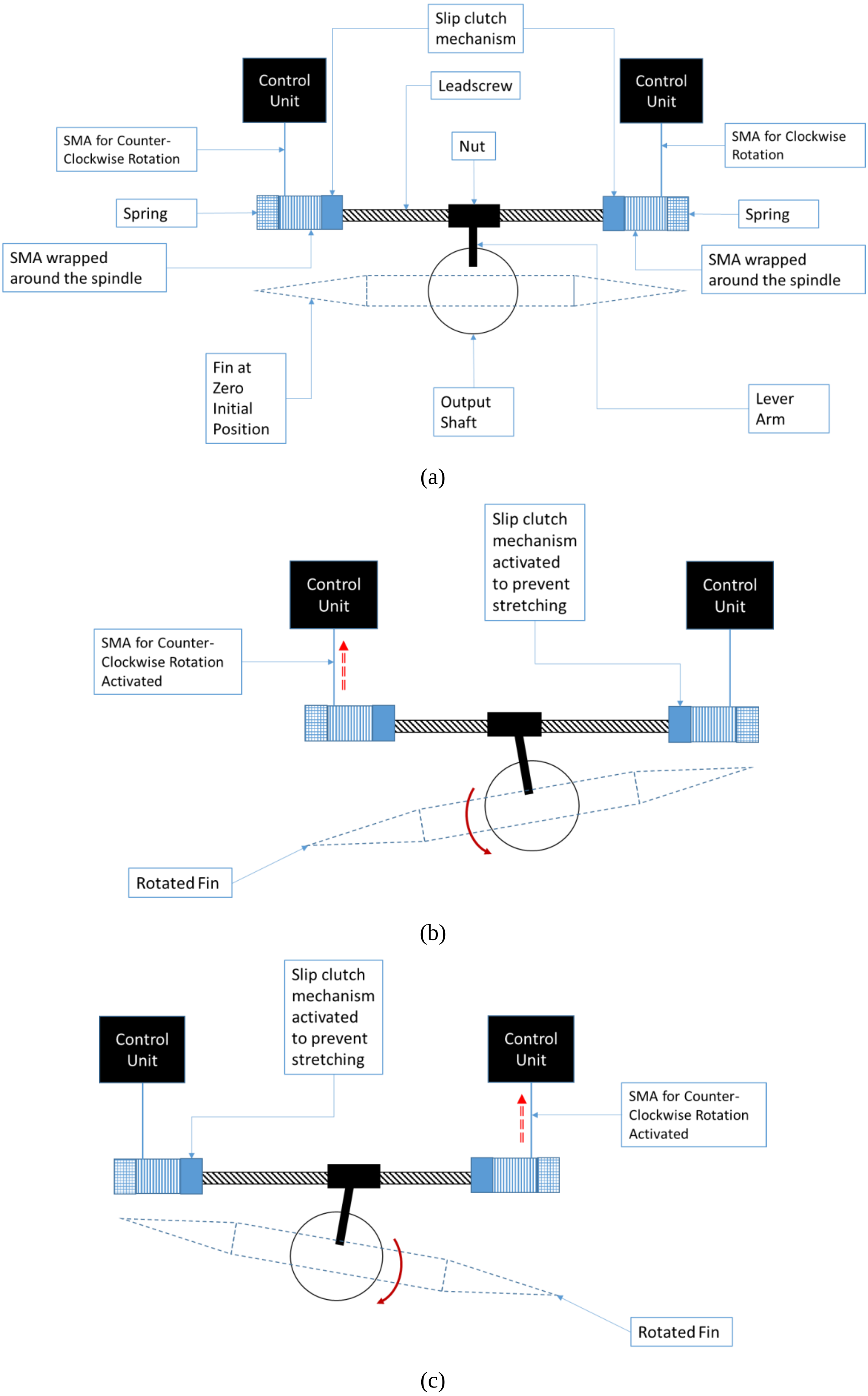

Figure 67: Concept 1 - Replacement of a Servo Motor

A clutch would need to be included to minimize overstretching of the wire that is not contracting. The clutch would need to disengage the non-contracting side when the tension exceeds a set limit but still allow for the extending wire to be wound around the spool. This can be assisted by a spring that will wind up the wire as it extends when the spool is free from the leadscrew.

This concept will induce a fin deflection similar to that of the generic missile. To achieve the desired (maximum) fin deflection of -12.7 degrees, the nut on the lead screw would need to be displaced by 12.85 mm. If the same leadscrew (5 mm pitch) used by the generic system in this study is used for this concept, the leadscrew would need to make 2.57 revolutions (5.14 revolutions from maximum rotated positions of the fin). The SMA envisaged for this concept would be Flexinol® wire. The wire would have to be 5.54 m for a more conservative strain of 3.5% to achieve the wire displacement required for the resultant revolutions with a spool diameter of 12 mm. The length wrapped around the spindle only needs to be about 200 mm, so the remainder would need to be placed accordingly.

The force at the end of the lever arm (76 mm) shown in Figure 67 would need to be 365.68 N to produce a torque of 27.79 Nm.

The input torque for the given lead screw would then need to be 0.3 Nm. For a 12 mm spool, the force required by the wire would need to be 25 N. Based on the datasheet obtained from Dynalloy [128], a cluster of 0.51 mm wire would have to be used. To achieve the force, a cluster of 8 strands, with a total area of 1.44 mm^2, would be needed at the SMA locations indicated in Figure 67.

To overcome the spring that will assist in winding up the wire when the spool is disengaged from the lead screw, additional pull force would be needed. To aid in this, additional wires can be added to the cluster to work against the spring force. The number of wires depends on the spring selected. This detail will be considered a detail design phase which is not part of this study.

As mentioned in Section 2.2.2, the response rate is determined by the heating of the wire, which is proportional to the rate and intensity of the current applied [129]. The limiting factor on the rate of response of the wire is the inertia of the load the wire has to pull, as damage in the wire can be introduced during fast operation. For fast contractions, the inertia should be kept low, and the current should be applied in short high magnitude surges. Heating the wire using current, starting from room temperature, will cause the wire to reach 100 °C in 1 millisecond [128]. For the wire to return to its initial position, it is required to be cooled for relaxation to occur. A cooling subsystem would have to be designed to satisfy this requirement. However, this will not be covered in this study. A practical cooling system that would allow the system to function as described will be assumed for system completeness.

6.1.1.1 Force Generation FR1

Concept 1 uses Flexinol® Wire to rotate the output shaft of the actuator, which rotates the missile control fins. The Flexinol® Wire was envisioned to replace the DC servo motors from the generic ASYS. Therefore, the evaluation for the force generation involves understanding the force required by the wire to replicate the control fin deflection.

The aerodynamic load determined in Section 4.2 was the basis of this evaluation. As previously discussed, a wire bundle would be required. The bundle details were determined in APPENDIX G. Each cable would therefore only be required to exert 25 N to rotate the leadscrew described above. The detail of this evaluation can be seen in APPENDIX G.

Following a discussion [130] (see APPENDIX H) with Flexinol® manufacturers (the selected Shape Memory Alloy similar to Nitinol®), Dynalloy INC, Flexinol® was capable of producing the determined force. This concept, therefore, meets the requirement FR1.

6.1.1.2 Structural Integrity FR4

The recommended work for the Flexinol® is 0.0981 Nm per strand of wire, and in this concept, the work is calculated to be 4.84 Nm which is 49 times higher than the recommended value. Therefore, the Flexinol® would be able to produce the force required. However, it would have to operate beyond its recommended limit, and therefore repeatability would be an issue. The repeatability in this context would have to be evaluated in a future study. The Flexinol® may, therefore, experience some structural damage after continuous use as the SMA is susceptible to high stresses according to the design data sheet [43] and the email discussion with the manufacturer [130]. It also mentions that the memory strain will decrease, causing the SMA not to perform as required and could impact requirement FR1a. Therefore, this concept does not meet requirement FR4.

6.1.1.3 Bandwidth FR7

The system to be evaluated can be seen in Figure 68. The effect of the Flexinol® on the bandwidth of the system was evaluated using the following transfer function (in the frequency domain), which was adapted from Senthilkumar *et al*. [131]:

$$G(s) = \frac{0.0643}{(s + 0.1)V} \tag{20}$$

Equation 20 is based on the outcome of the work done by Senthilkumar *et al*. [131]. The constants were determined experimentally as described in that study.

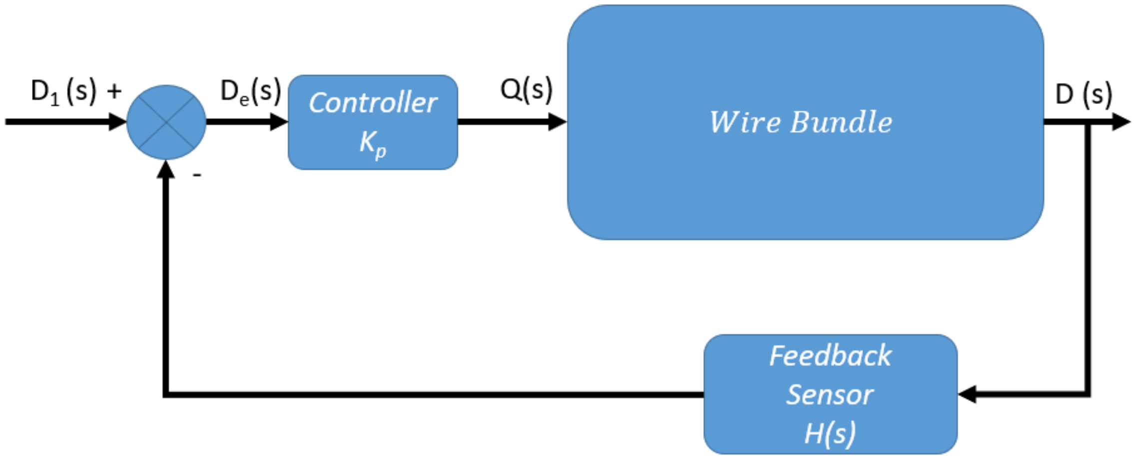

Figure 68: Flexinol® force generation system block diagram

The *"Wire Bundle"* seen in Figure 68 was the focus when the transfer function was determined for the Nitinol® wire in Senthilkumar *et al*. [131] and therefore was considered to be suitable for the use for the Flexinol® The input to the Wire Bundle is heat energy *Q* and the displacement of the nitinol wire bundle *D*. In order to develop a closed system to evaluate the bandwidth, additional components were included. As seen in Figure 68, D_1 is the displacement input signal. D_e the difference between the input signal and the output measured by the feedback sensor. A controller and a feedback sensor were also included to create a closed-loop system to evaluate the bandwidth. The inertia of the load connected to the Flexinol® was not included as the focus is on the mechanism that generates the force. A proportional controller (K_p) was selected to multiply the difference of the input from the output of the system. This does not consider any losses due to the load that has to be pulled or the hysteresis the Flexinol® would experience. The gear ratio, provided by the lead screw, in this system is used to amplify the force the Flexinol® wire can produce and transform the linear displacement into a rotational displacement of the control fin. This is not included in this calculation. Although the gear forms part of the system described, it was not included in the closed-loop system evaluated using MATLAB as the focus was on the bandwidth of the system in terms of the output displacement.

The variables and constants are described in Table 32.

Table 32: Variables and constants for the Nitinol® Wire

Variable/Constant	Description	Value	Units
K_p	Proportional Controller Constant	0.001	-
V	Wire volume	7.94×10^{-6}	m^3
$H(s)$	Feedback Function	1	-

The Bode diagram from MATLAB can be seen in Figure 69.

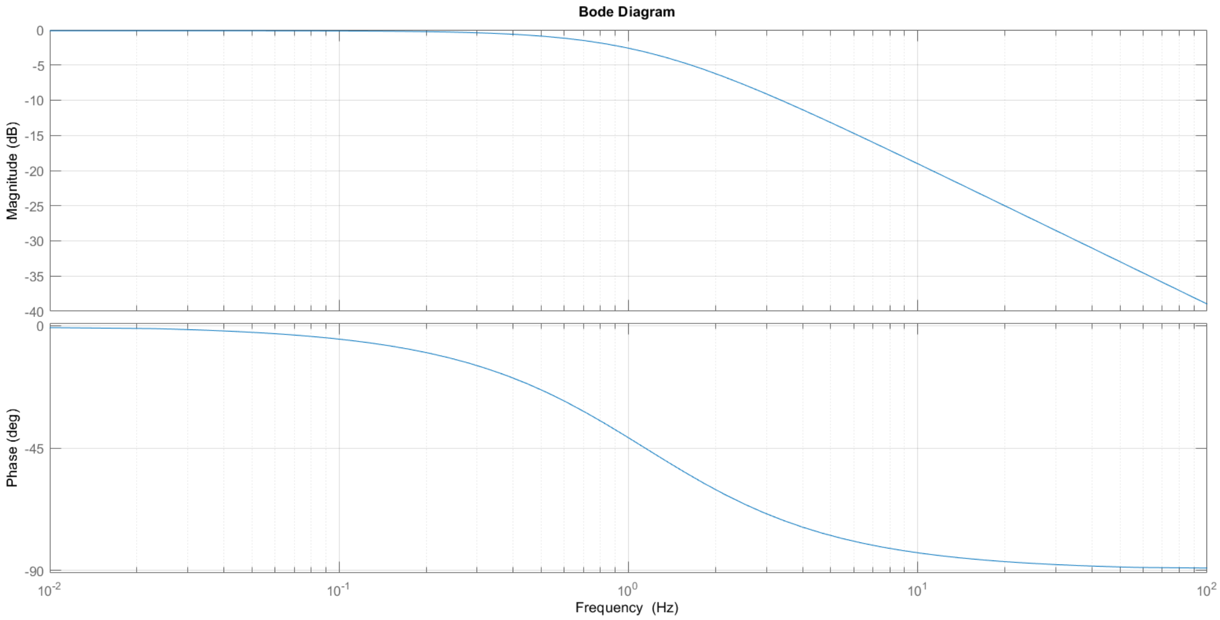

Figure 69: Bode Diagram - Wire Bundle

Unity feedback was selected for this analysis. Therefore, the feedback function has a value of 1.

The bandwidth was determined to be 1.14 Hz. The value for K_p was initially assumed and alternated to achieve the bandwidth result. Based on Nitinol® studies relating to the bandwidth of the wire, such as Sunjai Nakshatharan *et al*. [132], the bandwidth should be in the range of 0.3 to 2 Hz [133].

The literature also mentions that a significant contributing factor to the bandwidth includes the cooling of the wire to return it to the initial set point and compensating for the hysteresis in operation [43]. As previously mentioned, the cooling of the wire was not defined, and the hysteresis of the wire was not considered. Therefore, the result calculated was simplistic concerning the bandwidth of the wire. If these factors are considered as well as the leadscrew and the inertia of the missile fin used for the generic actuation system, the bandwidth will decrease significantly. Therefore, based on the range defined in the existing studies, the bandwidth is below the required bandwidth and is therefore not acceptable. The requirement FR7 is not satisfied.

Given that the rate of cooling has an impact on the bandwidth of the wire, an improvement with regard to these rates should improve the bandwidth. An example of improving the bandwidth through reducing the cooling cycle was shown by Tadesse [134]. Depending on the cooling method, the heat transfer rate can be improved. Further investigation is required to establish the level of improvement that can be achieved; however, this is beyond the scope of this work.

6.1.1.4 Operation Time FR2

The wire is required to operate for 180 s to meet the operational time requirement. The fatigue life of the SMA wire is a necessary factor to consider when evaluating the operation time of the FGM.

The fatigue life is affected by the mechanical loading and thermal loading, as mentioned by Pelton [135]. Thermal loading can be due to the environment (soaking in a -55ºC environment in carriage flight) or due to the joule heating required for the actuator to function and the cooling of SMA to return it to its initial position. The mechanically induced fatigue is due to the contractions and extensions of the wire. As mentioned in Middleton [57], the SMA wire can withstand 10^7 cycles of load. This would be dependent on the wire diameter, the relevance of the load applied, and certain other factors.

To verify if the wire would be able to survive the operation time, the number of cycles would have to be known. If we use the required bandwidth of the system, 25 Hz, as the duration of a cycle, and if the total operation time is 180 s, then there would be 4500 cycles. Assuming the loading of the wire is within its acceptable range, then it should last the duration of the operation time. Therefore, the Flexinol® wire should meet the requirement FR2.

6.1.1.5 Storage FR5

According to Duerig [44], Ni-Ti alloys, like Flexinol®, have been used as permanent Class III medical devices implanted inside a patient's vena cava as a filter to prevent possible embolisms. From this, it can be assumed that such material (used for Nitinol® wire) has a near-infinite shelf life. Flexinol® wire is only affected during prolonged exposure to high temperatures outside its transformation range [43]. Therefore, assuming the storage environment is temperature-controlled within a suitable range, the wire should meet the requirement FR5.

6.1.2 Concept 2

As shown in Section 2.5, changing the incidence angle of the control surface has an impact on its lift properties.

The idea behind this concept, seen in Figure 70, is to mimic a fin deflection by morphing the control fin structure by adjusting the leading and trailing edge in opposite directions (simulating a rotating fin), to generate the required force. This concept uses bistable/multi-stable structures in conjunction with Macro Fibre Composite (MFC) to actuate the leading and trailing edge of the control fin. In a similar method used by Bilgen *et al*. [18], an MFC (see Section 2.1) laminate structure would be bonded to the multi-stable surfaces to be deflected. The multi-stable surface is indicated by the diagonal hashed rectangle in Figure 70. The multi-stable structure forms part of the internal structure of the control fin. The outer surface, in contact with the airflow, would need to be a flexible skin to ensure a seamless aerodynamic surface. The inner space between the multi-stable structure and the flexible skin would require a support structure to maintain rigidity inflight. The flexible skin and inner support structure will not be covered in this study. This structure's design needs to be such that the impact on the MFC actuator is minimal and that it does not deform due to the airflow. The complexity of the structure's design is not in the scope of this study and should be done as future work.

In this application, the multi-stable structures would be applied to the leading and trailing edges of the control fins. The control surfaces would ideally be manipulated (the leading and the trailing edge would move in opposite directions) to mimic a rotating fin. When a current is applied to the MFC laminates, it provides the necessary actuation to snap the multi-stable structure into one of its pre-set stable states. As shown in Figure 70, the MFC actuators would be bonded on the top and bottom of the multi-stable structures on either side of the rigid support to facilitate deflections in both directions.

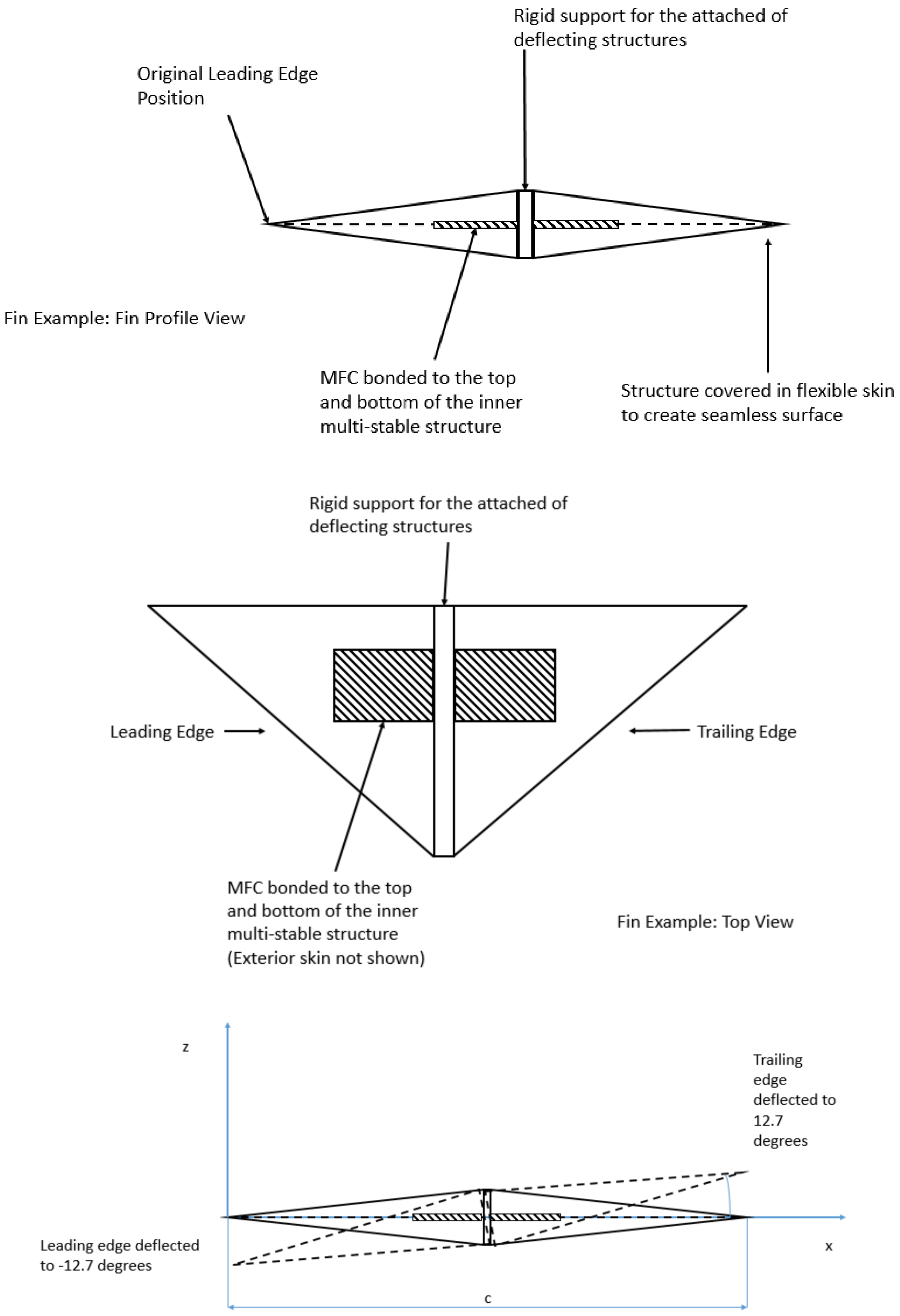

Figure 70: Concept 2 – Illustration of Leading and Trailing edge Actuation

The fin geometry in Figure 70 is only for illustration purposes. The fin geometry is envisioned to be the same as the generic missile fin, as seen in Figure 64. Multi-stable structures are developed, as discussed in Chapter 1. The structure would be processed to produce the necessary stable states that will mimic the deflections for the fin. The required deflections will be based on the generic missile's fin deflection to achieve the required force.

The rate of response of the multi-stable structure and the load-bearing capacity of the structure (due to the aerodynamic loading that would be experienced in flight) are related to other parameters. They will be determined as required.

6.1.2.1 Force Generation FR1

The second concept falls under the Alteration of Tail category. The force will be generated based on the fin's geometry and the deflection of the fin. The leading and trailing surfaces of the fin for this concept will be deflected to mimic the rotational deflection of the generic actuator system.

It was determined that the generic fin would require a deflection of -12.7 degrees to produce the required load to maintain the necessary g manoeuvre. This would mean the deflected fins (the horizontal fins in the "+" configuration as seen in Section 11.A.4) would require the leading edge to deflect -12.7 degrees and the trailing edge to deflect +12.7 degrees to achieve the same effect as the rotated generic actuator fin.

As described in Daynes *et al*. [136], the energy required to change the position of a generic control surface is related to the work done by the aerodynamic loads. However, for bistable structures, the type of structure used in this concept, the energy required to change the control surface position is a function of both the aerodynamic work done and the energy required to alter the form of the structure. This is highlighted in Equation (**21**):

$$W_a = W_f + W_b \tag{21}$$

Where W_a is the total energy required for bistable structure snap-through, W_f is the work done by the aerodynamic load, and W_b is the energy required to deform the bistable structure with no aerodynamic loading.

Equation (**21**) refers to the work the MFC actuator has to do in order to alter the control surface. The approach to determine the work done by the actuator was adapted from Daynes *et al*. [136] for this analysis.

If we assume a bistable or multi-stable structure was designed to produce the required deflections for the required g manoeuvre, as previously mentioned, the deflections of the leading and trailing surfaces of the fin are meant to mimic a generic control fin. Therefore, the loading of the fin should be the same as the generic missile fin. Thus, for this study, this concept's deflection was assumed to be as shown in Figure 71.

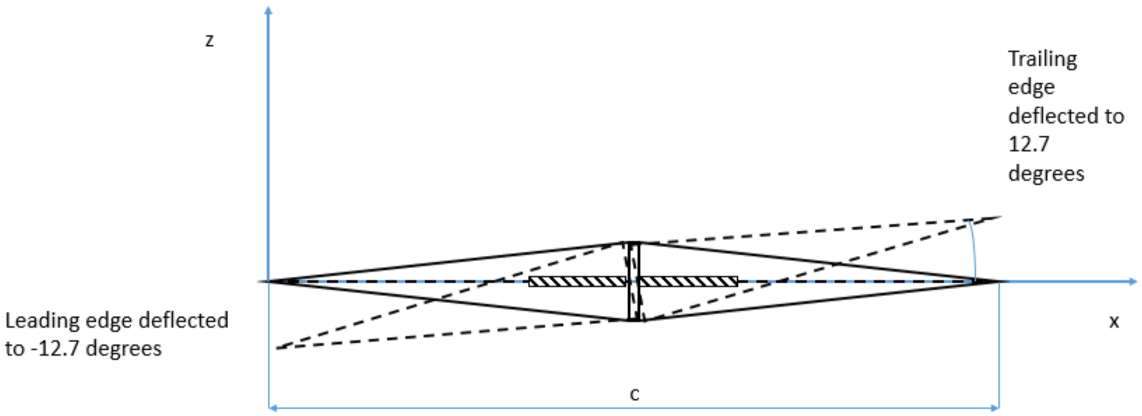

Figure 71: Fin leading and trailing surface deflection mimicking the generic fin rotation

For this concept, the analysis for the force generation will focus on the MFC actuator, the Piezoelectric patch. It is used to move the bistable/multistable structures, which forms part of the leading and trailing surfaces of the fin. The analysis would assess the capability of providing the necessary work W_a as discussed previously. Using the W_a, the force generated was determined.

MFC patches can induce flexure. This characteristic ability was utilised in this concept, as explained earlier in the chapter. In a previous study by Bowen *et al*. [38], MFC actuators were used to deflect an aluminium plate. The experimental setup was as shown in Figure 25.

For this study, the deflection expected by the bistable structure was approximated based on the deflection of beams. This approach would provide the basis of the method to determine the force required to deflect the relevant structure. The approximation of the beam deflection was compared to the results from the test carried out in by Zhang *et al*. [39] shown in Table 4 of that study which was similar to the study in C. R. Bowen *et al*. [38]. A cantilever beam, with the same geometry and material properties as the aluminium beam used in the study by Zhang *et al*. [39], was the basis of the approximation.

Based on the force due to the extension of the MFC d33 P1 patches [36] and the placement of the actuator on the aluminium plate, a moment would be induced in the plate, which was approximated along the central axis of the plate at the centre of the MFC patch as shown in Figure 72.

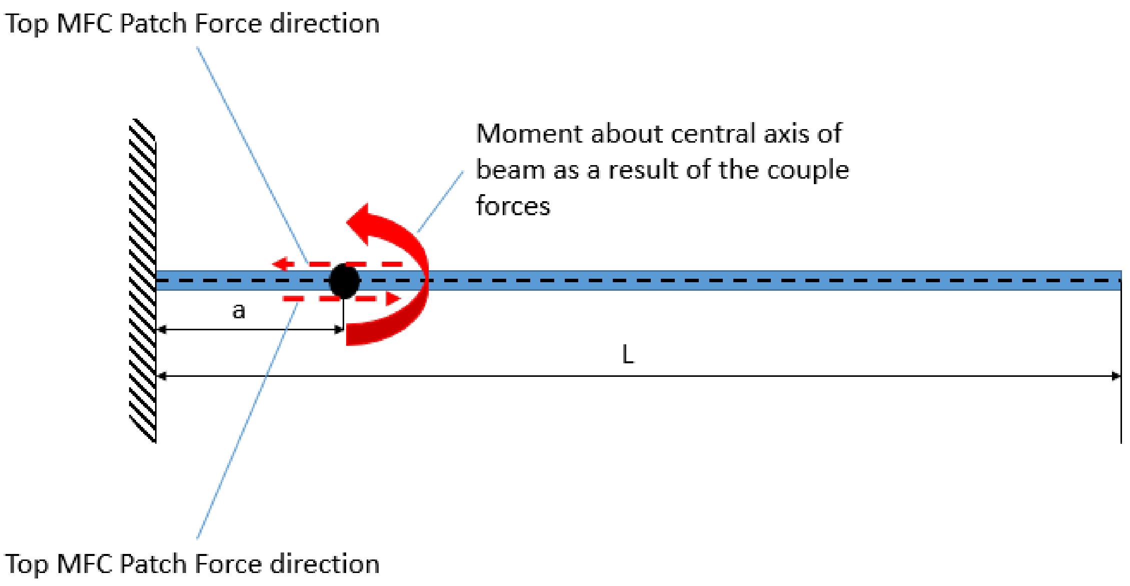

Figure 72: Resultant load due to MFC patch placement and force application

The moment applied to achieve the same plate end deflection would need to be 0.2 Nm. This equates to a force applied by the patches of 102 N, which is below the maximum force ability of the patch [36]. The experimental results were then plotted against an approximation of a beam with a moment acting at the same location as the MFC patch. As seen in Figure 73, the deflection of the plate from the study by Zhang *et al*. [39], and the approximation of the experiment based on a moment at the point indicated in the beam in Figure 72, differed from one another. This could be attributed to the way the MFC patch deforms the material of the plate, which is not modelled in this beam approximation or there could be missing information from the study by Zhang *et al*. [39].

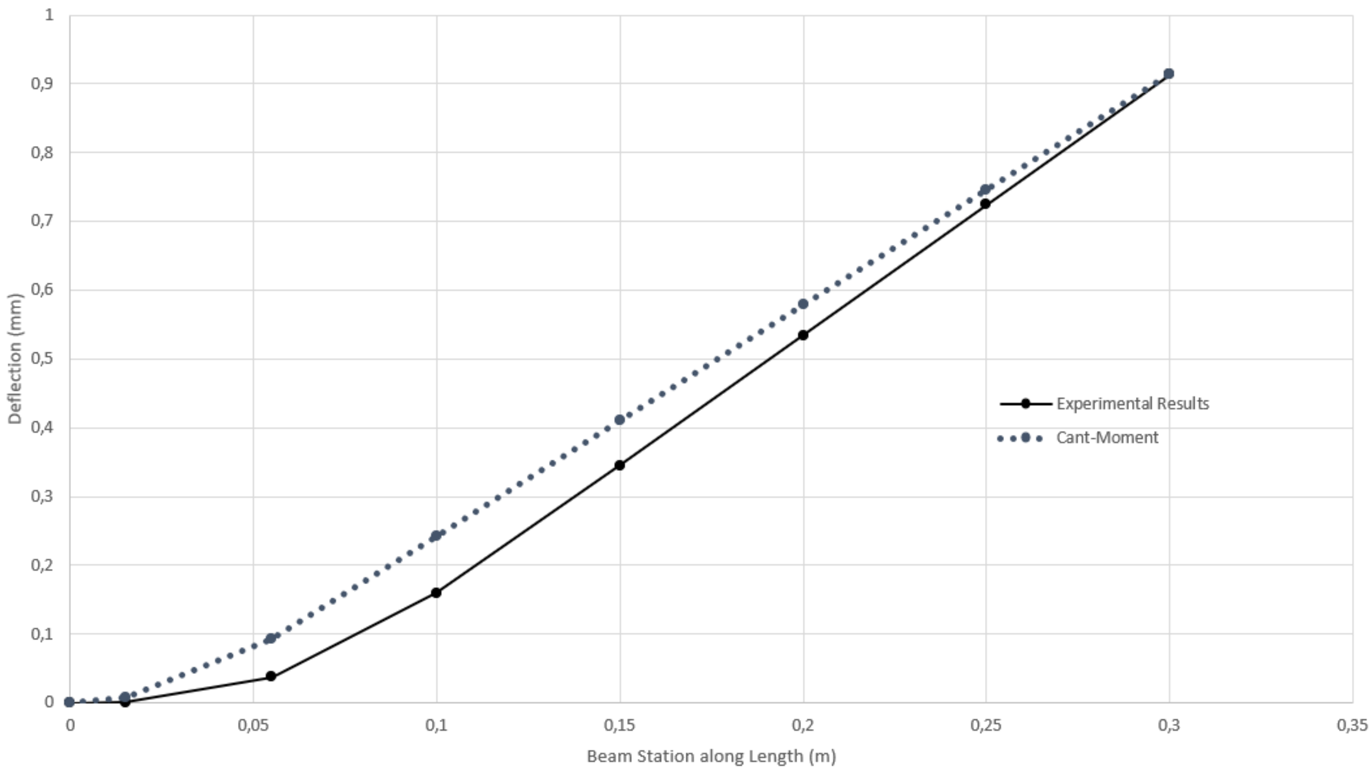

Figure 73: Deflection model comparison to determine the best approximation for the experimental results

In Figure 73, the solid line indicates the experimental results achieved by Zhang *et al*. [39], the dotted line indicates a cantilever beam with a moment applied at the experimental MFC location. The calculations relating to the creation of Figure 73 can be seen in APPENDIX I.

The deflection of this beam is as follows (adapted from Roark and Young [137]):

$$z_A = \frac{M}{2EI}(L^2 - a^2) \tag{22}$$

Where z_A is the displacement measured at the end of the beam (which is expressed as D_y in Figure 25), M is the applied moment, a is the distance the applied moment is from the free end, L is the length of the surface to be deflected, E is the Young's Modulus, and I is the moment of inertia.

The moment (M) is created from the force applied by the MFC patch (P) and the distance r_c to the centre of rotation shown in Figure 72.

$$M = Pr_c \tag{23}$$

The applied force was determined by rearranging Equation (**22**) and substituting in Equation(**23**) as shown in Equation (**24**):

$$P = \frac{2EIz}{r_c(L^2 - a^2)} \tag{24}$$

The deflection will be in the direction of the moment shown in Figure 72 based on the force directions of the patches shown.

This load is the force required to deform the beam structure. The work done can be determined as follows:

$$W_b = Pz \tag{25}$$

This was considered to be the work required to deform the leading or trailing structures of the fin. To fully define the work required from the actuator, the work done in resisting the aerodynamics loading, W_f, was defined.

According to Daynes *et al*. [136], a simulation was carried out to determine the aerodynamic loading on the bistable composite structure. The aerodynamic load distribution on the fin surface has not been defined. This aerodynamic load was assumed to be the normal force the fin would experience acting at the aerodynamic centre. Using the C_N calculated for the tail, using the method from Fleeman [60], the normal force can be determined based on the following equation:

$$N = qS_wC_N \tag{26}$$

Where N is the Normal Force, and C_N is the coefficient of the normal force. The load acting on the leading surface is illustrated in Figure 74.

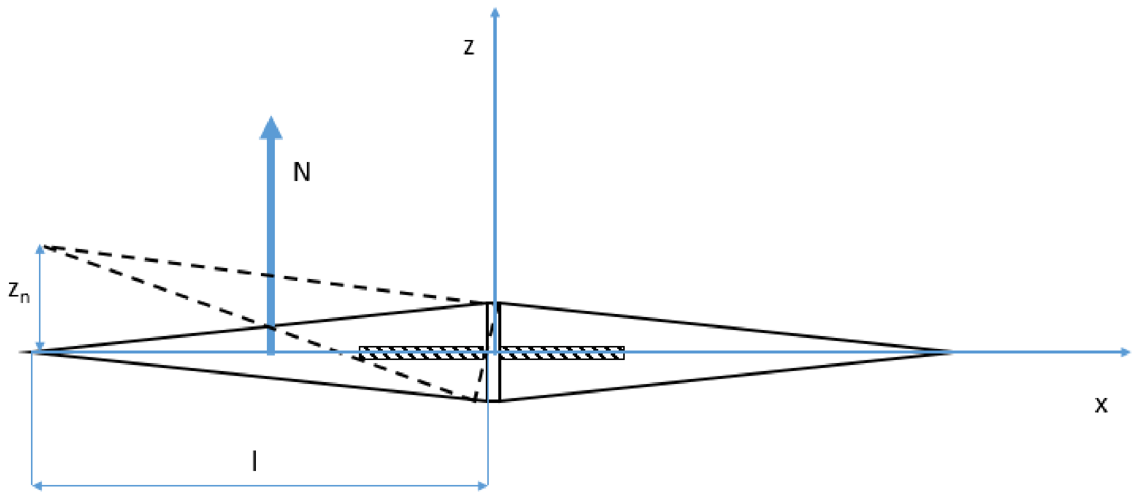

Figure 74: Aerodynamic load case for Concept 2

The aerodynamic centre of the fin is dependent on the flow velocity. At low Mach numbers, the aerodynamic centre is located at about 25 % of the mean aerodynamic chord (C_{MAC}) and for high Mach numbers (in the hypersonic range), it moves towards 50 % [60]. Since the Mach number for this study is high, the aerodynamic centre would tend to be more towards the centre of the C_{MAC}. So, for this study, the normal force was assumed to act at 30 % of the cord, as this falls within the ranges described. The normal force applied would deflect the leading surface by a distance z_n in the direction of the applied force. The work done in moving the leading surface, W_f, over this distance was considered as follows:

$$W_f = N z_n \tag{27}$$

W_f was considered to be the work required to maintain a zero-fin deflection if subjected to the aerodynamic load alone. Therefore, the work required by the actuator W_a can be determined based on the relationship, which includes the influence of the work done to deform the structure and the work done to overcome the aerodynamic loading.

In some instances, the aerodynamic load may assist the deflection of the control surface if the load acts in the same direction as the required deflection. The actuator would have to resist the aerodynamic load to prevent the control surface from exceeding the required deflection, and it will also be assisted by the bistable structure's "snap" ability. The highest work required to be done by the actuator is expected when the aerodynamic load acts in the opposite direction to the required deflection. This case was assessed.

If the leading surface of the control fin is considered to mimic a fin deflection of -12.7 degrees, the leading edge would have to be deflected in the negative *z*-direction, according to Figure 74's axis system, by -12.7 degrees. The displacement can be calculated as follows:

$$z = -Lsin\theta \tag{28}$$

Where *L* is the length of the leading surface of the fin, measured from the hinge line to the leading edge, and θ is the fin deflection required. Therefore Equation (24) becomes:

$$P = \frac{-2EILsin\theta}{r_c(L^2 - a^2)} \tag{29}$$

If the displacement of the leading edge is assumed to be the distance the object travels when the force *P* is applied, the work done to deform the structure would therefore be as follows:

$$W_b = \frac{2EIL^2sin^2\theta}{r_c(L^2 - a^2)} \tag{30}$$

Therefore, the work required (substituting Equations (27) and Equation (30) into Equation (**21**)) by the actuator can be expressed as:

$$W_a = Nz_n + \frac{2EIL^2sin^2\theta}{r_c(L^2 - a^2)} \tag{31}$$

For the actuator to be effective, the force generated would have to overcome the aerodynamic load and alter the structure as required. To determine the force required, Equation (31) becomes:

$$F_a = \frac{Nz_n}{z_a} + \frac{2EIL^2sin^2\theta}{z_ar_c(L^2 - a^2)} \tag{32}$$

Where F_a is the force generated by the actuator and z_a is the distance over which the actuator's force generated is required to work, which is the sum of the deflection distance due to the aerodynamic load and the distance the leading-edge travels to the required deflected position. Where:

$$z_a = z_n + z \tag{33}$$

If a bistable laminate composite made from T300/976 is used with the material properties shown in Table 33 from K. Y. Chang *et al*. [138] and cross-sectional properties shown in Figure 75, the force required by the actuator, F_a, would have to be 9495.84 N (see APPENDIX I).

Table 33: T300/976 material properties [138]

E_1 / GPa	E_2 / GPa	G_{12}^0 / GPa	ν_{12}	X_T / MPa	X_C / MPa	Y_T / MPa	Y_C / MPa	S_{12} / MPa	α
139.76	12.96	6.96	0.23	1516.9	1592.7	44.5	253.0	106.9	2.44×10^{-8}

$$I = \frac{bh^3}{12}$$

Figure 75: Cross-section of the bistable laminate composite

According to the MFC d33 patch technical data sheet [36], it is able to produce a blocking force of 923 N and a free strain displacement of 150 µm. Based on the required force, a single MFC patch would not suffice.

The other factor affecting the deflection of the control surface is displacement. In Zhang *et al*. [39], the maximum deflection of the aluminium plate was 0.914 mm. Based on the information provided in Zhang *et al*. [39], it is assumed that this is achieved based on some displacement (which is not the same as the free strain displacement) of the MFC patch, which is not explicitly mentioned and may be the reason for the deviation of the calculated and experimental results shown in Figure 73. The deformation of the control surface structure due to the displacement of the bonded MFC patches would therefore have an influence on the deflection of the control surface. The displacement required by the MFC patches to achieve the needed control surface structure deformation would have to be determined to ensure the structure would be able to achieve the required deflection.

The force required is not achievable, the displacement or deformation required of the MFC patch would need to be determined as the deflection of the fin structures becomes the determining factor if the force would be able to be generated. Therefore, this concept, with the given information, does not meet requirement FR1. Based on the information obtained regarding the MFC actuator and its application, the effects of modification cannot be predicted. Further investigation into the necessary patch displacement would have to be carried out.

6.1.2.2 *Structural Integrity FR4*

The bistable structure would be required to withstand at least the aerodynamic loads, which would result in a bending moment and a shear force at the origin of the beam structure, as shown in the free body diagram in Figure 76. The total load F_a was assumed to act at the free end of the cantilever beam as this would result in the highest bending moment at the fixed end of the beam. This would be a more conservative approach.

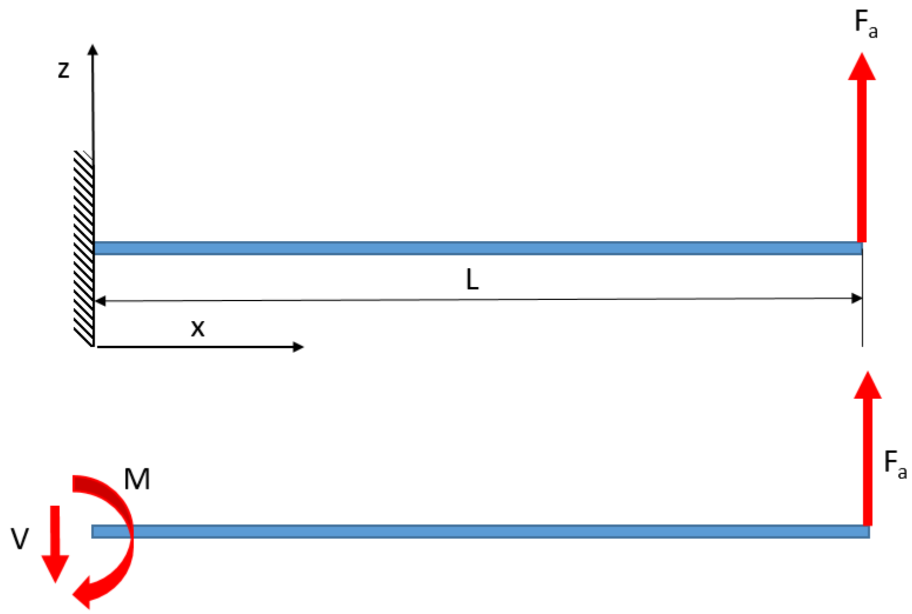

Figure 76: Free Body Diagram of the fin bistable structure

In Figure 76, F_a is 1685 N based on the load required for the missile to perform the 30 g manoeuvre, the shear force *V* at the fixed end is 1685 N, and the bending moment *M* at the fixed end of a 110 mm beam is 185.35 Nm (see APPENDIX I).

Degradation of the bistable laminate structure would result in a possible failure of the fin to achieve the desired deflection. This failure would prevent the required lift force from being generated, and therefore the actuator would not effectively manoeuvre the missile. The bistable laminate structure is a composite structure, and the behaviour of this type of material often varies due to different material properties in different directions. For this study, and for a first-order approximation to evaluate the structural integrity, the Maximum Strain Failure Criterion was applied.

According to R. Reid [139], the Maximum Strain Failure Criterion is similar to the Maximum Shear Stress theory, except strains are compared instead of stress with regard to the failure of the material.

Based on the Maximum Strain Failure Criterion, lamina failure is a result of either normal strain exceeding the maximum allowable strain in tension or compression (or shear) strain exceeding the maximum allowable shear strain for the lamina material. Failure is said to have occurred if any of the following strain criteria are not met:

$$\epsilon_1 \geq \epsilon_{1t}^* \tag{34}$$

or

$$\epsilon_1 \leq \epsilon_{1c}^* \tag{35}$$

or

$$\epsilon_2 \geq \epsilon_{2t}^* \tag{36}$$

or

$$\epsilon_2 \leq \epsilon_{2c}^* \tag{37}$$

or

$$|\gamma_{12}| \geq \gamma_{12}^* \tag{38}$$

This theory can also be expressed in terms of stresses as follows:

$$\sigma_1 - v_{12}\sigma_2 \geq X_t \tag{39}$$

or

$$\sigma_1 - v_{12}\sigma_2 \leq X_c \tag{40}$$

or

$$\sigma_2 - v_{21}\sigma_1 \geq Y_t \tag{41}$$

or

$$\sigma_2 - v_{21}\sigma_1 \leq Y_c \tag{42}$$

or

$$|\tau_{12}| \geq S \tag{43}$$

To evaluate the structure as described, the principal stresses were determined. The principal stresses were determined using the stress-transformation equations from Jones [140]:

$$\sigma_1 = \sigma_x \cos^2\theta \tag{44}$$

$$\sigma_2 = \sigma_x \sin^2\theta \tag{45}$$

$$\tau_{12} = -\sigma_x\, sin\,\theta\, cos\,\theta \tag{46}$$

For the x-y plane, σ_x refers to the stress in the x-direction, θ is the fibre orientation of the composite material, σ_1, σ_2 and τ_{12} are the principal stresses in the 1 and 2 directions and principal stress in the 1-2 plane. Based on the load case shown in Figure 76, the bending stress in the x-direction equates to the σ_x as the axial stress when considering the section under tension. There is no stress in the y-direction due to the load condition considered; therefore, σ_y is zero. The bending stress was determined as follows:

$$\sigma_x = \frac{My}{I} \tag{47}$$

For a moment, M, of 185.35 Nm, a distance from the neutral axis to the edge of the beam cross-Section, y, of 1 mm, and a moment of inertia, I, of 157.33 mm^4, would result in a maximum bending stress of 1178 MPa.

The shear reaction load in the x-y plane, based on the load case in Figure 76, was used to determine the shear stress, τ, as follows:

$$\tau = \frac{VQ}{Ib} \tag{48}$$

Where V is the shear force, I is the moment of inertia, b is the width of the section. Q is the first moment of the area above the area of interest of the structure that the MFC actuator will deform, envisioned as a beam for this study. For the sheer force of 1685 N, and I of 157.33 mm^4, Q of 0.236 mm^3, and b of 236 mm, the shear stress would be 0.0107 MPa.

If we consider the neutral axis of the beam structure, the shear stress would be at a maximum. However, the bending stress contribution to the tensile stress would be zero. At the edge of the beam, the bending stress contribution to the tensile stress would be at its maximum, and the shear stress, τ_{xy}, would be zero. For this study, the failure at the beam edge was considered as it would fail in bending first. Therefore, the principal stress is the bending stress. Therefore, σ_1 is 1178 MPa. Due to the loading of the beam, σ_2 and τ_{12} are equal to zero.

Based on the failure criterion in terms of stress, the outcomes of the assessment are seen in Table 34.

Table 34: Failure Criterion Evaluation

	Criterion	Result	Outcome
1	$\sigma_1 - v_{12}\sigma_2 \geq X_t$	1.2E+09	Fail
2	$\sigma_1 - v_{12}\sigma_2 \leq X_c$	1.2E+09	Pass
3	$\sigma_2 - v_{21}\sigma_1 \geq Y_t$	3E+08	Pass
4	$\sigma_2 - v_{21}\sigma_1 \leq Y_c$	3E+08	Fail
5	$\lvert\tau_{12}\rvert \geq S$	0	Fail

Therefore, the failures indicated in Table 34 show that the composite fails based on the Maximum Strain Failure Criterion (1), (4) or (5). Given that the structure is not currently able to withstand the aerodynamic loads, it will not be able to withstand the inclusion of the load due to the MFC actuator combined. Therefore, this concept does not comply with the requirement.

Changing the layup by increasing the ply number would improve the stiffness of the structure, as mentioned in Anto [141]. It was also mentioned that ply orientation plays a role in stiffness, with the stiffness being higher when the ply orientation is in the same direction as the tensile loading. Therefore, altering the layout for the concept could improve the structural integrity. This would need reinvestigation to determine the change required to improve the structure. The change in the force required to alter the structure would also have to be investigated as increasing the ply number would increase the thickness of the structure. This would require a high load from the actuator to deflect as required.

6.1.2.3 Bandwidth FR7

The effect of the Piezoelectric MFC actuator on the bandwidth of the system was evaluated by reviewing the literature. In Fichera *et al*. [55], an MFC actuator was used for a camber morphing trailing edge. The morphing of the trailing edge is similar to the morphing of the surfaces used in this concept. In Fichera *et al*. [55], the bandwidth was determined through dynamic testing. The actuator was able to achieve a bandwidth of 25 Hz. The actuators consisted of an MFC patch sandwich (which is two MFC patches with a 0.012 mm steel shim in between), 0.5 mm aluminium sheet metal, and fixed at the end with a non-deforming ABS plastic slider. It was shown that the bandwidth achieved was similar to that of the structure's first bending mode. Therefore, the construction of the actuator plays a role in the bandwidth of the system, as mentioned in Wu *et al*. [56], where it states the effect of the mechanical structure on the bandwidth and resonance and also indicates the influence of the electrical circuit. They affirm that PZT actuators have high-frequency bandwidths greater than 1 kHz. These high bandwidths are probably determined with the piezoelectric device alone without any additional components connected. If the mechanical components are considered, the bandwidth will be reduced. If the bandwidth achieved in S. Fichera *et al*. [55] was 25 Hz, a fin made from steel, as described for Concept 1 (See APPENDIX G), would add additional load to the system lowering the bandwidth below 25 Hz. Given that high bandwidths are possible, components could be adjusted to achieve the necessary response time. However, at this stage, for this concept, it is assumed that the actuator would not meet requirement FR7.

6.1.2.4 Operation Time FR2

As mentioned in the previous section, the operation time refers to the duration the FGM would have to operate. The missile is meant to operate for 180 s, and therefore the force mechanism should operate, at a minimum, for the same duration of time, unless there is an alternate requirement or specification that it doesn't have to do so.

The operation time for the MFC actuator will be limited by the battery power supply and MFC actuator, whilst the bistable laminate structure will be limited by its fatigue life.

As previously mentioned, the power supply is considered to be uncapped. The limitations of the power supply will therefore not be discussed in this study. It is important and should therefore be evaluated in a future study.

According to the MFC datasheets [36], the operational lifetime at 2kVp-p is 10^7 cycles. If the actuator is required to operate at a bandwidth of 25 Hz, the MFC actuator would be needed to achieve 4500 cycles which is lower than the operational lifetime specified. Therefore, the actuator would be able to meet the requirement FR2.

Specific information regarding the fatigue life of the T300/976 composite was not available at the time. However, a study was done on the fatigue life of carbon/epoxy laminate composites, which is the category of composites T300/976 would fall under. The fatigue life of the test specimens range from 25900 to 818355 cycles according to Reis *et al*. [142], which is well above the estimated cycles from the calculation for the MFC actuator, and therefore would be able to meet requirement FR2.

6.1.2.5 Storage FR5

According to the MFC actuator datasheet [36], the MFC patches are environmentally sealed. The limits of the sealing were not found. The storage of the MFC actuator requirements dictates that the actuator must be stored within the temperature range of 10-60° C and less than 70% humidity. Due to the placement of the MFC actuator within the actuator system, they are subjected to the same storage specifications as other weapon systems. This is usually an environmentally controlled facility as laid out in a Military Standard [124]. The actuator can be stored for 20 years (with maintenance at 6 to 7 years) according to the manufacturer Smart-Material [37]. See APPENDIX J for the email from Smart-Material affirming this statement.

The bistable laminate composite, being a carbon composite, tends to degrade when exposed to the natural environment [143]. The composite would form part of the internal structure of the fin and would be sealed to prevent exposure to the external environment, delaying the rate of degradation. This type of composite is also used in aviation/aerospace applications [144] and thus would be required to survive the operational environment for those applications which have a variety of harsh environmental conditions. This material would most probably be able to survive typical weapon storage, especially if it is a controlled environment.

Therefore, this concept for the FGM meets requirement FR5.

6.1.3 Concept 3

As seen in Chapter 1, various flow actuators use Adaptive Structure/Smart Materials to operate. This concept uses Adaptive Structures in the form of flow actuators to regulate the interaction of the fluid (air) of the fluidic control system and the airflow over the surface. Synthetic jet actuators, diaphragms oscillated using piezoelectric actuators, are built into a control fin, as illustrated in Figure 77. This will be used in conjunction with Free Wing. The Free Wing is a self-stabilising fin, with a centre of rotation ahead of the fin’s centre of pressure. An illustration of the fin’s cross-section can be seen in Figure 78.

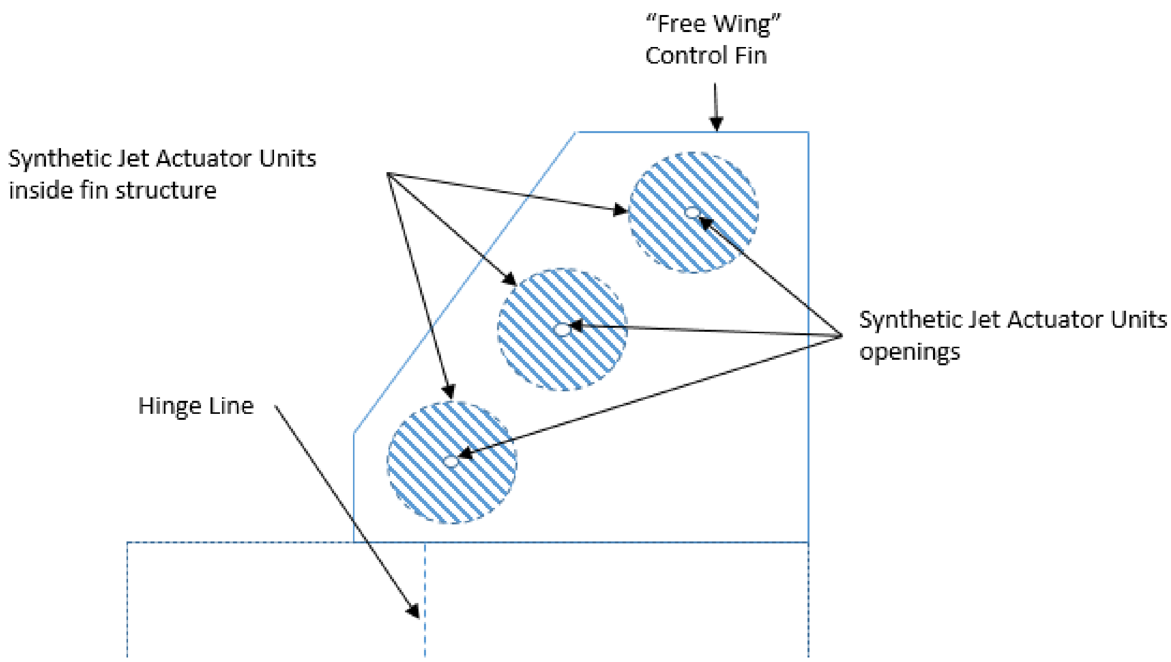

Figure 77: Concept 3 - Synthetic Jet Actuation - Flow Effector

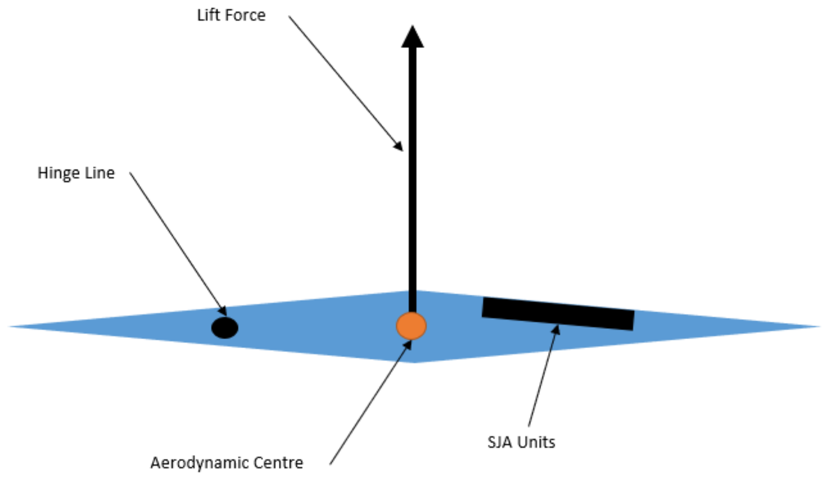

Figure 78: Supersonic Free Wing Illustration

As described in Porter *et al*. [145], the Free Wing is free to rotate about a spanwise axis. Instead of the control tab, the synthetic jet actuators will be used instead to control the fin rotation. Therefore, this concept would straddle both the Tail Fin Rotation and Flow Effector categories.

When the actuators are active on one fin, an improvement in the lift is achieved by delaying the separation of the boundary layer. This is achieved by vortices that are ejected from the orifices on the

fin's surface. Oscillations of the diaphragm like membrane generate the vortices. This lies beneath the opening on the fin's surface.
The description of how the boundary layer is altered is discussed in Section 2.5. This modification of the boundary layer changes the effective shape of the control fin. This change in the effective shape could shift the fin's centre of pressure which should induce a pitching moment of the fin.

This concept generates force in two ways. The first is based on the normal force coefficient, which is a function of the Mach number, angle of attack, aspect ratio and wing planform area of the control surface. The second is based on the influence of synthetic jets.

For this study, the flow has a velocity of Mach 4. This means that there would be shock-induced boundary layer interactions. As explained in Verma *et al*. [146], these phenomena cannot be avoided at supersonic velocities and are said to be complex physical interactions. Flow control techniques, which included the application of synthetic jets, have been the subject of many recent studies as a means to reduce the effects of shock-induced boundary layer interactions [146]. The purpose of flow control highlighted in Verma *et al*. [146] is to encourage a reduction in the negative influence of Flow Separation or to influence Compressible Mixing, with the aim of improving the overall performance. Altering the flow characteristics of the incoming boundary layer by introducing energy to its mean velocity profile is considered as the initial step with regard to flow control according to Verma *et al*.[146] and Blinde [147].

It was shown in Verma *et al*. [146] and Vadillo *et al*. [148] that synthetic jets can be used to control the shock strength, and it is both the unsteadiness and the separation of the boundary which makes these devices a good choice for hinge less control for the purpose of drag reduction. However, this result was obtained based on transonic speeds and most of the other studies described in Verma *et al*. [146] results were based on subsonic velocities. There were some promising results using Micro Jets at supersonic velocities; however, this is not the same as synthetic jets because micro jets make use of an additional gas supply. The Micro Jets, together with the transonic synthetic jet results from the other studies in Verma *et al*. [146], indicated that there is a possible use for synthetic jets for control in supersonic flow, but further investigation, beyond the scope of this study, is required to determine the viability of this control option in the context of this study. Therefore, it was decided that this concept will not be further analysed. This concept was discounted at this stage to highlight the Smart Material device as a system for flow control and to indicate the shortcomings of such a device for use in the defined application of this study.

6.1.4 Concept 4

Smart Materials can be used to open and close the openings of a bleed port system [95] or a Passive Porosity-Based Flow Control system [149]. Airflow from the high-pressure zone of an aerofoil passes through the wing structure, through openings on the wing surface, to the low-pressure zone of the aerofoil. This is illustrated in Figure 79.

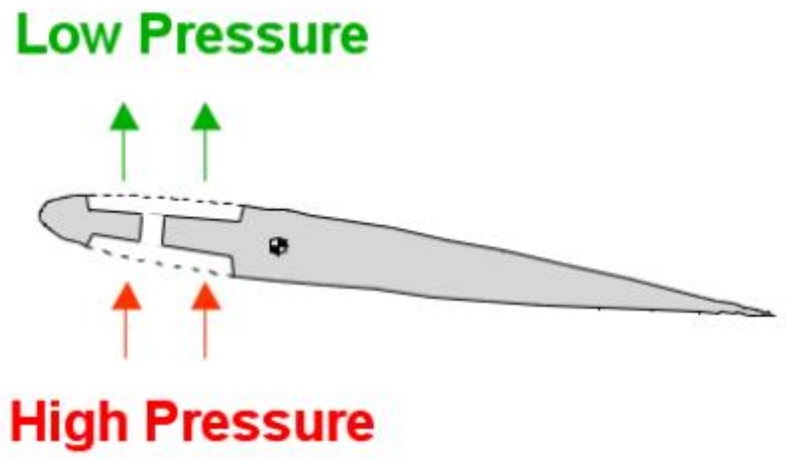

Figure 79: Passive porosity illustration [150]

Based on the finding by Bauer [98], the “Lift Dumping”, as described in Section 2.8, was considered as the method to alter the lift for the lift surface. As mentioned in Section 2.8, this system could be utilised for different flight regimes, and hence it was considered for this study.

To ensure the airflow is not bled from the high-pressure region to the low pressure, the openings on the upper and lower surface of the wing would need to be controlled so that they can be opened and closed when necessary. The mechanism to open and close the openings of the wing’s upper and lower surfaces can be controlled using Smart Materials. For this concept, a piezoelectric actuator will be employed to control the openings.

Piezoelectric actuators, as seen in Figure 80, will be used to allow a cover plate to slide to open and close on the upper and lower surfaces.

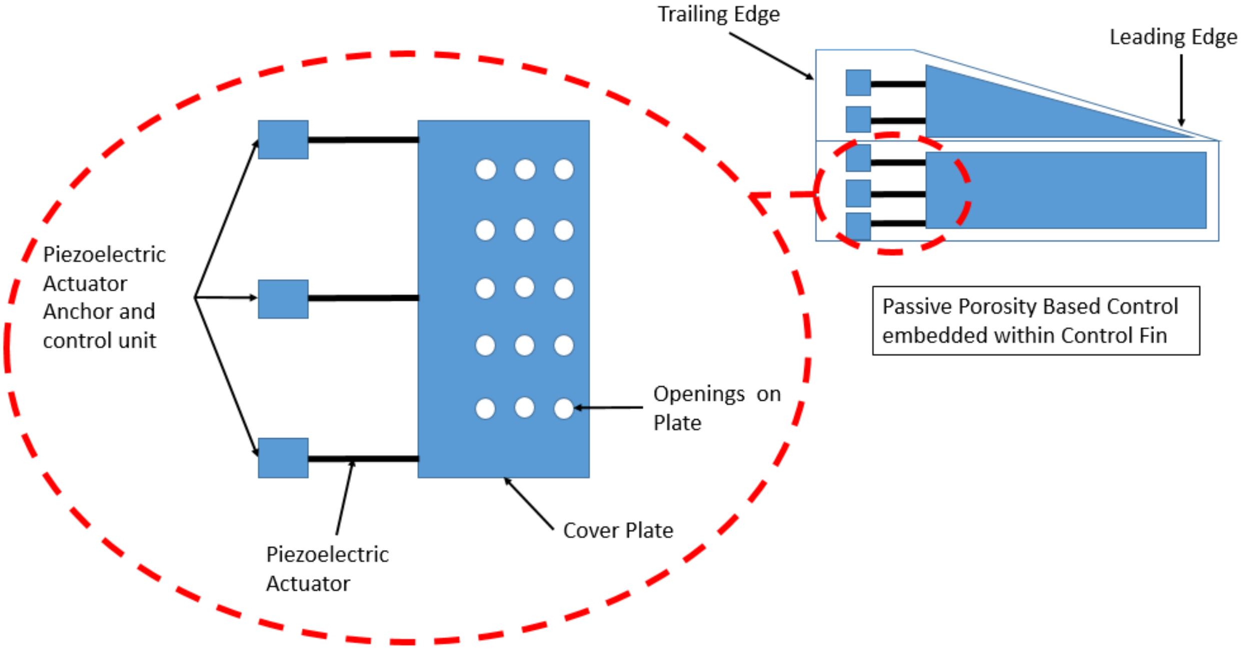

Figure 80: Concept 4 – Passive Porosity Based Control

Similar to the structure discussed in Barrett *et al*. [151] (as seen in Figure 81)

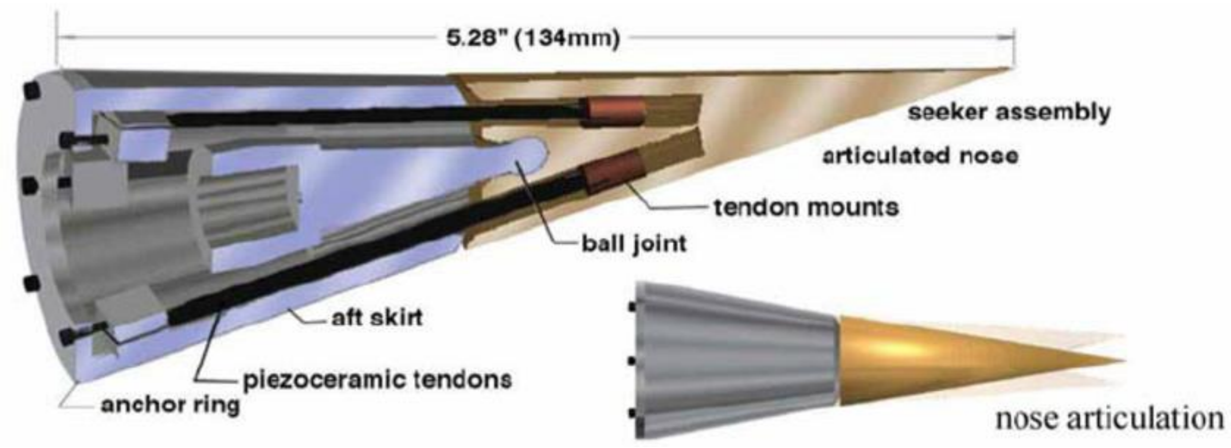

Figure 81: Piezoelectric Actuator in Munition [152]

The piezoelectric actuators pull the plate in one direction to align the plate holes with the holes on the fin surface, which allows the air to bleed through the fin, altering the lift. When required, the plate is pushed back, blocking the holes on the fin surface. The plate will have to be relatively low in mass so that the work done by the actuators is also low.

6.1.4.1 Force Generation FR1

The piezoelectric actuators will form part of a Passive Porosity-Based Flow Control system. The actuators will be used to push a plate that will allow for the opening of the holes on the upper and lower surfaces, which will allow the movement of air from the high pressure to the low-pressure surfaces. This mechanism will be used for Lift Dumping [96]. It is important to note this mechanism does not rotate the fin, as is the case in a conventional application. Therefore, the coefficient of normal force for the fin, as described by Fleeman [60], is only altered by the change to the missile's angle of attack.

The C_N for the fin, for relatively small angles of attack between -20° to 20°, was plotted against the angle of attack in Figure 82.

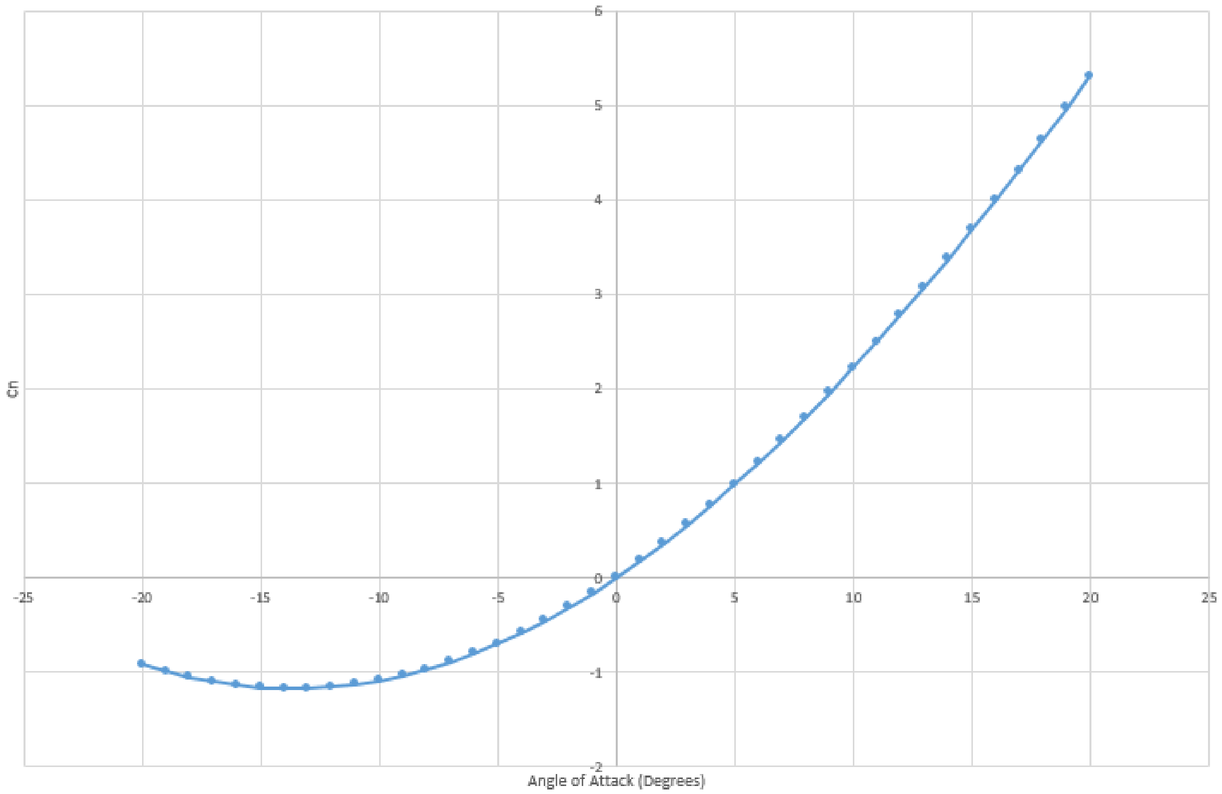

Figure 82: C_N vs α for the missile fin

The manoeuvring of the missile would have to be carried out in a different way compared to the generic missile with the rotating fin. The Lift Dumping would be used to manipulate the missile's angle of attack to achieve a certain normal force coefficient at the tail of the missile, which has an influence on the missile's lift. The magnitude of lift for the missile body is altered depending on the angle of attack. Therefore, the changes in total missile lift would need to be evaluated to determine the best "lift dumping" strategy for the tail fins. This strategy will not be characterised in this study.

For the requirement FR1a to be met, the ASYS would have to provide 1685 N of Normal force. This can be achieved by altering the missile's angle of attack between -1° to – 2° or 1° to 2°, as shown in Figure 83.

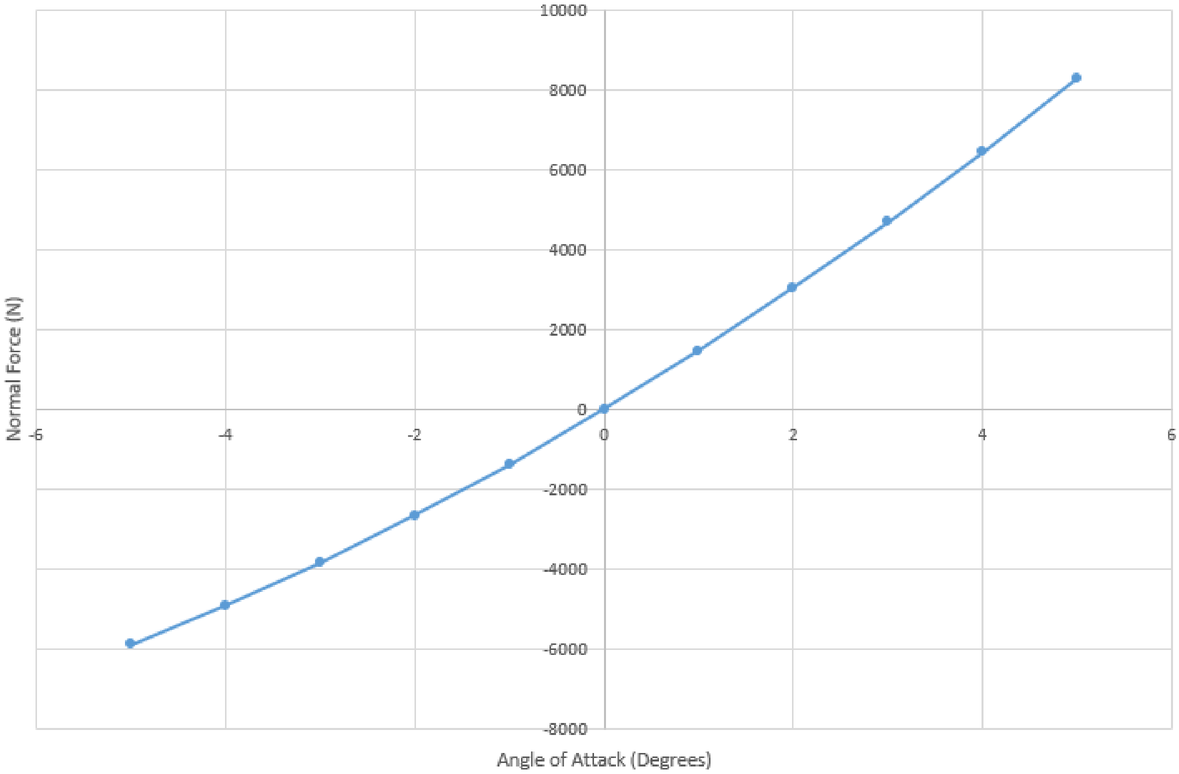

Figure 83: Normal force vs Angle of Attack

Therefore, using the fin (considering it forms part of the FGM), the force generation requirement, FR1a, is met. However, the change in angle of attack would also affect the normal force generated by the other missile lift surfaces. Therefore, the total normal force would differ from the normal force expected with the generic ASYS. The missile may therefore not be able to perform as expected. As mentioned previously, however, an alternative control method of manoeuvring that would include "Lift Dumping" and not fin deflection would have to be derived and applied.

The piezoelectric actuator role would only be used to open (and close) the holes that allow air to bleed from the high-pressure zone to the low-pressure zone. The plate within the fin that the actuator would have to push (or pull) would be subjected to the pressure induced by the external flow. The worst-case would be experienced in the high-pressure zone. This is illustrated in Figure 84.

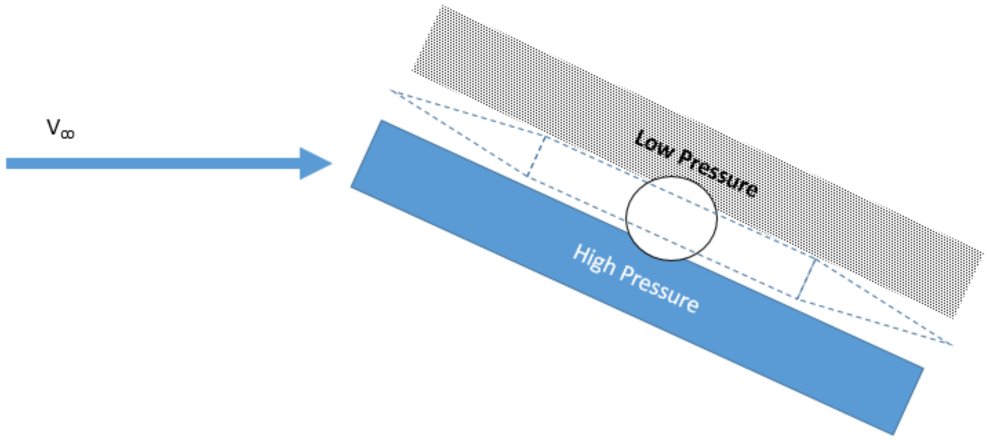

Figure 84: Illustration of High and Low Pressure of Fin due to free stream

For the case shown in Figure 84, the high pressure is on the lower side of the fin. Based on supersonic linear theory in J. D. Anderson [76], the coefficient of pressure on the lower surface of a flat plate is:

$$C_{p,l} = \frac{2\alpha}{\sqrt{M_\infty^2 - 1}} \tag{49}$$

And for the upper surface,

$$C_{p,u} = -\frac{2\alpha}{\sqrt{M_\infty^2 - 1}} \tag{50}$$

Where α is the angle of attack (degrees) and M_∞ is the Mach number of the free stream. Based on the cross-sectional geometry of the fin, it was assumed to behave like a flat plate where the pressure coefficient determined will be constant over the respective surfaces. Since,

$$C_p \equiv \frac{p - p_\infty}{q_\infty} \tag{51}$$

The pressure coefficient for the upper and the lower surfaces can therefore be written as follows:

$$C_{p,u} = \frac{p_u - p_\infty}{q_\infty} \tag{52}$$

$$C_{p,l} = \frac{p_l - p_\infty}{q_\infty} \tag{53}$$

Where q_∞ is the dynamic pressure:

$$q_\infty = \frac{1}{2}\rho_\infty V_\infty \quad (54)$$

The pressure p_u and p_l refer to the pressure on the upper and lower surfaces, respectively. The p_∞ refers to the free stream pressure, and the V_∞ is the free stream velocity. Using Equation (52) and Equation (53) in conjunction with Equation (54), the pressure on the lower surface can be determined.

$$p_l = C_{p,l} q_\infty + p_\infty \quad (55)$$

For an α of 20°, a q_∞ of 337.86 kPa, V_∞ of 1212 m/s, p_∞ of 32 kPa and a Mach number of 4, the pressure on the lower surface will be about 93 kPa.

Assuming this is the maximum angle of attack, this would be the maximum pressure that the plate within the fin would experience on the lower surface. This pressure applied over the area of the plate would equate to a force applied to the plate. This force is relevant as it relates to the frictional force the piezoelectric actuator would have to work against.

The exact dimensions of the plate must have to be determined based on the number of holes required and the exact placement of the porous surfaces on the fin's surface to have the desired Lift Dumping effect. This will not be covered in this study as the focus was on the effectiveness of the Smart Material in this application.

To evaluate the ability of the piezoelectric actuator to push the plate, the previously determined pressure (p_l) was assumed to be acting over the largest plate area (A) as this would result in the largest force applied to the plate (F), based on the following equation:

$$F = p_l A \quad (56)$$

The area for a single fin, 0.12 m^2, would be the largest area that could be considered for this study. Based on this area, the force applied to the plate would be 10.8 kN. The load is the basis of the friction force, which acts in the opposite direction to the direction the movement of the plate has to move. This is illustrated in the free body diagram of the plate Figure 85. It is assumed that the plate is constrained in all directions except for translation in the x-direction.

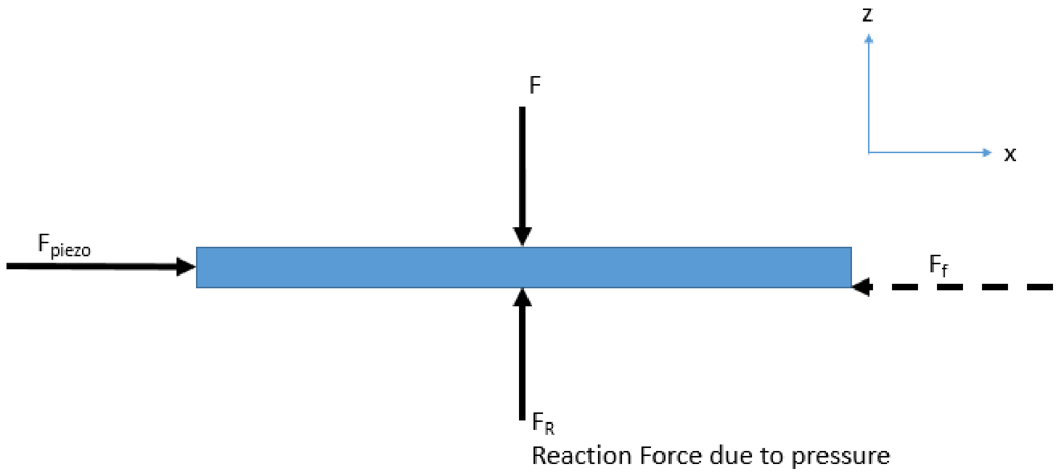

Figure 85: Plate free body diagram

The static friction force, F_f, is determined as follows:

$$F_f = \mu_s F$$

Where μ_s is the coefficient of static friction between the plate (assumed to be Aluminium) and the guiding rail within the fin (assumed to be titanium), which is 0.41 according to data found online [153], therefore, F_f would be 4443.51 N. The force applied by the piezoelectric actuator would have to be greater than this to commence movement of the plate initially, thereafter it would have to overcome the effect of the kinetic friction. The force due to kinetic friction is determined as follows:

$$F_{kf} = \mu_s F$$

This force acts in the same direction as F_f. Based on a kinetic friction coefficient of 0.38 [153], the force due to the kinetic friction would be 4118.38 N.

For a single linear piezoelectric actuator such as the P-845.60 by PI [41], which has a maximum push force of 3000 N, it would not be able to move the plate. Two of these actuators would have to be employed to move the plate. The friction force can be reduced if a lubricant is used on the sliding surfaces to reduce the coefficient of friction. This piezoelectric actuator can only apply a 700 N pull force. An additional mechanism would thus be required to aid the plate in returning to its initial position. This can be done by using a spring or another piezoelectric actuator pushing in the opposite direction (which adds an additional force the piezo actuator would have to work against).

This concept would therefore be able to work in a mechanism to open and close the holes of the Lift Dumping system, which allows the system to generate the required force provided the fin is at the required angle of attack. However, further investigation is required to determine the viability of this control option in the context of this study. Therefore, the requirement is not met.

6.1.4.2 Structural Integrity FR4

In this concept, as discussed previously, the actuators are affected by the pressure distribution experienced on the upper and lower surfaces of the fin. The only load considered in this study was the load the actuators would be subjected to is the load applied to move the plate into position. Other load cases should be identified and evaluated in a future study. As described in the previous section, the actuators would push the plate to open the holes on the surface of the fin, and they would require an additional mechanism to pull the plate back to its initial position. While the plate is pulled back, the actuators (used to initially push the plate) will be in compression. Based on the information provided by the manufacturer for the piezoelectric actuators, the actuator should not be preloaded with compressive stress exceeding 30 MPa [154]. The load applied to the plate to return it to its initial position is assumed to be the same as the load used to initially push the plate, as it would be required to overcome the same frictional resistance. The load would have to be applied over an area of 75 mm^2 (which seems possible given the available space) if two actuators are to be used to ensure the compressive stress is below 30 MPa. The actuators would therefore be able to withstand the loads applied and maintain their structural integrity. Therefore this concept meets requirement FR4 based on the evaluation carried out.

6.1.4.3 Bandwidth FR7

The actuator makes use of a Lead Zirconate Titanate piezoelectric stack. Lead Zirconate Titanate (PZT) stacks have been shown to operate at bandwidths in the kilohertz range [155].

The piezoelectric actuator is capable of producing no-load bandwidths up to 5.5 kHz [41], as mentioned in Section 2.2.2. Equations (**57**) and (**58**) from the PI Ceramic catalogue [156] can be used to determine the resonant frequency of a spring/mass system like the piezoelectric stacks.

$$f_0 = \left(\frac{1}{2\pi}\right)\sqrt{\frac{k_T}{m_{eff}}} \tag{57}$$

$$f'_0 = f_0\sqrt{\frac{m_{eff}}{m'_{eff}}} \tag{58}$$

Where f_0 is the resonant frequency of the no-load system, and k_T is the stiffness of the actuator. For the chosen piezoelectric actuator, the resonant frequency is 5500 *Hz* (based on the actuator's datasheet [41]), and it has an effective mass (m_{eff}) of 0.068 *kg* (calculated based on a third of the ceramic stack mass as described in the PI Ceramic catalogue [156]).

m'_{eff} is the effective mass, including the mass added to the system. For a 0.8 kg plate, the effective mass, including the added mass, would be 0.868 kg. Therefore, the resultant resonant frequency, f'_0, would be 1539.42 *Hz*.

The bandwidth Δf for the system can be estimated based on the adapted relationship between the resultant resonant frequency, f'_0 and the mechanical quality factor Q as shown in Equation (**59**)from Miller [157], where it is referred to as the bandwidth method:

$$Q = \frac{f'_0}{\Delta f} \tag{59}$$

The mechanical quality factor Q is a characteristic of piezoelectric systems that characterizes what PI Piezo Ceramics [156] refers to as the "sharpness of resonance". The inverse of this factor is related to the mechanical loss in the system and is determined as shown in Equation (**59**). The mechanical quality factor is determined experimentally as described by Holland and EerNisse [158]. The quality factor for the chosen piezoelectric actuator was not available. In a study by Nader *et al*. [159], the quality factors determined ranged from 50- 69 for different stack sizes. For a Q value greater than 62, a bandwidth greater than 25 Hz should be possible based on Equation (**59**).

Further details of the train of components would be required to assess this aspect completely. However, for this analysis, the FGM would meet requirement FR7.

6.1.4.4 Operation Time FR2

According to the piezoelectric actuator manufacturer, PI [41], the piezoelectric actuators are able to operate for 100^9 cycles. Based on this information, the piezoelectric actuator material used to create the tendons for this concept are assumed to have a similar operational life span. Therefore, they should be able to meet the requirement FR2.

6.1.4.5 Storage FR5

According to the design constraints stated in Barrett *et al*. [151], based on the life span information found online [160], munitions storage is usually 20 years in controlled storage conditions. Therefore, it can be concluded that the material selected for the piezoelectric actuators in Barrett *et al*. [151] should adequately meet the storage life span requirement. If the same materials are employed in Concept 4, then it would meet requirement FR5.

6.1.5 Concept 5

The concept, as seen in Figure 87, would essentially replace the generic servo motor and lead screw mechanism, as depicted in Figure 66. A Piezoelectric Linear actuator such as the P-845.60 by PI [41] would provide the force to rotate the output shaft of the actuator, which would result in rotation of the fin. The actuator would require a Displacement Amplification device in order to create the required fin deflection. This concept was based on and adapted from a study by Giurgiutiu & Pomirleanu [30].

The study by Giurgiutiu & Pomirleanu [30] describes the following parameters as important for the design of the Displacement Amplification device:

- Gain G
- Work Efficiency η_m
- Energy Transfer Coefficient E'_e
- Internal Stiffness k_i

Where the gain is the amplification factor of the Displacement Amplification device, the work efficiency is the ratio of the work going into the device, and the work coming out, the Energy Transfer Coefficient which is a characteristic of Smart Materials, and the Internal Actuator Stiffness is a characteristic of the selected actuator. Giurgiutiu & Pomirleanu [30] describe that the design should aim for a Displacement Amplification system with low gain and high energy transfer coefficient, which according to their study, is achievable. They mention that an optimum internal stiffness can be obtained, considering the work efficiency, based on the ratio of the energy transfer coefficient to the gain. Further investigation in this device was considered beyond the scope of this study as the focus is on the FGM. Therefore the detailed design of the Displacement Amplification device is for future work.

Based on the conceptual design described by Giurgiutiu & Pomirleanu [30], the work going into the Displacement Amplification device equates to the product of the force provided by the piezoelectric actuator F'_e and the actuator's displacement u'_e. The output of the device is the force required, F_e, to rotate the fin and required displacement, u_e, to provide the necessary fin deflection. The ratio of the work input and the work output forms the gearing ratio of the mechanism. If the same lever arm (76 mm) from the generic actuator system is used and the same hinge moment of about 28 Nm is required, then F_e would need to be about 369 N. To create the necessary deflection of 12.7 degrees, the linear displacement, u_e, of the lever arm would need to be about 17.2 mm for deflection in one direction.

The work efficiency is defined by Giurgiutiu & Pomirleanu [30] as seen in Equation (60):

$$\eta_m = \frac{F_e u_e}{F'_e u'_e} \tag{60}$$

Given that the piezoelectric actuator selected, the work efficiency of the Displacement Amplification would be 23.68. This is based on the force input of a single actuator. This is based on the process described by Giurgiutiu & Pomirleanu [30], seen in Figure 86. The gain G would need to be greater than 190.3.

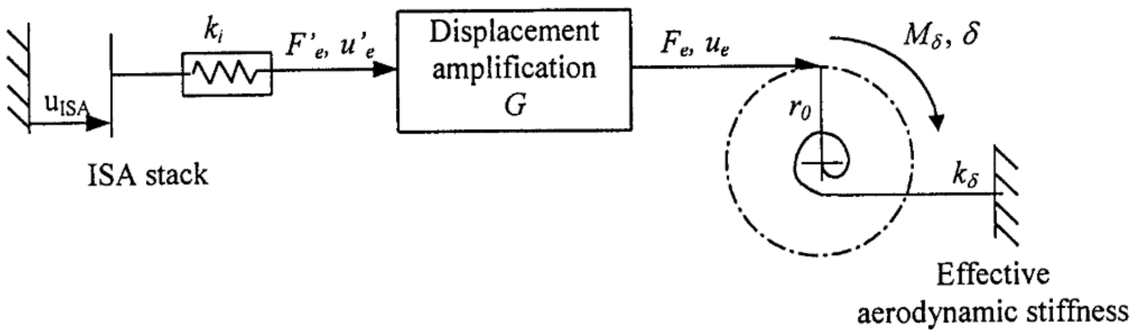

Figure 86: Model of Displacement Amplification process

The simplified concept can be seen in Figure 87. The concept as described would benefit from a spring to assist it in returning to its neutral position. A clutch and gear system could be used to switch between the deflections in either direction so that the piezo actuators only need to work in their respective directions.

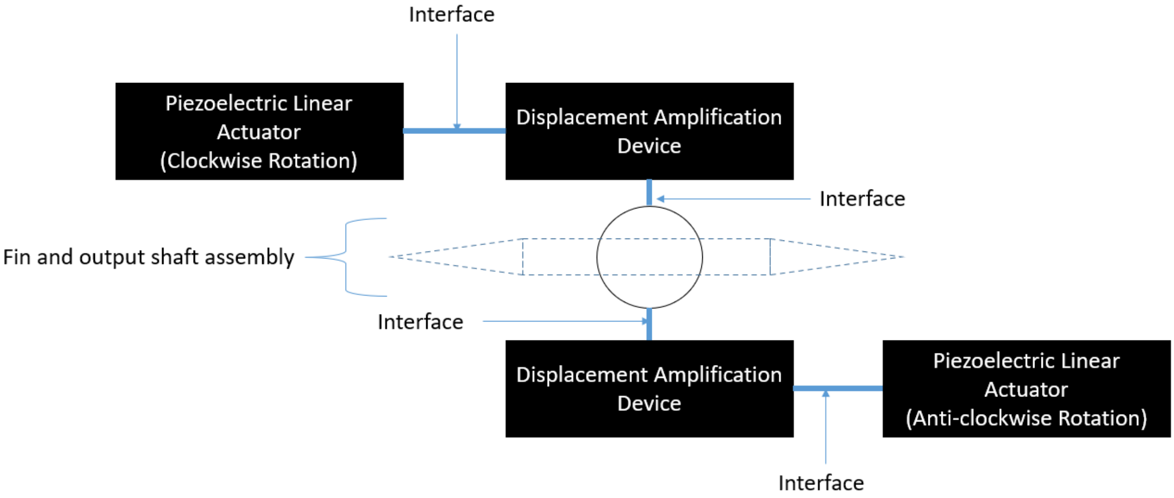

Figure 87: Concept 5 illustration

6.1.5.1 Force Generation FR1

For a single linear piezoelectric actuator such as the P-845.60 by PI [41], which has a maximum force of 3000 N. This would be able to provide the necessary hinge moment together with the Displacement Amplification device and therefore would allow for the aerodynamic force to be created. Therefore, it meets the requirement FR1.

6.1.5.2 Structural Integrity FR4

Based on the information provided by the manufacturer for the piezoelectric actuators, the actuator should not be preloaded with compressive stress exceeding 30 MPa [154]. The details of the Displacement Amplification device would be required to fully assess this requirement. Assuming this device would also have to withstand the applied loads, the structural integrity would be created to meet the requirement FR4.

6.1.5.3 Bandwidth FR7

The piezoelectric actuator is capable of producing no-load bandwidths up to 5.5 kHz [41], as mentioned in Section 2.2.2. Equation (57) can be used to determine the resonant frequency of a spring/mass system like the piezoelectric stacks.

As described for Concept 4 in Section 6.1.4.3, the required bandwidth should be achievable for this type of actuator.

Therefore, for this analysis, the FGM would meet requirement FR7.

6.1.5.4 Operation Time FR2

According to the piezoelectric actuator manufacturer, PI [41], the piezoelectric actuators are able to operate for 100^9 cycles. Based on this information, the piezoelectric actuator material used to create the tendons for this concept are assumed to have a similar operational life span. Therefore, they should be able to meet the requirement FR2.

6.1.5.5 Storage FR5

According to the design constraints stated in Barrett *et al*. [151], based on the life span information found online [160], munitions storage is usually 20 years in controlled storage conditions. Therefore it can be concluded that the material selected for the piezoelectric actuators in Barrett *et al*. [151] should adequately meet the storage life span requirement. Therefore, it would meet requirement FR5.

6.2 Summary of Concept Generation

During this process, five concepts were developed. Three concepts were designed to rotate or simulate a rotated fin. The other two were designed to be Flow Effector concepts. The summary of their performance in meeting the requirements can be seen in Table 35.

Table 35: Summary of Concepts and Requirements

	Requirement				
FGM	FR1	FR2	FR4	FR5	FR7
1	Y	Y	N	Y	N
2	N	Y	N	Y	N
3	-	-	-	-	-
4	N	Y	Y	Y	Y
5	Y	Y	Y	Y	Y

In Table 35, Y indicates that the requirement was satisfied, and N indicates that the requirement was not met.

It is important to note that the requirements evaluated in this study were elicited with the FGM as the focus. The intention with the requirements baseline developed was to allow different Smart Materials to be used in different conceptual configurations to aid in answering the research question.

Concept 1 was able to meet the force generation (FR1), operational time (FR2) and storage (FR5) requirements. It fell short with regards to the Structural Integrity (FR4) and the bandwidth (FR7) requirements. It may be possible to improve the structural integrity by reducing the work per wire strand through an alternate configuration. As previously mentioned, the bandwidth could also be improved. However, further investigation is needed for these requirements to establish the level of improvement that can be achieved. This is beyond the scope of this study.

Concept 2 was unable to meet FR1 and FR4. The limitation in achieving the force requirement was the force produced and the displacement of the MFC actuator. The structural integrity was limited due to the composite construction. Further investigation is needed to establish the level of improvement that can be achieved when modifying the concepts to meet these requirements.

For Concept 3, as mentioned in Section 6.1.3, the literature indicates that there is a possibility to use synthetic jets for control in supersonic flow, but further investigation is required to determine the viability of this control option in the context of this study. Therefore, this concept was not investigated further in this study.

For Concept 4, as mentioned in Section 6.1.4. The mechanism was still able to meet some of the requirements. However, due to the uncertainty with regard to control effectivity in supersonic flow, it doesn’t meet the force generation requirement.

Concept 5 was able to me*et al*l the requirements. It should be noted that the concept depends on the Displacement Amplification device that was considered a “black box” for this concept.

With the concepts defined and the successful concepts identified, the outcomes from Step 3, seen in Figure 62 and defined in Section 3.5, have been achieved. The next step was then initiated, starting with the design decision tool development.

7. Design Decision Tool Development

The next step in this study was to develop a method of evaluating the concepts as described in Section 3.4. This method or framework would be constructed as a decision-making tool. Concepts for missile FGMs should be able to use this tool to evaluate their performance compared to the design objectives and each other. This chapter includes the first part of Step 4 as described in Chapter 3 of the study, as illustrated in Figure 88.

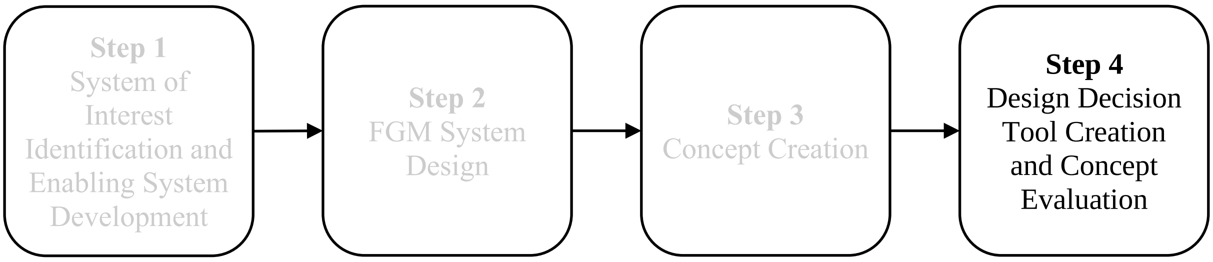

Figure 88: Part 1 of Step 4

The tool was constructed using the system requirements from the Systems Engineering approach followed in this study. The purpose of the tool was to evaluate how well the concepts achieved the requirements, to rank them based on their performance and to compare them with the generic FGM. The output of this tool was a performance score for the FGMs evaluated to be used as a decision input for design selection.

A simplified illustration of the tool can be seen in Figure 89.

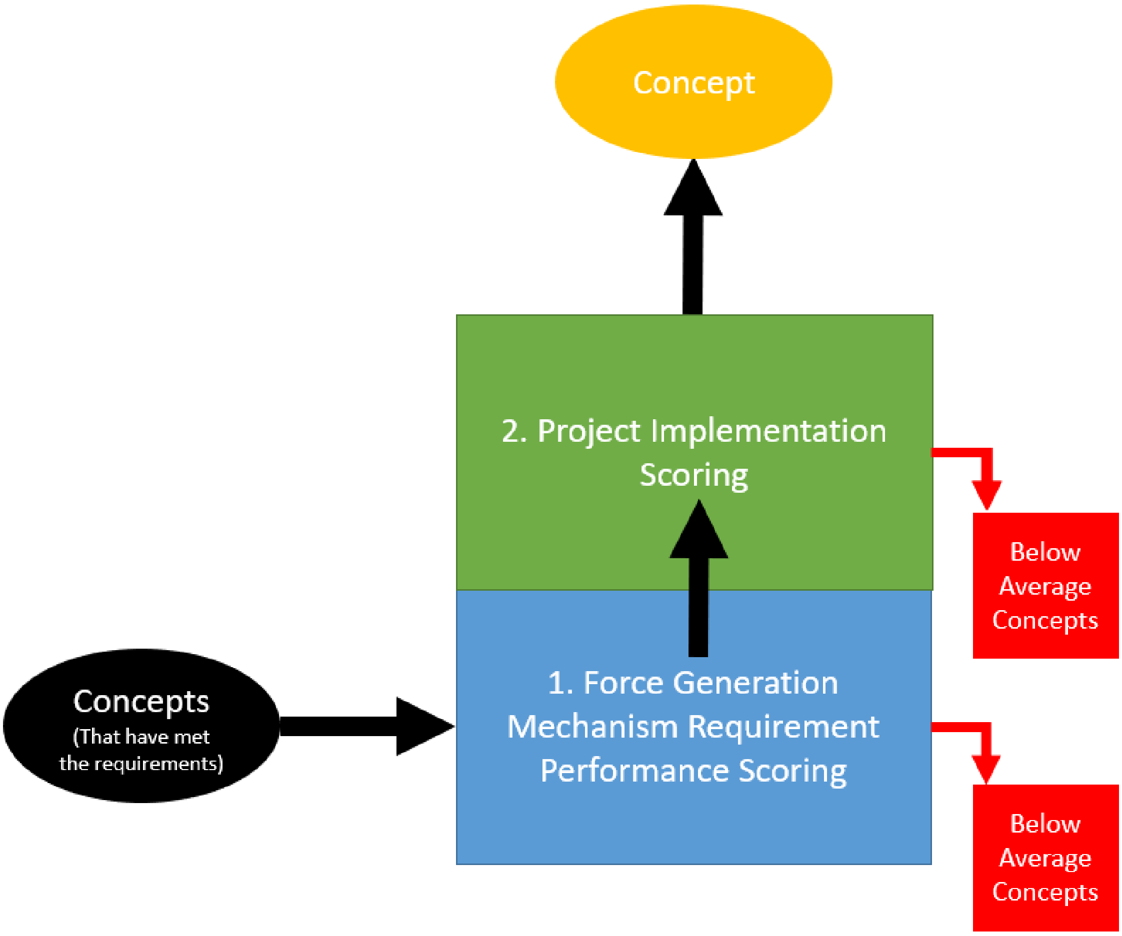

Figure 89: Illustration of the decision tool

7.1 The Vision for the Tool

The vision for the tool is for concepts that me*et al*l the requirements to proceed to the first stage, the Force Generation Mechanism Requirement Performance Scoring, where the concepts will be scored based on the requirements and the Measures of Effectiveness identified in Section 5.1.7. The scoring of the concepts is based on how well they meet the FGM system requirements. For the concepts with scores that are deemed acceptable, they would be able to move to the next level of the tool, the Project Implementation Scoring stage.

At this stage, the concepts will be assessed and scored based on how effective they are at meeting the project related criteria. For the concepts which make it through this filter, the final decision is then selected by carrying out a design review selecting the highest performing concept.

7.2 Force Generation Mechanism Requirement Performance Scoring

Cross [122] states that design alternatives can only be evaluated based on the design objectives. In the case of the FGM, the requirements of the system are the objectives of the design. The list of requirements is summarized in Table 36.

Table 36: Design Objectives

Label	Requirements	Quantity
FR1	The FGM shall generate the required force when required	1685 N (Minimum Required)
FR2	The FGM shall perform during the entire operational period.	>180s
FR4	The FGM shall withstand the loads during operation	1685 N
FR5	The FGM shall be able to be functional after a set storage period	Ten years (MIL-STD Conditions)
FR7	The FGM shall have a no-load bandwidth greater than 25 Hz	> 25 Hz

The design objectives were evaluated against the Measures of Effectiveness (MOEs) to identify which would have the most impact on the decision-making process. In order to evaluate the design objectives against the MOEs, a House of Quality (adapted from UWS Business Solutions GmbH [161]) was employed to determine which objectives would have the most impact on the design. The House of Quality can be seen in Figure 90.

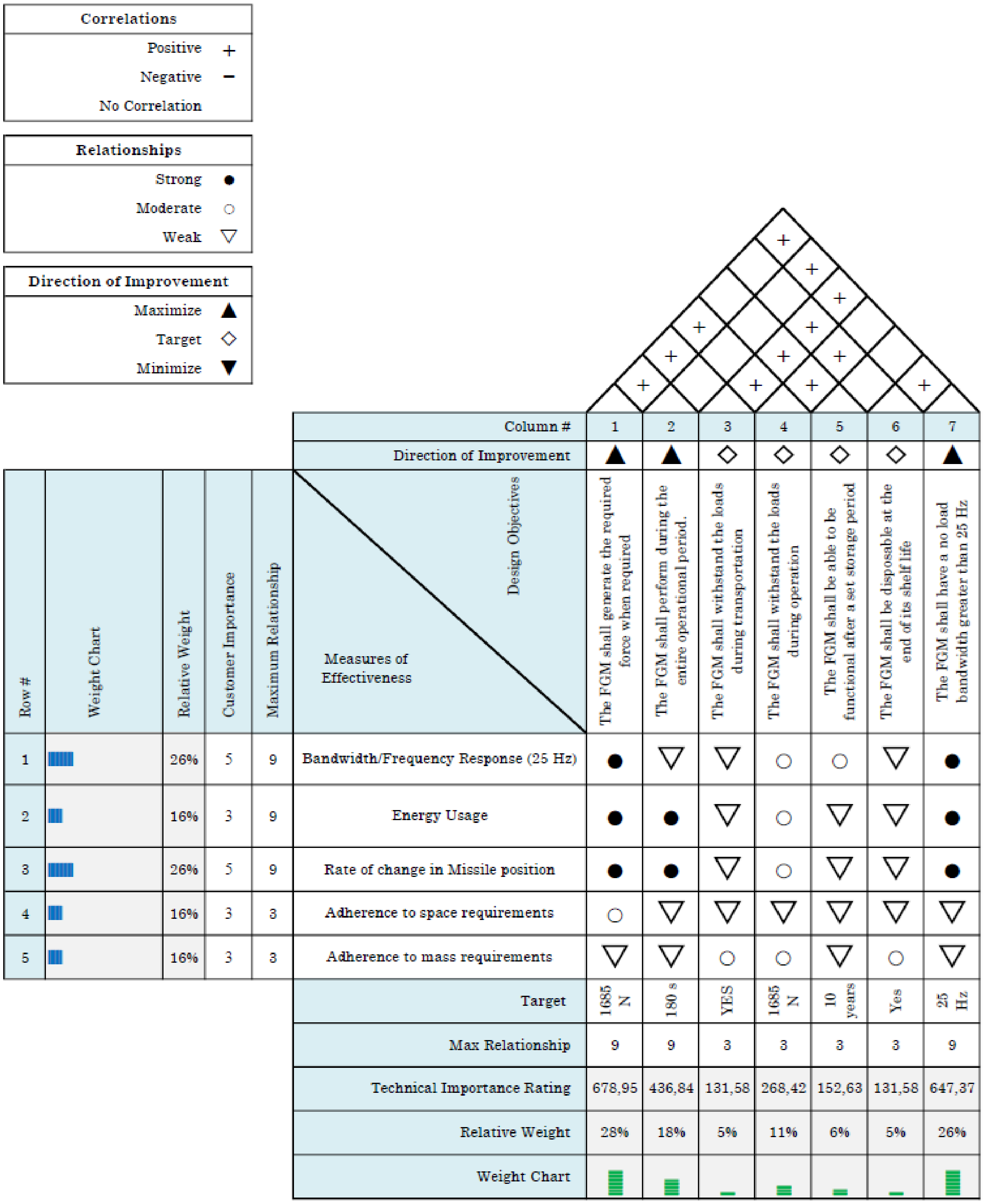

Figure 90: Evaluation of Design Objectives against Measures of Effectiveness using a House of Quality

The MOEs importance was rated out of five. The two measures related to meeting the bandwidth and the rate of change in the missile position were given the highest rating of five as these are directly related to the missile intercepting the target. The remaining three measures were given three each to share the remainder of the relative weighting.

As seen in Figure 90, the design objectives 1 to 7 all received an important technical rating and therefore were all included in the design decision tool.

HOQ is a tool used in Quality Function Deployment (QFD) [122]. The QFD method is used to determine the targets to be achieved by the design objectives of the product such that the MOEs are satisfied. Design objectives 1, 2, 4, and 7 have the highest number of strong relationships to the MOEs, as shown in Figure 90. The evaluation using the HOQ showed that the focus of the design is leaning towards the mechanism to generate the force required to alter the missile flight path.

Figure 91 illustrates the first stage of the tool based on the design objectives. It also highlights the mechanisms of this stage of the tool, which determines the path the ranked concepts will follow. The stage's operations, seen in Figure 91, use the design objectives, determined through the Requirements Analysis phase of the system development (refined by the MOEs) as the method to rank the concepts.

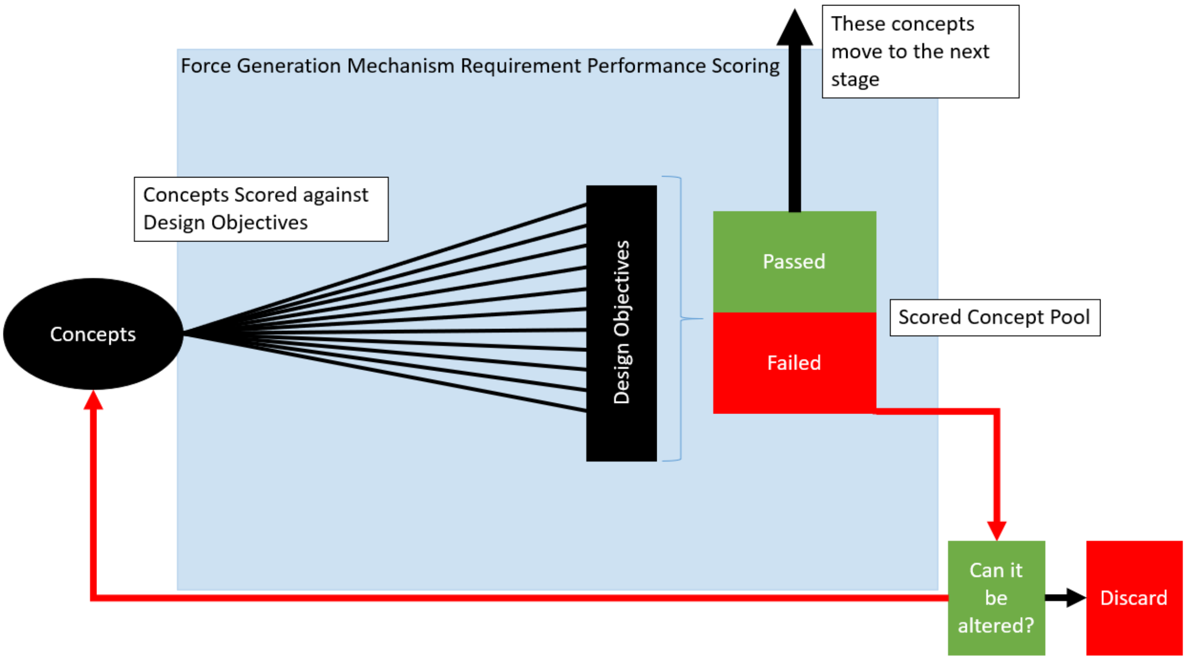

Figure 91: Actuator Filter Illustration

The scoring of the concepts in this stage is based on a scoring system developed using the Weighted Objective Method as described by Cross [122]. The method can be summarised as follows:

1. List the design objectives
2. Rank the design objectives
3. Assign relative weightings to the objectives
4. Establish performance parameters or utility scores for objectives
5. Calculate and compare the relative utility value of the alternative designs

This method is one of many multi-criteria decision-making methods. It was used to evaluate engineering design concepts as described by Cross [122]. A weighted scoring method is also described by Ulrich and Eppinger [112] and is mentioned in Honkala *et al.* [162]. This provided confidence in the use of the method; hence it was selected for the concept selection in this study.

As seen in Table 36, the design objectives have been listed for the FGM, so the first phase of the Weighted Objective Method has been satisfied. The next step is to rank the objectives.

Ranking the objectives can be done by comparing each objective against one another by arranging them in a matrix and scoring them with a "1" if it is more important than the other (a 0 if the opposite is true and ½ if they are of equal importance) and tallying the row scores. [122]

Once each objective has been compared, the row total will indicate the importance of each objective. The design objectives for this design were evaluated against one another, and this is shown in the matrix in Table 37.

Table 37: Evaluation of Design Objectives against one another

Design Objectives		FR1	FR2	FR4	FR5	FR7	Total	Rank	Relative weighting
1	FR1	-	0,5	0,5	1	0,5	2,5	1	11,63
2	FR2	0,5	-	0,5	0,5	0,5	2	4	9,30
4	FR4	0,5	0,5	-	1	0,5	2,5	1	11,63
5	FR5	0	0,5	0	-	0	0,5	5	2,33
7	FR7	0,5	0,5	0,5	1	-	2,5	1	11,63

A scoring system was developed using the rankings from Table 37.

A relative weighting was determined to indicate the design objective's importance, compared to other objectives, in numerical form. There are various ways in which this could be done. A simple method was used, as described in Cross [122]. In this method, the objectives are assigned a value based on their relative importance. The score for each objective was divided by the sum of all the scores and multiplied by 100. This allowed the development of relative weighting for the list of design objectives that added up to 100.

The relative weighting for this stage of the tool based on this design is shown in Table 37. The next step of the Weighted Objective Method is to determine the performance parameter scores of the objectives. In this step, the objectives are transformed into parameters that can be quantified. There are many methods to achieve the desired outcome, as explained in Cross [122]; however, for this study, the simple scale as described in Cross [122] will be used. The scale has five grades as follows:

1. Far below average (Score = 0)
2. Below average (Score = 1)
3. Average (Score = 2)
4. Above average (Score = 3)
5. Far above average (Score = 4)

The scale relates to the performance criteria stated in Table 36. This scale will be applied to each concept that passes through this stage, assessing each concept against each design objective and scoring them accordingly.

The scores for each design objective are then multiplied by the relative weight generated previously to obtain a weighted score. The weighted scores are then summed together for each concept to give an evaluation total.

If a concept achieves an average score (2) for each design objective, then the evaluation total will be the total of the relative weightings and the average score. For this design, the average total score would be 200.

Any concept with a score below this average value is not considered worthy of entering the next stage. The unsuccessful concepts will pass through a final decision question, “Can it be altered?” as seen in Figure 90. This question will assess if a concept can be adjusted with minimum effort in order to improve its performance in an effort to improve its evaluation score. The minimum effort mentioned refers to a small adjustment to a concept’s design that has a small or negligible impact on the project schedule or cost to carry out the change. If the concept cannot be improved, then it will be disregarded for this application. If it is possible to adjust the design with minimum effort, then the concept will be re-scored post adjustment. If it turns out to be an unsuccessful concept again, it will be set aside for the time being. Should a concept achieve an above-average total score, it will be able to pass through to the next stage.

7.3 Project Implementation Scoring

The purpose of the Project Implementation scoring is to evaluate the performance of the concepts from a project perspective. This final stage evaluates concepts against the following set of implementation criteria:

1. Technology Readiness
2. Cost
3. Manufacturability
4. Mission Performance

Technology Readiness refers to the maturity of a technology. It is measured using the Technology Readiness Level scale one to nine, where one is the lowest, where the research is still in its infancy, and nine is the highest, referring to a "Flight Proven" technology. [163]. Figure 92, taken from Mai [163], highlights each technology readiness level.

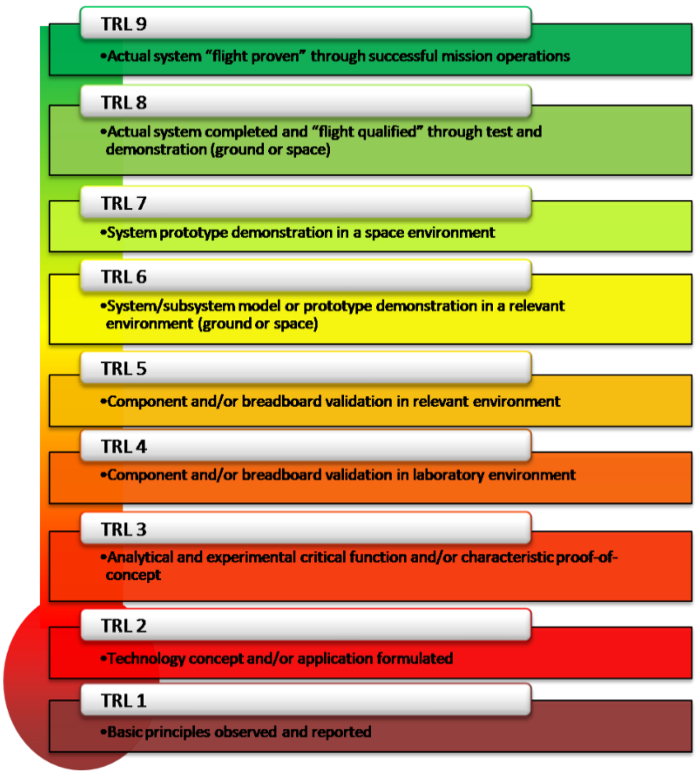

Figure 92: Technology readiness levels [163]

This is an important criterion to consider as it indicates how ready the technology being considered is for the concept to be implemented and what additional work is required to improve its readiness.

Cost refers to the financial implication of using or producing the concept. This can include the cost of the materials, cost of manufacturing and cost of any related processes. [122]

Manufacturability speaks to the ease of producing the concept. This may influence the cost and time to produce the concept.

The mission requirements refer to the requirements from the previous filter. The ranking of the criteria would be carried out as before using the Weighted Objective Method (see Table 38).

Table 38: Evaluation of Final Filter Criteria against one another

		1	2	3	4	Total	Rank	Relative Weighting
Technology Readiness	**1**	-	1	1	0,5	2,5	1	3,85
Cost	**2**	0	-	1	0	1	3	1,54
Manufacturability	**3**	0,5	0	-	0	0,5	4	0,77
Mission Requirements	**4**	0,5	1	1	-	2,5	1	3,85

The relative weighting was arranged in accordance with the totals in Table 38, and the weightings add up to 10. As before, the next step of the Weighted Objective Method is to determine the performance parameter scores of the criteria. For this study, we will be using a simple scale, as described in Cross [122].

The scale has five grades:

1. Far below average (Score = 0)
2. Below average (Score = 1)
3. Average (Score = 2)
4. Above average (Score = 3)
5. Far above average (Score = 4)

The Technology Readiness score range is from 6 to 9. The cost of the concepts will be evaluated against each other. They will be ranked and scored accordingly. Manufacturability will be evaluated based on the criteria in Table 39. The Mission Requirements refers to the adherence and achievement of design objectives and the selection criteria from the first filter. The assessment for this criterion will be based on the score from the previous filter. Table 39 details how the concepts will be scored.

Table 39: Decision Criteria Scoring Description

<table>
<tr><th rowspan="2">Decision Criteria</th><th rowspan="2">Acceptable Value</th><th colspan="5">Score</th></tr>
<tr><th>0</th><th>1</th><th>2</th><th>3</th><th>4</th></tr>
<tr><td>Technology Readiness</td><td>1-9</td><td colspan="2">1-5</td><td>6</td><td>7-8</td><td>9</td></tr>
<tr><td>Cost</td><td>Concept costs will be evaluated against one another, ranked and scored</td><td colspan="2">High cost</td><td>Average</td><td colspan="2">Low cost</td></tr>
<tr><td>Manufacturability</td><td>Ease of manufacturability</td><td>Very Difficult</td><td>Difficult</td><td>Average</td><td>Easy</td><td>Very Easy</td></tr>
<tr><td rowspan="2">Mission Requirements</td><td rowspan="2">Based on the score from the previous filter</td><td colspan="2">Low</td><td>Average</td><td colspan="2">High</td></tr>
<tr><td colspan="2">< 0</td><td>0</td><td colspan="2">> 0</td></tr>
</table>

This scale will be applied to each concept that passes through this stage, assessing each concept against each criterion and scoring them accordingly. As before, the scores for each design objective are then multiplied by the relative weight to obtain a weighted score. These scores are then added together for each concept to give an evaluation total.

From the evaluation totals, a suitable concept is expected to emerge. The other concepts will not be considered going forward in the study, though they could possibly be used in other studies, provided they meet the design criteria and are reassessed for suitability.

Once the concepts have been evaluated using the tool, a concept design review must be held. The agenda of the review would be to do the following:

1. Give an overview of the process used.
2. Describe the concepts generated (discussing how the concepts function, their advantages and disadvantages)
3. Describe the outcomes at the end of each stage of the tool
4. Propose the plan going forward
5. Gain stakeholder acceptance regarding concept selection

Following the review, changes may be required; however, if the concept selection is accepted, the design can advance to the next stage.

7.4 Design Decision Tool Creation Summary

An initial part of Step 4, mentioned in Section 3.5, was to create a design decision tool for the purpose of scoring, ranking and comparing mature concepts. The tool created is able to do the following:

- Score the performance of each mature concept using the requirements baseline.
- Score the concepts' performance with regard to meeting project implementation criteria.
- Compare the concepts with one another.

With the tool created, the mature concepts could then be assessed, the final part of Step 4.

8. Application of Design Decision Tool

In this chapter, the concepts were evaluated based on the design decision tool developed in Chapter 7. This chapter describes the outcome of the second part of Step 4, as illustrated in Figure 93.

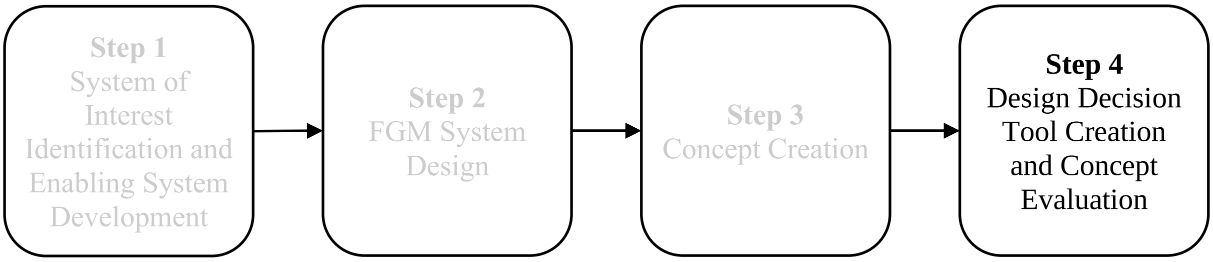

Figure 93: Part 2 of Step 4

The first FGM evaluated was the mechanism used in the Generic Actuator and will be referred to as the Generic FGM. The calculations and the outcome for the Generic FGM evaluated in this tool can be seen in APPENDIX F.

8.1 FGM Requirement Performance Scoring Results

Concept 5 met all the requirements defined for the FGM system. Using the calculated weighting, the concepts were scored. The results can be seen in Table 40.

Table 40: Scoring for the FGM Requirement Performance Scoring Results

					Generic			Concept 5		
System Specification Reference	**Design Objectives**	**Relative Weight**	**Quantity**	**Tolerance**	**Value**	**Score**	**Weighted Score**	**Value**	**Score**	**Weighted Score**
FR1	The FGM shall generate the required force when required	25,00	1685 N	Minimum	2022,34	3,00	75,00	3000,00	4,00	100,00
FR2	The FGM shall perform during the entire operational period.	20,00	180 s	± 10 s	180,00	2,00	40,00	>>180	4,00	80,00
FR4	The FGM shall withstand the loads during operation	25,00	Yes	Yes	Yes	2,00	50,00	Yes	2,00	50,00
FR5	The FGM shall be able to be functional after a set storage period	5,00	YES	-	Yes	2,00	10,00	Yes	2,00	10,00
FR7	The FGM shall have a no load bandwidth greater than 25 Hz	25,00	25 Hz	± 5 Hz	36,38	3,00	75,00	39,70	3,00	75,00
						Total	**250,00**		**Total**	**315,00**

Based on the scoring system developed, a score greater than or equal to 200 is an acceptable FGM and which would allow the concept to move onto the next stage.

Concept 5 scored above 200 and performed better than the generic FGM. Concept 5 and the generic FGM then moved to the next stage of performance evaluation.

8.2 Project Implementation Scoring

8.2.1 Setup and evaluation

Chapter 7 describes the criteria that will be used to assess the concepts as follows:

1. Technology Readiness
2. Cost
3. Manufacturability
4. Mission Requirements

The outcome of the evaluation can be seen in Table 41.

Table 41: Project Implementation Scoring Results

		Generic			Concept 5		
Decision Criteria	**Relative Weight**	**Value**	**Score**	**Weighted Score**	**Value**	**Score**	**Weighted Score**
Technology Readiness	3,85	9	4	15,4	6	2	7,7
Cost	1,54	Average	2	3,08	High	1	1,54
Manufacturability	0,77	Very Easy	4	3,08	Very Difficult	0	0
Mission Requirements	3,85	Average	2	7,7	High	3	11,55
		Total	12	29,26	Total	6	20,79

The servo motor within the generic actuator would be considered to be at technology readiness level 9, as it has already been tested and used successfully in the operation context [87]. Therefore, based on the scoring system developed, the generic actuator with the servo motors would score the highest points. Concept 5 was given a score of 6 for technology readiness as piezoelectric actuators used in these concepts have been used before; however, details of their use in the exact mission context was not evident in the literature.

With regard to the cost, off the shelf actuators with a frame should be lower priced than designing a servo motor from first principles or buying a frameless rotor and stator and then designing a frame to house them. This is based on the minimal effort required to incorporate a bought-out system compared to designing and developing one. This work has already been carried out by the original equipment manufacturer, and choosing their hardware reduces the cost due to the design and development time being eliminated. Therefore, it was assumed to be an average cost. Concepts 5 would have a relatively high impact on the cost to incorporate the mechanism into an existing generic ASYS. This also includes the impact of the design of the Displacement Amplification device.

The manufacturability of the servo motor to be used within the actuator would be considered to be easy as the manufacturing of the servo motor is done by the motor manufacturer. As the motor already exists and assuming the manufacturing processes are well defined, this hardware can be considered simple to manufacture. The same can be said about the actuator used in Concept 5. However, there might be some difficulty in manufacturing other connected components. The piezoelectric actuator is an existing device.

The servo motor was considered to be the baseline in the previous filter, and therefore would be considered to be average based on the score it received, based on the missile performance, which relates to the mission requirements of the weapon. Concept 5 scored higher than the average of 200 and higher than the generic FGM; therefore, Concept 5 scored a high value.

Overall, the servo motor scored higher than Concept 5 due to its Technology Readiness and Cost. The score for these decision criteria could be improved through further investigation and testing related to the operational context and further design work relating to the Displacement Amplification device.

8.2.2 Summary of the Project Implementation Outcome

This tool's stages were designed such that it should identify the best concept based on a project perspective through a scoring method. A discussion of the evaluation of the concepts and the effectiveness of the design decision tool was also conducted thereafter.

9. Discussion

The goal of the four-step approach described in Chapter 3 was to answer the research question mentioned in Section 1.3:

> *Can existing Smart Materials satisfy all the requirements of an FGM that alters the flight path of a BVR supersonic missile?*

The outcome from the study indicates that it is possible for Smart Materials to satisfy all the system requirements of a supersonic BVR missile FGM used to change the missile's flight trajectory. The approach in this study identified key inputs that aided in answering this research question.

The SOI, the FGM, was made evident through the research question. The identification of the influences relating to the SOI's enabling systems and operational context formed the first step of this study. It emerged, from the literature, that the enabling systems and operational context were the missile system, the actuation system, and the missile's operational environment.

The conceptual missile design ensued (refer to APPENDIX A and Section 4.2) to understand the inputs for the FGM. The process allowed for a BVR missile system to be defined using the process defined by Fleeman [60] through predefined mission requirements. As described in the literature, the process is iterative in nature. For the purpose of this study, however, extensive resizing was not done as the focus was on the outcome of the process. Further iterative refinements through additional studies would enhance the response to the research question. Using minimal resizing, a conceptual missile system was developed.

The outcome from the process yielded inputs and outputs for the missile's actuation system, and it enhanced the definition of the operational context in terms of the environment and launch platform. The salient outputs that relate to the FGM included the following:

- Maximum Force required for manoeuvring the missile
- Tail actuation system
- Operational Time
- Operational Environment Conditions
- Mass requirement
- Volume requirement

The process followed for the ASYS allowed for a “bird’s eye view” approach of the actuator’s lifecycle to develop its requirements baseline, functional architecture and physical architecture. The SE process provided a framework that enabled an in-depth look at the various factors that influence the SOI.

An extensive analysis would provide a deeper appreciation of all the relevant factors associated with the design and further enhance the design. The outcome from this process was captured in APPENDIX D and summarized in Section 4.3. Using this knowledge as additional inputs, the context for the FGM design was determined.

The FGM system design also utilised the same process followed for the ASYS design. Many of the ASYS requirements filtered down to the FGM, which indicates that a more extensive functional breakdown could have yielded the necessary inputs for the FGM requirements. This can be expected as the FGM is a system element of the ASYS.

The validation process that followed was done according to the process described in the IEEE 1220 standard [11] and by Sparrius [13] The outcomes are covered in Sections 5.1 and 5.2. Through this process, it showed the link between the requirements and the stakeholder input.

The requirements baseline was then used to define the functional architecture for the SOI. The functional architecture from ASYS was used as input to this process because the FGM functions were considered to be sub-functions of the ASYS. The “Force Generation” subfunction from the ASYS was defined as the sole function of the FGM. The functional architecture was considered to be verified for the purpose of this study. A thorough verification process is, however, deemed necessary for further study. The Physical Architecture was developed from the Functional Architecture.

Due to the influence from the ASYS, the ASYS Physical Architecture selected during the ASYS design was used as input during this phase.

With the definition of the FGM Physical Architecture, the second objective for this study was achieved, and the FGM system design was considered complete. The outcome is covered in Sections 5.3, 5.4, and 5.5. As it was possible to develop various physical architectures for a given functional architecture of a system, the use of the selected architecture could unnecessarily constrain the FGM Physical Architecture development.

However, the SE process allowed for the architecture to be specified in such a way as to improve the possibilities for the concept choices that could be made. The architecture developed through this process was used to identify which physical architecture components would be able to incorporate Smart

Material actuators, as this was the main use of the Smart Material identified in the literature (see Section 2.2). Using the outcome from the second step, the third step was initiated to also address the third objective of the study; to generate FGM concepts using Smart Materials.

The FGM concept generation involved the creation of possible solutions to address the FGM physical architecture developed. The process utilised a Concept Combination Table to identify various solutions that could be used to create the physical architecture. Following this, two concept categories were identified: Tail Rotation and Flow effectors (dealing with changes to the boundary layer specifically). The constraint of an ASYS at the tail end of the missile did limit the concept creation and the possible utilisation of the Smart Materials. However, it was necessary to include the constraint to add additional focus to this study. Further study with alternative ASYS placement should be considered to evaluate the use of Smart Materials in those locations.

Five concepts were created, three relating to the tail rotation and two relating to the flow effector category. As identified in Section 2.2, the Smart Materials that were considered for this study were SMAs and Piezoelectric actuators. These concepts were assessed to see if they met the requirements for the FGM mechanism. A larger number of concepts could have been generated to showcase a variety of different ways the Smart Materials could be utilised. However, the number created was deemed sufficient to answer the research question.

For design requirement FR1, the force value is defined as the minimum value the FGM system needs to achieve to allow the missile to carry out the required 30g manoeuvre. The tolerance limits defined need to be assessed and verified in a further study. The upper limit was not defined as it was assumed the system would only utilise the force necessary to achieve the desired manoeuvre. Any force value generated above the minimum value was deemed acceptable because the system should be able to adjust itself not to exceed the structural limits of the missile system. An upper force limit would still need to be determined and verified. For the purpose of this study, the evaluation using the lower limit was sufficient. A force produced below the limit would not be effective in achieving the manoeuvre requirement. A force above the limit indicates the mechanism would allow the missile to achieve the manoeuvre. The requirement was dependant on factors such as the placement of the actuator system, the hinge line of the generic missile actuator, the missile flight velocity and altitude, amongst others.

The requirement, "Maintain the applied force for the required duration" (FR2), was determined in terms of the length of time the concept would be able to operate. The operation time was defined as the flight duration of 180s. This requirement is specific to the envisioned operation of the FGM system. Therefore, only mechanisms that would be able to meet or exceed the operation time would qualify to enter the decision tool. The requirement could be different for a different missile context or for a different method of operation. However, as it stands, this would be an effective way to identify which mechanism would be a suitable concept.

Evaluating the FGM's performance in meeting FR4 was based on the applied load. The requirement was not explicit on the type of loads that the structure would experience, which would be a limitation for this filter. Each mechanism was evaluated based on the effect of the aerodynamic load the system would be subjected to. Thermal and other structural loads were not evaluated. With conventional design processes, the surrounding structure would be better defined as the design progresses, and it would then allow for additional structural evaluation. Further investigation beyond the scope of this study would have to be carried out to determine all the relevant load cases.

The storage requirement, FR5, identifies the FGMs that would be suitable to meet the possible storage period. This period is specific to this context, and it is possible that a lower storage period could be defined.

The evaluation of FR7 focused on the FGM bandwidth with the influence of fin/load and without the influences from the environment. The assessment of the bandwidth was tailored to each mechanism based on the type of actuator mechanism selected. A thorough evaluation of this requirement would need to include all the relevant influences that impact the bandwidth. Bandwidth values higher than the required value should be acceptable if the influences from the other relevant systems are negligible. In reality, this would not be the case, as the other structures influences would tend to reduce the estimated bandwidth. A safety factor should be incorporated into the requirement to ensure the concepts that enter the design decision tool accommodate for additional connected structures. However, for this evaluation, this would be sufficient for a conceptual design choice.

From the assessment, only Concept 5 was successful across the board. Concepts 1 and 2 could possibly be modified to improve their shortcomings. This would, however, require further investigation and was considered to be beyond the scope of the study.

The first concept was not a viable option as part of an FGM for the defined context in this study. The force value that the Flexinol® wire, in conjunction with its connected tail fin, would be able to withstand the applied load. This was determined to be higher than the required value and marginally lower than the generic mechanism. The downfall of this concept was the structural integrity. The use of the wire beyond its recommended load limit was predicted to cause the deformation of the wire, preventing it from performing as required. Even though it would be able to pull the load required, it is not certain that it would be able to operate as such for the entire flight time; hence it did not meet that requirement.

This was based on the literature and the discussion with the manufacturer of the SMA wire. Testing of the wire under the specified conditions would provide better certainty with regard to the performance of the wire. During the missile flight, the maximum load is only expected when the missile needs to execute the high g manoeuvre. The frequency of this may be low, as for the majority of the flight, small adjustments should only be required to keep the missile flying a certain path.

This concept also failed to meet the third most important requirement, the bandwidth. The heating and cooling times of the wire play a major role in the response of the wire. While the heating of the wire is controlled by the current supplied, the cooling of the wire would require an additional system to ensure the rate of cooling is increased to improve the response time of the wire. Further study on this aspect is required. In a context where the structural integrity requirement could be achieved or if the bandwidth was acceptable, this concept could still be considered a viable option.

Concept 2 failed to meet the force generation, structural integrity and bandwidth requirement. Further investigation is required to verify the impact of the MFC on the bistable structure with regard to the deflection required. A structurally improved bistable/multistable construction should be considered to handle the loads. With regards to bandwidth, this concept would perform better for a system with lower response requirements.

Concept 3, using the jet actuators, requires further investigation and falls beyond the scope of this study, as it needs to determine the improvement in the lift that can be achieved, and also if it would be useful for missile control at supersonic speeds.

Regarding Concept 4, with the bleed port system, the impact on the control of the missile would require further investigation to determine the viability of its application.

For this study, only Concept 5 was considered mature enough to progress through to the decision process. The third step was completed with the creation of the concepts, which also allowed the third objective to be achieved. A design decision tool was required to assess the performance of the concepts and to check if it would outperform the generic FGM.

The creation of the Design Decision Tool was the fourth objective and the first part of the fourth step.

The purpose of the design decision tool was to evaluate the FGM system concepts. The mechanics of the tool were established to assess the performance of each concept. This was centred on the various requirements drawn from the SE process, which allowed the tool to verify compliance with system requirements.

With the tool developed, the fourth objective was achieved. The remainder of the fourth step of the method involved the evaluation of the concepts. This part of the method was created to address the fifth and final objective.

The summary of the results of the First Stage is presented in Table 42.

Table 42: Summary of FGM Requirement Performance Scoring stage

	Requirement										
FGM	FR1	Score	FR2	Score	FR4	Score	FR5	Score	FR7	Score	Total Score
Generic	75,00		40,00		50.00		10.00		75.00		250.00
5	100.00		80.00		50.00		10.00		75.00		315.00

Based on the decision tool designed, concepts then progressed through to the next stage after having satisfied the preceding stage. Some of the concepts that were not evaluated could be modified to ensure they meet the requirements as previously described, but this iteration was not done as part of this study. If different actuator system requirements were determined such that the higher-level system requirements are still met, the outcome of this filter could have been different.

The actuation system requirements were derived from the concept of use of the supersonic BVR missile. In a context where the demand on the system was lower with regard to aerodynamic loading and response time, the concepts that previously failed are expected to be successful. Alternative concepts of use should be considered in further studies. A shift in thinking with regard to how a missile can achieve its requirements could be investigated, as this may allow other concepts to be viable. This was not investigated in this study.

Based on the scoring system developed, the minimum acceptable score for a concept would be 200 points. The evaluation of the generic FGM yielded 250 points. This means that it performs above the viable limit. This was expected, as the solution has been successfully used as an FGM in contemporary missiles in this class as described in the literature. However, the points for the generic FGM should therefore be the new minimum acceptable score as the idea would be that the concepts developed should perform the same or better than the existing system.

The candidates that achieved total scores above the benchmark would be evaluated by the final stage of the tool, the Project Implementation Scoring. As mentioned in Section 7.3, the criteria for this filter relates to factors that affect project implementation, which was defined in this study as Technology Readiness, Cost, Manufacturability, and Mission Requirements. The outcome of this stage was to determine the most suitable candidate for the defined project context. As discussed previously in this chapter, the generic FGM and Concept 5 were assessed. The score achieved by candidates were compared and ranked with other candidates to determine the best solution. The outcome from this stage, in some cases, may not have been the best performer from the previous stage. This final stage would be effective in eliminating candidates that would have hindered the development cycle through extensive design iterations, long lead times from manufacturing, and high project costs.

The servo motor was assessed based on the evaluation criteria, and as seen in Table 40, the servo motor scored 21.50. This is marginally above the average score (20.00) that a concept could possibly achieve. Any concept scoring below this average score would not be a suitable selection based on the value system defined for this stage of the tool in this study. Those concepts may, however, still be viable actuator system concepts, but not for this particular progression through the process. Ideally, these should be documented and their viability recorded because they could be reused in the future, should there be a change in the selection criteria used in the third or foregoing filters.

Concept 5 scored above the average and, therefore, should be suitable for implementation. The concept with the highest-ranking score above the average should be selected. However, even though the purpose of the decision tool developed was to draw out a viable value system orientated concept, the relevant stakeholders could still choose another evaluated and viable concept.

If the servo motor, the generic FGM in this study, used within the generic actuator were a concept, this tool has indicated that it would be a viable option and that it is above the average score with respect to the “soft” evaluation criteria seen in the second filter. The performance of Concept 5 indicates that existing Smart Materials are capable of satisfying the requirements of a BVR supersonic missile actuator. This was also indicated in the literature. However, the limitation regarding the concept is the design of the Displacement Amplification device. The literature did indicate that such a device is possible. However, an example was not designed in this study. An evaluation using a suitable Displacement Amplification device should be carried out in a future study.

The tool was able to evaluate the performance of concepts and the generic FGM based on the FGM system requirements. From the concepts developed, only Concept 5 was determined to be suitable for this missile context. Therefore, the tool aided in answering the research question.

10. Conclusion and Recommendations for Future work

10.1 Conclusion

In this study, the requirements baseline for the FGM within the actuation system of a Beyond Visual Range (BVR) missile was created using the SE approach described in Section 2.1. The design process covered the major subsystems of the missile in order to appreciate the inputs related to the various interactions that would have an influence on the FGM. The requirements for this system were elicited through the SE approach adapted from IEEE 1220 standard, as described in Section 3.2. The SE approach took a holistic view to establish the necessary inputs and outputs of the FGM system developed in this study. The highlights for this approach included a requirement and Functional Analysis, which satisfied the first objective of the study. The outcomes led to defining the functional and physical architectures and thus achieving the second objective.

In response to the research question, concepts were generated, as described in Section 3.3, based on the mechanisms and Smart Materials described in Chapter 2. This aided in achieving the third objective.

An evaluation tool was developed to assess the mature concepts. The concepts performance were assessed on the basis of the system requirements defined by the developed physical architecture. This met the fourth objective. The tool was then applied to the concepts generated—the scoring of the system allowed for the ranking of actuator concepts to facilitate decision making. The tool was useful in indicating the best actuator system concepts, satisfying the fifth objective.

The concepts were generated using Smart Material and/or Adaptive Structures which were described in Section 2.2. These were created based on the two FGM categories outlined in Section 6.1. These include Tail Fin Rotation and Flow Effectors. The first, second and fifth concepts fell under the Tail Fin Rotation category. This category involved the manipulation of the tail control fin by using the Smart Materials/Adaptive Structure to achieve the desired tail fin deflection as defined in the conceptual missile design from Section 4.2.

The first concept made use of a Shape Memory Alloy, called Flexinol® wire. The second used MFC patches, a piezoelectric actuator, in conjunction with a bistable laminate. The third and fourth concepts are a part of the Flow Effector category. The third concept used synthetic jet actuators, made using a diaphragm actuated by a piezoelectric actuator to manipulate the flow over the tail control surface. The fourth concept used piezoelectric actuators to control a plate that was envisioned to open and close the upper and lower surfaces of the tail fin to manipulate lift on it. The fifth concept used piezoelectric actuators that were envisioned to rotate the missile control fin to alter the missile's flight path.

Only those concepts that met the system requirements and the generic force mechanism were evaluated through the design decision tool developed as presented in Chapter 8.

The generic FGM was evaluated by the tool for comparative reasons. Concept 5 that made use of a piezoelectric PZT linear actuator and a Displacement Amplification device was also able to be assessed, as it met the system requirements. Concept 5 scored above the generic force mechanism in both stages of the tool. This indicates that it would be possible for an existing Smart Material to replace a generic force generation.

Therefore, through this study, the research question was answered; existing Smart Materials were able to satisfy all the elicited requirements for a supersonic BVR missile.

10.2 Recommendations for future work

In this study, it was established that the following recommendations for future work should be considered:

1. Testing of the successful concept would be the next step in verifying the outcome of this study.
2. The evaluation of alternative weapons, such as glide bombs, should be carried out to determine if Adaptive Structures would be beneficial in a different weapon application.
3. An investigation into alternative missile control methodologies should be done to establish alternate requirements for missile control.
4. The improvement of the Smart Material abilities evaluated in this study should be a topic for future investigation - specifically focusing on the improvements that would enable their use in the application-defined in this study.
5. Improvements to the concepts to be able to meet the requirements defined in this study.

11. References

[1] Institute of Materials, (2006), “SMART MATERIALS.”

[2] R. Vos and R. Barrett, (2010), “Pressure adaptive honeycomb: a new adaptive structure for aerospace applications,” *Sensors Smart Struct. Technol. Civil, Mech. Aerosp. Syst.*, doi: 10.1117/12.847031.

[3] R. Barrett and R. Vos, (2008), “Post-buckled precompressed subsonic micro-flight control actuators and surfaces,” *Smart Mater. Struct.*, vol. 17, no. 5, pp. 1–12, doi: 10.1088/0964-1726/17/5/055011.

[4] G. Warwick, (2006), “Lockheed Martin and NextGen Aeronautics start fast-morphing UAV tests, turning attention to attack formation.” https://www.flightglobal.com/news/articles/lockheed-martin-and-nextgen-aeronautics-start-fast-morphing-uav-tests-turning-attention-to-attack-208463/ Accessed : [Mar. 19, 2020].

[5] G. Goldshine and G. Lacy, (1968), “High-response electromechanical control actuator,” no. 3, pp. 19–26.

[6] G. Shea, (2017), “NASA Systems Engineering Handbook Revision 2.”

[7] M. Ryschkewitsch, D. M. Schaible, and W. Larson, (2009), “THE ART AND SCIENCE OF SYSTEMS ENGINEERING.,” *Syst. Res. Forum*, pp. 81–100, doi: 10.1029/WR009i006p01555.

[8] INCOSE, (2015), *Systems engineering handbook : a guide for system life cycle processes and activities*, 4th Editio. John Wiley & Sons, Inc.

[9] UK INCOSE and APM, (2014), “Systems Engineering and Project Management Integration: V-model (Explanatory Note) Dovetailing Systems Engineering and Project Management Lifecycles Programme and Project Management Perspective.”

[10] BKCASE, (2019), “Systems Engineering Body of Knowledge.” https://www.sebokwiki.org/.

[11] IEEE Computer Society, (2005), *“IEEE Standard for Application and Management of the Systems Engineering Process” in IEEE Std 1220-2005 (Revision of IEEE Std 1220-1998)*, vol. 2005, no. September. .

[12] T. Doran, (2006), “IEEE 1220: For practical systems engineering,” *Computer (Long. Beach. Calif).*, vol. 39, no. 5, pp. 92–94, doi: 10.1109/MC.2006.164.

[13] A. Sparrius, (2016), *Denel Dynamics System Engineering Course Notes*. .

[14] “Success for first in-flight morphing aircraft, as small Californian start-up NextGen flies Boeing-aided MFX-1 model | News | Flight Global.” https://www.flightglobal.com/success-for-first-in-flight-morphing-aircraft-as-small-californian-start-up-nextgen-flies-boeing-aided-mfx-1-model-/69072.article?adredir=1 Accessed : [Jan. 17, 2021].

[15] N. M. Ursache, T. Melin, A. T. Isikveren, and M. I. Friswell, (2007), “Morphing winglets for

aircraft multi-phase improvement," in *Collection of Technical Papers - 7th AIAA Aviation Technology, Integration, and Operations Conference*, (2007), , vol. 2, pp. 1216–1227, doi: 10.2514/6.2007-7813.

[16] D. D. Smith, A. T. Isikveren, R. M. Ajaj, and M. I. Friswell, "MULTIDISCIPLINARY DESIGN OPTIMIZATION OF AN ACTIVE NONPLANAR POLYMORPHING WING."

[17] T. Melin, E. Tmelinbrisacuk, and M. I. Friswell, (2008), "Technology Integration for Active Poly-Morphing Winglets Development."

[18] O. Bilgen, A. F. Arrieta, M. I. Friswell, and P. Hagedorn, (2013), "Dynamic control of a bistable wing under aerodynamic loading," *Smart Mater. Struct.*, vol. 22, no. 2, doi: 10.1088/0964-1726/22/2/025020.

[19] F. Mattioni, P. M. Weaver, K. D. Potter, and M. I. Friswell, (2008), "The application of thermally induced multistable composites to morphing aircraft structures," *Ind. Commer. Appl. Smart Struct. Technol. 2008*, vol. 6930, no. March, doi: 10.1117/12.776226.

[20] S. W. Kim, J. Y. Lee, and K. J. Cho, (2013), "Towards a bistable morphing winglet for unmanned aerial vehicle(UAV)," (2013), , doi: 10.1109/ISR.2013.6695648.

[21] A. Gatto, F. Mattioni, and M. I. Friswell, (2009), "Experimental investigation of bistable winglets to enhance wing lift takeoff capability," *J. Aircr.*, vol. 46, no. 2, pp. 647–655, doi: 10.2514/1.39614.

[22] R. Barrett, (2004), "Adaptive aerostructures: the first decade of flight on uninhabited aerial vehicles," *Smart Struct. Mater. 2004 Ind. Commer. Appl. Smart Struct. Technol.*, vol. 5388, p. 190, doi: 10.1117/12.536681.

[23] R. Barrett, (1992), "Active plate and wing research using EDAP elements," *Smart Mater. Struct.*, vol. 1, no. 3, pp. 214–226, doi: 10.1088/0964-1726/1/3/005.

[24] R. Barrett, (1993), "Active Composite Torque-Plate Fins for Subsonic Missiles," (1993), .

[25] R. M. Barrett, (2004), "Adaptive aerostructures: the first decade of flight on uninhabited aerial vehicles," *Smart Struct. Mater. 2004 Ind. Commer. Appl. Smart Struct. Technol.*, vol. 5388, p. 190, doi: 10.1117/12.536681.

[26] R. Barrett, (1993), "Advanced Low-Cost Smart Missile Fin Technology Evaluation," Florida.

[27] G. Lee, (1999), "Range-Extended Adaptive Munition (REAM)," Del Mar, California.

[28] G. Lee, (2000), "40/50 Caliber Range-Extended Adaptive Munition (REAM)," Del Mar, California.

[29] G. Lee, (2003), "Shipborne Countermeasure Range-Extended Adaptive Munition (SCREAM)," Del Mar, California.

[30] V. Giurgiutiu and R. Pomirleanu, (2000), "SMART-MATERIAL ACTUATED MISSILE FLIGHT CONTROL SURFACES FEASIBILITY STUDY FINAL PROGRESS REPORT."

[31] F. T. Calkins, (2004), "Boeing's Morphing Aerostructures."

[32] D. M. Pitt, J. P. Dunne, and E. V. White, (2002), "SAMPSON smart inlet design overview and

wind tunnel test: I. Design overview," in *Smart Structures and Materials 2002: Industrial and Commercial Applications of Smart Structures Technologies*, (2002), , vol. 4698, pp. 13–23, doi: 10.1117/12.475064.

[33] "Fundamentals of Piezo Technology." https://www.piceramic.com/en/piezo-technology/fundamentals/ Accessed : [Feb. 21, 2021].

[34] R. Barrett, (2014), "20 Years of Adaptive Aerostructures in Flying Missiles, Munitions and UAVs," (2014), , doi: 10.1115/smasis2014-7662.

[35] Smart-Material, "MFC." https://www.smart-material.com/MFC-product-main.html Accessed : [Feb. 02, 2020].

[36] Smart Material, (2017), "Macro Fiber Composite (MFC) Datasheet," p. 8.

[37] T. Daue, (2019), "Email from smart-material.com regarding additional information MFC Actutors." .

[38] C. R. Bowen, P. F. Giddings, A. I. T. Salo, and H. A. Kim, (2011), "Modeling and characterization of piezoelectrically actuated bistable composites," *IEEE Trans. Ultrason. Ferroelectr. Freq. Control*, vol. 58, no. 9, pp. 1737–1750, doi: 10.1109/TUFFC.2011.2011.

[39] S. Q. Zhang, Y. X. Li, and R. Schmidt, (2015), "Modeling and simulation of macro-fiber composite layered smart structures," *Compos. Struct.*, vol. 126, no. February, pp. 89–100, doi: 10.1016/j.compstruct.2015.02.051.

[40] physikinstrumente, "P-845 Preloaded Piezo Actuators." https://www.physikinstrumente.com/en/products/linear-actuators/nanopositioning-piezo-actuators/p-845-preloaded-piezo-actuators-101215/#description Accessed : [Feb. 02, 2020].

[41] PI, "Preloaded Piezo Actuators P-845 Datasheet." https://static.physikinstrumente.com/fileadmin/user_upload/physik_instrumente/files/datasheets/P-845-Datasheet.pdf Accessed : [Jun. 12, 2019].

[42] J. Mohd Jani, M. Leary, A. Subic, and M. A. Gibson, (2014), "A review of shape memory alloy research, applications and opportunities," *Materials and Design*, vol. 56. Elsevier Ltd, pp. 1078–1113, doi: 10.1016/j.matdes.2013.11.084.

[43] Dynalloy Inc., "Technical Characteristics of Flexinol ® Actuator Wires," *http://www.dynalloy.com/*. http://www.dynalloy.com/pdfs/TCF1140.pdf Accessed : [Oct. 03, 2019].

[44] T. W. Duerig, (1994), "Present and Future Applications of Shape Memory and Superelastic Materials," *MRS Proc.*, vol. 360, p. 497, doi: 10.1557/PROC-360-497.

[45] D. Collins, (2017), "Why is the bandwidth of a servo control loop important?," *www.motioncontroltips.com/*. https://www.motioncontroltips.com/why-is-the-bandwidth-of-a-servo-control-loop-important/ Accessed : [Oct. 27, 2019].

[46] C. Lan and C. Fan, (2010), "Sensors and Actuators A : Physical An accurate self-sensing method for the control of shape memory alloy actuated flexures," *Sensors Actuators A. Phys.*,

vol. 163, no. 1, pp. 323–332, doi: 10.1016/j.sna.2010.07.018.

[47] D. Grant, (1997), “Variable Structure Control Of Shape Memory Alloy Actuators - IEEE Control Systems Magazine,” no. June 2016, doi: 10.1109/37.588180.

[48] M. Moallem and V. A. Tabrizi, (2009), “Tracking Control of an Antagonistic Shape Memory Alloy Actuator Pair,” vol. 17, no. 1, pp. 184–190.

[49] M. Moallem, (2003), “Deflection control of a flexible beam using shape memory alloy actuators,” *Smart Mater. Struct.*, vol. 12, no. 6, pp. 1023–1027, doi: 10.1088/0964-1726/12/6/022.

[50] D. Josephine Selvarani Ruth, S. Sunjai Nakshatharan, and D. Dhanalakshmi, (2014), “Differential resistance feedback control of a self-sensing shape memory alloy actuated system,” *ISA Trans.*, vol. 53, no. 2, pp. 289–297, doi: 10.1016/j.isatra.2013.11.002.

[51] G. Song, B. Kelly, and B. N. Agrawal, (2000), “Active position control of a shape memory alloy wire actuated composite beam,” *Smart Mater. Struct.*, vol. 9, no. 5, pp. 711–716, doi: 10.1088/0964-1726/9/5/316.

[52] G. Song, V. Chaudhry, and C. Batur, (2003), “Precision tracking control of shape memory alloy actuators using neural networks and a sliding-mode based robust controller,” vol. 12, pp. 223–231.

[53] Y. H. Teh and R. Featherstone, (2007), “Frequency response analysis of shape memory alloy actuators.”

[54] Yee Harn Teh and R. Featherstone, (2008), “An Architecture for Fast and Accurate Control of Shape Memory Alloy Actuators,” *Int. J. Rob. Res.*, vol. 27, no. 5, pp. 595–611, doi: 10.1177/0278364908090951.

[55] S. Fichera, I. Isnardi, and J. E. Mottershead, (2019), “High-bandwidth morphing actuator for aeroelastic model control,” *Aerospace*, vol. 6, no. 2, doi: 10.3390/aerospace6020013.

[56] C. C. Wu, C. C. Lee, G. Z. Cao, and I. Y. Shen, (2006), “Effects of corner frequency on bandwidth and resonance amplitude in designing PZT thin-film actuators,” *Sensors Actuators, A Phys.*, vol. 125, no. 2, pp. 178–185, doi: 10.1016/j.sna.2005.07.007.

[57] L. Middleton, (1988), “The effect of ageing and thermal cycling on the shape memory properties of nickel-titanium,” *Univ. Wollongong Thesis Collect. 1954-2016*.

[58] R. B. Williams, D. J. Inman, M. R. Schultz, M. W. Hyer, and W. K. Wilkie, (2004), “Nonlinear Tensile and Shear Behavior of Macro Fiber Composite Actuators,” *J. Compos. Mater.*, vol. 38, no. 10, pp. 855–869, doi: 10.1177/0021998304040555.

[59] Merriam-Webster, (2019), “missile.” //www.merriam-webster.com/dictionary/missile Accessed : [Dec. 12, 2019].

[60] E. L. Fleeman, (2006), *Tactical Missile Design*, 2nd Editio. American Institute of Aeronautics and Astronautics.

[61] SAAB, “IRIS-T short range air-to-air missile.” https://saab.com/air/weapon-systems/air-to-air-

missile-systems/iris_t/ Accessed : [Sep. 03, 2019].

[62] Denel Dynamics, “A-Darter.” http://www.deneldynamics.co.za/products/missiles/air-to-air-missiles/a-darter Accessed : [Sep. 03, 2019].

[63] Raytheon, “AIM-9X Sidewinder Missile.” https://www.raytheon.com/capabilities/products/aim-9x Accessed : [Sep. 03, 2019].

[64] Military.com, “AGM-114 Hellfire.” https://www.military.com/equipment/agm-114-hellfire Accessed : [Sep. 04, 2019].

[65] MBDA Missile Systems, “Brimstone.” https://www.mbda-systems.com/air-dominance/brimstone/ Accessed : [Sep. 04, 2019].

[66] https://www.globalsecurity.org/, “AIM-7 Sparrow.” https://www.globalsecurity.org/military/systems/munitions/aim-7.htm Accessed : [Sep. 04, 2019].

[67] Raytheon, “AMRAAM Missile.” https://www.raytheon.com/capabilities/products/amraam Accessed : [Sep. 04, 2019].

[68] MBDA Missile Systems, “Meteor.” https://www.mbda-systems.com/air-dominance/meteor/ Accessed : [Sep. 04, 2019].

[69] Raytheon, (2005), “AGM-65 Maverick Man-in-the-Loop Precision , Low Collateral Damage , Anti-tank , Anti-ship , Close Air Support Weapon.”

[70] https://www.naval-technology.com/, “AGM-88E Advanced Anti-Radiation Guided Missile (AARGM).” https://www.naval-technology.com/projects/agm-88e-advanced-anti-radiation-guided-missile-aargm/ Accessed : [Sep. 04, 2019].

[71] Raytheon, “Javelin Weapon System.” https://www.raytheon.com/capabilities/products/javelin Accessed : [Sep. 04, 2019].

[72] Raytheon, “Tomahawk Cruise Missile.” https://www.raytheon.com/capabilities/products/tomahawk Accessed : [Sep. 04, 2019].

[73] L. Pierrot and J. A. Vines, (1997), *A Look at Tomorrow’s Tactical Air Forces*. Diane Publishing.

[74] J. M. Gilmore, (2015), “Director, Operational Test and Evaluation - FY 2014 Annual Report.”

[75] T. Tyrell and C. Funk, (2014), “AIM-120C-5 Performance Assessment for Digital Combat Simulation Enhancement.”

[76] J. D. Anderson, (2011), *Fundamentals of Aerodynamics*, Fifth Edit. McGraw Hill.

[77] T. Benson, (2011), “Dynamics of Flight Vehicles,” *https://www.grc.nasa.gov/*. https://www.grc.nasa.gov/WWW/k-12/UEET/StudentSite/dynamicsofflight.html Accessed : [Jun. 22, 2014].

[78] S. S. Chin, (1961), “Missile configuration design.”

[79] W. C. Pitts, J. N. Nielsen, and G. E. Kaattari, “NATIONAL ADVISORY COMMITTEE FOR AERONAUTICS LIFT AND CENTER OF PRESSURE OF WING-BODY-TAIL

COMBINATIONS AT SUBSONIC, TRANSONIC, AND SUPERSONIC SPEEDS.”

[80] L. H. Jorgensen, (1973), “PREDICTION OF STATIC AERODYNAMIC CHARACTERISTICS FOR SPACE-SHUTTLE-LIKE AND OTHER BODIES AT ANGLES OF ATTACK FROM 0 ° TO 180 °.”

[81] J. N. Nielsen, (1960), *Missile Aerodynamics*. McGraw Hill.

[82] C. Kopp, (1986), “Quo Vadis - AMRAAM?,” *Aust. Aviat.*, vol. 1986, no. September.

[83] P. B. Jackson, (2010), “Overview of missile flight control systems,” *Johns Hopkins APL Tech. Dig. (Applied Phys. Lab.*, vol. 29, no. 1, pp. 9–24.

[84] M. A. Siddiqui and M. M. Siddiqui, (2015), “Mathematical modeling and analysis of an Actuator for aerospace vehicle,” vol. 1.

[85] C. NOOK, “Lead Screws Drive Missile Fin Actuation Systems.” https://www.helixlinear.com/blog/lead-screws/lead-screws-drive-missile-fin-actuation-systems/ Accessed : [Sep. 08, 2019].

[86] San Francisco Maritime National Park Association, (2013), “Chapter 5 Missile Control Systems.” https://maritime.org/doc/missile/part1.htm Accessed : [Sep. 08, 2019].

[87] https://www.globalsecurity.org/, “AIM-120 AMRAAM SLAMMER - Design.” https://www.globalsecurity.org/military/systems/munitions/aim-120-design.htm Accessed : [Sep. 04, 2016].

[88] T. Wright, (2007), “That Extra Little Lift,” *Air & Space Magazine*. https://www.airspacemag.com/history-of-flight/that-extra-little-lift-17186541/?all Accessed : [Sep. 08, 2019].

[89] A. Buonanno, (2005), “Aerodynamic Circulation Control For Flapless Flight,” Cranfield University, (2005), .

[90] Y. Yamada, I. Vasilieva, A. Takayama, E. F. Fukushima, and G. Endo, (2015), “Circulation-controlled high-lift wing for small unmanned aerial vehicle,” *Robomech J.*, vol. 2, no. 1, pp. 1–11, doi: 10.1186/s40648-015-0031-1.

[91] M. Jabbal, S. C. Liddle, and W. J. Crowther, (2010), “Active flow control systems architectures for civil transport aircraft,” *J. Aircr.*, vol. 47, no. 6, pp. 1966–1981, doi: 10.2514/1.C000237.

[92] Cranfield University, “Developing the next generation of Unmanned Aerial Vehicles (UAVs) with BAE Systems,” *https://www.cranfield.ac.uk/case-studies/research-case-studies/flaviir*. https://www.cranfield.ac.uk/case-studies/research-case-studies/flaviir Accessed : [Sep. 08, 2019].

[93] H. Pozniak, (2018), “Lighter, faster aircraft made possible with new ‘flapless’ flight systems,” *https://www.telegraph.co.uk/*. https://www.telegraph.co.uk/education/stem-awards/defence-technology/lighter-faster-aircraft-with-flapless-flight-systems/ Accessed : [Sep. 08, 2019].

[94] A. Buonanno and M. V. Cook, (2006), “Flight dynamic simulation of a flapless flight control

UAV," in *ICAS-Secretariat - 25th Congress of the International Council of the Aeronautical Sciences 2006*, (2006), , vol. 5, pp. 3244–3254.
[95] Center for Advanced Machine Mobility (CAMM) at Georgia Institute of Technology, "Past Research Projects." camm.gatech.edu/index.php?title=Past_Research_Projects Accessed : [Sep. 08, 2019].
[96] N. T. Frink, D. L. Bonhaus, V. N. Vatsa, S. X. S. Bauer, and A. F. Tinetti, (2003), "Boundary condition for simulation of flow over porous surfaces," *J. Aircr.*, vol. 40, no. 4, pp. 692–698, doi: 10.2514/2.3147.
[97] R. A. Wallis and C. M. Stuart, (1962), "On the Control of Shock-induced Boundary-Layer Separation with Discrete Air Jets," *Aeronaut. Res. Counc. Curr. Pap.*, no. 595.
[98] S. X. S. Bauer and G. Hernandez, (1988), "Reduction of cross flow shock - Induced separation with a porous cavity at supersonic speeds," (1988), , doi: 10.2514/6.1988-2567.
[99] C. A. Hunter, S. A. Viken, and R. M. Wood, "Advanced Aerodynamic Design of Passive Porosity Control Effectors 39th AIAA Aerospace Sciences Meeting & Exhibit 8-11 January 2001 / Reno , NV," no. January 2001.
[100] D. Corriveau, (2005), "Impact of nose-mounted micro-structures on the aerodynamics of a generic missile."
[101] F. C. Wong *et al.*, (2007), "Shape memory alloy actuated micro-flow effectors for vortex manipulation," *Trans. Can. Soc. Mech. Eng.*, vol. 31, no. 1, pp. 19–38, doi: 10.1139/tcsme-2007-0002.
[102] D. D. C. and N. Hamel, (2006), "Impact of Nose-Mounted Micro-Structures on the Aerodynamics of a Generic Finned Missile - Presentation."
[103] K. Maree *et al.*, (2016), *First steps in research*, Revised Ed. Van Schaik Publishers.
[104] S. Goddard, W & Melville, (2004), *Research Methodology: An Introduction*, Second Edi. Blackwell Publishing.
[105] John Dudovskiy, "Inductive Approach (Inductive Reasoning)." http://research-methodology.net/research-methodology/research-approach/inductive-approach-2/ Accessed : [Oct. 12, 2014].
[106] John Dudovskiy, "Deductive Approach (Deductive Reasoning)." http://research-methodology.net/research-methodology/research-approach/deductive-approach-2/ Accessed : [Oct. 12, 2014].
[107] J. Jesson and F. Lacey, (2006), "How to do (or not to do) a critical literature review," vol. 6, no. June, pp. 139–148, doi: 10.1080/15602210600616218.
[108] G. Viljoen, (2016), "The Application of Parameter Dependency Diagrams in System Design. A missile system design example," *INCOSE Int. Symp.*, vol. 26, no. 1, pp. 2287–2299, doi: 10.1002/j.2334-5837.2016.00295.x.
[109] M. Khalil, A. Hashish, and H. M. Abdalla, (2019), "A preliminary multidisciplinary design

procedure for tactical missiles,” *Proc. Inst. Mech. Eng. Part G J. Aerosp. Eng.*, vol. 233, no. 9, pp. 3445–3458, doi: 10.1177/0954410018797882.

[110] A. P. Frits, E. L. Fleeman, and D. N. Mavris, (2002), “Use of a Conceptual Sizing Tool for Conceptual Design of Tactical Missiles (U).”

[111] S. M. College and D. of Defense, (2001), *System Engineering Fundamentals*, 22060th–5565th ed. Defense Acquisition University Press Fort Belvoir, Virginia, MIT.

[112] K. Ulrich and S. Eppinger, (2020), *Product design and development*, 7th editio. McGraw-Hill Education.

[113] “The Most Advanced Air-to-Air Missile In The World.” https://www.saab.com/markets/india/gripen-for-india/technology/the-most-advanced-air-to-air-missile-in-the-world Accessed : [Feb. 25, 2021].

[114] “Gripen conducts high altitude firing with Meteor.” https://www.saab.com/newsroom/press-releases/2007/gripen-conducts-high-altitude-firing-with-meteor Accessed : [Feb. 25, 2021].

[115] “AIM-120 Advanced Medium-Range Air-to-Air Missile (AMRAAM).” https://www.airforce-technology.com/projects/aim-120-advanced-medium-range-air-to-air-missile-amraam/ Accessed : [Feb. 25, 2021].

[116] Montevideo Technology Inc., “BLHP-20-04-8P Brushless High Performance Servo Series.” https://www.slmti.com/products/brushless-dc-motors/high-performance/blhp-series/motor/blhp-20-04-8p Accessed : [Sep. 30, 2019].

[117] G. P. Sutton and O. Bilblarz, (2001), *Rocket Propulsion Elements*, Seventh. John Wiley & Sons, Inc.

[118] T. W. Howard and G. D. Davis, (1997), “Challenges in Missile Life Cycle System Engineering,” p. 26.

[119] C. S. Wasson, (2011), “System Phases, Modes, and States Solutions To Controversial Issues,” *21st Annu. Int. Symp. Int. Counc. Syst. Eng. INCOSE 2011*, vol. 1, pp. 278–292.

[120] J. Moubray, (2001), *Reliability-centered maintenance*. Industrial Press.

[121] A. Kaposi and M. Myers, (2001), *Systems for all*. Imperial College Press.

[122] N. Cross, (2008), *Engineering Design Mehods - Strategies for Product Design*, 4th ed., no. 1. John Wiley & Sons.

[123] IEEE Computer Society, (2005), “1220-2005 - IEEE Standard for Application and Management of the Systems Engineering Process,” doi: 10.1109/IEEESTD.2005.96469.

[124] United States of America Department Of Defence, (2014), *MIL-STD-810G: Environmental Test Methods Test Method Standard for Environmental Engineering Considerations*. .

[125] N. Hall, “Inclination effects on lift,” *www.grc.nasa.gov/*. www.grc.nasa.gov/www/k-12/airplane/incline.html Accessed : [Sep. 29, 2019].

[126] ArsenioDev, “Arduino rocket stabilization system [UD: 7/14/17],” *https://hackaday.io/*. https://hackaday.io/project/1742-arduino-rocket-stabilization-system-ud-71417 Accessed :

[Sep. 29, 2019].

[127] I. Todić, M. Miloš, and M. Pavišić, (2013), “Position and speed control of electromechanical actuator for aerospace applications,” *Teh. Vjesn.*, vol. 20, no. 5, pp. 853–860.

[128] http://www.dynalloy.com/, “Dynalloy Inc.” http://www.dynalloy.com/ Accessed : [Sep. 29, 2019].

[129] Images SI Inc., “Nitinol Wire Actuators.” https://www.imagesco.com/nitinol/wire.html Accessed : [Jan. 21, 2020].

[130] Dynalloy Inc.; JC Moonsamy, (2019), “Email Conversation with Dynalloy, Inc.” .

[131] P. Senthilkumar, G. N. Dayananda, M. Umapathy, and V. Shankar, (2012), “Experimental evaluation of a shape memory alloy wire actuator with a modulated adaptive controller for position control,” *Smart Mater. Struct.*, vol. 21, no. 1, doi: 10.1088/0964-1726/21/1/015015.

[132] S. Sunjai Nakshatharan, K. Dhanalakshmi, and D. Josephine Selvarani Ruth, (2016), “Effect of stress on bandwidth of antagonistic shape memory alloy actuators,” *J. Intell. Mater. Syst. Struct.*, vol. 27, no. 2, pp. 153–165, doi: 10.1177/1045389X14563865.

[133] A. Khan, Hamza; Manfredi, Luigi; Huan, Yu; Velsink, Florien; Cuschieri, (2016), “Analysis of performance and energy efficiency of thin shape memory alloy wire-based actuators,” no. June. pp. 0–4.

[134] Y. Tadesse, N. Thayer, and S. Priya, (2010), “Tailoring the response time of shape memory alloy wires through active cooling and pre-stress,” *J. Intell. Mater. Syst. Struct.*, vol. 21, no. 1, pp. 19–40, doi: 10.1177/1045389X09352814.

[135] A. R. Pelton, (2011), “Nitinol fatigue: A review of microstructures and mechanisms,” *J. Mater. Eng. Perform.*, vol. 20, no. 4–5, pp. 613–617, doi: 10.1007/s11665-011-9864-9.

[136] S. Daynes, P. M. Weaver, and K. D. Potter, (2009), “Aeroelastic study of bistable composite airfoils,” *J. Aircr.*, vol. 46, no. 6, pp. 2169–2173, doi: 10.2514/1.44287.

[137] R. J. (Raymond J. Roark, W. C. (Warren C. Young, and R. G. (Richard G. Budynas, (2002), *Roark’s formulas for stress and strain*. McGraw-Hill.

[138] K. Y. Chang, S. Llu, and fu K. Chang, (1991), “Damage Tolerance of Laminated Composites Containing an Open Hole and Subjected to Tensile Loadings,” *J. Compos. Mater.*, vol. 25, no. 3, pp. 274–301, doi: 10.1177/002199839102500303.

[139] R. Reid, (2007), “MECN3001 Aircraft Structures I Course Notes.” .

[140] R. M. Jones, (1999), *Mechanics of composite materials*. Taylor & Francis.

[141] A. Das Anto, S. Mia, and M. A. Hasib, (2019), “The influence of number and orientation of ply on tensile properties of hybrid composites,” *J. Phys. Mater.*, vol. 2, no. 2, p. 025002, doi: 10.1088/2515-7639/aaff7a.

[142] P. N. B. Reis, J. A. M. Ferreira, J. D. M. Costa, and M. O. W. Richardson, (2009), “Fatigue life evaluation for carbon/epoxy laminate composites under constant and variable block loading,” *Compos. Sci. Technol.*, vol. 69, no. 2, pp. 154–160, doi:

10.1016/j.compscitech.2008.09.043.

[143] G. C. Materials, (2003), "Journal of Reinforced Plastics Correlation of Accelerated Aging Test to," *J. Reinf. Plast. Compos.*, vol. 22, no. 09, doi: 10.1177/073168403033369.

[144] Toray Carbon Fibers America Inc, "Technical data sheet TORAYCA T300." https://www.fibermaxcomposites.com/shop/datasheets/T300.pdf Accessed : [Jun. 12, 2019].

[145] R. F. Porter, D. W. Hall, and R. D. Vergara, (1979), "Extended Analytical Study Of The Free-Wing/Free-Trimmer Concept," *NASA Contract Rep CR-3135*.

[146] S. B. Verma and A. Hadjadj, (2015), "Supersonic flow control," *Shock Waves*, vol. 25, no. 5, pp. 443–449, doi: 10.1007/s00193-015-0587-y.

[147] P. L. Blinde, R. A. Humble, B. W. van Oudheusden, and F. Scarano, (2009), "Effects of micro-ramps on a shock wave/turbulent boundary layer interaction," *Shock Waves*, vol. 19, no. 6, pp. 507–520, doi: 10.1007/s00193-009-0231-9.

[148] J. L. Vadillo, R. K. Agarwal, and A. A. Hassan, (2005), "Active control of shock/boundary layer interaction in transonic flow over airfoils," *43rd AIAA Aerosp. Sci. Meet. Exhib. - Meet. Pap.*, no. June, pp. 2319–2328.

[149] J. M. Kearney, (2015), "Aerodynamic Control Using Distributed Active Bleed," Georgia Institute of Technology, (2015), .

[150] N. T. Frink, S. X. S. Bauer, and C. a Hunter, (2002), "Simulation of Flows With Passive Porosity," *ICAS 2002 Congr.*, pp. 1–10.

[151] R. M. Barrett and G. M. Lee, (2004), "Design and testing of piezoelectric flight control actuators for hard-launch munitions," *Smart Struct. Mater. 2004 Smart Struct. Integr. Syst.*, vol. 5390, no. May 2010, p. 459, doi: 10.1117/12.536686.

[152] R. Barrett, (2011), "Adaptive Flight Control Actuators and Mechanisms for Missiles, Munitions and Uninhabited Aerial Vehicles (UAVs)," *Adv. Flight Control Syst.*, no. April 2011, doi: 10.5772/13796.

[153] www-eng.lbl.gov, "Coefficient of friction," *www-eng.lbl.gov*. http://www-eng.lbl.gov/~ajdemell/coefficients_of_friction.html Accessed : [Oct. 06, 2019].

[154] PI, "Piezoelectric Actuators." https://www.pi-usa.us/.

[155] T. C. Briles, D. C. Yost, A. Cingöz, J. Ye, and T. R. Schibli, (2010), "Simple piezoelectric-actuated mirror with 180 kHz servo bandwidth," *Opt. Express*, vol. 18, no. 10, p. 9739, doi: 10.1364/oe.18.009739.

[156] PI CERAMIC, (2016), "Piezoelectric Actuators." .

[157] J. M. L. Miller *et al.*, (2018), "Effective quality factor tuning mechanisms in micromechanical resonators," *ApPRv*, vol. 5, no. 4, p. 041307, doi: 10.1063/1.5027850.

[158] R. Holland and E. P. Eernisse, (1969), *Design of resonant piezoelectric devices*. M.I.T. Press.

[159] G. Nader, E. Carlos, N. Silva, and J. C. Adamowski, (2004), "Effective Damping Value of Piezoelectric Transducer Determined by Experimental Techniques and Numerical Analysis."

[160] http://www.globalsecurity.org/, “Trajectory Correctable Munition (TCM).” http://www.globalsecurity.org/military/systems/munitions/tcm.htm Accessed : [Oct. 06, 2019].

[161] UWS Business Solutions GmbH, “QFD: House of Quality.” www.uw-s.com/wp-content/uploads/2014/01/Full_HOQ_0.9.xlsx Accessed : [Jun. 09, 2018].

[162] S. Honkala, M. Hämäläinen, and M. Salonen, (2007), “Comparison of Four Existing Concept Selection Methods,” *DS 42 Proc. ICED 2007, 16th Int. Conf. Eng. Des. Paris, Fr. 28.-31.07.2007*, pp. 125-126 (exec. Summ.), full paper no. DS42_P_317.

[163] T. Mai, (2012), “Technology Readiness Level,” no. 2006, pp. 1–4.

[164] D. Mawby, (2004), “Ministry Of Defence MOD Architectural Framework Feedback from Community of Interest Workshops,” *Defense*, pp. 1–17.

[165] C. Michielssen, (2016), “AIM 120A AMRAAM.” http://modelrocketbuilding.blogspot.com/2016/11/stm-12-kitbash.html Accessed : [Dec. 12, 2019].

[166] Engineering ToolBox, (2003), “US standard atmosphere.” https://www.engineeringtoolbox.com/standard-atmosphere-d_604.html Accessed : [Aug. 31, 2016].

[167] Northrop Grumman Corporation (Former ATK Tacitcal Systems), (2000), “AMRAAM PEP Propulsion System.”

[168] T. L. Moore, (2011), “Solid propulsion enabling technologies and milestones for navy air-launched tactical missiles,” *AIAA Centen. Nav. Aviat. Forum “100 Years Achiev. Progress,”* no. 11.

[169] E. L. Fleeman, (2010), “Summary and Lessons Learned,” *Integr. Vlsi J.*, pp. 1–25.

[170] L. J. Clancy, (1975), *Aerodynamics*. Pitman Publishing Limited, London.

[171] L. THK Co., “Examples of Selecting a Ball Screw,” *https://tech.thk.com/en/*. https://tech.thk.com/en/products/pdf/en_b15_069.pdf#1 Accessed : [Oct. 03, 2019].

[172] Rexroth Bosch Group, “Rexroth Precision Ball Screw Assemblies End Bearings and Nut Housings.” https://www.ahrinternational.com/PDF_catalogues/Rexroth_STAR/RE83301_2009_09_KGTENGL_Precision_ball_screw_assemblies.pdf Accessed : [Oct. 03, 2019].

[173] S. S. Rao, (2004), *Mechanical vibrations*. Pearson Prentice Hall.

[174] G. A. Swift, (2011), “Thermophysical properties of lithium alloys for thermal batteries,” *Int. J. Thermophys.*, vol. 32, no. 10, pp. 2102–2111, doi: 10.1007/s10765-011-1081-0.

APPENDIX A: Missile Design

The missile design, as described in Fleeman [60], required the mission requirements to be defined. The missile mission requirements are usually derived from the client, together with other stakeholders. The additional context for the design is extracted from the evaluation of the Concept of Use of the weapon. Once this is completed, a baseline can be selected. This assists the design process as the baseline provides a starting point for the design of the missile. As described in Section 2.4, a BVR missile was selected.

The concept of use (CONUSE) describes how a product will be used in a variety of situations/scenarios as described by Mawby [164]. To generate the required inputs to develop an ASYS, the higher-level system, the missile, needed a concept of use to be defined.

The missile will have the following post-integration life profile:

1. Acceptance Testing (Using external power)
2. Be transported.
3. Be stored and remain in a dormant state.
4. Enter Maintenance State (after extended storage periods of 5 years (assumed) after each flight cycle) (Using External Power)
    a. Be powered.
    b. Be tested (within missile system)
    c. Be powered down.
    d. Be repaired (if required)
5. Carriage Flight
6. Be utilised by the missile system (Free Flight)
7. Decommission and dispose (if beyond proposed shelf life)

The concept of use of the BVR missile to be designed is to engage an oncoming target at a range of 120 km at 30000 ft. The missile would be launched from an aerial launch platform (like a fighter aircraft) with a velocity of Mach 0.9.

A.1 The Conceptual Generic Missile

Based on the Systems Engineering approach to this design, the conceptual design of the missile system was needed to develop the system requirements in which the ASYS would be used.

Missiles are complex systems with a design process that requires multidisciplinary inputs. For this study, the missile design method described by Fleeman [60] was used to develop a generic missile to determine the necessary system inputs to the missile's ASYS design. There are other methods to develop a missile system, for example, the method described by G. Viljoen [108]. However, the Fleeman approach was selected as the method of choice due to its use in other missile studies. [109][110]

The approach laid out in Fleeman [60] is illustrated in Figure 94.

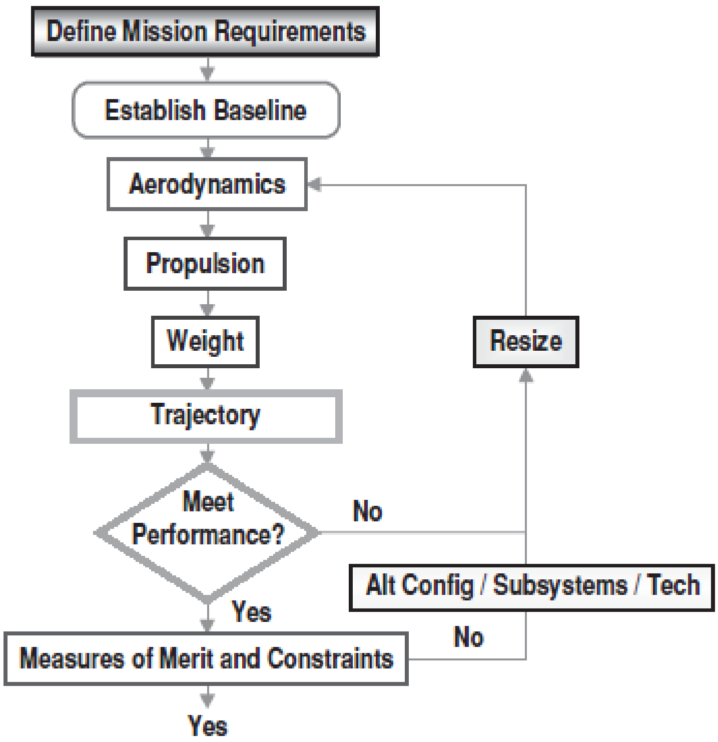

Figure 94: Fleeman's Missile Conceptual Design Approach [60]

A.2 Mission Requirements

The initial phase of the missile conceptual design process is to define the mission requirements for the missile system. These requirements are usually developed by an original equipment manufacturer (OEM) through market analysis and/or client needs.

The concept of use was introduced to assist in adapting and refining the mission requirements, as summarized in Table 43.

Table 43: Missile Performance Requirements

1	Range	120 km+
2	Launch Platform	Fighter Jet Aircraft (SAAB Gripen)
3	Launch Altitude	9144 m or 30000 ft.
4	Launch Platform Speed	Mach 0.9
5	Maximum Mass	160 kg
6	Maximum Carriage Volume	3.7mx0.35mx0.35m
7	Warhead Size	≥ 18kg Blast Fragmentation
8	Engaging Platform Speed	Mach 0.9
9	Engaging Platform Altitude	30000ft
10	Engaging Platform Maximum Manoeuvre	9 g

A.3 Missile Baseline Characteristics

The baseline to initiate the design for this study was the AIM-120 AMRAAM outer geometry. The outer missile dimensions and layout of the AIM-120A/B/C (pre-clipped wings) are illustrated in Figure 28 and Figure 95. The dimensions depicted in Figure 95 were used for the design of the BVR missile. These influenced the available space and placement of the subsystems.

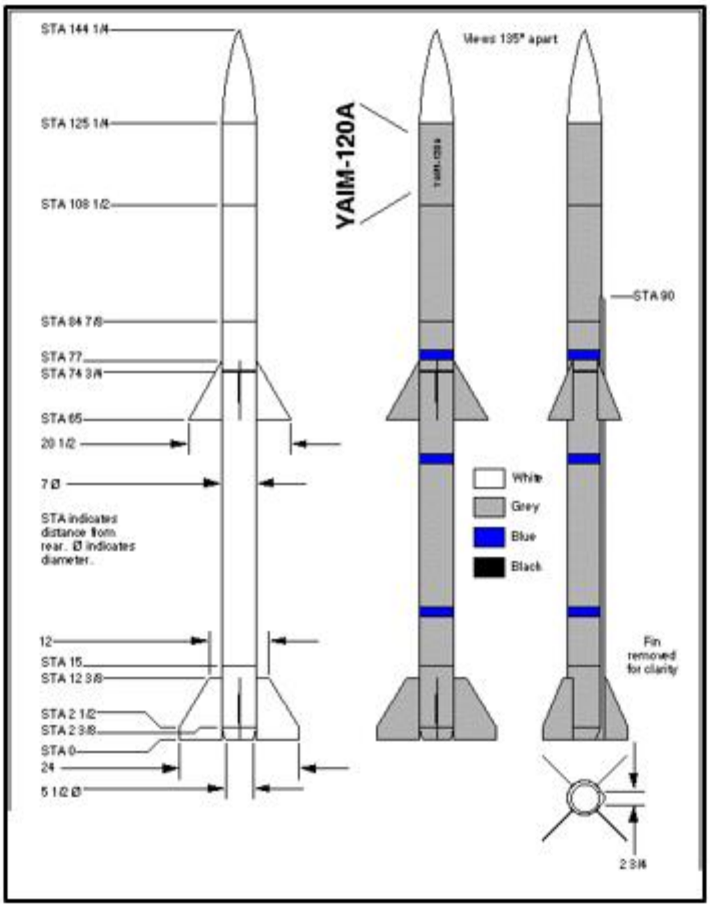

Figure 95: AIM-120A Geometry (from [165] **online)**

A.4 Aerodynamics

The missile aerodynamics are the next phase of the conceptual design [60]. The aerodynamic design for a missile includes the consideration of various types of subsystem layouts, changes in geometry, and the aerodynamic technology available.

The following parameters were identified from Fleeman [60] as outputs of the missile aerodynamic design process:

- Missile body length
- Nose geometry
- Wing geometry
- Control surface geometry
- Aerodynamic coefficients

There are advantages and disadvantages to the selection of specific parameters. The missile's performance is a crucial factor in the selection of various geometric parameters.

The missile aerodynamic characteristics, based on the design carried out, is shown in Table 44:

Table 44: Missile Aerodynamics Characteristics

Characteristic	**Value/Design Choice**
Missile Diameter	0.178 m
Nose Fineness (l_n)	2.71
Dome Geometry	Von Karman
Nose Bluntness	20 %
Missile Length	3.664 m
Boat Tail	None
Missile Body Geometry	Axisymmetric
Body Centre of Pressure	73% of the Nose Length (0.350 m)
Wing Design	Delta
Fin Design	Cropped Delta
Coefficient of Normal Force Prediction ($C_{N\ Total}$)	5.49
Normal Force Curve Slope	6.14/rad
Wing Centre of Pressure	1.80 m (0.090 m from Wing Leading Edge)
Tail Centre of Pressure	3.39 m (0.081 m from Tail Leading Edge)
Lift to Drag ratio (L/D)	2.19
Induced Drag Coefficient (C_{Di})	1.5
Total Coefficient of Drag (C_D)	2
Flight Control	Tail Control
Missile Configuration	X configuration
Static Stability	Statically Stable
Missile Tail Sizing	0.233 m^2
Hinge Moment (total for two fins)	46.2 Nm

Fleeman begins the aerodynamic design by defining the missile diameter. The diameter selected for this design was 0.178 m, based on the missile baseline selected, and was deemed acceptable due to reasons outlined in A.3.

The nose fineness defines the ratio of the nose length over the missile diameter. The value of 2.71 was based on the AIM-120 (nose length of 0.483 m and a diameter of 0.178 m from Figure 95), close to the typical ratio for supersonic missiles [60].

A Von Karman dome geometry was selected based on the AIM 120 seen in Figure 95 and the advantages when flying at high Mach number and high altitude [60]. A nose bluntness of 20 % was selected to reduce localised stress concentration and heating of the nose tip. The effect on the body wave drag would be relatively small, as described in Fleeman [60].

The missile length and axisymmetric body were based on the AIM 120, as seen in Figure 95. A boat tail was not selected for the missile to simplify the aerodynamic calculations.

The centre of pressure was initially calculated based on an angle of attack of 10 degrees and a body fineness ratio (length of the body over the length of the nose) of 7.61 (based on the AIM 120 dimensions in Figure 95).

Delta and cropped delta were selected for the wing and fins designs, respectively. Delta wings or fins are commonly used for supersonic missiles [60]. The AIM 120D also has delta wings. The related geometric characteristics were calculated for this study.

The coefficient of normal force is a calculated value based on the geometry of the body, wings and fin. The Coefficient of Normal Force (C_N) for the entire missile was determined based on the requirement (Cf. Section A.2) for the missile to achieve a 30g manoeuvre. The C_N was determined to be 5.49 at Mach 4 and 30000 ft. This C_N was redefined as C_{NReq}, the required C_N.

The C_N values for the missile body ($C_{N\ Body}$), the wings ($C_{N\ Wings}$) and the Tail fins ($C_{N\ Fins}$) were determined for a constant tail fin deflection (δ) at different missile angles of attack (α). These coefficients were used to determine the moments of the missile's centre of gravity and thereafter the related Coefficient of Pitching Moment (C_M) for the missile.

First, the required Turn Radius was defined based on the required 30 g maneuverer using the following equation from Fleeman [60]:

$$n = \frac{V^2}{gR_T}$$

Where V is the velocity (m/s) of the missile, g is the acceleration due to gravity (9.81 m/s^2), n is the required g acceleration (m/s^2), and R_T is the Turn Radius in metres.

Rearranging the equation to solve for the Turn Radius R_T,

$$R_T = \frac{V^2}{gn} \tag{61}$$

A velocity of 1212 m/s would result in a Turn Radius of 4997 m. The required C_N total can be determined using Equation **(62)** from Fleeman [60]:

$$R_T = \frac{2W}{gC_N S_{Ref}\rho} \tag{62}$$

Substituting Equation **(61)** into Equation **(62)**, C_N can be determined from Equation **(63)**:

$$C_N = \frac{2Wn}{V^2 S_{Ref}\rho} \tag{63}$$

Where g is 9.81m/s^2, the missile reference area, S_{Ref} is 0.025 m^2, an air density ρ of 0.458kg/m^3 (at 30000 ft. [166]) and a weight W of 1540.17 N, the C_N total (required) is determined to be 5.49. This does not include interactions between the body, wings and tail fins.

This C_N was used to determine the load acting on the tail fins and the deflection. The C_N was evaluated at different angles of attack and different tail fin deflections. This was done to determine the conditions where the required C_N would be achieved. The results from the evaluation can be seen in APPENDIX C.

The relationship between the missile's C_N and C_M was established to evaluate trim condition, the tail fin deflection that would be required (δ_{Req}) to achieve C_{NReq} and a C_M of zero. Figure 96 depicts this relationship.

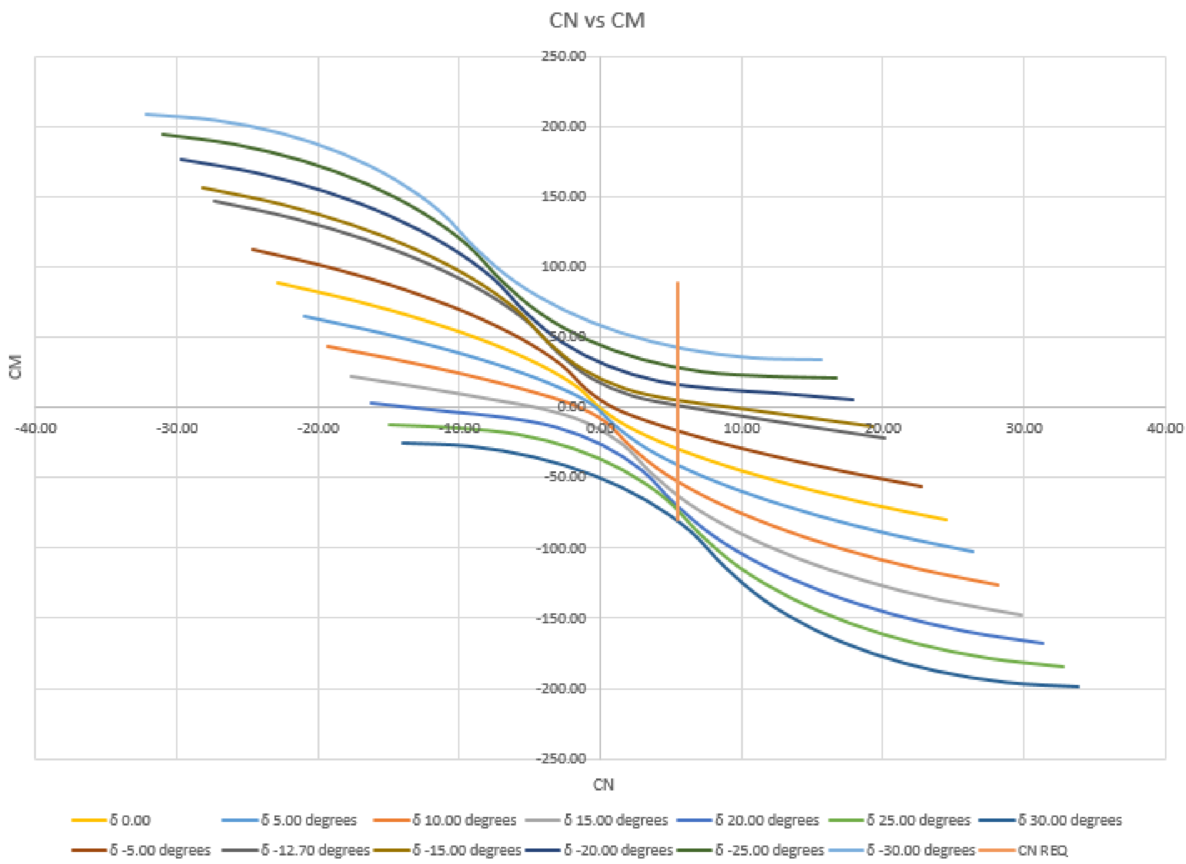

Figure 96: C_N vs C_M

Based on Figure 96, the deflection that allows for the sustained g manoeuvre was determined to be -12.7°. This was based on the curve that passes through the x-axis at the required C_N value, which indicates the fin deflection that achieves the required Normal Force coefficient for a zero Moment coefficient. A negative fin deflection is defined as the "leading edge down - trailing edge up" deflection of the tail fin, as seen in Figure 97.

The conditions to produce the required C_N are highlighted in Table 45

Table 45: Conditions for the Required C_N

Angle of Attack α (degrees)	Tail Deflection δ (degrees)
14.92	-12.7

The initial angle of attack of 14.92 degrees allows for the C_N to be achieved at -12.7 degrees tail deflection. These values are used going forward as the maximum control manoeuvre condition with this tail deflection as the maximum tail deflection for the generic actuator.

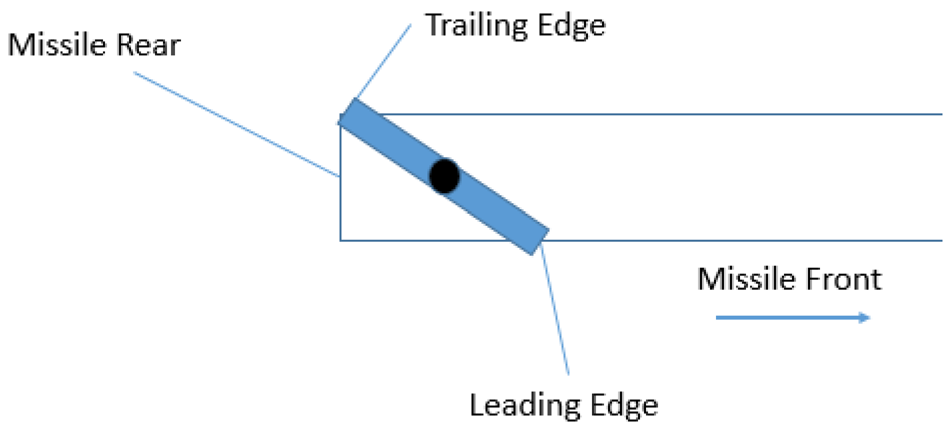

Figure 97: Fin Deflection

The missile will be flying in the "+" configuration. Therefore, the total tail $C_{N\ Tail}$ is assumed to act on two fins instead of four based on the missile orientation. The "+" configuration is the case where the missile flies with two tail fins in a horizontal orientation and two in a vertical orientation, and the fin set can be visualized as a "+" when viewed from the front or back of the missile.

This load is a result of the missile and fin geometry. To counteract this load and to allow for manoeuvring of the missile, the servo motors provide a force to rotate the tail fin to position it in the flow. The force produced by the motors combined with a gearing ratio needs to be equal to the externally applied load to maintain a fin position of higher than the applied load to move the fin. The normal force at the centre of pressure (CP) of the fin is used to determine the hinge moment of the hinge line of the tail. This is the moment that the servo motor is meant to match and, in some instances, overcome to produce the deflection required.

The normal force, the point of application (the CP), and the resultant moment are illustrated in Figure 98.

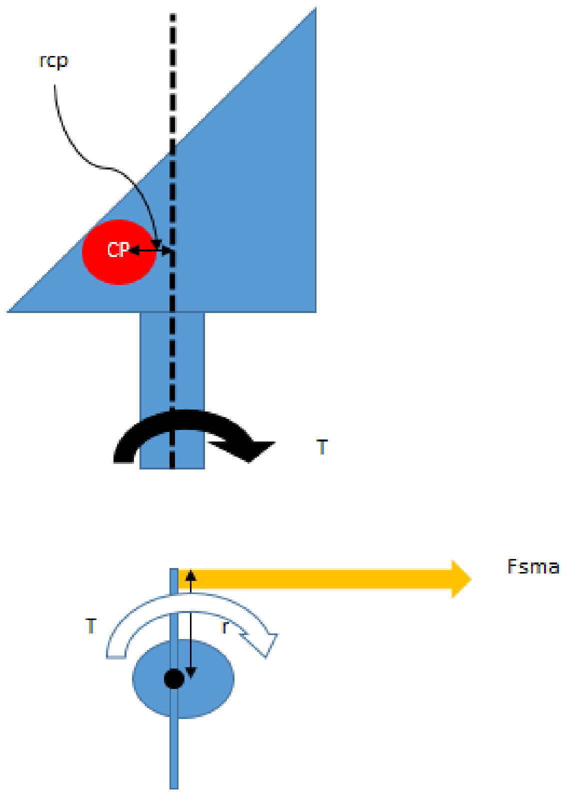

Figure 98: Normal force interaction with the missile tail Fin

In Figure 98, the force (≈1685 N) is acting into the page perpendicular to the surface of the fin at the CP location indicated. The moment arm, r_{cp} (calculated to be 13.74 mm), is the distance from the CP to the hinge line (axis of rotation) of the fin. The hinge moment or torque T (23.15 Nm) is the result of the product of the force and the moment arm r. The load the servo motor (in conjunction with a gearing mechanism) is required to maintain the fin position is F_{SM} which would have to act in the opposite direction to the resultant load at the end of the lever arm, r, to counteract the torque. For this study, it was decided to increase the torque requirement by 20 % (this was assumed for the calculation, and it should be verified in a future study). This was done to ensure the FGM produces sufficient load and would always be able to overcome the applied load, assuming the 1685 N is the maximum load the fin experiences. The target torque requirement is, therefore, 27.78 Nm.

The Normal Force Curve Slope was calculated as described in Fleeman [60]. Based on the asymmetric body of AIM 120, an assumed roll angle of zero, the wing and fin areas and Mach 4, the Normal Force Curve Slope for the missile was found to be 6.14 rad^{-1}.

The wing and tail aerodynamic centres are related to the missile's velocity. For low Mach numbers, the aerodynamic centre is closer to the leading edge and as the missile velocity increases (up to hypersonic flight), it can shift to 50 % of the mean aerodynamic chord. The aerodynamic centre for the missile was calculated based on the AIM 120 geometry in Figure 95. It was determined to be 0.090 m from the wing's leading edge and 0.081 m from the leading edge of the tail fin, measured along the Mean Aerodynamic Chord (MAC). This calculation was necessary for the stability predictions for the missile.

The lift to drag (*L/D*) ratio was determined based on the equation found in Fleeman [60]. The coefficient of drag (excluding induced drag) for the missile was calculated based on AIM-120's geometry. The *L/D* ratio was determined to be 2.19 based on the previously calculated C_N.

Induced Drag is a contributing factor to the total drag of the missile. The induced drag coefficient is influenced by the geometry of the lifting surface and the lift experienced by the lifting body. The total induced drag coefficient for the missile was calculated to be 1.5.

If one considers the induced drag coefficient and the previously calculated drag coefficient (excluding the induced drag, C_{do}), the total drag coefficient C_d was calculated to be 2.

For this missile, tail control was selected based on AIM 120. This will have an impact on the actuator design, and defining it at this stage allows for the generation of critical requirements for the actuator to be designed (the system of interest for this study).

The missile configuration for the flight was selected to be flying in the "+" configuration as this allows for a simpler normal force calculation and evaluates a more conservative load case for the missile fins. The flight configuration influences the actuator design.

Missile static stability is a vital characteristic to consider during missile design—the position of the aerodynamic surfaces and centre of gravity of the missile influence the missile's stability. Static stability in pitch is defined by a negative slope of the pitching moment against the angle of attack. This means that when the angle of attack increases in upwards pitching motion, the pitching moment due to the aerodynamic loading is such that it forces the missile nose down, this decreases the angle of attack. For a statically unstable missile, the converse is true. For this design, the missile was selected to be statically stable with the CP rear of the CG by 0.88 times the diameter of the missile as selected by Fleeman [60]

The missile's tail was sized based on the method described in Fleeman [60]. Based on the AIM 120 geometry and a Mach number of 4, the tail area was estimated to be 0.233 m^2.

The hinge moment is an important factor to consider for generic missile design. It is the result of the normal force acting on the control surface at a distance away from the hinge line of the control surface (a rotating fin). Based on a normal force of 3.37 kN (for two fins), a distance of 0.081 m (x_{AC}) from the tail fins MAC leading edge, and the hinge line at 30 % of the C_{MAC}, the hinge moment was calculated to be 46.2 Nm or about 23.1 Nm per fin.

A.5 Propulsion

After the aerodynamic characteristics were assessed, the next step was propulsion design. [60]

A variety of propulsion choices exist for missiles [60]. These include.

- Solid Rockets
- Ducted Rockets
- Scramjets
- Ramjets
- Turbofan/Turbojet

The propulsion selected for the conceptual missile is highlighted in Table 46. These design characteristics were considered due to their influence on the actuator design.

Table 46: Propulsion Characteristics

Characteristic	Value/Design Choice
Rocket Motor	Solid Rocket Propulsion (AIM-120)
Propellant Mass	52 kg
Velocity (not including Drag)	1312 m/s
Thrust	18 kN
Burn Time	7 s
Total Impulse	126 kNs
Propellant	Reduced-Smoke Hydroxyl-Terminated Polybutadiene
Motor Case	Steel

This design was based on the AIM-120 propulsion system. Therefore, solid rocket propulsion is the propulsion method of choice. The AIM 120 propulsion system is described in Figure 99.

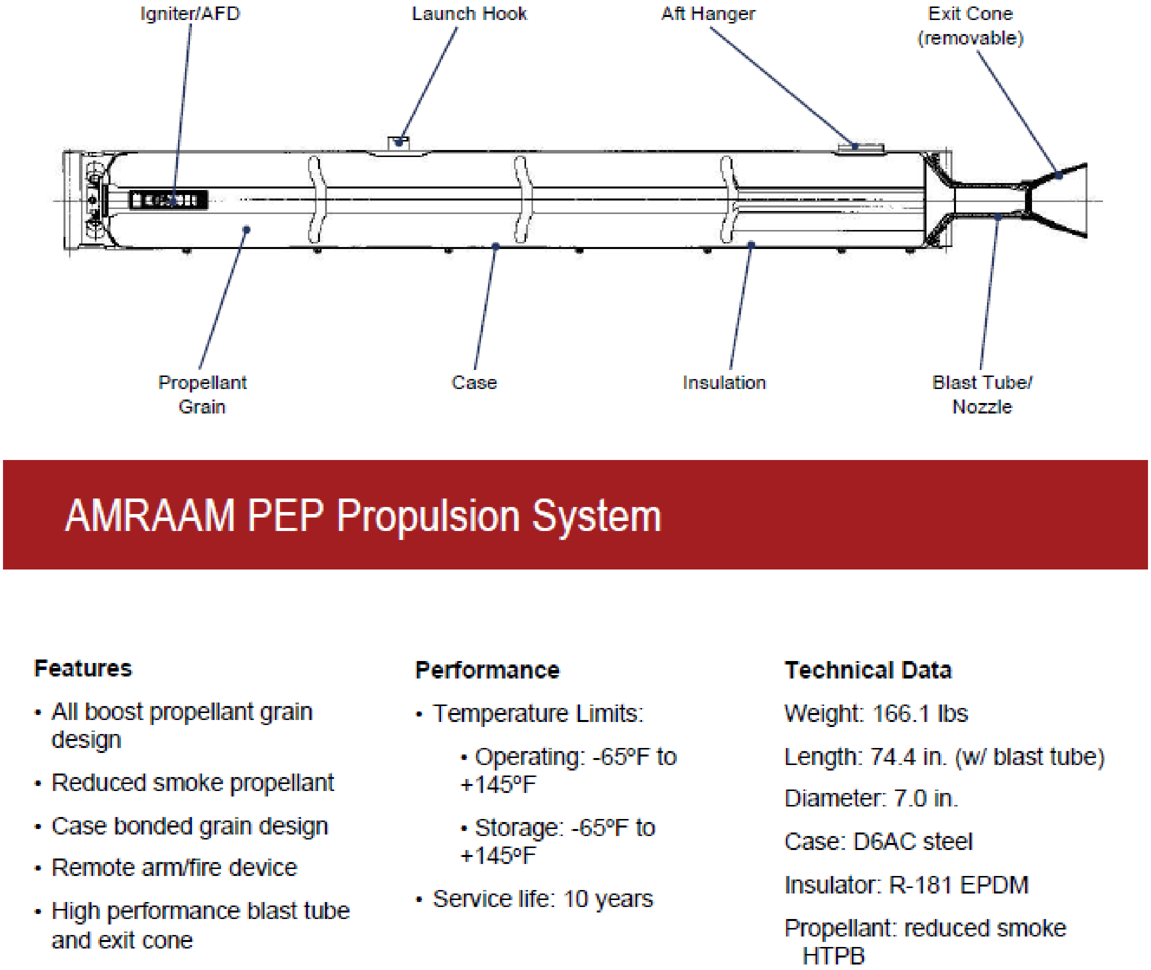

Figure 99: AIM-120 Rocket Motor Layout [167]

The rocket motor mass can be seen in Table 46. The ratio of propellant mass to the missile mass is therefore about 0.33 when the missile mass is 157 kg.

The velocity achievable (excluding drag) based on the ratio, after the propellant is spent, is 1312.5 m/s, assuming the missile is launched at Mach 0.9 at 30000 ft.

The I_{sp} was assumed to be 250 s which falls within the range of solid propellant rocket motors (no further information was found at the time of the study). The thrust was calculated to be 18 kN based on an assumed throat area of 0.046 m^2.

The Total Impulse was calculated to be 126 kNs based on an assumed burn time of 7 s.

The AIM-120 rocket motor uses a reduced-smoke hydroxyl-terminated polybutadiene propellant [167]. This propellant has an average I_{sp} (similar to the assumed value mentioned previously) density, is relatively safe to handle and has low observables. [60]

The rocket motor casing was based on the AIM 120, which is made from DA6C Steel. [167]

A.6 Missile Weight (Mass and Structure)

The next phase of the conceptual design was the missile weight (Mass and Structure design).

The missile mass and structure are important considerations for the actuator design as it gives rise to interface requirements and constraints. The design areas considered as influences to the actuator design are described in this section.

The mass of the missile was established based on the mass requirement. The mass of the subsystems was based on this mass value, the AIM 120 geometry and the estimated linear volumes from Fleeman [60]. This can be seen in Table 47.

Table 47: AIM-120 Layout summary

Subassembly	Weight	Length	Density (kg/m)
Radome	5.95kg	480mm	12.4
Radar Electronics	13.7kg	425mm	32.2
Guidance Section	19.6kg	606mm	32.3
Warhead	23kg	251mm	91.6
Rocket motor	75.3kg	1500mm	50.2
Actuator	14.4kg	410mm	35.1
Wings, fins	5kg	n/a	
Total	157kg	3654mm	43.0

The warhead mass is larger than the specified warhead mass of 18 kg. The additional mass can be redistributed to other subsystems where applicable to meet the requirements of the design for both the warhead and the missile.

The missile's centre of gravity was determined to be situated 1.986 m from the nose based on the calculated masses and their corresponding centres of gravity.

The missile layout was based on the AIM 120 baseline, as seen in Figure 100.

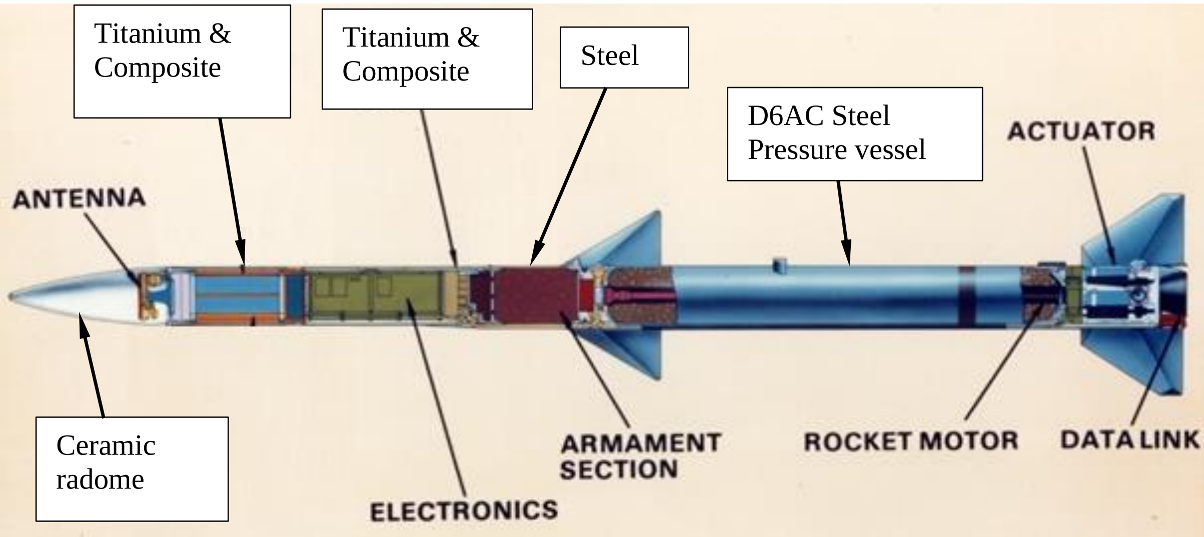

Figure 100: AIM 120 Baseline Layout [82]

The materials selected for the missile can be seen in Table 48:

Table 48: AIM-120 Structure summary

Subassembly	Material	Comments
Radome	Ceramic radome material	-
Front Section	Titanium [168]	Composite wrapped; manufacturability/cost & insulation
Warhead	Steel	
Rocket motor	Steel [167]	D6AC steel pressure vessel
Actuator sleeve	Steel	
Wings, fins	Steel	Future composite to save 50% mass

The reasons for the selection were based on the Functional Requirements of the various subassemblies in Table 48, including the requirements relating to, amongst others, mass, thermal effects and radar permeability. Further investigation is required to verify the material selection, but this should be sufficient for a first iteration.

The actuator sleeve or shroud material was initially defined as steel. The actuator design in the next sections will give a better insight into the material to be chosen.

A missile detailed structure design includes joints and other considerations that fall outside the scope of this study. A basic layout and design for the initial baseline can be seen in Figure 100.

During its flight, the missile is expected to experience some thermal loading, and it is expected to be significant since the missile will be operating at Mach 4. This is due to the recovery temperature being proportional to the square of the free-stream Mach (M_∞) number. Assuming a recovery factor (r) of 1 and a free stream temperature (T_∞) of 228.7 K at altitude 30000 ft., the recovery temperature ($T_{Recovery}$) is expected to be as follows based on Figure 101:

$$T_\infty = T_{Free\ Stream}(1 + 0.2rM_\infty^2)$$

$$= 960.5K = 687.4°C$$

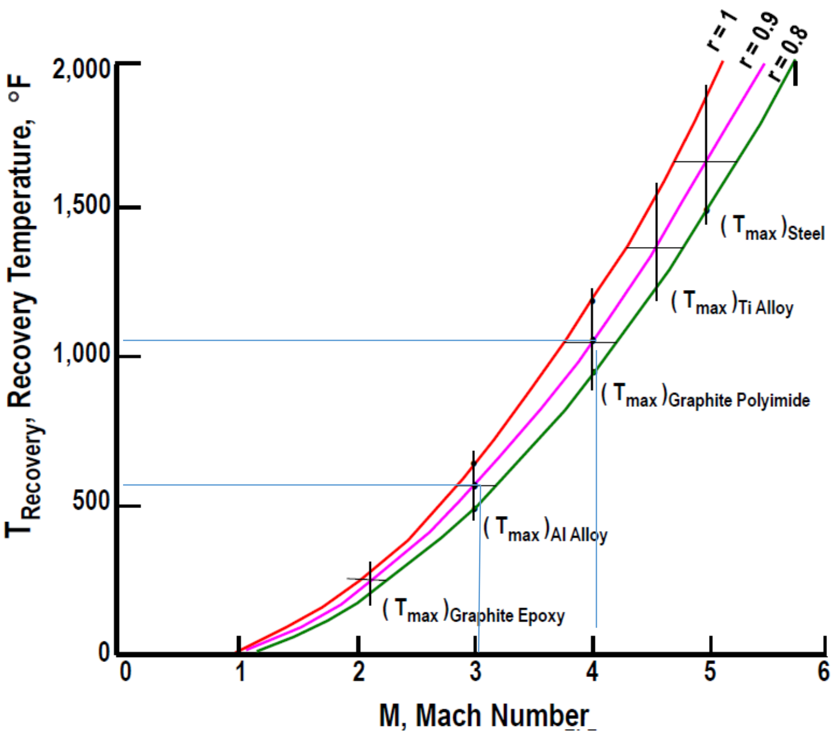

Figure 101: Recovery Temperature vs Mach Number [60]

The stagnation temperature (T_0) at the stagnation points is expected to be as follows:

$$\frac{T_0}{T_\infty} = 1 + \frac{\gamma - 1}{2} M_\infty^2$$

$$T_0 = T_\infty \left(1 + \frac{\gamma - 1}{2} M_\infty^2\right)$$

For a free stream temperature of 229.73 K at 30000 ft., a specific heat ratio γ of 1.4 and a Mach number of 4, the stagnation temperature would be:

$$T_0 = 964.86\, K$$

Even though the time the missile spends flying at Mach 4 is short, the heat transferred to the missile structure is noteworthy. High temperatures can affect the structural integrity of the missile, so the correct materials and thermal insulation methods need to be selected based on the external conditions expected.

The missile's first Body Bending Mode (ω_B) is an important structural factor to consider during the conceptual design, as seen in Fleeman [60]. Assuming that all the material that makes up the missile has a combined stiffness (*E*) of that of steel (210 GPa), the skin thickness (*t*) is 2 mm, the missile mass (*W*) is 157 kg, and the length to diameter (*l/d*) ratio is 18, the calculated natural frequency (*f*) in Hertz (*Hz*) for the first Body Bending Mode was therefore estimated as:

$$\omega_B = 18.75 \sqrt{\frac{Et}{W \frac{l}{d}}} \tag{64}$$

$$\omega_B = 302.33\, rad/s$$

$$f = \frac{\omega_B}{2\pi} = 48.11\, Hz$$

According to Fleeman [60], as a rule of thumb, the first body bending mode should be at least twice the flight control system's actuator bandwidth. This was used as the basis of the bandwidth requirement later in the study.

The maximum allowable buckling stress due to a bending moment ($\sigma_{Buckling\ Bending}$) was calculated to indicate the loads the missile structure would be able to endure. With a shroud of D6AC steel, whose modulus of elasticity (*E*) is 210GPa, the shroud thickness (*t*) 2 mm and the shroud radius (*r*) of 88.9 mm, for *t/r* equal to 0.0226, $\sigma_{Buckling\ Bending}$ would be.

$$\sigma_{Buckling\ Bending} = E \times 0.35 \left(\frac{t}{r}\right) = 1634\ MPa \tag{65}$$

The expected carriage loads on the missile should be much lower than the free flight loads. Higher loads would be expected for an ejection launch (compared to a rail launch). To future proof the missile for ejection launch platforms, the relevant loads were used to determine the missile structure requirement.

Assuming a 20 g ejection load, the mass distribution in front of the rocket motor is 10.7 kN.m. There the thickness *t* required would be 0.39 mm.

As calculated, a thin skin will suffice. However, a limiting factor to skin thickness is the manufacturability of the element. [60]

A.7 Trajectory and Flight Performance

The next phase of the conceptual design is the missile flight performance and trajectory.

The factors that influence missile trajectory and performance are the closing velocity and the end-game manoeuvre [60]. These factors will determine if the missile can intercept the intended target after the range requirement has been met [60]. The zero-lift drag coefficient is a driving factor in the calculation of the missile range [60]. An assumption can be made that for the majority of the flight, the missile will fly at an approximate zero angle of attack. [60]

Other influences on the range include the time of flight, seeker gimbal angle, and fire control system [60]. These will, however, not be discussed as it is beyond the scope of this conceptual design. The parameters required for long-range are first considered.

The flight performance can be simulated and modelled using methods such as one degree of freedom (1-DOF) up to six degrees of freedom (6-DOF) simulations. For this conceptual design, only one degree of freedom was considered to simplify analysis as this was not the focus of the study.

A 1-DOF (Axial force (C_{DO}), thrust, weight) has good accuracy near zero Angle of Attack and can be used to simulate speed during the majority of the flight (based on the assumption made previously). At low angles of attack, which is assumed to occur for the majority of the missile flight, the normal force contribution does not significantly affect the missile trajectory [60]. A ballistic flight at a certain altitude would yield the highest range. At the end-game manoeuvre, the normal force and missile weight becomes very relevant [60].

The missile's flight time was determined based on a 1-DOF assessment. It was assumed that the missile travels along a straight path at a zero angle of attack. Two phases were considered for the flight, the Rocket Motor Burn Phase and the cruise phase.

During the Rocket Motor Burn Phase, the following was considered:

- A rocket motor burn time of 7 s
- A thrust of 18 kN
- An initial velocity of 1212 m/s
- A reference area of 0.025 m^2
- Coefficient of Drag of 2
- A missile mass of 157 kg
- Air density of 0.46 kg/m^3

Based on the sum of forces in the direction of flight (x-direction):

$$\sum F_x = ma$$

$$\therefore a = \frac{T - D}{m}$$

The acceleration, a, was determined to be 7.05 m/s2. The is displacement, s, of the missile from its initial position during this phase was determined as follows:

$$s = vt + \frac{1}{2}at^2$$

The displacement was determined to be 8.7 km.

During the cruise phase, it was assumed the missile would travel its expected range of 120 km. During this phase, the drag was assumed to be constant and slowly bleed off the missile's velocity. The incept velocity was then considered to be the final velocity, *v*, at the end of the phase. This velocity should be twice the target's velocity, according to Fleeman [60]. For a target velocity of M 0.9 at 30000 ft, the intercept velocity was determined to be 546 m/s.

Considering the initial velocity, u, to be 1212 m/s, the time taken to reach 120 km was determined as follows:

$$s = \frac{1}{2}(u + v)t$$

$$\therefore t = \frac{2s}{(u + v)}$$

The time taken was determined to be 126 s. This gives a total flight time of 133 s, given the simplicity of this approach. An operational flight time was considered to be 180 s to account for the effects of manoeuvring, normal force and the change in weight after the propellent was used. These effects would mean the missile would require more time to reach the target at 120 km, provided it still achieve the intercept velocity.

The required 30g manoeuvre would require sufficient normal force to achieve the manoeuvre. The normal force coefficient, calculated in Section A.4, was based on the missile geometry and adjusted accordingly to achieve the 30 g manoeuvre.

According to Fleeman [60], a high speed and long-range flight are attained by a significant total impulse. The total impulse (*I)* of the missile has the following relationship:

$$I_{sp} = \frac{I}{mg}$$

If this equation is rearranged, the following is obtained:

$$I = I_{sp}mg \tag{66}$$

It is therefore related to the propellant mass (m), acceleration due to gravity (g) and specific impulse (I_{sp}). There are other factors, such as the drag force coefficient needs to be optimized to achieve the required range [60].

A.8 Measures of merit and performance Evaluation

The next phase examined if the missile met the required performance criteria by assessing the measures of merit and constraints.

The Measures of Merit were adapted from the missile mission requirements as defined at the beginning of this section. Various parameters were varied in an iterative process to move towards meeting the range and manoeuvre requirement. These included propellant mass, the addition of propulsion pulses and the change in missile diameter.

Additional Measures of Merit, according to Fleeman [60], include:

- Missile Robustness
- Warhead Lethality
- Miss Distance
- Carriage and Launch Observables
- Other Survivability Considerations
- Reliability
- Cost
- Launch Platform Integration

Robustness refers to the ability of the missile to survive various environmental flight conditions and any changes in those conditions. These can include, amongst others, changes to weather, temperature variation, and changes in altitude. [60]

Warhead lethality relates to the effectiveness of a warhead on an intended target. [60]

Miss Distance refers to the missile's performance concerning the interception of the intended target. The miss distance influences the effectiveness of the warhead and overall missile performance. The circular error probable (CEP) relates to the circular region where the miss distance will be close to the target 50 % of the time. The conservative approach for conceptual design is to assume 3σ (which is three times the CEP or 1σ), meaning the missile has a miss distance probability of 99%. [60]

Carriage and Launch Observables are measures of the missile’s launch platform’s radar cross-section (RCS) and the missile’s rocket plume signature. [60]

Other Survivability Considerations refers to the missile's RCS and the stand-off distance from possible threats. [60]

Reliability relates to the missile's ability to perform when required. The missile's overall reliability is related to the reliability of its subsystems. [60]

A missile's cost is important to consider in the design of a tactical missile. The cost of the missile filters up from the cost to produce its subsystems. Missile cost can affect design decisions which could impact missile performance. [60]

Launch Platform Integration measure refers to the level of impact the missile has on the launch platform. This is usually considered earlier in the design process. The iterative approach helps to refine the design to fit a selected launch platform should the type of platform be a constraint. [60]

The Measures of Merit influence on the actuator system to be developed were considered during the evaluation.

These measures were based on the primary function of the actuator within the missile system context. The primary function of the actuator is to provide the means to manoeuvre the missile in flight. This would include altering the missile's flight path or maintaining the missile's heading.

A.9 Summary of the Missile Design

The importance of the missile design highlighted the various areas which have an impact on the actuator design. The selection of the missile baseline indicated the placement of the actuator system, including the surrounding systems that would have an impact, like the rocket motor. The missile propulsion design highlighted the factors such as the space available and the operating environment. The aerodynamic design indicated the aerodynamic loads, which had an impact on the structural design and actuator selection. The missile weight assisted in the mass estimation for the actuator system. The centre of gravity of the weapon had an impact on the hinge line position and the centre of pressure. The trajectory, flight performance and the measures of merit are influenced by the actuator system together with the other missile systems.

This design developed the context and set the platform for the ASYS design. It gave the inputs for the elicitation of the requirements and functions of the actuator system.

A.10 Additional Generic Force Generation Mechanism considerations

A.10.1 Missile Manoeuvring

A.10.1.1 Response Time

It was previously mentioned that the missile's response time is the sensitivity of the angle of attack (α) to the missile's turn rate ($\dot{\gamma}$.), which was measured based on the ratio $\alpha/\dot{\gamma}$. The actuator system influence on the missile's response time is captured in the turn rate performance defined by $\dot{\gamma}$.

According to Fleeman [60], the turn rate performance is defined as follows:

$$\dot{\gamma} = gn/V = \left[qS_{Ref}C_{N\alpha}\alpha + qS_{Ref}C_{N\delta}\,\delta - W\cos\gamma \right]/[(W/g)V] \tag{67}$$

Where *g* is the acceleration due to gravity, *n* is the g manoeuvre, *v* is the velocity of the missile, *q* is the dynamic pressure (S_{Ref} is the reference area, $C_{N\alpha}$ is the normal force curve slope due to the angle of attack, and the $C_{N\delta}$ is the normal force derivative due to pitch control deflection, *W* is the mass of the missile, *α* is the angle of attack, *δ* is the control surface deflection, and *γ* is the flight path angle (assumed to be zero for this study due to constant altitude used in this study).

Fleeman [60] indicates the actuator impacts the $C_{N\alpha}$, the $C_{N\delta}$, *δ* and *W*. $C_{N\alpha}$ is related to the ratio of the tail area (S_T) (which forms part of the actuator system in this study), and the missile S_{ref}. $C_{N\delta}$ would be related to the deflection of the tail control surface. *δ* would also be related to the tail's deflection. The mass of the actuator system would influence the missile's *W*. Based on the generic actuator for this study, the $C_{N\alpha}$ contribution from the tail was determined to be 1.03rad^{-1}. With the body's contribution of 2 rad^{-1} and the wing's contribution of 1.03 rad^{-1}, the $C_{N\alpha}$ for the missile would be 16.6 rad^{-1}, which is 0.29 deg^{-1}, according to Equation (68).

$$C_{N\alpha} = C_{N\alpha\,Wing}(S_W/S_{Ref}) + C_{N\alpha\,Tail}(S_T/S_{Ref}) + C_{N\alpha\,Body} \tag{68}$$

This is based on an S_T/S_{ref} of 9.38 and an S_w/S_{ref} of 4.82.

The contribution and influence of the tail towards $C_{N\delta}$ are illustrated by the slope of the curve for $C_{N\,Tail}$ and $C_{N\,Total}$ in Figure 102. Based on a linear approximation, the slope of the $C_{N\,Tail}$ curve is 0.295 deg^{-1}. As seen in Figure 102., the tail is the main contributor towards the $C_{N\delta}$ as the $C_{N\,Body,}$ and $C_{N\,Wing}$ have no slope. Therefore, the total $C_{N\delta}$ would also be 0.295 deg^{-1}.

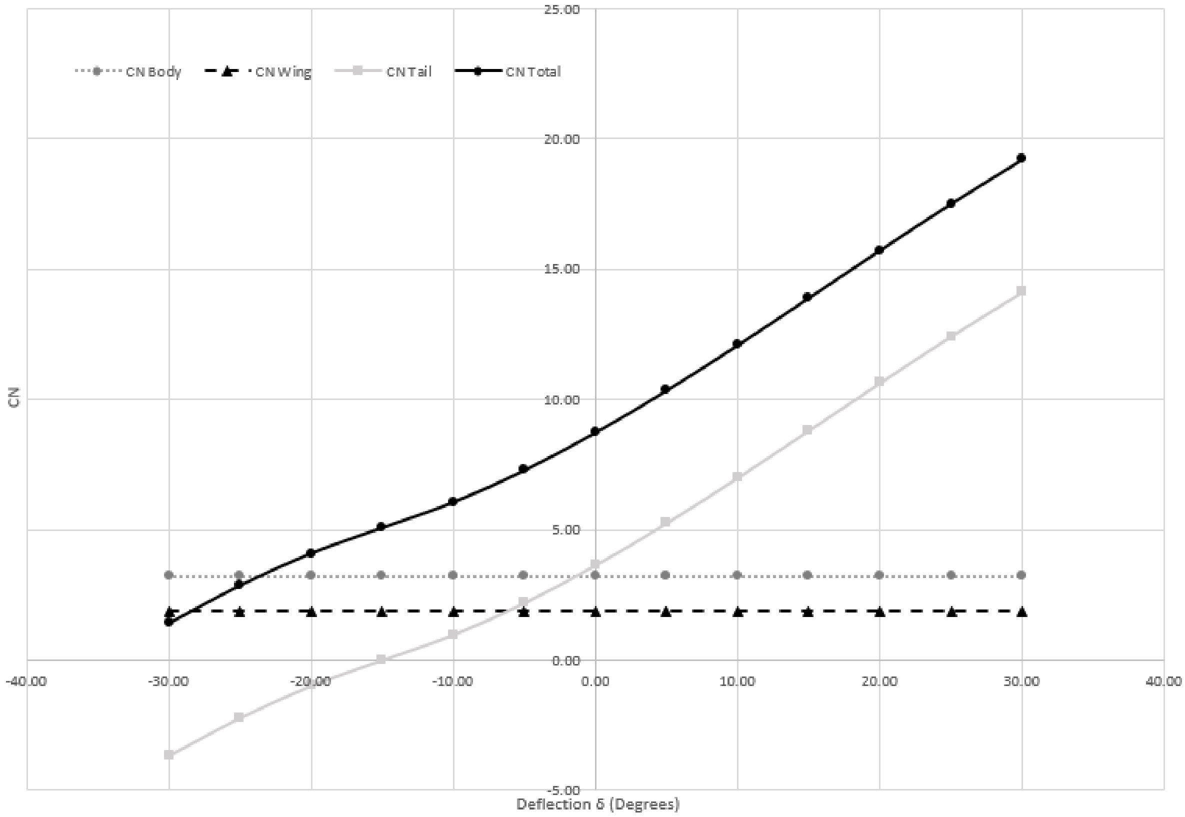

Figure 102: CN vs δ

As shown in SectionA.4, at an angle of attack of 14.92 degrees, the missile is trimmed with a tail deflection δ of -12.7 degrees. This deflection would be required for a sustained 30 g manoeuvre at Mach 4. According to Fleeman [60], this gives control effectiveness, *α/δ*, of -1.18. This deflection was used as the maximum deflection for this study and was therefore used as *δ* for the evaluation of the turn rate performance.

The system of interest for the actuator was the FGM, which is the servo motor for the generic actuator. The selected motor for this study has a mass of 0.516 kg, as mentioned in the Montevideo Technology Inc. servo motor datasheet [116]. There would be four motors, one for each of the four tail control surfaces of the actuator system. This would mean the total mass of the servo motors combined would be 2.064 kg. In Section A.6, the mass summary of the AIM-120 missile, the baseline of the conceptual missile used for this study, estimated that the actuator mass was 14.4 kg. The mass of the servo motors is below this actuator mass and therefore means the motor selection would be a valid option as the FGM for the generic actuator. The mass of the missile, *W*, used for this evaluation included the actuator mass from the summary as this forms part of the generic actuator used on the conceptual missile design. The missile mass is 157 kg. Assuming the missile reaches its maximum velocity of Mach 4 when all the propellant (52 kg) is spent and is then required to perform the 30 g manoeuvre, the mass of the missile would be reduced to 105 kg. This would be considered as *W* for the turn rate performance.

Therefore, based on Equation (67), the turn rate performance would be 20.95 °/s, which is greater than the intended target's turn rate performance of 16.64 °/s, which means that the missile is capable of intercepting the target.

The response time for 14.92 degrees angle of attack is 0.712 s.

A.10.1.2 Missile Miss Distance

As previously described, the miss distance for an effective navigation ratio (N) of 3 is as described by Equation (69) according to Fleeman [60].

$$\sigma_{MAN} = g n_T \tau^2 e^{-(t_O/\tau)[(t_O/\tau)^2/2]} \quad (69)$$

For a target acceleration of 9 g, a time constant τ of 0.44 s, a time to go (t_O) of 0.41 s, and acceleration due to gravity of 9.81 m/s^2, the miss distance was calculated to be 11.48 m.

The actuator system has an impact on the missile time constant τ. The calculation is described later in Section A.10.3.

A.10.2 Missile Aerodynamics

A.10.2.1 Contribution to the Normal Force

The contribution to the Normal Force of the missile is evaluated by assessing the actuator system's influence on the normal coefficient of the entire weapon as described previously. For the total C_N of 5.50, the tail contribution, C_{NTail}, is 0.4.

The C_{NTail} for the generic actuator system is a function of the tail fin area and the deflection of the fin. The servo motor for the generic actuator has a direct impact on the deflection.

A.10.2.2 Impact on Drag.

The induced drag contribution due to the actuator system's control surface was determined to be 0.22 based on the induced drag calculation previously described. The C_{NTail} is the main influence from the actuator system.

A.10.3 Missile Guidance and Control

A.10.3.1 Time constant

Based on the calculation previously described by Fleeman [60], the missile time constant τ is 0.444 s. The actuator system has a direct impact on the deflection δ, the pitching moment control effective $C_{M\delta}$, the deflection (slew) rate $\dot{\delta}$, and the turn rate performance $\dot{\gamma}$. The FGM has an influence on all of these.

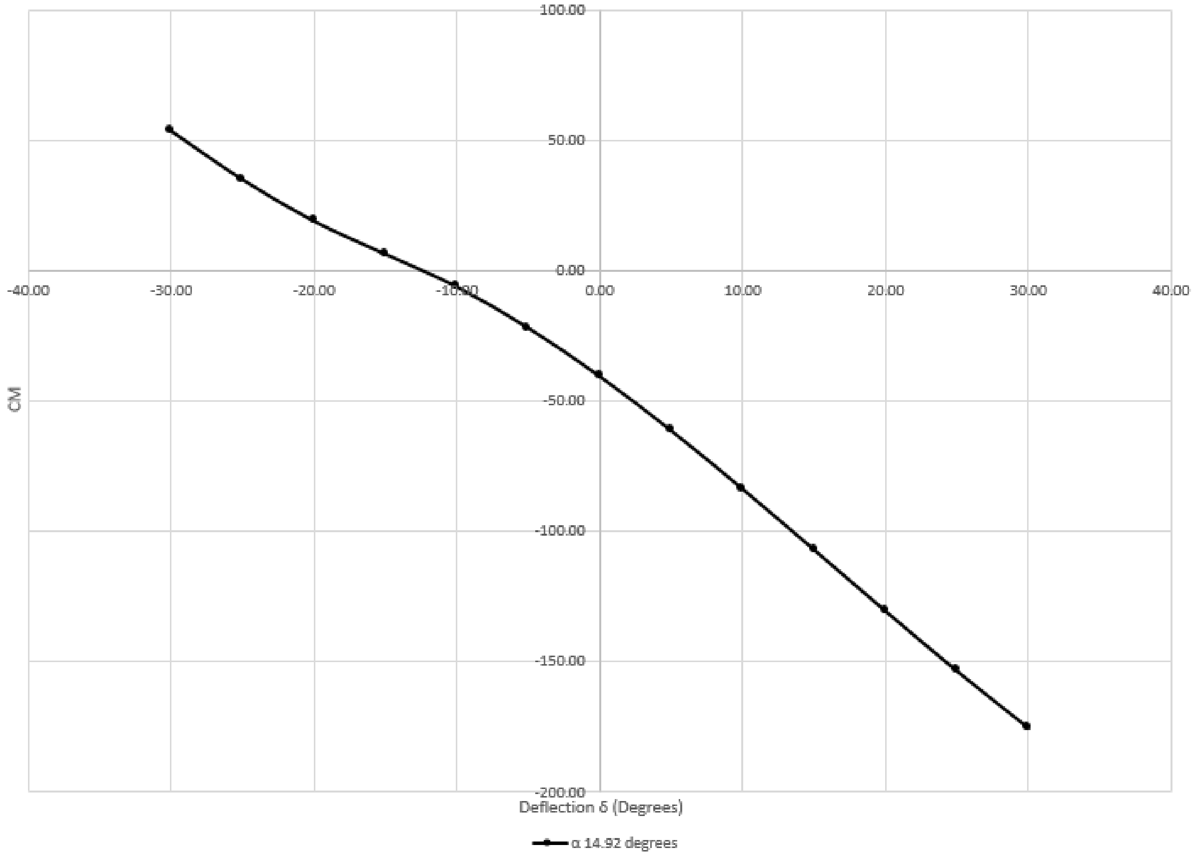

Figure 103: CM vs Delta at 14.95 degrees

The slope of the curve in Figure 103 is -3.787. This slope is the pitching moment control effectiveness derivative $C_{M\delta}$.

A.10.4 Missile Airframe

A.10.4.1 Effect of loading on Structure

The actuator system is loaded subject to aerodynamic loads, which is a function of altitude, geometry and velocity. The actuator system is meant to be designed to withstand these loads and work against them in order to manoeuvre the missile. The loading around the actuator region would affect the interface to the missile airframe. For this evaluation, the focus was on the loading that would impact the FGM in a direct manner. This would be the hinge moment the normal force would cause acting on the tail fin. The FGM would be expected to withstand and overcome this load to produce the necessary fin deflections. The hinge moment was determined to be 46.2 Nm. To withstand this load and to operate when this load (assumed to be the maximum loading) is applied, it was decided that the motor should provide 20 % more torque to operate under load for the purpose of the study. This would mean that the servo motor should be able to hold the fin in its desired position regardless of the load applied, within the range the control fins would experience.

A.10.4.2 Influence due to Rocket motor.

The thermal data for the rocket motor selected for the conceptual missile design was not available and thus could not be included in this study. Therefore, to estimate the heat the actuator system would experience, the heat transfer from the rocket motor to the exterior surface of the rocket motor casing was estimated.

In G. P. Sutton *et al*. [117], which describes the transient heat transfer from the combustion chamber to the motor casing wall and through it, the temperature of the blast tube internal wall was determined based on Figure 104.

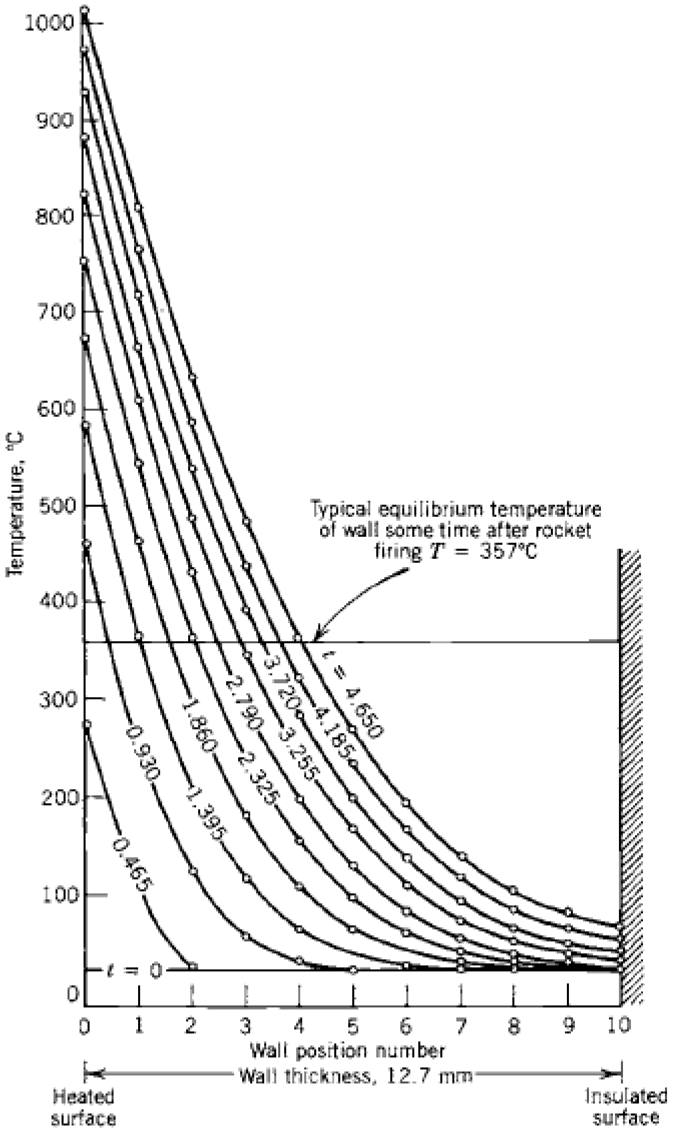

Figure 104: Typical temperature distributions through a motor casing thrust chamber wall as a function of heating time [117]

The internal temperature (T_i) was assumed to be the typical equilibrium temperature, namely 357°C, described in Figure 104. Through conductive heat flow, the surface on the outside of the blast tube will eventually reach this temperature. The temperature inside the actuator system would start from an extremely low temperature (at the minimum operating temperature of the motor) and would start to increase as soon as the rocket motor is ignited and would continue to increase until all the propellant is burnt. According to Montevideo Technology Inc.[116], the maximum operating temperature is 220°C. As a similar type of motor is in use in the AIM-120, it is expected that the temperature does not reach a temperature higher than the maximum rate operating temperature during the flight time.

A.10.5 Missile Mass

A.10.5.1 Percentage contribution

As previously described, the generic actuator system would contain four servo motors of 0.516 kg each, which make the total mass for the FGM 2.064 kg. This makes up 14.3 % of the 14.4 kg actuator, described in Section A.6. It is important to note that there are other structures that make up the ASYS and will also contribute to the total ASYS mass.

A.10.6 Missile Stability

A.10.6.1 Effect of force generation location

The positioning of the servo motor, the FGM within the actuator system, has an influence on the centre of gravity of the missile but has no direct effect on the centre of pressure of the weapon. This generic FGM placement would be similar to that of the AIM-120 baseline. The placement of the fins on the conceptual missile is also similar to the AIM 120. Therefore, the conceptual missile's stability is expected to at least be similar to that of the baseline selected.

A.10.7 Missile Flight Time

A.10.7.1 Operational Time

The overall effect of the actuator on the operational time encompasses the time the actuator is able to operate as well as the effects of its mass and its influence on drag. The mass and the drag would tend to bleed energy from the system, reducing the missile's operational time. However, for this study, the operational time of the 180s was considered as the structures that would influence the mass and drag were not designed.

APPENDIX B: Advantages and Disadvantages of Tail and Canard Control

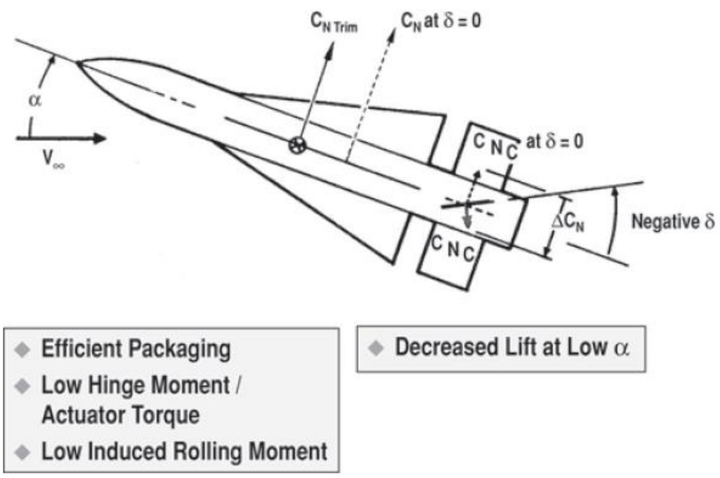

Figure 105: Advantages and disadvantages of Tail Control [60]

Figure 105 illustrates the advantages and disadvantages of tail control. Figure 106, also taken from Fleeman [60], illustrates the benefits of tail control over canard control at high angles of attack.

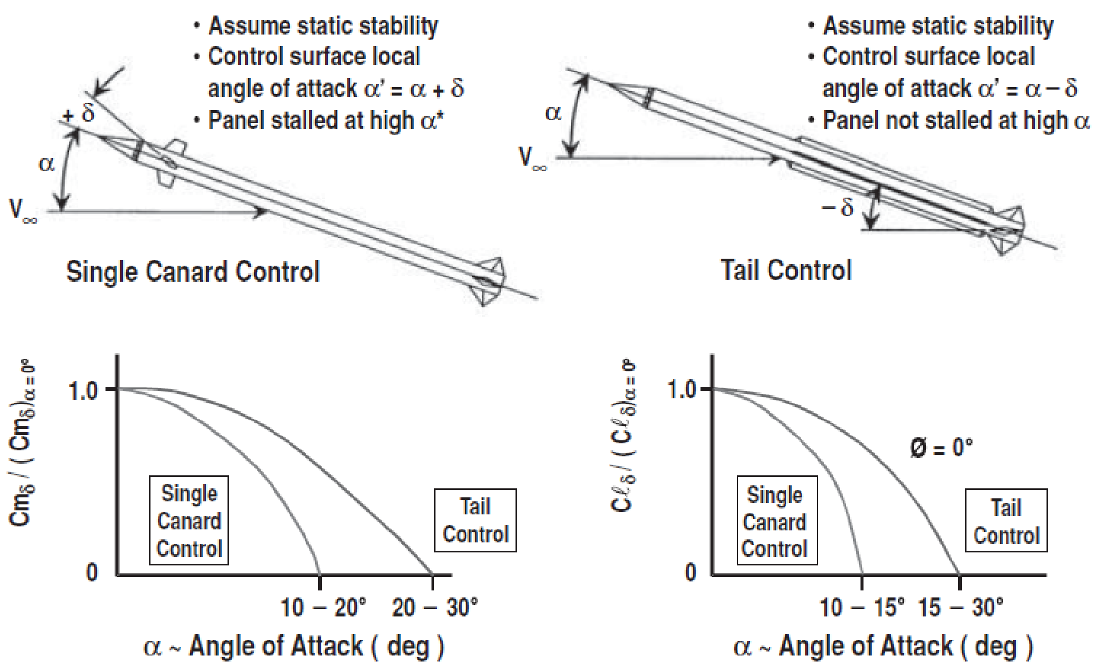

Figure 106: The benefits of Tail Control vs Canard control at high angles of attack [169]

Regarding Canard control, Figure 107 highlights the advantages and disadvantages of having control surfaces at the front of a missile.

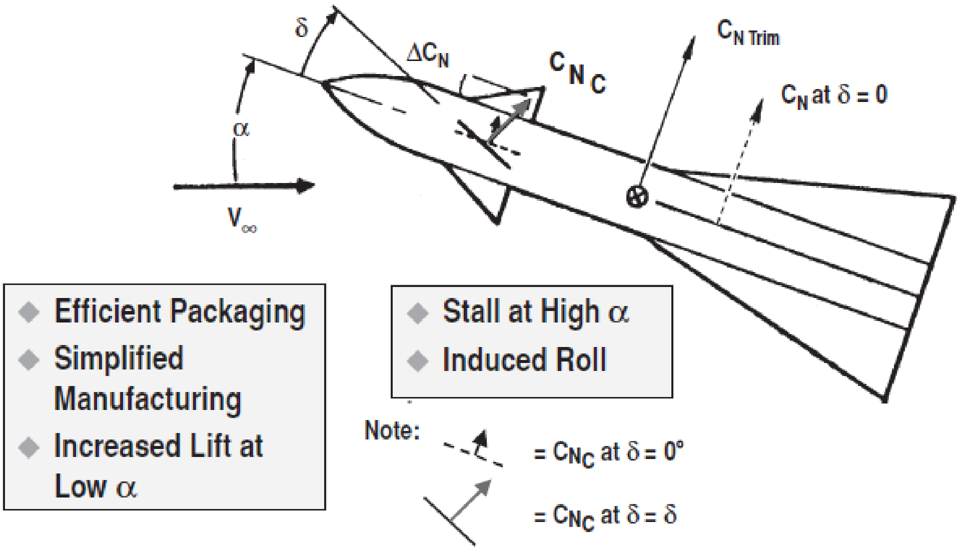

Figure 107: Advantages and Disadvantages of Canard Control [60]

APPENDIX C: Normal Force Coefficient calculation

The normal force coefficient (C_N) was calculated as part of the aerodynamics characterization phase of Fleeman's missile design process [60]. The C_N was used to determine the load required to sustain the 30 g manoeuvre, which was considered to be the maximum loading the actuator would have to withstand. The data represented in Figure 96 was sourced from Table 49 to Table 62.

The curve that crossed the x-axis at the point indicated by the vertical line (the required C_N Line) was considered to be the fin deflection and the angle of attack that would result in a stable 30 g manoeuvre.

In the tables to follow:

- δ refers to the deflection angle of the tail fin.

- α refers to the missiles angle of attack in flight; the values are given in degrees and radians, the latter used for inputs to the coefficient calculations.

- $\alpha+\delta$ refers to the combination of the angle of attack missile and tail deflection; this gives the total tail deflection relative to the missile flight path.

- $C_{N\ \mathrm{Body}}$ refers to the normal force coefficient of the missile body. The calculation was based on the equation from the following equation from Fleeman [60]. The lift to diameter ratio, *l/d,* for the missile was 20.58.

$$C_{N\,Body} = \sin(2\alpha)\cos(\alpha/2) + 2(l/d)\sin^2\alpha$$

- $C_{N\ \mathrm{Wing}}$ refers to the normal force coefficient of the missile wing. The calculation was based on the equation from the following equation from Fleeman [60]. The wing area, *Sw*, used for this 0.025m^2

$$C_{N\,Wing} = \left[4\frac{\sin\alpha\cos\alpha}{\sqrt{M^2-1}} + 2\sin^2\alpha\right]\frac{S_W}{S_{REF}}$$

- $C_{N\ \mathrm{Tail}}$ refers to the normal force coefficient of the missile tail. The calculation was based on the equation from the following equation from Fleeman [60]

$$C_{N\,Tail} = \left[4\frac{\sin(\alpha+\delta)\cos(\alpha+\delta)}{\sqrt{M^2-1}} + 2\sin^2(\alpha+\delta)\right]\frac{S_T}{S_{REF}}$$

- C_N refers to the total normal force coefficient of the missile. The calculation was based on the equation from the following equation from Fleeman [60]

$$C_N = C_{N\,Body} + C_{N\,Wing} + C_{N\,Tail}$$

- N_{tail} refers to the total normal force generated by the missile tail section.

- $N_{tail\ per\ fin}$ refers to the normal force generated by the missile tail fin. This is based on the number of normal forces producing surfaces which two in this analysis due to the "+" flight configuration of the missile.
- *M* refers to the pitching moment as a result of the tail fins normal force.

- C_M refers to the normal force coefficient of the missile body. The calculation was based on the equation from the following equation adapted from L. J. Clancy [170]. The *q* refers to the dynamic pressure, and *d* is the missile's diameter in this analysis.

$$C_M = \frac{M}{qS_{REF}d}$$

Table 49: Normal Force and Pitching Moment Results for a Constant 0 Degree Fin deflection

δ	0.00	degrees	0.00	rad							
α		α+δ		CN Body	CN Wing	CN Tail	CN	CM	Ntail	Ntail per fin	M
Degrees	Radians	Degrees	Radians						(N)	(N)	(Nm)
-30.00	-0.52	-30.00	-0.52	-9.46	-4.55	-8.84	-22.84	88.92	-74428.50	-37214.25	133259.70
-25.00	-0.44	-25.00	-0.44	-6.61	-3.61	-7.03	-17.24	75.89	-59151.90	-29575.95	113736.01
-20.00	-0.35	-20.00	-0.35	-4.18	-2.72	-5.28	-12.18	61.54	-44465.49	-22232.75	92229.21
-15.00	-0.26	-15.00	-0.26	-2.26	-1.88	-3.66	-7.80	46.31	-30815.52	-15407.76	69395.42
-10.00	-0.17	-10.00	-0.17	-0.90	-1.14	-2.21	-4.25	30.65	-18616.74	-9308.37	45933.25
-5.00	-0.09	-5.00	-0.09	-0.14	-0.50	-0.98	-1.62	15.06	-8239.80	-4119.90	22562.14
0.00	0.00	0.00	0.00	0.00	0.00	0.00	0.00	0.00	0.00	0.00	0.00
5.00	0.09	5.00	0.09	0.49	0.50	0.98	1.97	-13.06	8239.80	4119.90	-19576.64
10.00	0.17	10.00	0.17	1.58	1.14	2.21	4.93	-26.74	18616.74	9308.37	-40069.76
15.00	0.26	15.00	0.26	3.25	1.88	3.66	8.80	-40.61	30815.52	15407.76	-60864.44
20.00	0.35	20.00	0.35	5.45	2.72	5.28	13.45	-54.27	44465.49	22232.75	-81335.41
25.00	0.44	25.00	0.44	8.10	3.61	7.03	18.74	-67.30	59151.90	29575.95	-100865.50
30.00	0.52	30.00	0.52	11.13	4.55	8.84	24.52	-79.31	74428.50	37214.25	-118863.94

Table 50: Normal Force and Pitching Moment Results for a Constant 5 Degree Fin deflection

δ	5.00	degrees	0.09	rad							
α		α+δ		CN Body	CN Wing	CN Tail	CN	CM	Ntail	Ntail per fin	M
Degrees	Radians	Degrees	Radians						(N)	(N)	(Nm)
-30.00	-0.52	-25.00	-0.44	-9.46	-4.55	-7.03	-21.03	65.62	-59151.90	-29575.95	98337.38
-25.00	-0.44	-20.00	-0.35	-6.61	-3.61	-5.28	-15.50	53.49	-44465.49	-22232.75	80162.89
-20.00	-0.35	-15.00	-0.26	-4.18	-2.72	-3.66	-10.56	40.72	-30815.52	-15407.76	61025.39
-15.00	-0.26	-10.00	-0.17	-2.26	-1.88	-2.21	-6.36	27.70	-18616.74	-9308.37	41509.00
-10.00	-0.17	-5.00	-0.09	-0.90	-1.14	-0.98	-3.02	14.82	-8239.80	-4119.90	22211.56
-5.00	-0.09	0.00	0.00	-0.14	-0.50	0.00	-0.64	2.49	0.00	0.00	3725.95
0.00	0.00	5.00	0.09	0.00	0.00	0.98	0.98	-12.57	8239.80	4119.90	-18836.19
5.00	0.09	10.00	0.17	0.49	0.50	2.21	3.20	-28.89	18616.74	9308.37	-43298.33
10.00	0.17	15.00	0.26	1.58	1.14	3.66	6.38	-45.35	30815.52	15407.76	-67956.17
15.00	0.26	20.00	0.35	3.25	1.88	5.28	10.42	-61.43	44465.49	22232.75	-92068.26
20.00	0.35	25.00	0.44	5.45	2.72	7.03	15.19	-76.67	59151.90	29575.95	-114908.53
25.00	0.44	30.00	0.52	8.10	3.61	8.84	20.55	-90.61	74428.50	37214.25	-135787.82
30.00	0.52	35.00	0.61	11.13	4.55	10.67	26.34	-102.81	89831.13	44915.57	-154074.35

Table 51: Normal Force and Pitching Moment Results for a Constant 10 Degree Fin deflection

δ	10.00	degrees	0.17	rad							
α		α+δ		CN Body	CN Wing	CN Tail	CN	CM	Ntail	Ntail per fin	M
Degrees	Radians	Degrees	Radians						(N)	(N)	(Nm)
-30.00	-0.52	-20.00	-0.35	-9.46	-4.55	-5.28	-19.28	43.22	-44465.49	-22232.75	64764.26
-25.00	-0.44	-15.00	-0.26	-6.61	-3.61	-3.66	-13.88	32.67	-30815.52	-15407.76	48959.07
-20.00	-0.35	-10.00	-0.17	-4.18	-2.72	-2.21	-9.11	22.11	-18616.74	-9308.37	33138.97
-15.00	-0.26	-5.00	-0.09	-2.26	-1.88	-0.98	-5.12	11.87	-8239.80	-4119.90	17787.32
-10.00	-0.17	0.00	0.00	-0.90	-1.14	0.00	-2.04	2.25	0.00	0.00	3375.37
-5.00	-0.09	5.00	0.09	-0.14	-0.50	0.98	0.34	-10.08	8239.80	4119.90	-15110.24
0.00	0.00	10.00	0.17	0.00	0.00	2.21	2.21	-28.40	18616.74	9308.37	-42557.88
5.00	0.09	15.00	0.26	0.49	0.50	3.66	4.65	-47.50	30815.52	15407.76	-71184.74
10.00	0.17	20.00	0.35	1.58	1.14	5.28	8.00	-66.17	44465.49	22232.75	-99159.99
15.00	0.26	25.00	0.44	3.25	1.88	7.03	12.16	-83.84	59151.90	29575.95	-125641.38
20.00	0.35	30.00	0.52	5.45	2.72	8.84	17.01	-99.98	74428.50	37214.25	-149830.85
25.00	0.44	35.00	0.61	8.10	3.61	10.67	22.38	-114.10	89831.13	44915.57	-170998.23
30.00	0.52	40.00	0.70	11.13	4.55	12.46	28.13	-125.78	104891.79	52445.89	-188503.02

Table 52: Normal Force and Pitching Moment Results for a Constant 15 Degree Fin deflection

δ	15.00	degrees	0.26	rad							
α		α+δ		CN Body	CN Wing	CN Tail	CN	CM	Ntail	Ntail per fin	M
Degrees	Radians	Degrees	Radians						(N)	(N)	(Nm)
-30.00	-0.52	-15.00	-0.26	-9.46	-4.55	-3.66	-17.66	22.39	-30815.52	-15407.76	33560.44
-25.00	-0.44	-10.00	-0.17	-6.61	-3.61	-2.21	-12.43	14.06	-18616.74	-9308.37	21072.65
-20.00	-0.35	-5.00	-0.09	-4.18	-2.72	-0.98	-7.88	6.28	-8239.80	-4119.90	9417.29
-15.00	-0.26	0.00	0.00	-2.26	-1.88	0.00	-4.14	-0.70	0.00	0.00	-1048.87
-10.00	-0.17	5.00	0.09	-0.90	-1.14	0.98	-1.06	-10.32	8239.80	4119.90	-15460.82
-5.00	-0.09	10.00	0.17	-0.14	-0.50	2.21	1.57	-25.91	18616.74	9308.37	-38831.93
0.00	0.00	15.00	0.26	0.00	0.00	3.66	3.66	-47.01	30815.52	15407.76	-70444.29
5.00	0.09	20.00	0.35	0.49	0.50	5.28	6.27	-68.32	44465.49	22232.75	-102388.57
10.00	0.17	25.00	0.44	1.58	1.14	7.03	9.75	-88.57	59151.90	29575.95	-132733.11
15.00	0.26	30.00	0.52	3.25	1.88	8.84	13.98	-107.14	74428.50	37214.25	-160563.70
20.00	0.35	35.00	0.61	5.45	2.72	10.67	18.83	-123.47	89831.13	44915.57	-185041.27
25.00	0.44	40.00	0.70	8.10	3.61	12.46	24.17	-137.07	104891.79	52445.89	-205426.90
30.00	0.52	45.00	0.79	11.13	4.55	14.15	29.83	-147.54	119152.86	59576.43	-221103.83

Table 53: Normal Force and Pitching Moment Results for a Constant 20 Degree Fin deflection

δ	20.00	degrees	0.35	rad							
α		α+δ		CN Body	CN Wing	CN Tail	CN	CM	Ntail	Ntail per fin	M
Degrees	Radians	Degrees	Radians						(N)	(N)	(Nm)
-30.00	-0.52	-10.00	-0.17	-9.46	-4.55	-2.21	-16.21	3.79	-18616.74	-9308.37	5674.03
-25.00	-0.44	-5.00	-0.09	-6.61	-3.61	-0.98	-11.20	-1.77	-8239.80	-4119.90	-2649.03
-20.00	-0.35	0.00	0.00	-4.18	-2.72	0.00	-6.90	-6.28	0.00	0.00	-9418.90
-15.00	-0.26	5.00	0.09	-2.26	-1.88	0.98	-3.17	-13.27	8239.80	4119.90	-19885.06
-10.00	-0.17	10.00	0.17	-0.90	-1.14	2.21	0.17	-26.15	18616.74	9308.37	-39182.51
-5.00	-0.09	15.00	0.26	-0.14	-0.50	3.66	3.02	-44.52	30815.52	15407.76	-66718.34
0.00	0.00	20.00	0.35	0.00	0.00	5.28	5.28	-67.83	44465.49	22232.75	-101648.11
5.00	0.09	25.00	0.44	0.49	0.50	7.03	8.02	-90.72	59151.90	29575.95	-135961.69
10.00	0.17	30.00	0.52	1.58	1.14	8.84	11.56	-111.87	74428.50	37214.25	-167655.43
15.00	0.26	35.00	0.61	3.25	1.88	10.67	15.81	-130.63	89831.13	44915.57	-195774.11
20.00	0.35	40.00	0.70	5.45	2.72	12.46	20.62	-146.45	104891.79	52445.89	-219469.93
25.00	0.44	45.00	0.79	8.10	3.61	14.15	25.87	-158.83	119152.86	59576.43	-238027.71
30.00	0.52	50.00	0.87	11.13	4.55	15.70	31.37	-167.41	132181.04	66090.52	-250886.24

Table 54: Normal Force and Pitching Moment Results for a Constant 25 Degree Fin deflection

δ	25.00	degrees	0.44	rad							
α		α+δ		CN Body	CN Wing	CN Tail	CN	CM	Ntail	Ntail per fin	M
Degrees	Radians	Degrees	Radians						(N)	(N)	(Nm)
-30.00	-0.52	-5.00	-0.09	-9.46	-4.55	-0.98	-14.98	-12.04	-8239.80	-4119.90	-18047.66
-25.00	-0.44	0.00	0.00	-6.61	-3.61	0.00	-10.22	-14.34	0.00	0.00	-21485.22
-20.00	-0.35	5.00	0.09	-4.18	-2.72	0.98	-5.92	-18.85	8239.80	4119.90	-28255.09
-15.00	-0.26	10.00	0.17	-2.26	-1.88	2.21	-1.93	-29.10	18616.74	9308.37	-43606.75
-10.00	-0.17	15.00	0.26	-0.90	-1.14	3.66	1.62	-44.75	30815.52	15407.76	-67068.92
-5.00	-0.09	20.00	0.35	-0.14	-0.50	5.28	4.64	-65.34	44465.49	22232.75	-97922.16
0.00	0.00	25.00	0.44	0.00	0.00	7.03	7.03	-90.23	59151.90	29575.95	-135221.23
5.00	0.09	30.00	0.52	0.49	0.50	8.84	9.83	-114.03	74428.50	37214.25	-170884.00
10.00	0.17	35.00	0.61	1.58	1.14	10.67	13.39	-135.37	89831.13	44915.57	-202865.84
15.00	0.26	40.00	0.70	3.25	1.88	12.46	17.59	-153.61	104891.79	52445.89	-230202.78
20.00	0.35	45.00	0.79	5.45	2.72	14.15	22.32	-168.20	119152.86	59576.43	-252070.74
25.00	0.44	50.00	0.87	8.10	3.61	15.70	27.41	-178.70	132181.04	66090.52	-267810.12
30.00	0.52	55.00	0.96	11.13	4.55	17.05	32.73	-184.80	143580.46	71790.23	-276945.31

Table 55: Normal Force and Pitching Moment Results for a Constant 30 Degree Fin deflection

δ	30.00	degrees	0.52	rad							
α		α+δ		CN Body	CN Wing	CN Tail	CN	CM	Ntail	Ntail per fin	M
Degrees	Radians	Degrees	Radians						(N)	(N)	(Nm)
-30.00	-0.52	0.00	0.00	-9.46	-4.55	0.00	-14.00	-24.61	0.00	0.00	-36883.85
-25.00	-0.44	5.00	0.09	-6.61	-3.61	0.98	-9.24	-26.91	8239.80	4119.90	-40321.41
-20.00	-0.35	10.00	0.17	-4.18	-2.72	2.21	-4.69	-34.68	18616.74	9308.37	-51976.78
-15.00	-0.26	15.00	0.26	-2.26	-1.88	3.66	-0.48	-47.71	30815.52	15407.76	-71493.16
-10.00	-0.17	20.00	0.35	-0.90	-1.14	5.28	3.24	-65.57	44465.49	22232.75	-98272.74
-5.00	-0.09	25.00	0.44	-0.14	-0.50	7.03	6.38	-87.74	59151.90	29575.95	-131495.28
0.00	0.00	30.00	0.52	0.00	0.00	8.84	8.84	-113.53	74428.50	37214.25	-170143.55
5.00	0.09	35.00	0.61	0.49	0.50	10.67	11.66	-137.52	89831.13	44915.57	-206094.42
10.00	0.17	40.00	0.70	1.58	1.14	12.46	15.18	-158.34	104891.79	52445.89	-237294.51
15.00	0.26	45.00	0.79	3.25	1.88	14.15	19.29	-175.36	119152.86	59576.43	-262803.59
20.00	0.35	50.00	0.87	5.45	2.72	15.70	23.86	-188.07	132181.04	66090.52	-281853.15
25.00	0.44	55.00	0.96	8.10	3.61	17.05	28.77	-196.09	143580.46	71790.23	-293869.19
30.00	0.52	60.00	1.05	11.13	4.55	18.17	33.85	-199.17	153004.76	76502.38	-298489.26

Table 56: Normal Force and Pitching Moment Results for a Constant -5 Degree Fin deflection

δ	-5.00	degrees	-0.09	rad								
α		α+δ		CN Body	CN Wing	CN Tail	CN	CM	Ntail	Ntail per fin	M
Degrees	Radians	Degrees	Radians						(N)	(N)	(Nm)
-30.00	-0.52	-35.00	-0.61	-9.46	-4.55	-10.67	-24.67	112.41	-89831.13	-44915.57	168470.11
-25.00	-0.44	-30.00	-0.52	-6.61	-3.61	-8.84	-19.06	99.20	-74428.50	-37214.25	148658.33
-20.00	-0.35	-25.00	-0.44	-4.18	-2.72	-7.03	-13.92	83.94	-59151.90	-29575.95	125802.33
-15.00	-0.26	-20.00	-0.35	-2.26	-1.88	-5.28	-9.43	67.13	-44465.49	-22232.75	100599.24
-10.00	-0.17	-15.00	-0.26	-0.90	-1.14	-3.66	-5.70	49.26	-30815.52	-15407.76	73819.66
-5.00	-0.09	-10.00	-0.17	-0.14	-0.50	-2.21	-2.85	30.88	-18616.74	-9308.37	46283.83
0.00	0.00	-5.00	-0.09	0.00	0.00	-0.98	-0.98	12.57	-8239.80	-4119.90	18836.19
5.00	0.09	0.00	0.00	0.49	0.50	0.00	0.99	-0.49	0.00	0.00	-740.45
10.00	0.17	5.00	0.09	1.58	1.14	0.98	3.70	-10.91	8239.80	4119.90	-16348.07
15.00	0.26	10.00	0.17	3.25	1.88	2.21	7.35	-22.01	18616.74	9308.37	-32978.03
20.00	0.35	15.00	0.26	5.45	2.72	3.66	11.83	-33.45	30815.52	15407.76	-50131.59
25.00	0.44	20.00	0.35	8.10	3.61	5.28	17.00	-44.90	44465.49	22232.75	-67292.38
30.00	0.52	25.00	0.44	11.13	4.55	7.03	22.70	-56.01	59151.90	29575.95	-83941.62

Table 57: Normal Force and Pitching Moment Results for a Constant -10 Degree Fin deflection

δ	-10.00	degrees	-0.17	rad							
α		α+δ		CN Body	CN Wing	CN Tail	CN	CM	Ntail	Ntail per fin	M
Degrees	Radians	Degrees	Radians						(N)	(N)	(Nm)
-30.00	-0.52	-40.00	-0.70	-9.46	-4.55	-12.46	-26.46	135.39	-104891.79	-52445.89	202898.78
-25.00	-0.44	-35.00	-0.61	-6.61	-3.61	-10.67	-20.89	122.69	-89831.13	-44915.57	183868.74
-20.00	-0.35	-30.00	-0.52	-4.18	-2.72	-8.84	-15.74	107.25	-74428.50	-37214.25	160724.65
-15.00	-0.26	-25.00	-0.44	-2.26	-1.88	-7.03	-11.17	89.53	-59151.90	-29575.95	134172.36
-10.00	-0.17	-20.00	-0.35	-0.90	-1.14	-5.28	-7.32	70.08	-44465.49	-22232.75	105023.48
-5.00	-0.09	-15.00	-0.26	-0.14	-0.50	-3.66	-4.30	49.49	-30815.52	-15407.76	74170.24
0.00	0.00	-10.00	-0.17	0.00	0.00	-2.21	-2.21	28.40	-18616.74	-9308.37	42557.88
5.00	0.09	-5.00	-0.09	0.49	0.50	-0.98	0.01	12.07	-8239.80	-4119.90	18095.74
10.00	0.17	0.00	0.00	1.58	1.14	0.00	2.72	1.66	0.00	0.00	2488.12
15.00	0.26	5.00	0.09	3.25	1.88	0.98	6.11	-6.18	8239.80	4119.90	-9256.34
20.00	0.35	10.00	0.17	5.45	2.72	2.21	10.38	-14.84	18616.74	9308.37	-22245.18
25.00	0.44	15.00	0.26	8.10	3.61	3.66	15.37	-24.08	30815.52	15407.76	-36088.56
30.00	0.52	20.00	0.35	11.13	4.55	5.28	20.96	-33.61	44465.49	22232.75	-50368.50

Table 58: Normal Force and Pitching Moment Results for a Constant -12.70 Degree Fin deflection

δ	-12.70	degrees	-0.22	rad							
α		α+δ		CN Body	CN Wing	CN Tail	CN	CM	Ntail	Ntail per fin	M
Degrees	Radians	Degrees	Radians						(N)	(N)	(Nm)
-30.00	-0.52	-42.70	-0.75	-9.46	-4.55	-13.39	-27.39	147.33	-112720.43	-56360.21	220795.05
-25.00	-0.44	-37.70	-0.66	-6.61	-3.61	-11.64	-21.86	135.21	-98035.94	-49017.97	202624.94
-20.00	-0.35	-32.70	-0.57	-4.18	-2.72	-9.83	-16.73	119.96	-82760.19	-41380.09	179770.88
-15.00	-0.26	-27.70	-0.48	-2.26	-1.88	-8.00	-12.14	102.05	-67357.30	-33678.65	152929.92
-10.00	-0.17	-22.70	-0.40	-0.90	-1.14	-6.21	-8.25	82.02	-52295.30	-26147.65	122922.42
-5.00	-0.09	-17.70	-0.31	-0.14	-0.50	-4.52	-5.16	60.50	-38031.83	-19015.91	90666.71
0.00	0.00	-12.70	-0.22	0.00	0.00	-2.97	-2.97	38.13	-25000.28	-12500.14	57150.65
5.00	0.09	-7.70	-0.13	0.49	0.50	-1.61	-0.63	20.25	-13596.61	-6798.31	30341.41
10.00	0.17	-2.70	-0.05	1.58	1.14	-0.49	2.22	8.02	-4167.32	-2083.66	12014.62
15.00	0.26	2.30	0.04	3.25	1.88	0.42	5.55	1.04	3507.30	1753.65	1562.16
20.00	0.35	7.30	0.13	5.45	2.72	1.52	9.68	-5.92	12765.41	6382.71	-8869.03
25.00	0.44	12.30	0.21	8.10	3.61	2.85	14.57	-13.72	24023.15	12011.57	-20561.18
30.00	0.52	17.30	0.30	11.13	4.55	4.39	20.06	-22.13	36938.45	18469.23	-33161.69

Table 59: Normal Force and Pitching Moment Results for a Constant -15 Degree Fin deflection

δ	-15.00	degrees	-0.26	rad							
α		α+δ		CN Body	CN Wing	CN Tail	CN	CM	Ntail	Ntail per fin	M
Degrees	Radians	Degrees	Radians						(N)	(N)	(Nm)
-30.00	-0.52	-45.00	-0.79	-9.46	-4.55	-14.15	-28.15	157.14	-119152.86	-59576.43	235499.59
-25.00	-0.44	-40.00	-0.70	-6.61	-3.61	-12.46	-22.68	145.66	-104891.79	-52445.89	218297.41
-20.00	-0.35	-35.00	-0.61	-4.18	-2.72	-10.67	-17.57	130.74	-89831.13	-44915.57	195935.06
-15.00	-0.26	-30.00	-0.52	-2.26	-1.88	-8.84	-12.98	112.83	-74428.50	-37214.25	169094.68
-10.00	-0.17	-25.00	-0.44	-0.90	-1.14	-7.03	-9.06	92.48	-59151.90	-29575.95	138596.60
-5.00	-0.09	-20.00	-0.35	-0.14	-0.50	-5.28	-5.92	70.31	-44465.49	-22232.75	105374.06
0.00	0.00	-15.00	-0.26	0.00	0.00	-3.66	-3.66	47.01	-30815.52	-15407.76	70444.29
5.00	0.09	-10.00	-0.17	0.49	0.50	-2.21	-1.22	27.90	-18616.74	-9308.37	41817.42
10.00	0.17	-5.00	-0.09	1.58	1.14	-0.98	1.74	14.23	-8239.80	-4119.90	21324.31
15.00	0.26	0.00	0.00	3.25	1.88	0.00	5.14	6.39	0.00	0.00	9579.85
20.00	0.35	5.00	0.09	5.45	2.72	0.98	9.14	0.99	8239.80	4119.90	1476.51
25.00	0.44	10.00	0.17	8.10	3.61	2.21	13.93	-5.47	18616.74	9308.37	-8202.14
30.00	0.52	15.00	0.26	11.13	4.55	3.66	19.34	-12.79	30815.52	15407.76	-19164.68

Table 60: Normal Force and Pitching Moment Results for a Constant -20 Degree Fin deflection

δ	-20.00	degrees	-0.35	rad							
α		α+δ		CN Body	CN Wing	CN Tail	CN	CM	Ntail	Ntail per fin	M
Degrees	Radians	Degrees	Radians						(N)	(N)	(Nm)
-30.00	-0.52	-50.00	-0.87	-9.46	-4.55	-15.70	-29.70	177.01	-132181.04	-66090.52	265282.00
-25.00	-0.44	-45.00	-0.79	-6.61	-3.61	-14.15	-24.37	167.42	-119152.86	-59576.43	250898.22
-20.00	-0.35	-40.00	-0.70	-4.18	-2.72	-12.46	-19.36	153.71	-104891.79	-52445.89	230363.73
-15.00	-0.26	-35.00	-0.61	-2.26	-1.88	-10.67	-14.81	136.33	-89831.13	-44915.57	204305.09
-10.00	-0.17	-30.00	-0.52	-0.90	-1.14	-8.84	-10.88	115.78	-74428.50	-37214.25	173518.92
-5.00	-0.09	-25.00	-0.44	-0.14	-0.50	-7.03	-7.67	92.72	-59151.90	-29575.95	138947.19
0.00	0.00	-20.00	-0.35	0.00	0.00	-5.28	-5.28	67.83	-44465.49	-22232.75	101648.11
5.00	0.09	-15.00	-0.26	0.49	0.50	-3.66	-2.67	46.51	-30815.52	-15407.76	69703.84
10.00	0.17	-10.00	-0.17	1.58	1.14	-2.21	0.51	30.06	-18616.74	-9308.37	45046.00
15.00	0.26	-5.00	-0.09	3.25	1.88	-0.98	4.16	18.96	-8239.80	-4119.90	28416.04
20.00	0.35	0.00	0.00	5.45	2.72	0.00	8.17	13.55	0.00	0.00	20312.70
25.00	0.44	5.00	0.09	8.10	3.61	0.98	12.69	10.36	8239.80	4119.90	15519.54
30.00	0.52	10.00	0.17	11.13	4.55	2.21	17.89	5.82	18616.74	9308.37	8721.74

Table 61: Normal Force and Pitching Moment Results for a Constant -25 Degree Fin deflection

δ	-25.00	degrees	-0.44	rad							
α		α+δ		CN Body	CN Wing	CN Tail	CN	CM	Ntail	Ntail per fin	M
Degrees	Radians	Degrees	Radians						(N)	(N)	(Nm)
-30.00	-0.52	-55.00	-0.96	-9.46	-4.55	-17.05	-31.06	194.40	-143580.46	-71790.23	291341.07
-25.00	-0.44	-50.00	-0.87	-6.61	-3.61	-15.70	-25.92	187.29	-132181.04	-66090.52	280680.63
-20.00	-0.35	-45.00	-0.79	-4.18	-2.72	-14.15	-21.05	175.47	-119152.86	-59576.43	262964.54
-15.00	-0.26	-40.00	-0.70	-2.26	-1.88	-12.46	-16.60	159.30	-104891.79	-52445.89	238733.76
-10.00	-0.17	-35.00	-0.61	-0.90	-1.14	-10.67	-12.71	139.28	-89831.13	-44915.57	208729.33
-5.00	-0.09	-30.00	-0.52	-0.14	-0.50	-8.84	-9.48	116.02	-74428.50	-37214.25	173869.50
0.00	0.00	-25.00	-0.44	0.00	0.00	-7.03	-7.03	90.23	-59151.90	-29575.95	135221.23
5.00	0.09	-20.00	-0.35	0.49	0.50	-5.28	-4.29	67.33	-44465.49	-22232.75	100907.66
10.00	0.17	-15.00	-0.26	1.58	1.14	-3.66	-0.94	48.67	-30815.52	-15407.76	72932.41
15.00	0.26	-10.00	-0.17	3.25	1.88	-2.21	2.92	34.79	-18616.74	-9308.37	52137.73
20.00	0.35	-5.00	-0.09	5.45	2.72	-0.98	7.19	26.12	-8239.80	-4119.90	39148.89
25.00	0.44	0.00	0.00	8.10	3.61	0.00	11.71	22.92	0.00	0.00	34355.73
30.00	0.52	5.00	0.09	11.13	4.55	0.98	16.65	21.65	8239.80	4119.90	32443.42

Table 62: Normal Force and Pitching Moment Results for a Constant -30 Degree Fin deflection

δ	-30.00	degrees	-0.52	rad							
α		α+δ		CN Body	CN Wing	CN Tail	CN	CM	Ntail	Ntail per fin	M
Degrees	Radians	Degrees	Radians						(N)	(N)	(Nm)
-30.00	-0.52	-60.00	-1.05	-9.46	-4.55	-18.17	-32.18	208.78	-153004.76	-76502.38	312885.02
-25.00	-0.44	-55.00	-0.96	-6.61	-3.61	-17.05	-27.27	204.68	-143580.46	-71790.23	306739.70
-20.00	-0.35	-50.00	-0.87	-4.18	-2.72	-15.70	-22.60	195.34	-132181.04	-66090.52	292746.95
-15.00	-0.26	-45.00	-0.79	-2.26	-1.88	-14.15	-18.30	181.05	-119152.86	-59576.43	271334.57
-10.00	-0.17	-40.00	-0.70	-0.90	-1.14	-12.46	-14.50	162.25	-104891.79	-52445.89	243158.00
-5.00	-0.09	-35.00	-0.61	-0.14	-0.50	-10.67	-11.31	139.51	-89831.13	-44915.57	209079.92
0.00	0.00	-30.00	-0.52	0.00	0.00	-8.84	-8.84	113.53	-74428.50	-37214.25	170143.55
5.00	0.09	-25.00	-0.44	0.49	0.50	-7.03	-6.04	89.73	-59151.90	-29575.95	134480.78
10.00	0.17	-20.00	-0.35	1.58	1.14	-5.28	-2.56	69.49	-44465.49	-22232.75	104136.23
15.00	0.26	-15.00	-0.26	3.25	1.88	-3.66	1.48	53.40	-30815.52	-15407.76	80024.14
20.00	0.35	-10.00	-0.17	5.45	2.72	-2.21	5.95	41.95	-18616.74	-9308.37	62870.58
25.00	0.44	-5.00	-0.09	8.10	3.61	-0.98	10.74	35.49	-8239.80	-4119.90	53191.92
30.00	0.52	0.00	0.00	11.13	4.55	0.00	15.68	34.22	0.00	0.00	51279.61

APPENDIX D: Actuator System Design

The Systems Engineering approach was also used for the design of the missile's Actuator System (ASYS).

The main stages of the process followed (adapted from IEEE 1220 [12][123]) are:

1. Requirements Analysis
2. Requirements Validation
3. Functional Analysis
4. Functional Verification
5. Synthesis
6. Design Verification
7. System analysis
8. Control

D.1 Requirements Analysis

Requirement Analysis involves the evaluation of the needs of the stakeholders and the operational context. It is necessary to carry out a Requirements Analysis in order to gather the correct inputs to establish a more defined baseline of design inputs. During this process, the system requirements are specified. [123]

The requirements for the actuator system are derived from the missile system. This is influenced by the stakeholders (this includes the Client, the end-user and the original equipment manufacturer (OEM)) as well as the operational context.

D.1.1 Stakeholder needs, expectations and constraints.

Table 22 highlights the needs, expectations and constraints for all relevant stakeholders. For this study, only the stakeholder inputs seen in Table 22 were identified. These inputs will be used for the design going forward.

Table 63: Stakeholder Needs, Expectations and Constraints

Stakeholder		Needs, expectations and constraints
End-User (Pilot)	(a)	The Actuator must alter the missile flight path to intercept the intended target
	(b)	The Actuator must maintain the missile flight path
	(c)	The Actuator must not interfere with the launch platform
OEM of Missile	(d)	The Actuator must alter the missile flight path to intercept the intended target
	(e)	The Actuator must maintain the missile flight path
	(f)	Fit within the designated missile volume
	(g)	Operate within a required timeframe
	(h)	Must not interfere with the launch platform
Client	(i)	The Actuator must alter the missile flight path to intercept the intended target
	(j)	The Actuator must maintain the missile flight path
	(k)	The Actuator must not interfere with the launch platform

In Table 22, it can be seen that there are some similar requirements when comparing the inputs from the different stakeholders.

Therefore, it was deemed necessary to consolidate this table into Table 64:

Table 64: Consolidated Actuator System Stakeholder input

	Actuator System Requirements
1.1.1	The Actuator must alter the missile flight path to intercept the intended target
1.1.2	The Actuator must maintain the missile flight path
1.1.3	The Actuator must not interfere with the launch platform
1.1.4	Fit within the designated missile volume
1.1.5	Operate within a required timeframe

D.1.2 Project constraints

Project constraints are necessary inputs to consider, as they can have a significant impact on the design of a product. Examples of these constraints could include financial, end-user certificates, technology, suppliers and client constraints [123]. For this study, only the constraints highlighted in this chapter were identified to showcase the process followed.

D.1.3 End Date

The conceptual design is to be completed in six months.

D.1.4 Technology

Alternative technology and actuation methods should be investigated instead of generic missile actuation methods.

D.1.5 Operational Context

The operational context refers to the environment in which the product to be designed would be required to function. It includes everything that has an influence on the operation of the product, whether it be constraints or system inputs.

D.1.6 Concept of Use envisioned for the Missile Actuator System

As described in Section 4.2, the Concept of Use (CONUSE) describes how the product will be used in a variety of situations, and the CONUSE for the missile system was described. The system of interest, the missile actuator system, would have a CONUSE as follows:

Assist the higher-level missile system in intercepting a target at a range of 120 km by executing flight altering commands by providing the required forces to keep the missile travelling along a required trajectory towards the target for as long as required by the missile system.

For a better understanding of how the actuator will be used post-integration, the mission and life profiles were defined (see Section D.1.8). The context diagram, shown in Section D.1.8, also gives some insight into the environment where and how the actuator will be used.

D.1.7 External Constraints

External constraints refer to environmental and physical constraints that influence the system to be designed.

The actuator will form part of the missile system and will, therefore, be subjected to the same external environment (refer to Table 65). Based on the location of the actuator unit within the missile structure (refer to Section A.6), there would be effects due to the interface to the missile system. Therefore, the following external constraints were identified:

Table 65: Actuator External Constraints

	Constraint	**Limits (Minimum and/or maximum)**
1.3.1	**Operating environment**	
1.3.1.1	Temperature	-40 to +85 Degrees Celsius
1.3.1.2	Aerodynamic Loads	1685 N (Maximum load expected)
1.3.1.3	Aerodynamic Heating	334.76 K (for t = 90s) 891 K (Maximum temperature)
1.3.1.4	Vibration	Refer to MIL-STD-810G
1.3.1.5	G-Loading	30 g
1.3.2	**Missile Airframe**	
1.3.2.1	Airframe interface	Lap Joint at the rear of Rocket Motor
1.3.2.2	Space available	0.0074 m^3 (0.178 m Diameter)
1.3.3	**Rocket Motor**	
1.3.2.1	Thermal Loading	373- 473 K
1.3.2.2	Space available	0.08 m (Blast tube diameter)

The operating environment for the actuator would be the same environment the missile system would experience. The temperature is the expected environmental temperature range during the missile operation; this excludes the aerodynamic heating. The aerodynamic loads experienced by the actuator would be as a result of the placement of the subsystem in the missile layout and the missile system aerodynamics.

The aerodynamic loads acting on the actuator have been estimated to be 1685 N based on the initial calculations based on the conceptual missile design by Fleeman [60].

The aerodynamic heating was based on the following aerodynamic heating prediction from Fleeman [60]:

$$Q = 345\,\rho^{0.8}\,M^{2.8}/x^{0.2} \qquad (70)$$

In Equation (**70**), Q represents the heat transfer rate, ρ is the density of air, M is the Mach number, and x refers to the distance from the leading edge (in this case, the nose tip is the leading edge). At 30000 ft., the air density is about 0.467 kg/m^3. At Mach 4 and 3.55 m from the leading edge (assumed actuator location based on the position of the leading edge), the heat transfer rate is about 7.06 kW/m^2.

The skin temperature experienced during flight is estimated as follows:

$$T_{skin} = (T_{skin})_{max} + [(T_{skin})_i - (T_{skin})_{max}]e^{-Qt/\{(c\rho z)_{skin}[(T_{skin})_{max} - (T_{skin})_i]\}} \quad (71)$$

$$(T_{skin})_{max} = T_0[1 + 0.2rM^2] \quad (72)$$

In Equation (**71**) and Equation (**72)**, Q refers to the heat transfer rate, t is the duration of the flight (at the specified Mach number), c is the specific heat for aluminium (the assumed skin material), ρ_{AL} is the density of the skin material, z is the thickness of said material, $(T_{skin})_{max}$ is the maximum temperature, T_o is the temperature at the specified altitude and the $(T_{skin})_i$ is the initial skin temperature.

The skin temperature estimate was determined to be 334.76 K for a flight time of 90 s, with a possible maximum skin temperature of 891 K. These are assumed to be the aerodynamic heating for the actuator.

The vibration refers to the vibration spectrum the missile will experience. This includes both carriage flight (experienced while still on the aircraft store) and free flight (in flight) vibration. Carriage flight vibration values are based on typical fighter aircraft flight vibration taken from [124]. The free-flight vibration is based on military test specifications and established test data. Vibration test specifications should be evaluated based on the standard.

The g-loading was specified during the conceptual missile design. This is the expected worst case the missile is expected to see when engaging its specified target.

The Missile Airframe constraints refer to the limitations imposed onto the actuator system based on its attachment to the missile system. The joint between the actuator and the missile is an important consideration when defining the airframe constraints. The space/volume allocated to the actuator is a limiting factor. It is based on inputs from the conceptual design in Chapter A.6.

Due to the decision to have the actuator at the rear of the missile, the rocket motor would influence the actuator's operation. The thermal loading during and after the rocket motor is fired is a limiting factor. The rocket motor temperature values in Table 23 are based on rocket motor blast tube temperatures discussed in G. P. Sutton *et al*. [117]. The space available is influenced by the rocket motor blast tube. The blast tube diameter is based on the rocket motor's throat area, 0.003 m^2, which is a throat diameter of 0.061 m. According to Fleeman [60], the blast tube diameter is larger than the throat diameter, and therefore a diameter of 0.08 m was assumed.

D.1.8 Scenarios or Mission Profiles

Defining scenarios or mission profiles allows one to outline how the system will operate or be operated by the end-user. The mission profile defined in this section is arranged in chronological order and highlights the various scenarios the actuator will face during its period of operation.

1. Once power is received from the launch platform, the system functional test is performed.
2. After the initial functional test, if the test was successful, then the actuator enters a standby mode. If not, it enters a failure mode, and a power reset from the launch platform is required.
3. Once the missile system is launched and is clear of the launch platform, the actuator will be fully functional.
4. The actuator will maintain the missile flight path towards the intended target by executing guidance and control commands.
5. The actuator will alter the missile flight path to intercept the intended target by executing guidance and control commands.
6. If the missile does not intercept the target or is required to end its mission, the actuator shall enter a flight termination mode such that the missile tumbles towards the ground.

D.1.9 Measures of Effectiveness

The Measures of Effectiveness (MOE) refers to limits by which the system satisfies its mission when used by the end-user in the correct operational environment [10]. The MOE is meant to be defined in terms of anticipated outputs of the system but must be independent of any final design chosen. According to the INCOSE Systems Engineering Handbook [8], the defined MOE should be able to identify the overall performance of the final solution chosen.

The defined MOEs will be used to check if the actuator system meets or exceeds the requirements needed for the subsystem to be an effective solution of the intended missile system.

1. Bandwidth/Rate of Response
2. Energy Usage
3. Rate of change in Missile pitching moment
4. Adherence to space requirements
5. Adherence to mass requirements

D.1.10 Define system boundaries and external interfaces.

The definition of system boundaries assists in characterising other interacting systems which are out of the system designer's control. The external interfaces can be defined, and a greater understanding can be obtained as to the input and output requirements of the system to be designed.

Figure 108 is an illustration of the ASYS and its related systems interaction. This illustration was created based on the inputs from the missile design (see APPENDIX A) and other information related to the life cycle of the actuator system (derived from the missile system).

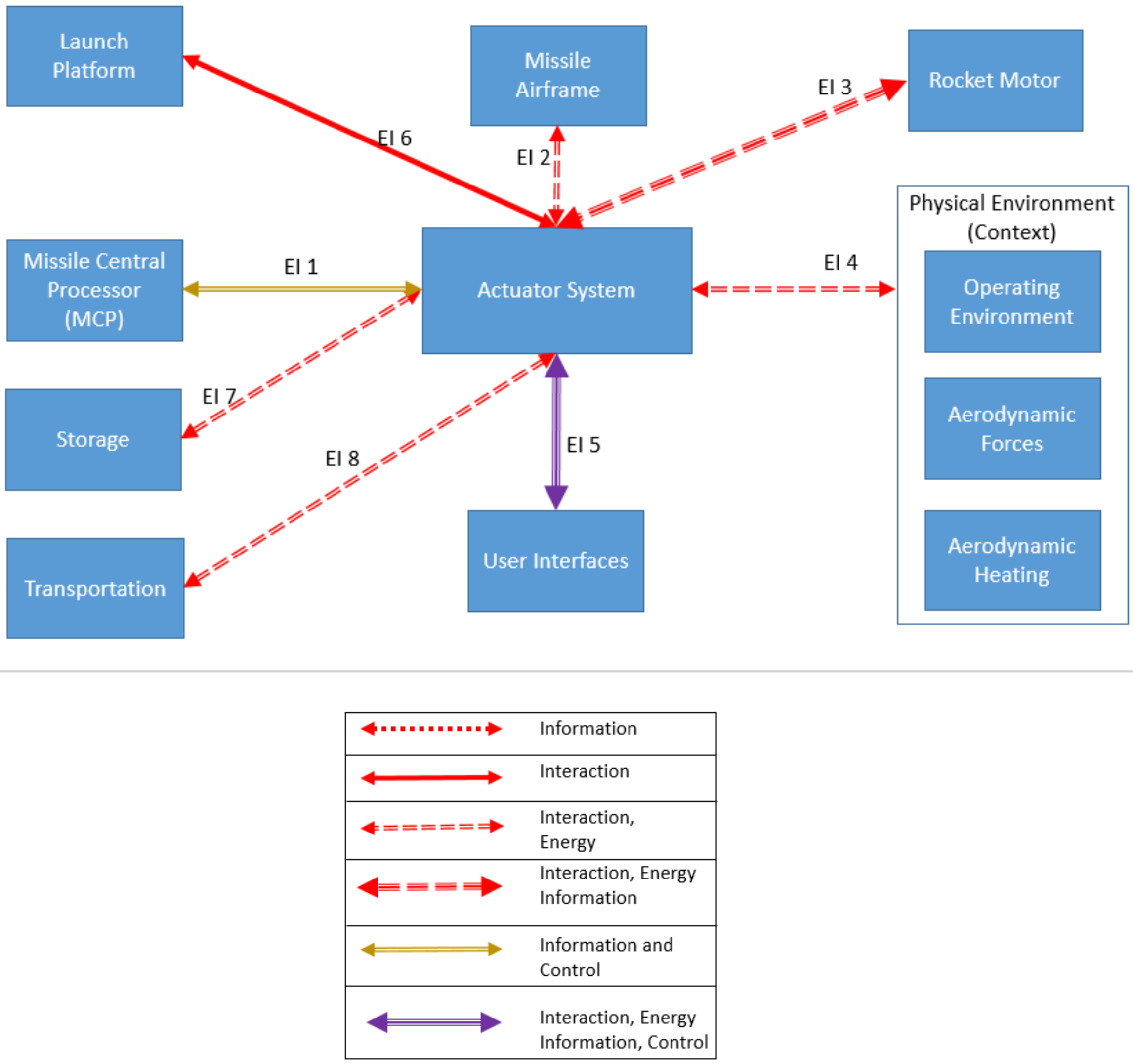

Figure 108: Context Diagram: Actuator System - External Interfaces

Figure 108 depicts the external interfaces (the arrows labelled EI 1-8). The details of these interfaces are as follows:

1. The interface to the Missile Central Processor (MCP) is a communications link. The link is required for the MCP to send the actuator system information and to receive feedback from the actuator. (Information and Control)
2. The interface to the missile airframe refers to the physical connection the actuator will have with the rest of the missile system. (Interaction and Energy)
3. The rocket motor interface relates to the influence the rocket motor would have on the actuator. This was considered based on the general placement of a tail ASYS. The rocket motor affects the immediate environment of the actuator system due to the thermal impact. The rocket motor also constrains the volume the actuator can occupy. (Interaction, Energy and Information)

4. The physical environment is a significant influence on the actuator system. The physical environment refers to the operating environment and the aerodynamic loads that the actuator would have to overcome to function effectively. (Interaction, Energy)
5. The user interface refers to the interface the actuator would have before, during and after integration to the missile system. This would involve the consideration of human factors and other design criteria to ensure it can be integrated on the higher system level. (Interaction, Information, Control, Energy)
6. The launch platform has a direct influence on the volume the system can occupy. The interface is, therefore, a constraint to the actuator system. (Interaction)
7. The storage of the ASYS, before and after integration, is an interface that would have an influence on the volume. There may also be environmental effects that may affect the actuator system. (vibration, temperature, humidity and other environmental factors) (Interaction, Energy)
8. The transportation of the actuator, like the storage interface, also has a similar influence on the actuator system. (Interaction, Energy)

In Figure 108, the different arrows used to depict the various flows between interfaces for the context diagram are defined. The flows such as information, control, energy and interaction were considered.

Information flow refers to the flow of data feedback or measurements at the relative interfaces. Control flow refers to the control data sent at a specific interface that alters the function of the system. Energy flow refers to thermal energy and vibration. Interaction flow refers to the physical influence surrounding systems have on the actuator system. This relates to the space constraints the actuator would experience.

D.1.11 Utilisation Environment

The actuator shall withstand the same environment as the next higher-level system, the BVR missile described in APPENDIX A.

D.1.12 Life Profile

The Life Profile refers to the item's post-development life cycle, which includes where it will be used, how it will be integrated, how it will be accepted, user training, system support, and end of life processes (decommissioning and disposal). [10]

In order to define the life profile, the various processes post-integration of the system were envisioned, based on the Systems Engineering Body of Knowledge [10], and the following life profile was determined:

1. Acceptance Testing (Performance related testing pre-integration to the next higher-level system)
2. Physical integration to the missile system
3. Be transported.
4. Remain in a dormant state.
5. Enter Maintenance State
    a. Be powered.
    b. Be tested (within missile system)
    c. Be powered down.
    d. Be repaired (if required)
6. Be utilised by the missile system.
7. Decommission and dispose (if beyond proposed shelf life)

Acceptance testing was considered as a part of the life profile as the ability to interface to the actuation would be necessary if the system is to be tested for acceptance before the next level integration, and therefore the interface would be a design consideration.

Physical integration to the missile system was included in the life profile as it was decided that there would be an influence on the design of the system.

The remainder of the life profile was determined based on the life of the actuator incorporated into the missile system—the typical shelf life for a missile is 10 to 20 years [118]. The shelf life of the missile system would give rise to a shelf-life constraint for the actuator. The shelf life of weaponry is a concern, and an accurate performance specification could assist in developing products with better shelf life [118]. This points to the necessity of Systems Engineering as a basis for the design and to develop a maintenance plan.

D.1.13 Functional Requirements

Deriving the Functional Requirements (as well as the Performance Requirements, as seen in Section 1.10 of this chapter) involves evaluating what the requirements of the system would have over its life profile [10].

The following list describes the functions identified (based on the life profile seen in Section D.1.12) that the actuator is required to perform:

1. Generate the required normal force (to generate the required missile pitching moment)
2. Physical termination of missile flight (Once In-Flight termination mode)
3. Receive information from missile MCP.
4. Send information to missile MCP.
5. Assist in altering the missile flight path.
6. Assist in maintaining missile flight path.
7. Monitor force generation.
8. Run Pre-programmed flight paths.
9. Run built-in maintenance tests.
10. Be transported.
11. Be stored.
12. Be Programmable
13. Be Disposable at the end of its shelf life.

It is important to note that during the process of deriving the Functional Requirements, the actuator was considered as a whole, and the Functional Requirements defined are that of the entire system. The functions relating to the defined requirements are described in this chapter. The links between the life profile of the actuator and the functions defined can be seen in Table 66. The grey cells in the matrix depict the link between life profile and functional requirement.

Table 66: Actuator Life Profile and Actuator Functional Requirements

	FR1	FR2	FR3	FR4	FR5	FR6	FR7	FR8	FR9	FR10	FR11	FR12	FR13
LP1	■	■	■	■	■	■	■	■	■				
LP2	■	■	■	■				■	■	■			
LP3										■			
LP4											■		
LP5			■	■			■	■	■			■	
LP6	■	■	■	■	■	■	■	■	■				
LP7													■

D.1.14 Performance Requirements

The Performance Requirements were based on the Functional Requirements developed in the previous section. The Performance Requirements are defined to characterise how well the function needs to be executed in order for the system to be valid based on the defined MOE [10].

The following list showcases the previously defined functions and their related Performance Requirements:

1. Generate the required normal force (to generate the required missile pitching, yaw or roll moment)
    a. Generate a force to allow the missile to achieve a manoeuvre limit of 30 g (1685 N (Minimum Required))
    b. Ensure Interfaces withstand generated forces (Reserve Factor > 1)
2. Physical termination of missile flight (Once In-Flight termination mode)
    a. Provide the means to terminate the flight (Not considered in this study)
3. Receive information from missile MCP.
    a. Information to be transferred at a rate of system-level defined communication frame rate
4. Send information to missile MCP.
    a. Information to be transferred at a rate of system-level defined communication frame rate
5. Assist in altering the missile flight path.
    a. Operate at a bandwidth of at least 50 Hz
    b. Generate sufficient force to alter missile flight path as required (1685 N (Minimum Required))
    c. Maintain the required applied force for the required duration of 200 ± 5s
6. Maintain missile flight path.
    a. Operate at a bandwidth of at least 50 Hz
    b. Generate sufficient force to alter missile flight path as required (1685 N (Minimum Required))
    c. Maintain the required applied force for the required duration of 200 ± 5s
7. Monitor Force generation
    a. Measure force generated output at 800 Hz ± 10 Hz
    b. Record force generated output at 800 Hz ± 10 Hz
    c. Feedback measurements within the system to allow for system adjustment at 800 Hz ± 10 Hz
8. Run Pre-programmed flight paths.
    a. Operate at a bandwidth of at least 50 Hz
    b. Generate sufficient force to alter missile flight path as required (1685 N (Minimum Required))
    c. Maintain the required applied force for the required duration of 200 ± 5s
    d. Information to be transferred to and from MCP at a rate of 800Hz ± 10 Hz
9. Run built-in maintenance tests.

a. Operate at a bandwidth of at least 50 Hz
b. Generate sufficient force to alter missile flight path as required (1685 N (Minimum Required))
c. Maintain the required applied force for the required duration of 200 ± 5s
d. Information to be transferred to and from MCP at a rate of 800Hz ± 10 Hz

10. Be transported.
    a. Endure all transportation within transportation packaging based on the Military Standard [124]
11. Be stored.
    a. Have a Shelf life of 10 years?
    b. Endure conditions within packaging based on the Military Standard [124]
12. Be Programmed
    a. Allow for multiple programming updates/modifications.
    b. Allow access from the outside for programming.
13. Be disposable at the end of its shelf life.
    a. Must adhere to environmental standards

D.1.15 State and Mode Analysis

D.1.15.1 Modes

A mode is a label given to a set of user-based capabilities that can be used to command and control the system to achieve the required outcomes of the system. [119]

The modes are defined as follows:

a) Power Off Mode refers to the mode when the system is not powered either from within the missile or an external source.
b) Power-On Mode is when the actuator system is powered from within the missile.
c) External Power Mode is when the actuator system is powered from outside the missile.
d) Standby Mode is the mode the actuator enters where it awaits instruction.
e) Operational Mode is when the actuator is able to execute the flight commands received from the MCP.
f) Flight Termination mode is when the actuator performs a flight termination action.
g) Test Mode is a mode used during the testing of the actuator. Within this mode, there are various built-in tests that assess the performance of the system.

h) Failure mode is entered into once the actuator does not receive any feedback from the missile MCP. Upon entering this mode, the actuator then performs a series of system checks (built-in tests) to identify and resolve the problem.

i) Repair mode allows the system to be adjusted to resolve issues affecting the functioning of the actuator.

Figure 109 highlights the modes. These modes are derived from the life profile of the actuator. Each blue block refers to a distinct mode, and the arrows indicate the conditions for each mode. The modes defined in Figure 109 are the internal modes of the actuator.

Table 67 illustrates the relationship between the defined modes and the previously defined Functional Requirements of the actuator system. The grey cells of the matrix depict the link between the functional requirement and the modes.

The complete correlation between the actuator modes and the missile system modes were not evaluated in this study.

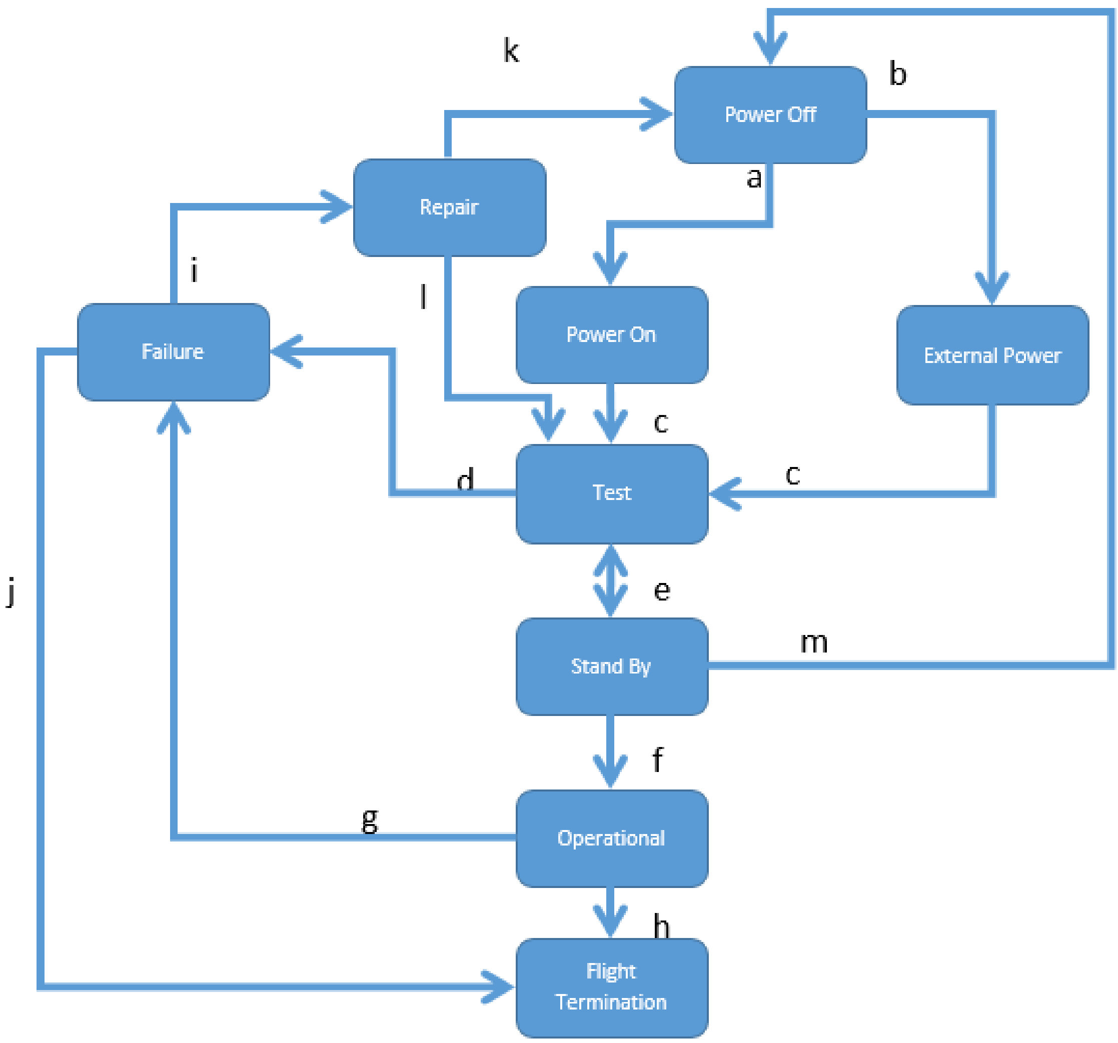

Figure 109: Modes of Operation

The various conditions are defined as follows:

a) Refers to the fulfilment of the request from the Missile MCP to enter the Power On mode.
b) An external user initiates the External Power mode (for test purposes only).
c) After the power initiation has taken place (Power On/External Power modes) and the system is fully powered, the actuator system enters a test mode. Built-in tests are carried out to assess the integrity of the system.
d) If a failure occurs, the system enters a failure mode.
e) If the tests are successful, the system enters a standby mode. If required, the actuator system will be instructed to return to the test mode during system testing or maintenance.
f) When required by the missile system, the actuator is requested to enter the operational mode (by the MCP).

g) Should a failure occur with the actuator system, or if there is a communication failure between the MCP and actuator, the system enters a failure mode.
h) If a request is received from the MCP, the actuator enters flight termination mode.
i) If the failure can be resolved internally or by an external user (during maintenance or acceptance testing), the system will enter a repair mode.
j) If the failure cannot be resolved during free flight, the MCP will request the actuator to enter a flight termination mode.
k) During maintenance testing or acceptance testing, the system will reset itself if required by the solution to repair the failure and enter a Power Off mode.
l) If the solution to resolve the issue does not require a system reset, the system will enter the test mode.
m) If required by the external user during acceptance testing/maintenance testing, the system can be manually switched to power off mode.

Table 67: Modes and associated Functional Requirements

	Power On	Standy By	Operational	Test	Maintenance	Failure	Flight Termination	Power Off	External Power
FR1			■	■					
FR2							■		
FR3	■	■	■	■	■	■	■		
FR4	■	■	■	■	■	■	■		
FR5			■	■			■		
FR6			■	■			■		
FR7	■	■	■	■	■	■	■		■
FR8				■					■
FR9					■				■
FR10								■	
FR11								■	

D.1.15.2 The Impact of Failure modes

Assessing the Failure modes of a system is necessary in order to ensure a system continues to operate as intended. The conditions/events related to a failure occurring is referred to as Failure Modes in J. Moubray [120]. As described in J. Moubray [120], it is crucial to define the functions and the Performance Requirements of the system to gain a better understanding of what the possible failure modes will be for the system.

Once failure occurs, the system enters a failed state, also called a functional failure. It is named as such since the system is unable to function as intended [120]. The failed state for the actuator is a sub-state of the Termination State. Within the failed state, there are two lower states, namely the Internal Power Failure State or the External Power Failure State. The latter refers to a failed state experienced during testing and maintenance. During this period, the actuator can be repaired if required.

The former refers to when the missile is using the actuator in captive and free flight. During these periods, the actuator is not accessible for repair. It, therefore, results in the flight termination mode for the actuator, which in free flight would cause the missile to tumble from the sky, or in captive flight, it would send a signal to the missile that it is non-functional, which in turn would relay the message to the launch platform.

The possible failure events or failure modes identified are as follows.

1. A delay greater than 2 ms between messages received from the MCP.
2. A repeated delay greater than 2 ms between messages received from the MCP.
3. A delay greater than the 2 ms between messages received from the MCP and the Force Generated
4. A reduced pitching rate of the missile due to a reduced force generation rate
5. A reduced roll rate of the missile due to a reduced force generation rate
6. A reduced yaw rate of the missile due to a reduced force generation rate
7. The actuator does not receive sufficient/any power for the system to operate.
8. After repair mode, the system powers down and does not Power-On.

The effects of these failures aid in understanding the impact on the surrounding systems. The effects of the failures are linked to the failure events, as detailed and discussed in J. Moubray [120], and are described as follows:

1. A delay greater than 2 ms between messages received from the MCP.
   - 1.1. A delay in messages is recorded in a log file based on an internal timer running out.
   - 1.2. It is a threat to the surrounding environment.
   - 1.3. The delay has an impact on the performance of the missile and could result in the missile missing its target.
   - 1.4. The missile, due to the actuator not functioning correctly, could intercept something unintended.
   - 1.5. If experienced in free flight, no repairs are possible. A system check, power cycle and a system reset may be necessary.

2. A repeated delay greater than 2 ms between messages received from the MCP.
    2.1. A delay in messages is recorded in a log file based on an internal timer running out.
    2.2. It is a threat to the surrounding environment.
    2.3. The delay has an impact on the performance of the missile and could result in the missile missing its target.
    2.4. The missile, due to the actuator not functioning correctly, could intercept something unintended.
    2.5. If experienced in free flight, no repairs are possible. A system check, power cycle and a system reset may be necessary.
3. A delay greater than the 2 ms between messages received from the MCP and the Force Generated
    3.1. A delay in messages is recorded in a log file based on an internal timer running out.
    3.2. It is a threat to the surrounding environment.
    3.3. The delay has an impact on the performance of the missile and could result in the missile missing its target.
    3.4. The missile, due to the actuator not functioning correctly, could intercept something unintended.
    3.5. If experienced in free flight, no repairs are possible. A system check, power cycle and a system reset may be necessary.
4. A reduced pitching rate of the missile due to a reduced force generation rate
    4.1. A reduced pitching rate can be visually seen by the missile not effectively heading towards the target.
    4.2. It is a threat to the performance of the missile.
    4.3. There is an impact on the performance of the missile and could result in the missile missing its target.
    4.4. The missile, due to the actuator not functioning correctly, could intercept something unintended.
    4.5. If experienced in free flight, no repairs are possible. A system check, power cycle and a system reset may be necessary.
5. A reduced roll rate of the missile due to a reduced force generation rate
    5.1. A reduced roll rate can be visually seen by the missile not effectively heading towards the target.
    5.2. It is a threat to the performance of the missile.
    5.3. There is an impact on the performance of the missile and could result in the missile missing its target.
    5.4. The missile, due to the actuator not functioning correctly, could intercept something unintended.

5.5. If experienced in free flight, no repairs are possible. A system check, power cycle and a system reset may be necessary.

6. A reduced yaw rate of the missile due to a reduced force generation rate
    6.1. A reduced yaw rate can be visually seen by the missile not effectively heading towards the target.
    6.2. It is a threat to the performance of the missile.
    6.3. There is an impact on the performance of the missile and could result in the missile missing its target.
    6.4. The missile, due to the actuator not functioning correctly, could intercept something unintended.
    6.5. If experienced in free flight, no repairs are possible. A system check, power cycle and a system reset may be necessary.
7. The actuator does not receive sufficient/any power for the system to operate.
    7.1. The system is non-responsive to the MCP or an external user. No information is received or logged by the actuator.
    7.2. It is a threat to the functioning of the missile system.
    7.3. There is an impact on the operation of the missile.
    7.4. The missile, due to the actuator not functioning, would not be used.
    7.5. If experienced in free flight, no repairs are possible. A system check, power cycle and a system reset may be necessary during testing or maintenance by an external user.
8. After repair mode, the system powers down and does not Power-On.
    8.1. The system is non-responsive to the MCP or an external user. No information is received or logged by the actuator.
    8.2. It is a threat to the functioning of the missile system.
    8.3. There is an impact on the operation of the missile.
    8.4. The missile, due to the actuator not functioning, would not be used or will be terminated during free flight.
    8.5. If experienced in free flight, no repairs are possible. A system check, power cycle and a system reset may be necessary during testing or maintenance by an external user.

The actuator is an important system with regard to flight path alteration of the missile system. Highlighting the criticality of the failures was needed to assess as they impact the surrounding systems and influence the missile operation. For this study, the failures were assumed to have equal importance. The delay times in the failure mode analysis were assumed values. These values should be determined based on the needs of the system once components have been selected.

D.1.15.3 States

A system is in a state when the behaviour it showcases remains constant or steady for a meaningful period [121]. In a particular state, a variety of modes can occur as long as they align with the values of that state.

The states identified for the actuator are the Dormant State, Operational State and Termination State. These are indicated in Table 68 and are linked to the modes which align to the state values.

Table 68: States and associated Modes

Mode	State		
	Operational	Termination	Dormant
Power On	■		
Stand By	■		
Operational	■		
Test	■		
Maintenance	■		
Failure	■	■	
Flight Termination		■	
Power Off			■
External Power			■

D.1.16 Technical Performance Measures

These are usually related to the measures of effectiveness. For this study, the Performance Requirements for the Functional Requirements will be used as the technical performance measures along with the measures of effectiveness mentioned in this chapter.

D.1.17 Physical characteristics

The actuator must fit within the space allocated in the missile. The missile's diameter is 178 mm, and the volume available is 0.0074 $m^{3.}$

D.1.18 Human factors

The actuator must have an external interface to a human user. The interface would allow for programming, maintenance and integration. These human factors have been identified in previous sections.

D.2 Requirements Validation

Validation of the outputs from the Requirements Analysis process is necessary to ensure the system will meet the required outcomes. The validation processes stated in A. Sparrius [13] involve:

- Examination of all requirements individually and as groups to see if they have been formulated correctly.
- Compared to the stakeholder requirements and possibly reviewed by the stakeholders
- Compared to the constraints of the project
- Compared to the external constraints
- Determine and fix any requirement issues.

The requirements have been evaluated and can be assumed to be validated for this study.

D.3 Functional Analysis

Based on the function requirement list of this appendix, the main Functional Requirements of the actuator were identified. This was done by evaluating the purpose of the system based on the higher-level system requirements.

From the missile level design, the actuator is to be designed to aid in the manoeuvring of the missile. Therefore, the primary Functional Requirements of the actuator are to execute commands to alter and maintain the missile flight path. The other Functional Requirements listed can be considered to be secondary Functional Requirements that aid in achieving the primary Functional Requirements.

In order to define the actuator functions, a Functional Flow Block Diagram (FFBD) was generated. According to the Systems Management College [111], functional flow block diagrams are useful in functionally defining the system requirements.

In this study, functions are high-level operations performed by the system, and Functional Requirements are required on a lower level to achieve the higher functions. The Functional Requirements and other supporting detail developed previously were to create a deeper understanding of the ASYS. This understanding provided the insights that aid in the defining of the system functions.

The functional flow diagram in Figure 110 illustrates the primary functions of the actuator in terms of its sub-functions. The format of the diagrams that follow was based on the functional flow block diagrams from Systems Management College [111]:

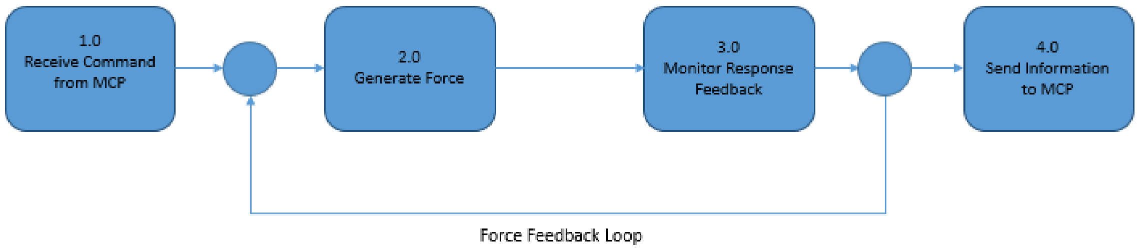

Figure 110: Actuator System-Level Functional Flow Block Diagram

The input from and the outputs to the missile system are not illustrated in Figure 110. It can be seen that the information enters the system at 1.0 Receive Command from the MCP function. It then enters the 2.0 Generate Force function, which then enters the 3.0 Monitor Response Feedback function. After this, the system then enters the 4.0 Send Information to MCP function.

An FFBD is meant to define functions and not define solutions for the system to be designed. The process of defining lower-level functional decomposition was carried out to determine the lower-level functions. This is required to develop the Functional Architecture required to carry out the design according to Systems Management College. [111]

In Figure 110, the first function, 1.0 Receive Command from MCP, can be broken down, as seen in Figure 111. The solid blue blocks depicted in the functional decomposition can be considered to be the reference functions. The blue outlined white blocks reference the sub-functions, products of the functional decomposition.

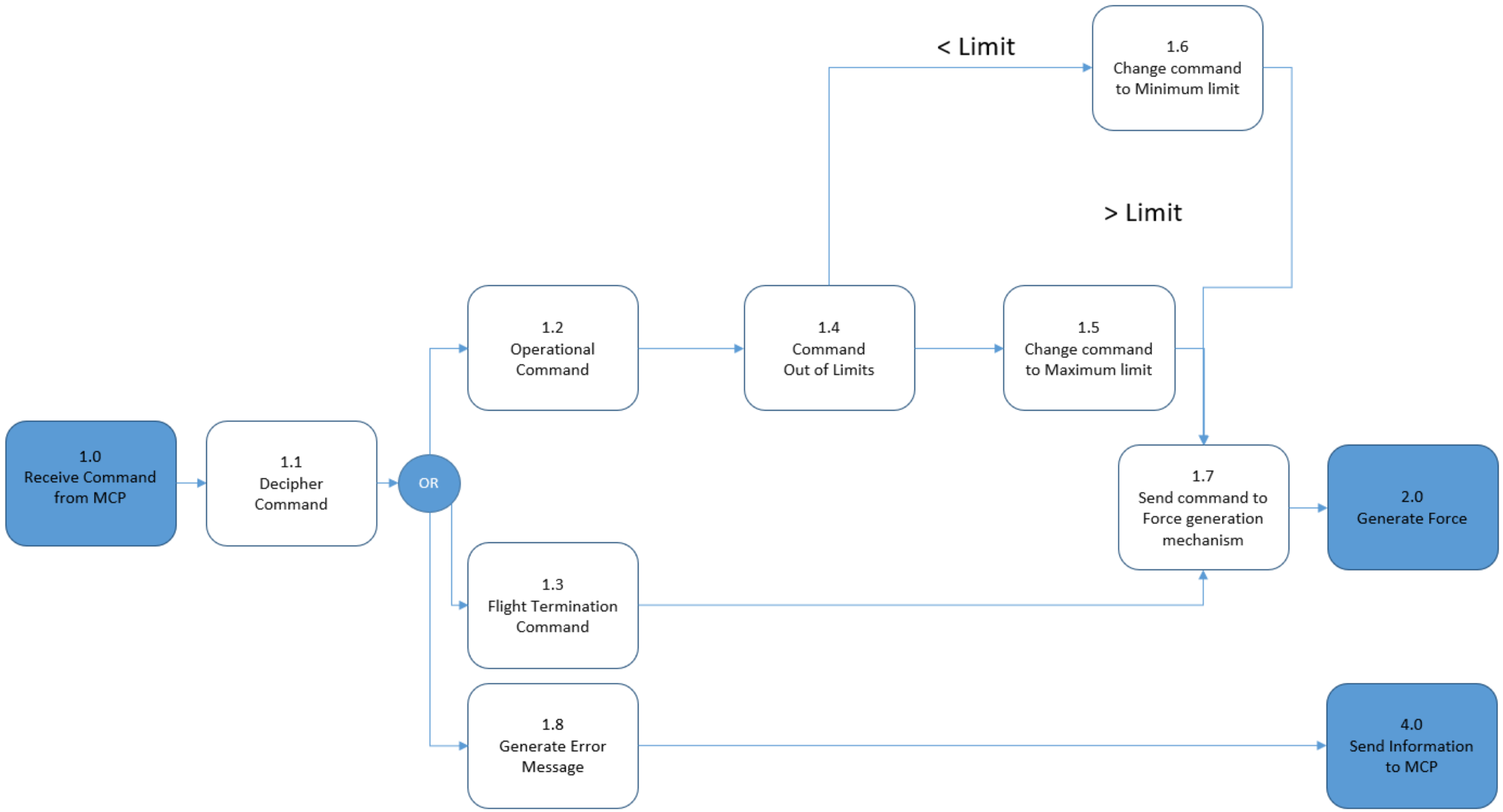

Figure 111: Functional Decomposition of Receive Command from MCP Function

In Figure 111, 1.0 Receive Command from the MCP function would require a receiving unit to receive the information from the MCP. The receiving unit would then begin the process to inform the system to generate a force. After the command from the MCP is received, the actuator system must 1.1 Decipher the command to determine if it is an Operational command, a Flight Termination command or neither of the two.

An Operational Command will activate the 1.2 Operational Command function. This will check if the command is within limits. If the command is out of limits, the system will enter the 1.4 Command out of Limits function. This function will deal with the out of limit command. If the command is higher than the upper limit, the system will enter a 1.5 Change command to Maximum limit function where the command is changed to the maximum upper limit. If it is lower than the lower limit, the command will be changed to the lower limit by 1.6 Change command to Minimum limit function. The altered commands will then enter the 1.7 Send to the Generate Force function.

A 1.3 Flight Termination command function will be activated if the command received is as such. The function will send the pre-programmed flight termination information to function 1.7 Send to the FGM. Once the 1.7 Send to the FGM function has received the required inputs, it is then sent to the 2.0 Generate Force function.

If the command received from the MCP cannot be deciphered, then the system (1.1 Decipher Command) will enter the 1.8 Generate Error function, and it will generate a response to the command and submit it to the MCP (4.0 Send Information to MCP function).

The sub-functions between the 2.0 Generate Force Function and the 3.0 Monitor the Response feedback can be broken down as seen in Figure 112 and Figure 114:

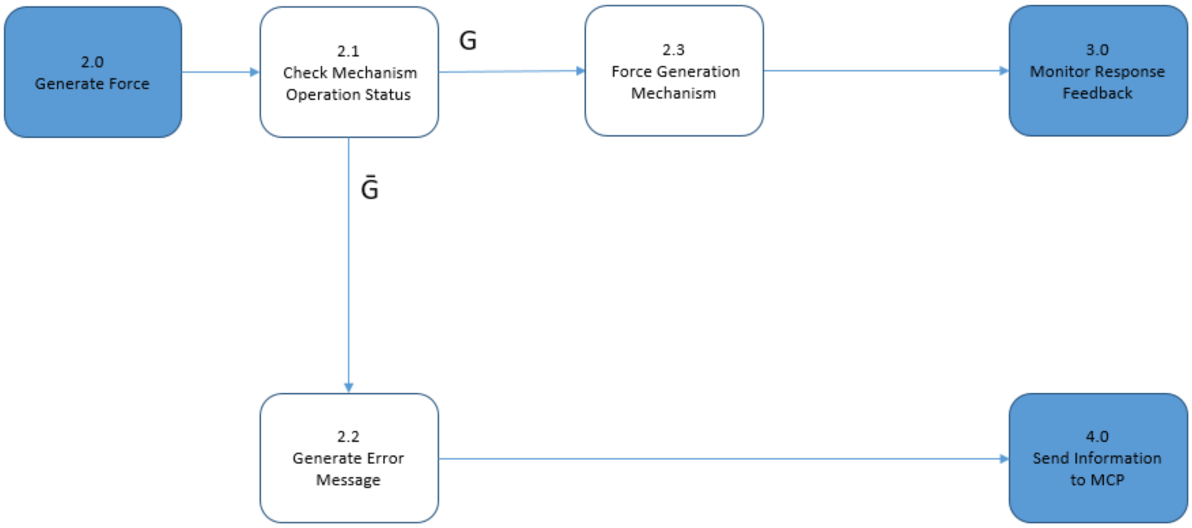

Figure 112: Functional Decomposition of the Generate Force Function

Once the command reaches the 2.0 Generate Force function, the system must check the operational status of the FGM (2.1 Check Mechanism Operational Status function).

If the system detects that there is a fault/error from the system, a "No Go" path is taken, denoted by the $\bar{G}$. It enters a 2.2 Generate Error Message function which generates a message with the error description that will then be sent to the 4.0 Send information to MCP function.

If the mechanism's status is acceptable, a "Go" path is taken, denoted by the G. The system then enters the 2.3 FGM function, which would then ideally be able to increase, decrease or maintain the force required from the missile system. The 2.3 FGM function could be broken down into the sub-functions seen in Figure 113:

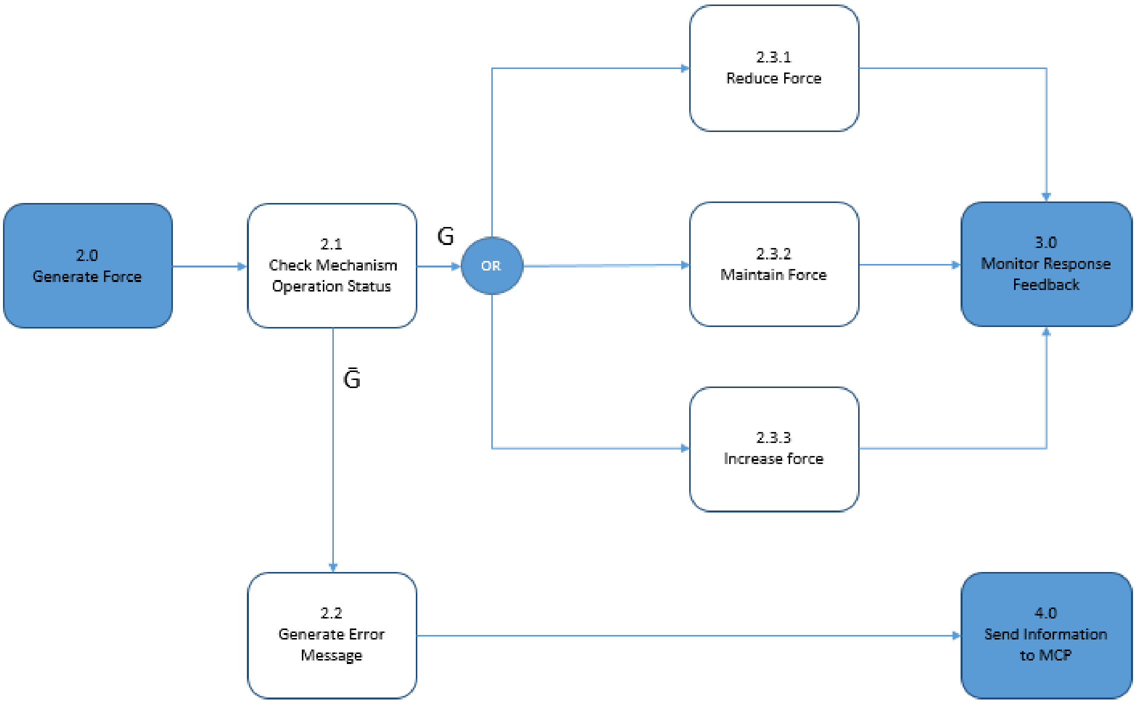

Figure 113: Functional Decomposition of the FGM Function

These sub-functions would include a 2.3.1 Reduce Force function, a 2.3.2 Maintain Force function and a 2.3.3 Increase Force function. The system will enter each of these functions depending on the overall missile system requirement. Once the function has been performed, the system will enter the 3.0 Monitor Response Feedback function.

Once the system enters the 3.0 Monitor Response Feedback function, the sub-functions involved can be seen in Figure 114:

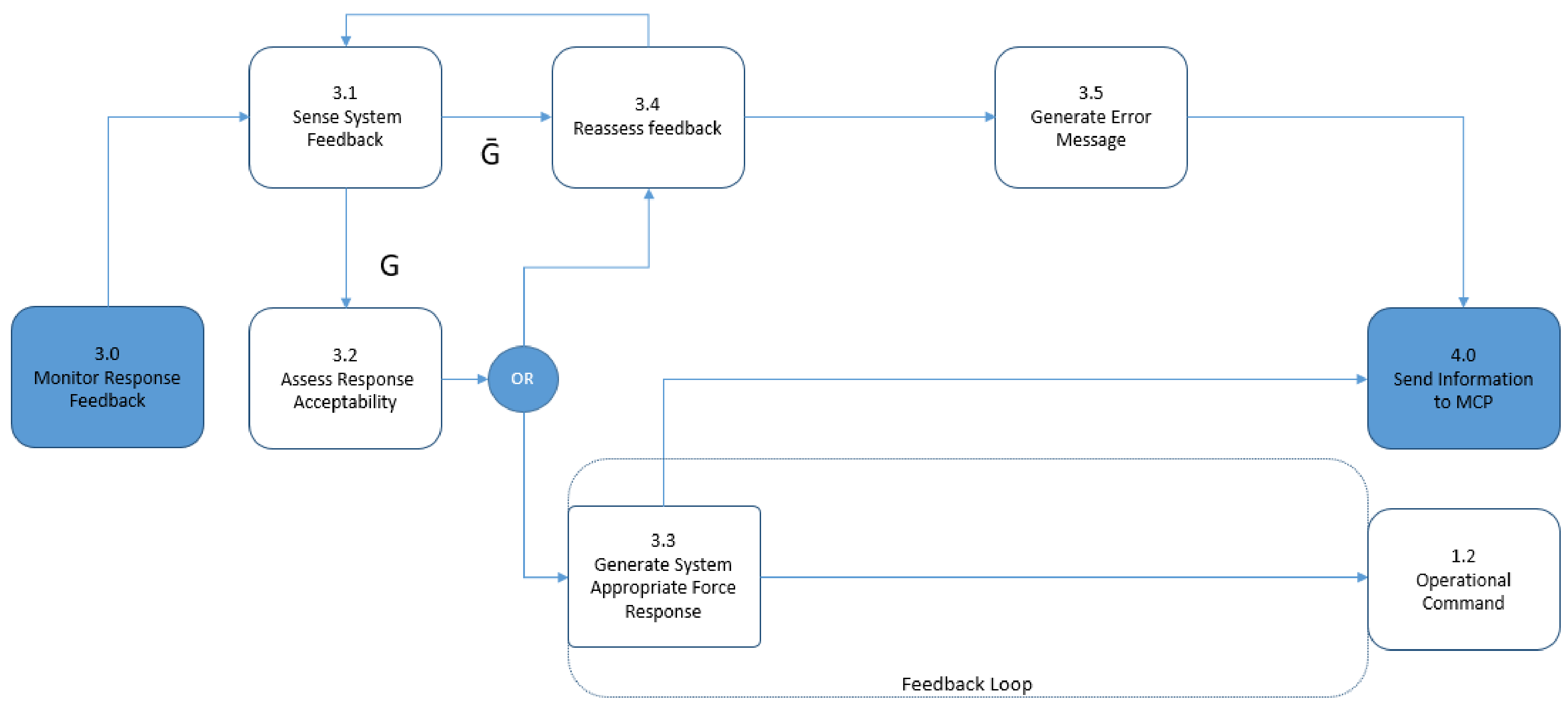

Figure 114: Functional Decomposition of the Monitor Response Feedback Function

In Figure 114, the sub-functions of the 3.0 Monitor Response Feedback Function have been identified. Once the 3.1 Sense System Feedback function has received the feedback signal from the 2.0 Generate Force Function, it then enters 3.2 Assess Response Acceptability function via the "Go" path denoted G. If the feedback is acceptable, then the system enters 3.3 Generate System Appropriate Force Response, it is then fed into the 4.0 Send Information to MCP function and the 2.0 Generate Force Function. If the feedback is not acceptable, the system enters a 3.4 Reassess Feedback Function, which requests the system to enter the 3.1 Sense System Feedback function, and 3.5 Generate Error Message function (which is sent to the 4.0 Send Information to the MCP function). If the force feedback cannot be sensed, the system also enters the 3.4 Reassess Feedback function via the "No Go" path denoted $\bar{G}$. This function simultaneously enters the 3.1 Sense System Feedback and 3.5 Generate Error Message functions again (which is sent to the 4.0 Send Information to the MCP function).

In order to be able to transfer and process information and to perform the physical functions required, a power source would be required. This would be a high-level function and would be associated with the primary functions, as can be seen in Figure 115:

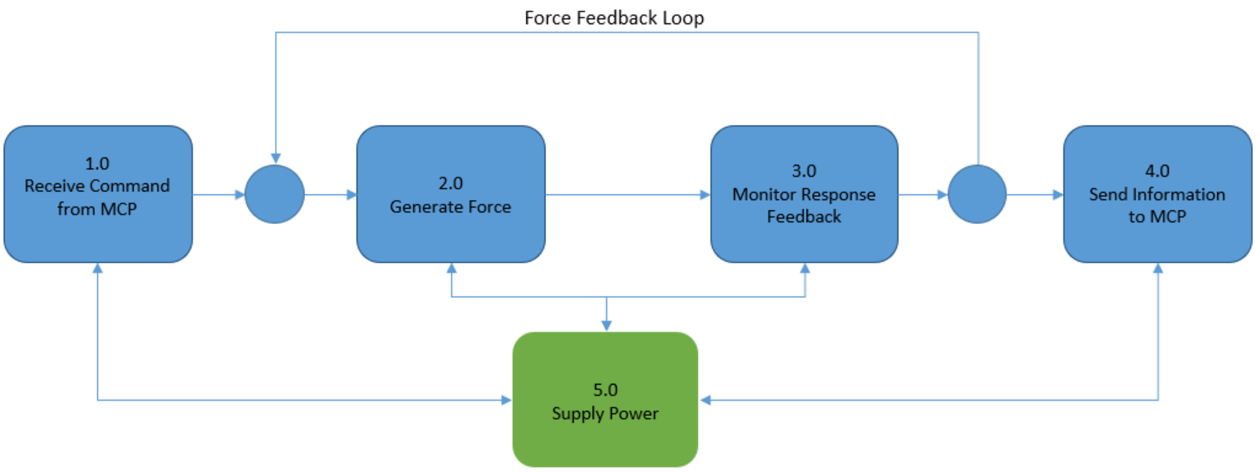

Figure 115: The Updated Primary Functional Flow Diagram

The Supply Power function would be accessed to carry out each of the primary functions and their associated sub-functions. A current would be requested through the Supply Power function depending on the requirement from each other function and sub-functions.

D.4 Functional Verification

The purpose of Functional Verification is to verify the totality of the functional structure developed in the previous section. The verification involves evaluating the functions against the system requirements.

The Functional Verification will be carried out in the following ways:

- Tabulation of the system requirements and their associated functions
- Activity diagram

The tabulation of the system requirements and the associated functions will highlight the downwards and upwards traceability of the requirements and derived functions. An activity diagram can showcase the actuator during operation. This would allow for the derived functions to be evaluated, to elicit any additional functions required, to determine any emerging functions, and to find redundant or unnecessary functions. For this study, a tabulation of requirements and functions was employed.

Table 69 highlights the relationship between the system requirements and the system functions.

Table 69: Downward and Upward traceability of System Requirements

Index	System Requirements and Constraints	Function	Functional Requirements	Performance Requirements
1.1.1	The Actuator must alter the missile flight path to intercept the intended target	1.0; 2.0; 3.0; 4.0; 5.0	1;2;5;6;7,9	1a;2a;2b;5a;6a;7a;7b;7c,9a
1.1.2	The Actuator must maintain the missile flight path	1.0; 2.0; 3.0; 4.0; 5.0	1;2;5;6;8;9	1a;2a;2b;5a;6a;8a;8b;8c;9a
1.1.3	The Actuator must not interfere with the launch platform	-	3	3a
1.1.4	Fit within the designated missile volume	-	3	3a
1.1.5	Operate within a required timeframe	1.0; 2.0; 3.0; 4.0; 5.0	7;8	7a;8a

D.5 Physical Architecture Design

D.5.1 Architecture Definition

During the Physical Architecture design or the process of Synthesis [10], the functional building blocks are transformed into physical blocks that details the organisation layout of crucial components, internal and external interfaces and relevant design constraints. A preferred solution is selected from a set of concepts.

The Physical Architecture is the representation of the physical elements that make up the internal structure of a system. The physical elements are derived from the functions the systems are required to perform. The system functions are as follows:

1. Receive Command from MCP
2. Generate Force
3. Monitor response Feedback.
4. Send Information to MCP
5. Supply Power

These functions and their related sub-functions were evaluated to develop suitable architecture as a first step. The top-level functions were separated into mechanical and electronic subsystems depending on the main focus of the function. In Figure 116, the demarcation of the subsystems depending on the functions are illustrated.

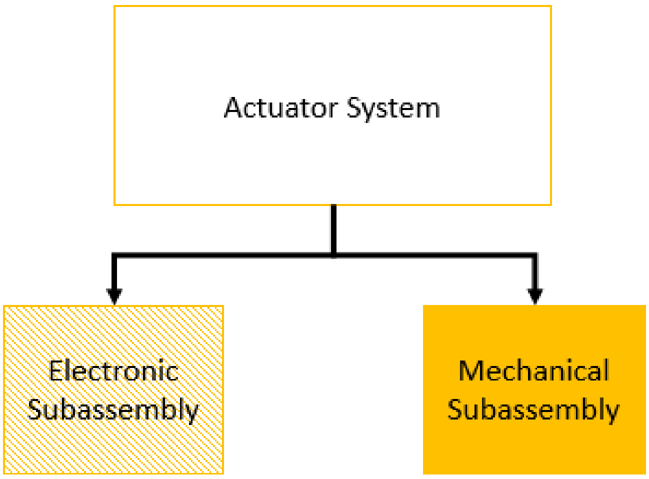

Figure 116: Initial Architecture Breakdown

The electronic architecture will handle the following functions:

- Receive Command from MCP
- Monitor response Feedback.
- Send Information to MCP
- Supply Power

The mechanical architecture will mainly focus on the "Generate Force" function.

The hatched blocks will refer to electronic architecture, and the solid colour blocks will denote mechanical architecture.

During the next step, the functions were evaluated to determine if there would be a possible Physical Architecture. The electronic assembly was assessed first.

In order to receive or send a command (information in a data form), a processing device/processor would be required. To monitor the response feedback, an encoder would be required to measure the force output. A battery system provides the Supply Power function.

Within the mechanical assembly, the Generate Force function would require a Force Generation mechanism, a primary structure to transfer the load through the actuator (like a bulkhead) and a shroud to encapsulate the inner components to protect them from the external environment during flight.
The next step was to break down the structure further by considering the sub-functions to identify the Physical Architecture better.

Focusing on the sub-functions between Function 1.0 and 2.0 (see Figure 111), the sub-functions would require electronic hardware and software to operate. The electronic hardware and software details are beyond the scope of this study, and therefore, further breakdown of these architecture components will not be discussed further.

For sub-functions between 2.0 and 3.0, electronic hardware and software would be required to ensure sub-functions 2.1 and 2.2 were possible. Sub-function 2.3 would require mechanical hardware. The sub-functions of 2.3, Reduce Force, Maintain Force, and Increase Force (2.3.1, 2.3.2 and 2.3.3, respectively) would require the mechanical hardware to be adjustable.

The encoder would handle this sub-function. The actuator electronic hardware and software would handle the remaining sub-functions. The diagram in Figure 117 illustrates the decomposition of the architecture.

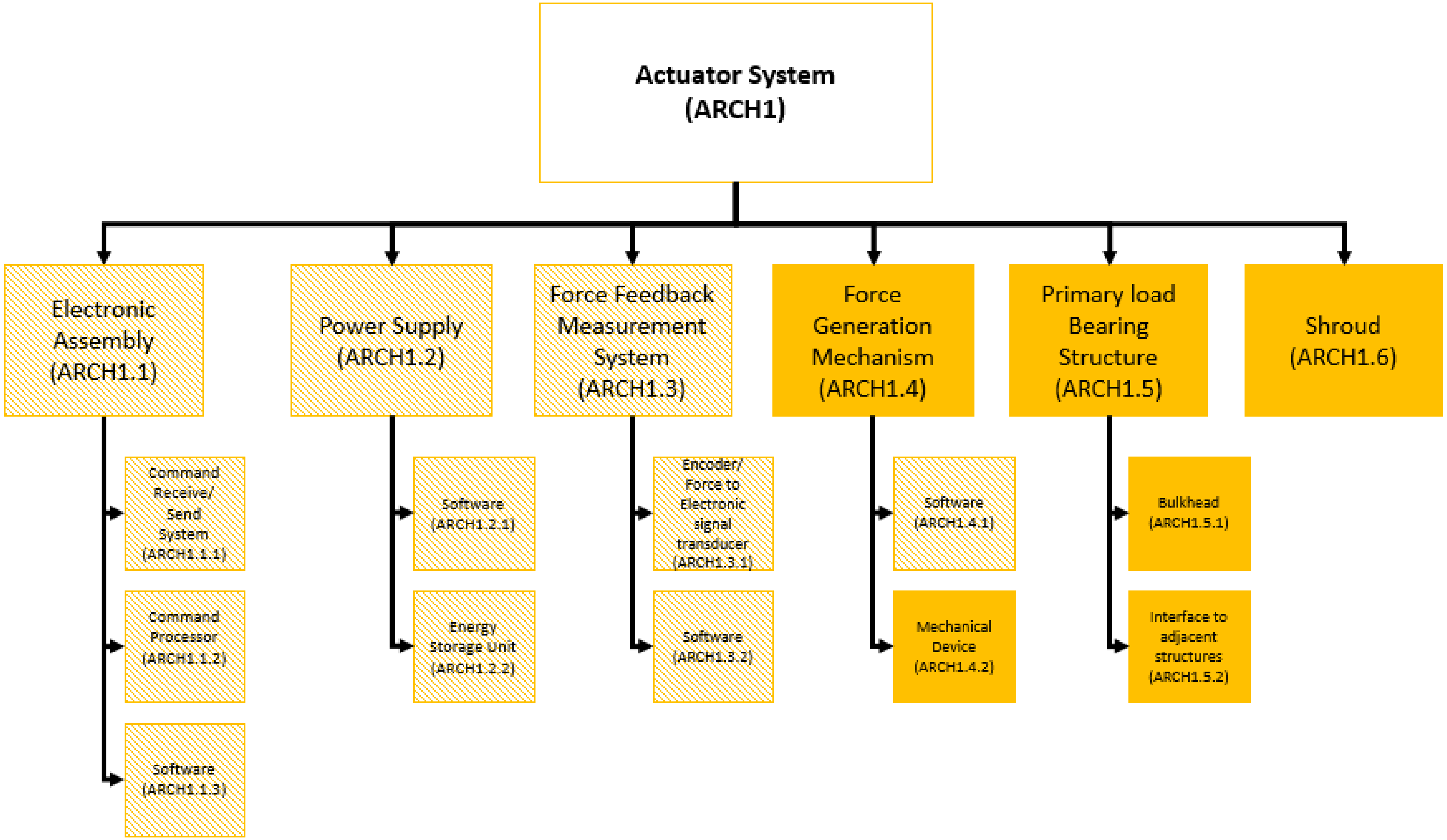

Figure 117: Actuator Physical Architecture based on Functions – Type A

The architecture decomposition of the actuator is only a single approach to the architecture that would be able to achieve functions defined for the actuator. An alternative architecture can be seen in Figure 118.

In order to perform the functions for receiving commands (F1) and sending information (F4), and processing of the information received (sub-functions between F1, F2, F3, F4 and F5), a printed circuit board (PCB) with the relevant electronic components to aid in performing the receiving, sending and processing of information, would be required. The PCB would also provide the physical interface for the system subsystems. Software would be required to aid in the processing of the information, for the power management of the system and to interface and manage the interaction between the system subsystems (for functions F1, F2, F3, F4 and F5 and sub-functions between F1, F2, F3, F4 and F5).

The generate force function (F2) and the function to monitor the response feedback (F3) could be carried out by the same subsystem/assembly.

The primary structure and shroud of the actuator, which would be required to transfer the loads through the structure generated by the force generation and the shielding of the internal actuator components from the operating environment, are a result of the force generation function (F2), the operating environment requirement and the missile airframe aerodynamics (see 5.1.3). The Supply Power function (F5) would be achieved with an energy storage system.

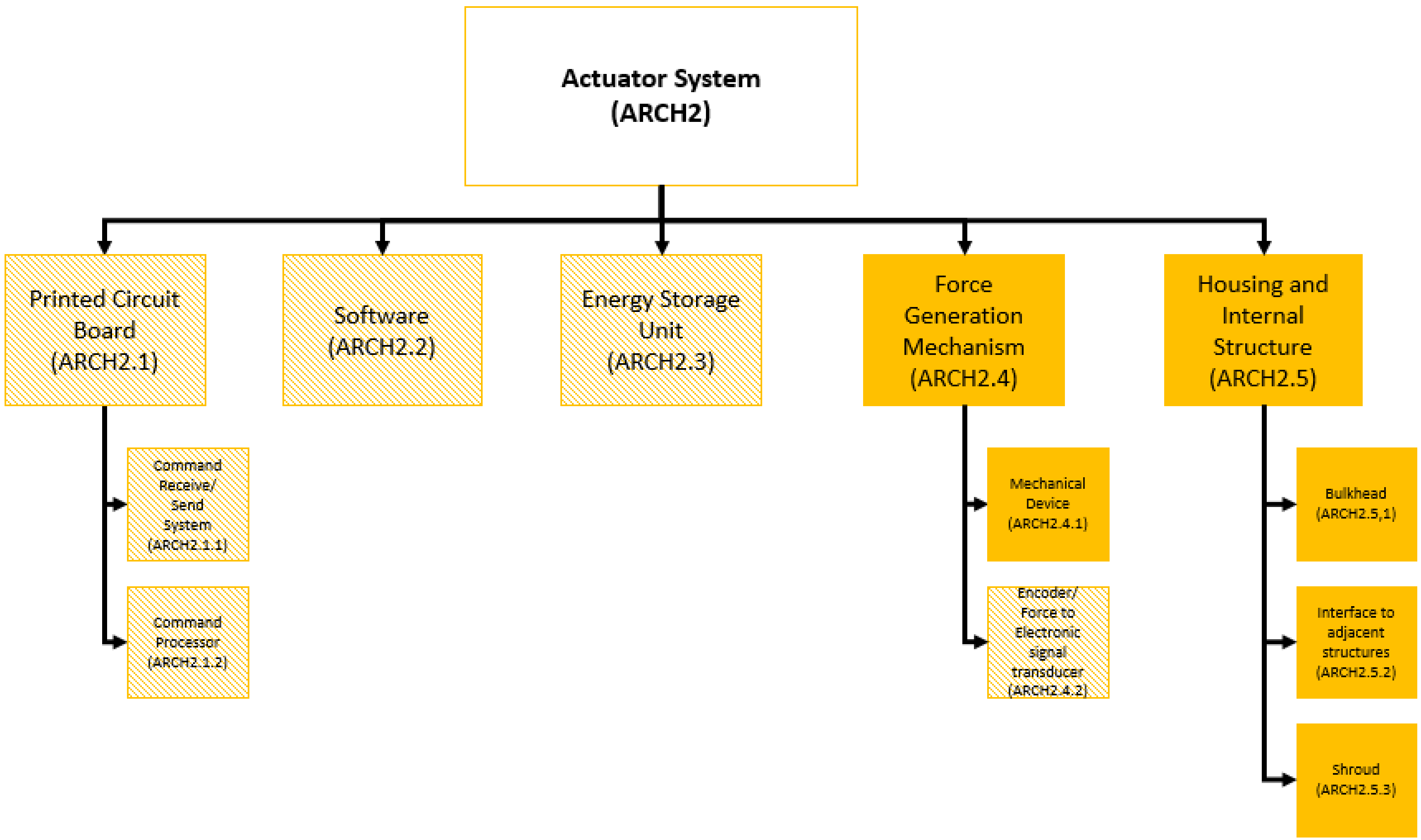

Figure 118: Physical Architecture based on Functions – Type B

Table 30 illustrates the relationship between the defined architecture and the main functions of the system. In places where the architecture is linked to more than one function, it refers to the architecture assisting in performing some of the functions.

Table 70: Relationship between the system architecture and the central system functions

		Functions				
		F1.0	F2.0	F3.0	F4.0	F5.0
		Receive Command from MCP	Generate Force	Monitor Response Feedback	Send Information to MCP	Power Supply
Architecture	ARCH1.1.1	■			■	
	ARCH1.1.2	■	■	■	■	
	ARCH1.1.3	■			■	
	ARCH1.2.1	■	■	■	■	■
	ARCH1.2.2					■
	ARCH1.3.1			■		
	ARCH1.3.2		■	■		
	ARCH1.4.1		■			
	ARCH1.4.2		■			
	ARCH1.5.1	■	■	■	■	■
	ARCH1.6	■	■	■	■	■
	ARCH2.1.1	■			■	
	ARCH2.1.2	■	■	■	■	■
	ARCH2.2	■	■	■	■	■
	ARCH2.3	■	■	■	■	■
	ARCH2.4.1		■			
	ARCH2.4.2			■		
	ARCH2.5.1	■	■	■	■	■
	ARCH2.5.2		■			
	ARCH2.5.3	■	■	■	■	■

The Architecture Selection process is described in the following section.

D.5.2 Architecture Selection

The process of Architecture Selection is required to determine the most suitable system architecture to use for the concept generation. According to Cross [122], the practice relating to evaluating design alternatives is to evaluate them based on a set list of objectives. Through the Systems Engineering approach followed in the previous sections, a list of design objectives can be drawn up. This will be based on user requirements, Functional Requirements, Performance Requirements, operational context requirements, and the defined functions of the system.

The method proposed by Cross [122] for evaluating alternatives, the Weighted Objective Method, was demonstrated through examples of concept evaluation. This method was employed for the architecture selection.

As per the procedure of the Weighted Objective Method (WOM), the design objectives were determined and listed. For the Architecture Selection, the design objectives were referred to as Selection Criteria (SC). This can be seen in Table 71.

Table 71: Selection Criteria

	Selection Criteria
SC1	**Simplicity**
SC2	**Allows for objective design**
SC3	**Maturity**

Simplicity (SC1) refers to the complexity of the Physical Architecture created to carry out the system functions. It was decided that a favourable architecture for this study would have a reduced complexity to achieve better groupings of subsystems to ease the conceptual design phase.

The "Allows for objective design" criterion (SC2) relates to how well the architecture is perceived to reduce restrictions in finding solutions for the architectural components. An architecture with fewer built-in constraints would be more favourable as it would allow for greater creativity during the conceptual design.

Maturity (SC3) refers to the state of maturity of the Physical Architecture developed; more specifically, it refers to how well are the architectures broken down into the lowest components and if there is a possibility that it can be broken down further.

The next step in the WOM is to rank the selection criteria. The process of ranking a selection criterion by comparing it to the other selection criterion was selected as the system of ranking. If a criterion is more important than another, then it will be assigned a 1 in the ranking matrix. If it is not as important, it will be assigned a 0. The matrix will be generated by assessing each of the selection criterion rows sequentially. The ranking matrix can be seen in Table 72.

Table 72: Selection Criteria Ranking Matrix

Selection Criteria	SC1	SC2	SC3	Row Totals
SC1	-	0	0	0
SC2	1	-	1	2
SC3	1	0	-	1

In the matrix in Table 72, the row totals highlight the importance of each objective and rank them accordingly, with the highest-ranking score being the objective perceived to be the most important and the lowest the least. In this case, selection criterion 2 (SC2) is ranked the highest. The weightings for the criteria were assigned, as seen in Table 73.

Table 73: Weightings of Ranked Design Objectives

Weighting	Selection Criteria
50	SC2
25	SC3
12.5	SC1

Based on the selection criteria determined, the architectures will be assessed according to their adequacy. The architecture will be scored off a five-point scale, from zero to four. The definition of the scoring can be seen in Table 74.

Table 74: Scoring Scale and Definition

Scoring Scale	Scoring Definition
0	Inadequate
1	Weak
2	Satisfactory
3	Good
4	Excellent

The architectures were then evaluated using the WOM. The evaluation can be seen in Table 75.

Table 75: Architecture Evaluation using the Weighted Objective Method

			Architecture Alternatives			
	Selection Criteria	**Weight**	**ARCH1**	**Weighted Value**	**ARCH2**	**Weighted Value**
SC1	**Simplicity**	12.5	2	0.16	4	0.32
SC2	**Allows for objective design**	50	2	0.04	4	0.08
SC3	**Maturity**	25	2	0.08	2	0.08
	Total			**0.28**		**0.48**

For SC1, ARCH2 was deemed to be twice as simple and had better subsystem groupings compared to ARCH1. ARCH1 was given a two as it was of satisfactory adequacy in being able to achieve the functions of the actuator system. ARCH2 was, however, seen as a better structure in this regard.

For SC2, ARCH1 was deemed satisfactory as it would allow for an objective design. However, ARCH2 was considered better due to the groupings of its subsystems.

Both ARCH1 and ARCH2 were considered to be on par concerning maturity. They both can be further broken down into smaller components, but for this study, it is sufficient.

As in Table 75, the second architecture (ARCH2) was found to be better than the two architectures developed, with a total of 0.48. Therefore, going forward, ARCH2 will be used for the conceptual design.

APPENDIX E: Brushless DC motor datasheet

The information in this appendix was obtained from Montevideo Technology Inc. [116].

Montevideo Technology, Inc. A Motor And Control Company TORQUE SYSTEMS (/)

BLHP-20-04-8P

Brushless High Performance Servo Series

DESIGN FEATURES

- High temperature operation up to 220°C
- Specs reflect high energy/high temp SmCo magnets
- Optional NdFeB magnets
- 3-phase Delta winding standard; Wye optional
- Class 'H' insulation standard
- Adheres to MIL design standards
- ABEC 3 bearings standard
- Feedback sensor options available

Contact Us (/contact-us) about this motor

DOWNLOAD DRAWINGS

(/images/Products/BLHP/diag_sensor/BLHP-20-04-8P.gif)
Housed w/ Halls

(/images/Products/BLHP/diag_senslss/BLHP-20-04-8P.gif)
Diagram Drawing

(/images/Products/BLHP/diag_sensor/FBLHP-20-04-8P.gif)
Frameless w/ Halls

(/images/Products/BLHP/diag_senslss/FBLHP-20-04-8P.gif)
Frameless Sensorless

SIZE PARAMETERS (APPROXIMATE)

Parameter		
	Units	Value
Number of Poles		
	P	8
Thermal Resistance, $_r$		
	°C/W	4.00
Max. Continuous Stall Torque, T_{cs}		
	mN-m	397.37
Motor Constant, K_m		
	mN-m/$W^{1/2}$	93.71
Hysteresis Drag Torque, T_f		
	mN-m	11.30
Viscous Damping		
	mN-m/RPM X 10^{-5}	53.67
Detent Torque, T_{fmax}		
	mN-m	19.07
Inertia, Sensorless, J_m		
	g-cm ^{2}	134.17
Inertia, w/halls, J_m		
	g-cm ^{2}	148.29
Weight, housed, W		
	g	515.96
Weight, frameless, W		
	g	391.22

(/contact-us/regional-sales-representatives)

WINDING DATA AT 24 VDC (APPROXIMATE)

Customize this Motor
Enter a new voltage and no load speed to view new winding data and new Torque vs. Speed curve
Metric | Imperial

Voltage:
24 V

No Load Speed:
2064 RPM

Ambient Temperature:
25 °C

Operating Temperature:
125 °C

Parameter		
	Units	Value
Torque Constant, K_t		
	mN-m/A	110.87
Voltage Constant, K_e		
	V/kRPM	11.63
No Load Speed, NLS		
	RPM	2064
Electrical Time Constant, t_e		

mS	0.71
Mechanical Time Constant, Sensorless, t_m	
mS	1.53
Mechanical Time Constant, w/Halls, t_m	
mS	1.69
Resistance at @25°C, R_m	
Ohm	1.4
Inductance, L_m	
mH	1
Max. Continuous Power Output at 100°C Rise	
W	57.81
Max. Continuous Torque Output at 100°C Rise	
mN-m	364.88
Max. Continuous Speed Output at 100°C Rise	
RPM	1513

(/contact-us/regional-sales-representatives)

Rotation is counter-clockwise as viewed from the lead wire side with **this excitation sequence and phase relationship (/excitation-sequence)**.

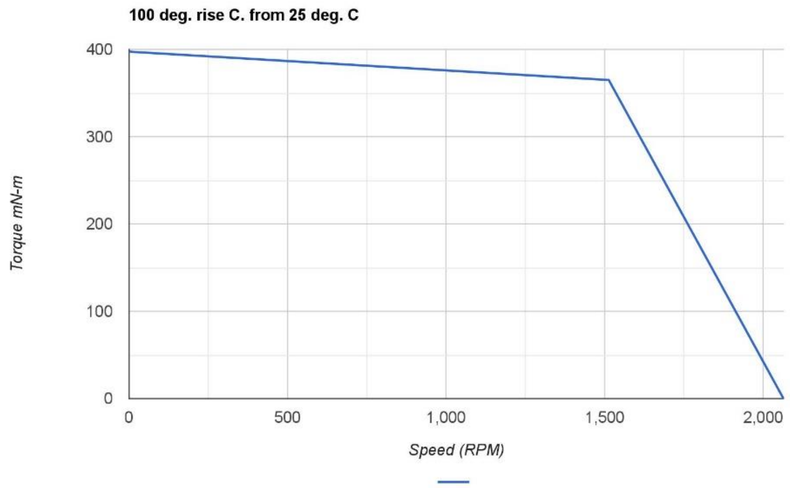

Montevideo Technology, Inc. (/)
A Motor And Control Company
TORQUE SYSTEMS

Montevideo Technology Inc. (MTI)
8201 109th Street
Pleasant Prairie, WI 53158
Phone: 262-764-6495 (tel:2627646495)
Email: websales@slmti.com (mailto:websales@slmti.com)

QUALITY MANAGEMENT

ISO9001 CERTIFIED (/Portals/0/Documents/0083453-01-SL-Montevideo-Technology-Inc-Recert-JC.pdf) AS 9100

OUR AFFILIATES

APPENDIX F: Generic Force Generation Mechanism Calculations

F.1 Force Generation

As previously mentioned in this chapter, the generic actuator uses a servo motor to actuate fins, which together forms a significant part of the FGM. The motors provide the force to rotate the fins, and in turn, the fins, in the presence of the airflow, provide the required forces to manoeuvre the missile.

A brushless DC motor (See data sheet in APPENDIX E), together with a ball screw arrangement, is used to counter this torque and move the missile's control surface for the baseline missile actuator system [87].

The fin's hinge moment was determined as follows:

$$T = F \times r_{cp}$$

In this equation, r_{cp} is the distance (13.74 mm) from the centre of pressure to the hinge line of the fin, as seen in Figure 119. The force F is the normal force (≈1685 N) that acts on the fin, determined in APPENDIX A. The torque T (hinge moment) produced is 23.15 Nm. The torque was increased by an assumed value of 20 % to ensure the motor selected had sufficient capability to still manoeuvre when loaded. The torque value used in the analysis was, therefore, 27.78 Nm.

The lever arm, r, is measured from the centre of the fin output shaft to the point of contact of the ball screw spindle. This is illustrated in Figure 119. The lever arm was adjusted to reduce the load acting along the axis of the ball screw. For this analysis, a lever arm of 76 mm was selected based on the space available within the actuator system.

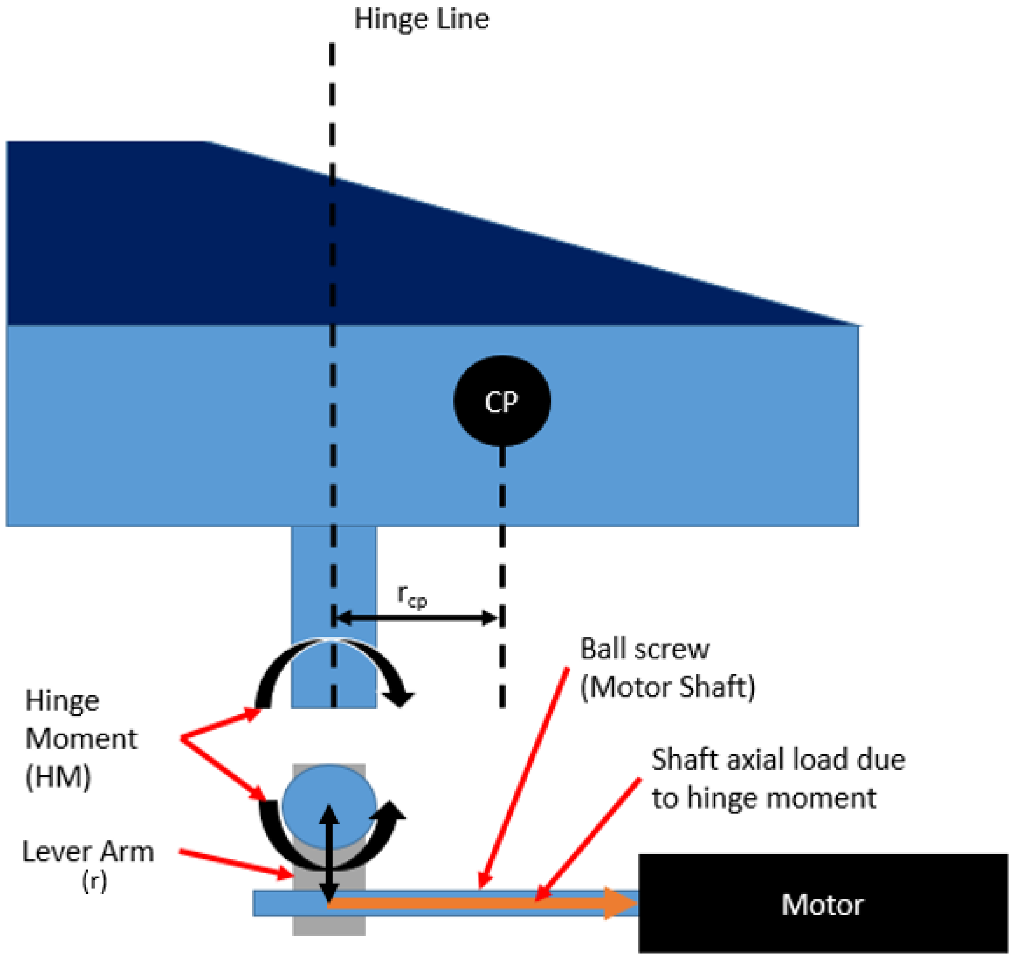

Figure 119: Illustration of lever arm distance

The BLHP-20-04-8P motor was selected due to its volume, which allows for four motors to be placed in the specified actuator volume and its torque rating. The motor torque is capable of producing the required linear force on the nut as shown in the calculation (from L. THK Co. [171]):

$$F_a = \frac{2 \times \pi \times \eta \times T_d}{P} \tag{73}$$

Where η is the efficiency of the ball screw (assumed to be 0.97), T_d is the torque developed by the motor (0.3 Nm), and P is the lead of the ball screw (5 mm). The force, F_a, produced is about 365.68 N. The specifications for a 12 mm diameter, 5 mm lead pitch ball screw (Part number 1521- 4 -6310) is an "off the shelf" item. [172]

The force, F_a, applied to the lever arm, which is assumed to be 76 mm in length (based on the available space within the actuator), connected to the output shaft would result in a torque of 27.79 Nm. This would equate to a force of 2022.34 N at the CP position.

Based on the information in the datasheet, the Servo Motor, the FGM of the generic actuator, is capable of producing the load required for the 30 g manoeuvre. Therefore, the servo motor meets requirement FR1.

F.2 Structural Integrity

The servo motor structure as a whole was evaluated regarding the structural integrity of the generic FGM. Assuming the servo motor uses a ball screw as its shaft, it allows for the translation of the torque from the motor into a linear force which is used to rotate the output shaft to the control fin using a lever arm. The motor shaft would have to withstand loads applied to the missile control fin. These loads affect the motor axially along the shaft of the motor.

As this type of FGM has already been deployed in an in-service missile actuator, it can be assumed that the motor can withstand the applied loading. Therefore, the requirement FR4 is satisfied.

F.3 Bandwidth

The bandwidth is the measure of the rate of response of the system to the input received. For the servo motor, Figure 120 illustrates the system (in the frequency domain) considered to determine the transfer function that would be used to evaluate the bandwidth of the generic actuators FGM.

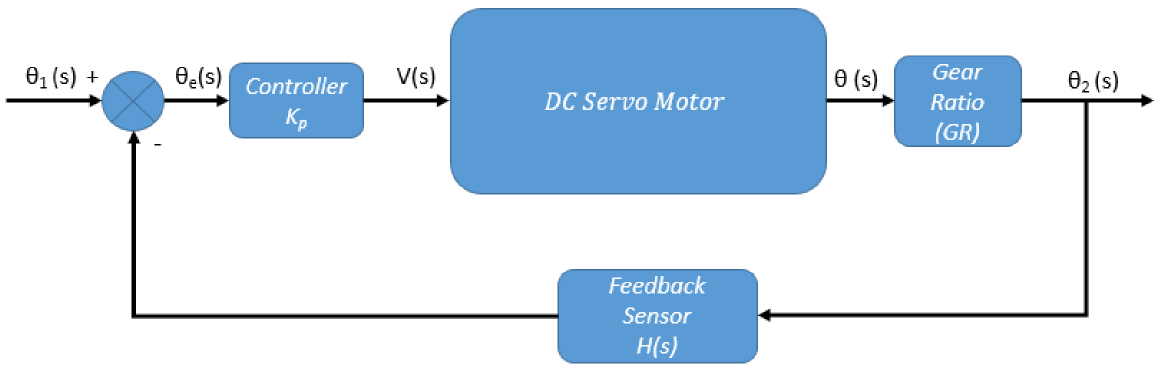

Figure 120: DC Servo Motor system block diagram

In Figure 120, θ_1 is the input signal, and θ_e is the difference between the input signal and the output measured by the feedback sensor. V is the voltage input to the servo motor. θ is the motor's output rotation, and θ_2 is the output rotation after the gearing ratio, which would be expected to be seen at the hinge line of the control surface, negating the effect of the inertia due to the components that follow after the servo motor. The transfer function was determined between the voltage input to the servo motor and the rotational displacement.

The transfer function of the DC Servo Motor for bandwidth assessment

The transfer function for the generic FGM was developed as follows:

$$T_M - c\dot{\theta} = J\ddot{\theta} \tag{74}$$

$$T_M = i(t)K_T \tag{75}$$

$$v(t) = Ri(t) + L\frac{di}{dt} + e_{bemf} \tag{76}$$

$$e_{bemf} = K_E\dot{\theta} \tag{77}$$

Substituting Equation **(75)** into Equation **(74)**, you get Equation **(78)**

$$i(t)K_T - c\dot{\theta} = J\ddot{\theta} \tag{78}$$

Substituting Equation **(77)** into Equation **(76)**, you get Equation **(79)**

$$v(t) = Ri(t) + L\frac{di}{dt} + K_E\dot{\theta} \tag{79}$$

If you take the Laplace transform of Equation **(78)** and Equation **(79)**, you get Equation **(80)** and Equation **(81)**, respectively.

$$I(s)K_T - cs\theta(s) = Js^2\theta(s) \tag{80}$$

$$V(s) = RI(s) + LsI(s) + K_E\theta(s) \tag{81}$$

Rearranging Equation **(80)** such that it solves for *I(s)* and substituting the rearranged equation into Equation **(81)**, we get the combined Equation **(82)** in terms of the system output over the input:

$$G(s) = \frac{\theta(s)}{V(s)} = \frac{K_T}{[JLs^3 + (RJ + cL)s^2 + Rcs + K_T K_E]} \tag{82}$$

The MATLAB code was as follows:

```
% Servo_Motor


% Controller


Kp = 1000;


Ki = 0;


Kd = 0;


controller = pid(Kp, Ki, Kd);


% Plant
R = 1.4; %Ohm
L = 1*10^-3; %mH to H
KE = (11.63/(1000*(0.104719755))); %V/kRPM to V/rad/s
Jload = 0.008139165; %Inertia of load (kgm2)

KT = 110.87/1000;%mNm/A to Nm/A
c = (53.67)/(1000*0.104719755); % mN-m/RPM X 10 -5 to Nm/RPM to Nm/rad/s
H = 1; %sensor feedback
GR = 92.6;%gear ratio
J = 14.829e-6 + (Jload*(1/GR)^2); %gcm2 to kgm2

num = [0 KT];
```

```
dem = [L*J (R*J)+(c*L) (KT*KE)+(R*c) 0];

plant = tf(num, dem);

% Feedback Sensor
sensor = tf(H, 1);

% Closed-loop system

sys = controller*plant;

closed_sys = feedback(sys, sensor, -1);

% Calculate bandwidth of the closed-loop system

figure; bode(closed_sys); grid on

bw = bandwidth(closed_sys)/(2*pi)
```

When considering the angular displacement, the inverse gear ratio is considered, as shown in Figure 121, as the gearing results in an angular displacement reduction.

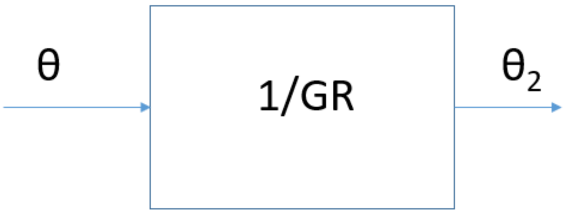

Figure 121: System block diagram for the Gear Ratio

The Missile fin load on the system was added to the inertia of the motor as follows:

$$J = J_m + J_L \left(\frac{1}{GR}\right)^2 \tag{83}$$

Where J_L is the load's inertia (kgm^2).

For the Missile Fin load, inertia was determined based on a steel plate with dimensions seen in Figure 122.

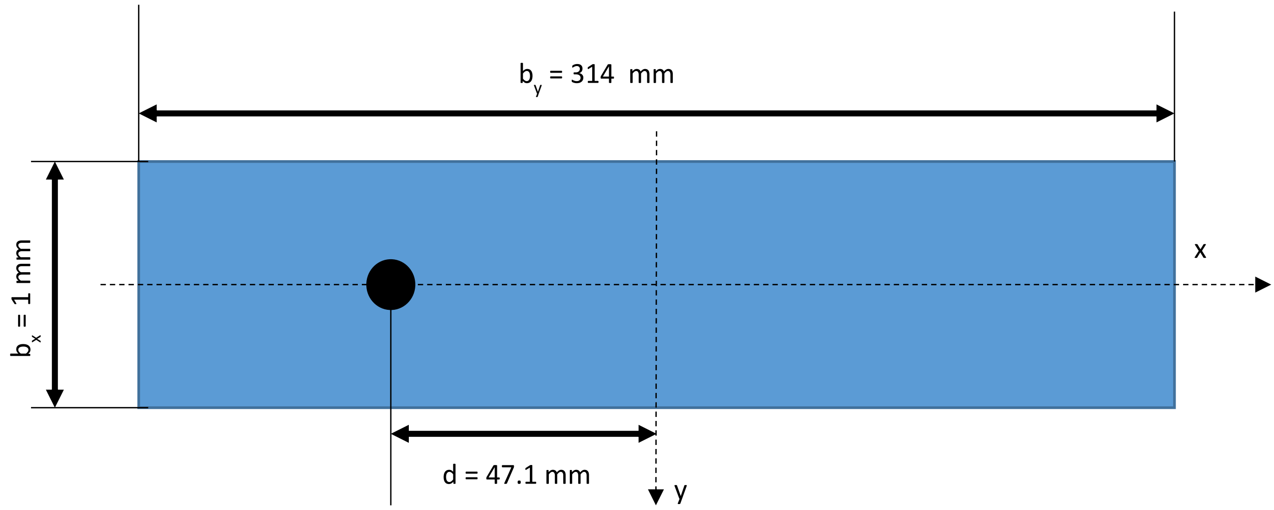

Figure 122: Fin Root chord and plate thickness

$$I_y = \frac{1}{12} b_y m^2 \tag{84}$$

$$I_x = \frac{1}{12} b_x m^2 \tag{85}$$

$$I_{y'} = I_y + md^2 \tag{86}$$

In Figure 122, *d* refers to the axis of rotation. The polar moment of inertia *J* was calculated about this position. In Equation (**84**) to (**86**), I_y refers to the mass moment of inertia about the *y* axis, b_y is the base dimension perpendicular to the *y* axis, I_x refers to the mass moment of inertia about the *x*-axis, by is the base dimension perpendicular to the *x*-axis, m refers to the mass of the fin and $I_{y'}$ refers to the mass moment of inertia about the centre of rotation based on parallel axis theorem. Only the influence of the inertia was evaluated for this system. Other factors like stiffness and damping of the load were not considered as part of the scope of the study. These factors can influence the performance of the system, and their impact should be evaluated in another study.

As seen in Figure 120, a controller, gear ratio and a feedback sensor were selected to create a closed-loop system to evaluate the bandwidth. A proportional controller (K_p) was selected to multiply the difference of the input from the output of the system.

The variables and constants are described in Table 76.

Table 76: Variable and constants for the Generic Actuator

Variable/Constant	Description	Value	Units
K_p	Proportional Controller constant	1×10^3	-
R	Servo Motor resistance [116]	1.4	Ω
K_E	Back EMF constant [116]	11.63	V/kRPM
J_m	Motor Inertia [116]	14.829×10^{-6}	kgm^2
c_t	Damping constant for the system [116]	0.5125	Nms/rad
K_T	Motor Torque Constant [116]	0.1109	Nm/A
$H(s)$	Feedback Function	1	-
GR	Gear Ratio	92.6	-
J_L	Missile Fin Load Inertia	8.14×10^{-3}	kgm^2

The Bode diagram for the Servo motor can be seen in Figure 123.

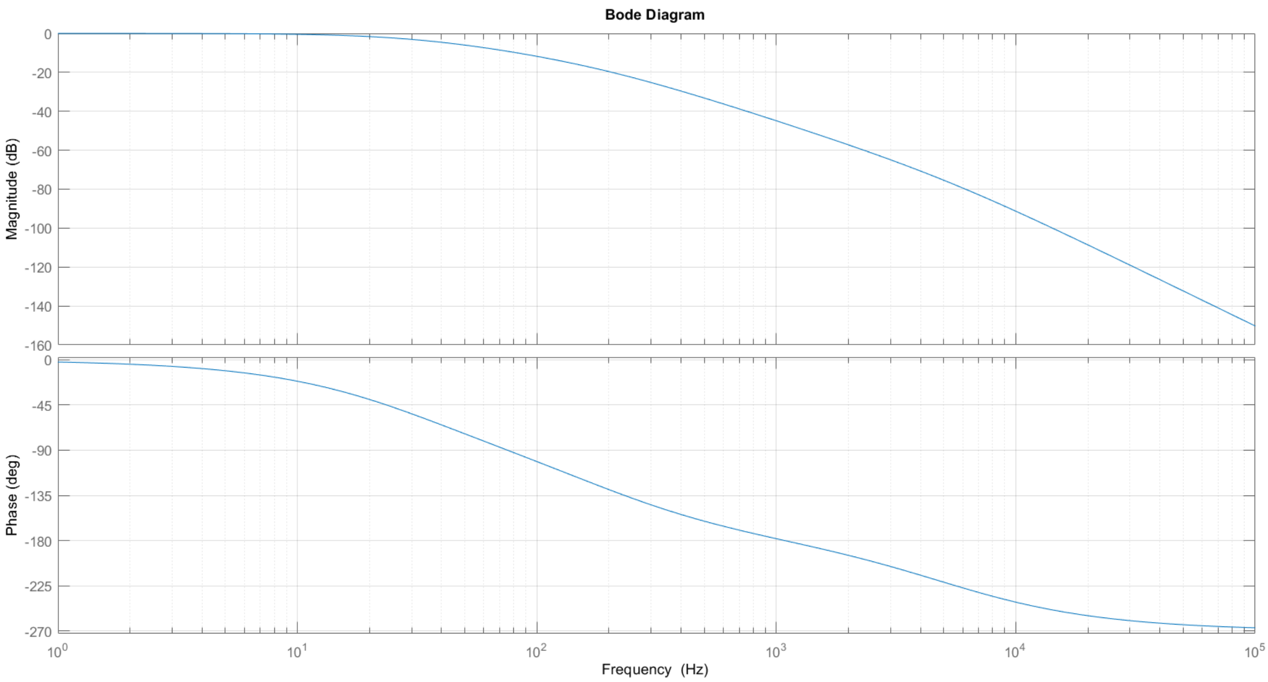

Figure 123: Bode Diagram - Servo Motor

The K_p value used was adjusted to achieve a critically damped system. This type of damping was selected as a critically damped system. It would tend to return to its position of rest in a relatively short period [173] which would allow the servo to achieve the fin deflection command in a shorter time. Improved values, additional or alternative controller configurations will not be analysed in this study as a first-order answer was able to be achieved with the initial controller.

The torque required by the motor to overcome the aerodynamic loading and to maintain the control surface position was determined to be 27.78 Nm. The selected motor can produce 0.3 Nm torque [116]. Therefore, a gearing ratio of 92.6 would be required to ensure the required output torque is achieved.

Unity feedback was selected for this analysis to simplify the calculation for this study. Therefore, the feedback function has a value of 1.

The bandwidth was determined to be 27 Hz. This is above the required bandwidth of 25 Hz and is therefore acceptable for this application. The requirement FR7 is therefore satisfied.

F.4 Operation Time

As mentioned in the previous section, the operation time refers to the duration the FGM would have to operate. The missile is meant to operate for 180 s. Therefore, the force mechanism should operate, at a minimum, for the same duration of time. This is true unless there is a requirement or specification that it does not have to do so.

The battery power supply will limit the operation time for the motor. According to [87] online the actuator for the AIM 120 uses lithium-aluminium batteries. Additional details were not able to be found. Therefore, a suitable similar battery was investigated.

Thermal Batteries are often used as a power supply for defence systems, according to Swift [174]. These batteries are electrically inert at low temperatures, which make them ideal for extended storage periods. The ignition is usually provided by an electric current. The batteries are electrochemical systems that require high temperatures to operate. The batteries are made up of Li/FeS2 couple to create power and an anode usually made from Lithium-Silicon or Lithium-Aluminium.

The voltage and current capabilities of the AIM 120 actuator batteries were also not available. Based on its in-service status, it was assumed that the batteries in the actuator system are capable of powering the servo motors (the servo motors are rated at 24 V) and allowing the missile to manoeuvre as required; hence the selection. Therefore, it was assumed that at a minimum, it would last 180 s. Therefore, the generic FGM meets requirement FR2.

F.5 Storage

Based on the use of DC motors as a component of the generic FGM for missile systems like the AIM-120, the motors would have to be able to be stored similarly to the system itself. As mentioned in Howard *et al*. [118], the typical shelf life of missiles is 10 to 20 years. Therefore, this meets requirement FR5.

APPENDIX G: Concept 1 Calculations

a) Force Generation Hinge Moment Calculation

Based on the torque, *T*, of 27.78 Nm to rotate the fin and a lever arm, *r*, of 76 mm, the force required was calculated as follows:

$$F = \frac{T}{r}$$

Therefore the force *F* required was 365.68 N. Based on the arrangement of the Flexinol® wire, as seen in Section 6.1.1 in Figure 67, the pull of the wire would provide the input torque to rotate the leadscrew. The rotation would allow the nut to move linearly and provide the need required force to rotate the fin output shaft. This is illustrated in the free body diagram of the fin output shaft and the lever arm in Figure 124.

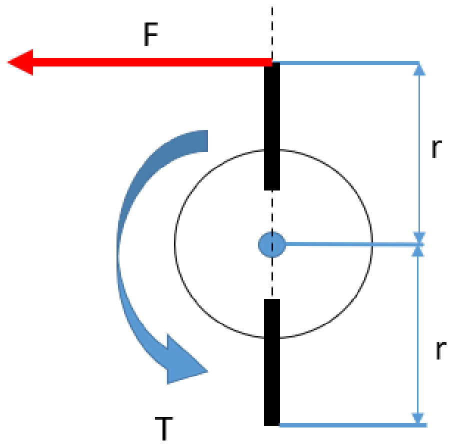

Figure 124: Free body diagram of the fin output shaft and the lever arm combination

From Figure 124:

$$\sum M = T = Fr$$

$$\therefore T = Fr$$

$$\therefore F = \frac{T}{r}$$

Based on the torque T of 27.78 Nm and the lever arm r of 56.60 mm mentioned previously, the force per wire, F, from the equation, would be 365.68 N.

Similar to the generic FGM, if the same leadscrew characteristics are considered, then the input torque to the leadscrew is 0.3 Nm. If a spool of diameter 12 mm is considered, then the force required by the Flexinol® wire is 25 N.

Based on the information provided by the Flexinol® wire manufacturer Dynalloy Inc. [128], the wire diameter (d) selected was 0.51 mm, which is able to produce a pull force of 3.56 N when heated [128]. About eight strands of this wire would have to be bundled together to produce the required pull force. This would result in a wire bundle of 1.35 mm in diameter (D). This was calculated as follows:

$$Single\ Wire\ Area = \pi r^2 = \pi \frac{d^2}{4}$$

$$\therefore Single\ Wire\ Area = 2.04 \times 10^{-7} m^2$$

$$Number\ of\ Strands = \frac{Force\ Required}{Force\ Produced} = \frac{25}{3.56} = 7.02$$

$$Wire\ Bundle\ Area = Single\ Wire\ Area \times Number\ of\ Strands$$

$$\therefore Wire\ Bundle\ Area = 1.46 \times 10^{-6}\ m^2$$

$$\therefore Bundle\ Wire\ Diameter\ (D) = \sqrt{\frac{4 \times Wire\ Bundle\ Area}{\pi}} \times 1000 = 1.35\ mm$$

b) The transfer function for bandwidth assessment

The transfer function from P. Senthilkumar *et al*. [131] is as follows:

$$G(s) = \frac{0.0643}{(s + 0.1)} = \frac{d(s)}{Q(s)}$$

In that study, the transfer function is based on the heat generated per unit volume of wire as was derived experimentally according to P. Senthilkumar *et al*. [131]. Where $d(s)$ refers to the function for wire displacement in the frequency domain and $Q(s)$ is the function of the heat generated per unit wire volume. To investigate the bandwidth of the wire length selected for this concept, the wire volume was included. Therefore the transfer function becomes:

$$G(s) = \frac{0.0643}{(s + 0.1)V}$$

The transfer function didn't include the inertia of the fin or the other components that would increase the load on the system. The inclusion of the components would increase the inertia of the system and would tend to decrease the bandwidth as the systems natural frequency would decrease based on simple harmonic motion:

$$\omega_n = \sqrt{\frac{K}{J}}$$

The MATLAB code was as follows:

```
% Controller

Kp = 0.001;

Ki = 0;

Kd = 0;

controller = pid(Kp, Ki, Kd);

% Plant
%R = 1.4; %Ohm
%L = 1; %mH
%KE = 11.63; %V/kRPM
%J1 = 148.29; %gcm2
%J2 = 300.00; %gcm2
%JT = J1+ J2;
%ct = 0.2;
%KT = 110.87;%mNm/A
H = 1; %sensor feedback
%GR = r*theta;%gear ratio
%s = tf('s');
%A = ((L*JT)*s^3)+(((R*JT)+(ct*L))*s^2)+(((KT*KE)+(R*ct))*s);
```

```
%num = [0.0643*Kp*H Kp*(H/Ki)];
%dem = [1 0.1 0];
l = 5.54; % m
d = 0.00051; %m
Ad = pi*(d^2)/4; %m2
Strands = 8;
AD = Ad*Strands; %m2
%D = d*Strands;%m
V = (AD)*l; %m3

%zeta = 0.7;

%wn = 40*2*pi; % needs to be in rad/s

%plant = tf(num, dem); % put in your plant transfer function here
%plant = (0.064)/((s + 0.1)*V);
num = 0.0643;
dem = [1 0.1];
plant = tf(num, dem);

% Feedback Sensor

sensor = tf(H, 1);

% Closed-loop system

sys = controller*plant*(1/V);

closed_sys = feedback(sys, sensor, -1);

% Calculate bandwidth of the closed-loop system

figure; bode(closed_sys); grid on

bw = bandwidth(closed_sys)/(2*pi)
```

c) Operational Time

According to D. Collins [45], bandwidth is defined as the rate of response of the system to given command input. In this analysis, it was assumed for the bandwidth evaluation that the given command would be equated to a single cycle of operation. During the operational cycle, the loading is meant to be within the expected loads of the system. Therefore, under normal operating conditions, the system should be able to perform under these conditions. Based on the required operation time of 180 s, the system would be required to respond to command inputs for the duration of the operating time. Therefore, the number of operation cycles was calculated as follows:

$$Operating\ Cycles = \frac{Operating\ Time}{Response\ Time}$$

$$Response\ Time = 1/Bandwidth$$

$$\therefore Operating\ Cycles = \frac{Operating\ Time}{1/Bandwidth} = \ Operating\ Time \times \ Bandwidth = 4500\ cycles$$

This is based on the required bandwidth of 25 Hz. In comparison with the load cycles of the nitinol wire, the operating cycles of this system fall below this value. Testing of the loading of the system would need to be carried out to verify this approach.

APPENDIX H: Email from Dynalloy Inc.

Erick Ortega <Erick.Ortega@dynalloy.com>

Wed 2019/02/20 21:41

To: Jeff <negative_pressure@hotmail.com>
Cc: Caroline Gonzalez <caroline.gonzalez@dynalloy.com>

Hi Jeff,

Pulling 490N over 12.85mm is possible but potentially not efficient. Typically, we recommended staying below 1kg*cm and your desired work is 64.2kg*cm.

To pull 490N 12.85mm will require several stands of wire strung in parallel. The length of your working wire can be found by taking your desired stroke and dividing it by the percent strain the can be created through the phase change ≈ 4%. Take 12.85mm/4% (or 3.5% for some safety margin) = 321.25mm.

Regarding the response time of the wire thicker wires require more power to head and longer cooling times. For details see the link below:
http://dynalloy.com/tech_data_wire.php

Thank you
Best Regards,

____

Erick Ortega | Customer Service

(714) 436-1206 main
(949) 502-8548 office
(714) 436-0511 fax

1562 Reynolds Avenue
Irvine, CA 92614

Alternate Contact: Jeff Brown (jeff.brown@dynalloy.com)

DYNALLOY, Inc.
Makers of Dynamic Alloys

From: Jeff <negative_pressure@hotmail.com>
Date: Monday, February 18, 2019 at 5:37 AM
To: Erick Ortega <Erick.Ortega@dynalloy.com>
Cc: Caroline Gonzalez <caroline.gonzalez@dynalloy.com>
Subject: Re: Flexinol product Information Request

Good Day Erick,

My apologies for the delayed response.

Thank you for the information.

The pull force required by the wire has changed to 490 N and the distance it has to travel is 12.85 mm. is there a wire length that would be able to meet this requirement?

Regarding the efficiency of the wire, I understand that it isn't as effective as other solutions. Is there a method to determine the rate of response of the nitinol wire?

I am currently using the study, Material Characterization of Nitinol wire for the design of actuator systems by SP Kennedy.

Kind Regards
JEFF

From: Erick Ortega <Erick.Ortega@dynalloy.com>
Sent: Friday, 25 January 2019 1:05 AM
To: Jeff
Cc: Caroline Gonzalez
Subject: Re: Flexinol product Information Request

The load of 270N over 34mm is possible with Flexinol® actuator wire but the length of the wire would be very long and require a large amount of power and a long cooling time. The 34mm actuation would require 875mm of straight working wire (16 parallel wires with 4% strain).

Please keep in mind there is also the question of efficiency. If your end task or device will require more than one-inch pound of work (or approximately 1 cm * kg) per second in order to operate, shape memory alloys may not be the most effective solution. The inherent efficiency of the shape memory alloys is relatively low compared to motors or solenoids capable of accomplishing the this much work. The SMAs excel in lower total work environments.

Best Regards,

____

Erick Ortega | Customer Service

(714) 436-1206 main
(949) 502-8548 office
(714) 436-0511 fax

1562 Reynolds Avenue
Irvine, CA 92614

Alternate Contact: Jeff Brown (jeff.brown@dynalloy.com)

DYNALLOY, Inc.
Makers of Dynamic Alloys

From: Jeff <negative_pressure@hotmail.com>
Date: Thursday, January 17, 2019 at 6:05 AM

To: Jeff Brown <jeff.brown@dynalloy.com>
Cc: Erick Ortega <Erick.Ortega@dynalloy.com>, Caroline Gonzalez <caroline.gonzalez@dynalloy.com>
Subject: Re: Flexinol product Information Request

Good Day Jeff,

Please see attached the form filled in as best I could. I am currently doing a feasibility study as part of my degree. I am identifying if SMA's can be used in place of generic actuation methods on air vehicle actuation systems.

Kind Regards

From: Jeff Brown <jeff.brown@dynalloy.com>
Sent: Wednesday, 16 January 2019 11:37 PM
To: Jeff
Cc: Erick Ortega; Caroline Gonzalez
Subject: Re: Flexinol product Information Request

Jeffrey Brown | 949-502-8540 direct | 714-436-1206 main

DYNALLOY, Inc.
Makers of Dynamic Alloys

From: Jeff <negative_pressure@hotmail.com>
Date: Wednesday, January 16, 2019 at 12:30 AM
To: Contact <Contact@dynalloy.com>
Subject: Flexinol product Information Request

Good Day,

I am looking for Flexinol product that can pull a load of 300 N over a distance of 35 mm. Do have something that could achieve this?

Kind Regards

APPENDIX I: Concept 2 Calculations

a) Force Generation Calculation

i. MFC patch deflection characterisation

The patch's deflection characterisation was carried out to determine the patch's effect on the bistable internal structure, as seen in Figure 70. The load conditions were compared to the results from S. Q. Zhang *et al*. [39]. These results can be seen in Table 77.

Table 77: Results of deflection of the aluminium plate from [39]

Θ^1 (mm)	Deflection (mm)
0	0
15	6.1445×10^{-4}
55	0.0372
100	0.1593
150	0.3453
200	0.5344
250	0.7242
300	0.9141

Moment (*M*) applied at the centre of the beam, at the centre of the patch length, with each station's deflection due to the load along beam determined as follows adapted from Roark and Young [137]:

$$z = z_A + \theta_A x + \frac{M}{2EI}\langle x - a\rangle^2$$

$$z_A = \frac{M}{2EI}(L^2 - a^2)$$

$$\theta_A = -\frac{M}{EI}(L - a)$$

- z is the deflection a position x
- z_A is the maximum deflection at the free end of the cantilever beam
- θ_A is the slope of the deflected beam

- x is the distance along the beam
- a is the distance from the free end of the cantilever beam (m) to where the moment is applied
- L is the length of the beam (m)
- E is the Young's Modulus (Pa)
- I is the Moment of Inertia (m^4)
- M is the applied Moment (Nm)

The aluminium plate was evaluated at the same stations as in S. Q. Zhang *et al*. [39]. The results can be seen in Table 78. The outcome of the calculation was corrected such that the deflection occurred in the same orientation as the experimental setup.

Table 78: Beam Deflection Evaluation

		z	
	Beam Station	**Results from** [39]	**Cantilever with a moment acting at the centre of the patch location**
x	0	0	0.000
	0.015	0.00061445	0.007
	0.055	0.0372	0.092
	0.1	0.1593	0.243
	0.15	0.3453	0.411
	0.2	0.5344	0.579
	0.25	0.7242	0.746
	0.3	0.9141	0.914

The results in Table 78 was used to create Figure 73.

ii. Force required Calculation

Based on Equation (32), the force was calculated

$$F_a = \frac{N z_n}{z_a} + \frac{2EIL^2 sin^2\theta}{z_a r_c (L^2 - a^2)} \quad (87)$$

Table 79: List of variables and quantities for the required force calculation

Variable	Quantity	Unit
N	*1685*	*N*
z_n	*0.0294*	*m*
L	*0.11*	*m*
E	13.22×10^{10}	*Pa*
I	1.573×10^{-10}	mm^4
θ	*12.7*	*Degrees*

The required force, F_a, using the values from Table 79, would therefore be 9495 N.

b) Structural Integrity

The shear and moment loads at the origin of the cantilever beam based on how the load is applied by the MFC patch would be determined as follows based on Figure 125:

$$\sum F_z = 0 = V$$

$$\therefore V = 0$$

$$\sum M_{origin} = 0 = M - M_{origin}$$

$$\therefore M_{origin} = M$$

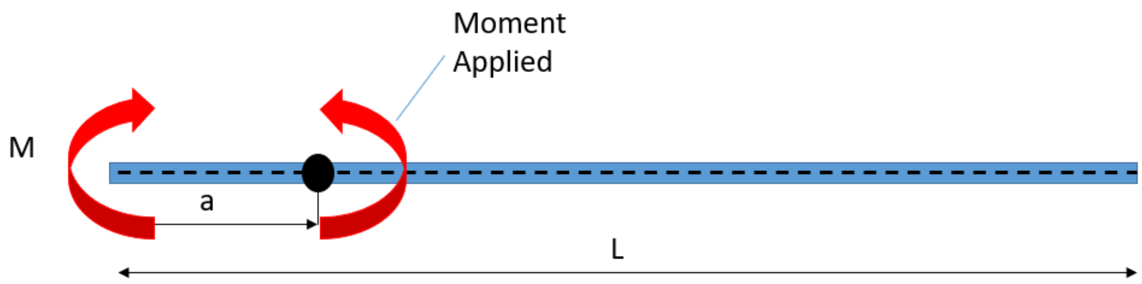

Figure 125: Moment applied to beam due to MFC Patches

Considering a worst case of a point load acting on the beam:

$$\sum F_z = 0 = F_a - V$$

$$\therefore V = F_a$$

$$\sum M_{origin} = 0 = F_a L - M$$

$$\therefore M = F_a L$$

APPENDIX J: Email from Smart-Material, the MFC manufacturer

RE: MFC information

Thomas Daue <t.daue@smart-material.com>

Sun 2019/04/07 17:27

To: 'Jeff' <negative_pressure@hotmail.com>
Cc: m.daue@smart-material.com <m.daue@smart-material.com>

Hello Jeff,

please see answers below.

best
Thomas Daue

e-mail: t.daue@smart-material.com
Phone: +1 941 870 3337
Fax : +1 941 847 0788
http://www.smart-material.com
MFC Forum: http://www.macrofibercomposite.com

From: Jeff [mailto:negative_pressure@hotmail.com]
Sent: Sunday, April 07, 2019 11:09 AM
To: sarasota@smart-material.com
Subject: MFC information
Importance: High

Good Day,

My name is Jeff, I am currently busy with my Masters Degree research and require some additional information regarding MFC actuators.

I am looking for following information:

Storage Requirements
10-60C, humidity < 70%

Storage life (without being used)
20 years, might require repoling after6-7 years

Sealing specification of the patches.
encapsulated in polyimide

Could you please assist me? Your help would be greatly appreciated.

Kind Regards

Jeff

Sent from Mail for Windows 10